

JUACEP Summer Program 2015 at Nagoya University



Table of Contents

<1> About the Program

a) Overview	...5
b) Participants	...6
c) Schedule	...8

<2> Classes & Events

a) Japanese Class	...12
b) Handcraft Exercise	...14
c) Field Trip	...15
d) Research Internship	...16
- Research Reports	...18
e) Workshop	
- The 13 th Workshop (for UM students)	...114
- The 14 th Workshop (for UCLA students)	...135

<3> Reports & Questionnaires on JUACEP Program

a) Reports	...156
b) Questionnaires	...179

<4> Appendix

a) Pictures	...184
b) Handout Materials	...191

<1>

About the Program

1-a. Overview

Short course (3 months) program 2015

for the students of University of Michigan...

Duration: May 14 - August 6, 2015

Research presentation: The 13th JUACEP Workshop on August 6

for the students of UCLA...

Duration: June 16 - September 4, 2015

Research presentation: The 14th JUACEP Workshop on September 2

This program was designed for graduate course students of University of Michigan and University of California, Los Angeles. The qualified students were selected among many excellent candidates of each university.

Each student belonged to a laboratory of Nagoya University according to his/her research interest being given a research topic and carried out the project in cooperation with the lab members under the supervising professor. At the same time most of them attended the optional Japanese language class (with credit), the hands-on engine assembly course and some special lectures organized for the program.

During the program period, they took part in the lab's ordinary events like seminars, sessions, trips, casual parties and so on. They acted as a regular member of laboratory. Teaching assistant assigned for the program in each laboratory supported the US students not only in research scenes but also in everyday life.

At the end of the program, they respectively completed a research report and gave a final presentation at the workshop about their research findings. Each NU supervisor evaluated the report and presentation, and the students were credited by Nagoya University. In the University of Michigan, the credits have been transferred to ME590/ENGR591 by the agreement.

1-b. Participants

	Students from University of Michigan	Advisors at Nagoya University
1	Emanuel CHIRAYATH	Prof. Jiro KASAHARA
	Aerospace Engineering	Aerospace Engineering
2	Fang DAI	Prof. Tatsuya SUZUKI
	Mechanical Engineering	Mechanical Science and Engineering
3	Ulka DANDEKAR	Prof. Hiroyuki ASANUMA
	Integrative Systems and Design	Molecular Design and Engineering
4	Yuting GAO	Prof. Ichiro NARUSE
	Chemical Engineering	Mechanical Science and Engineering
5	Xudong HAO	Prof. Yoji YAMADA
	Mechanical Engineering	Mechanical Science and Engineering
6	Chadwick HARVEY	Prof. Jiro KASAHARA
	Aerospace Engineering	Aerospace Engineering
7	Jiahong JU	Prof. Toshiro MATSUMURA
	Electrical Engineering and Computer Science	Electrical Engineering and Computer Science
8	Andrea MANOPPO	Prof. Fumihito ARAI
	Biomedical Engineering	Micro-Nano Systems Engineering
9	Haodong SHEN	Prof. Norihiko NISHIZAWA
	Electrical Engineering and Computer Science	Quantum Engineering
10	Goutham THANGARAJ	Prof. Kazuo SHIOKAWA
	Climate and Space Sciences and Engineering	Solar-Terrestrial Environment Laboratory
11	Chen WANG	Prof. Toshiro MATSUMOTO
	Mechanical Engineering	Mechanical Science and Engineering
12	Hanyi XIE	Prof. Noritsugu UMEHARA
	Mechanical Engineering	Mechanical Science and Engineering
13	Yalim YILDIRIM	Prof. Yasuhisa HASEGAWA
	Mechanical Engineering	Micro-Nano Systems Engineering

	Students from UCLA	Advisors at Nagoya University
1	Douglas CHEN	Assoc. Prof. Seiichi DEGUCHI
	Materials Science and Engineering	Energy Engineering and Science
2	Yifan JIANG	Prof. Hiroshi AMANO
	Electrical Engineering	Electrical Engineering and Computer Science
3	Austin KUO	Prof. Yoshikazu HAYAKAWA
	Mechanical and Aerospace Engineering	Mechanical Science and Engineering
4	Haroula KYRIACOU	Prof. Masahiro HIRASAWA
	Materials Science and Engineering	Molecular Design and Engineering
5	Hongyang LI	Prof. Yasutoshi IRIYAMA
	Materials Science and Engineering	Materials Science and Engineering

6	Xu LI	Prof. Fumihito ARAI
	Mechanical and Aerospace Engineering	Micro-Nano Systems Engineering
7	Antonio MARTINEZ	Prof. Nobuo KAWAGUCHI
	Electrical Engineering	Computational Science and Engineering
8	Jimmy NG	Prof. Yahachi SAITO
	Materials Science and Engineering	Quantum Engineering
9	Lindsey PERRY	Prof. Masahiro HIRASAWA
	Materials Science and Engineering	Molecular Design and Engineering
10	Jacob STREMFEL	Prof. Yang JU
	Materials Science and Engineering	Mechanical Science and Engineering

Instructors at Nagoya University

Ms. Sumie YASUI	Japanese Teacher
Prof. Yasuhiko SAKAI	Director of Creation Plaza
Asst. Prof. Kazue KANEKO	Creation Plaza
Masafumi NAKAKIMURA	Chief Technical Staff
Koji YAMAMOTO	Technical Staff
Shintaro GOTO	Technical Staff
Kiyonori SAITO	Technical Staff
Toshifumi ISOGAI	Technical Staff
Yuta ADACHI	Technical Staff

Coordinators of Partner Universities

Prof. Katsuo KURABAYASHI	Mechanical Engineering, Univ. of Michigan
Prof. Jenn-Ming YANG	Materials Science and Engineering, UCLA



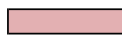




JUACEP Members

Prof. Yang JU	Mechanical Science and Engineering
Prof. Noritsugu UMEHARA	Mechanical Science and Engineering
Assoc. Prof. Yasumasa ITO	Mechanical Science and Engineering
Tomoko KATO	Administrative staff
Chiharu YADA	Administrative staff

JUACEP Summer Program 2015 Schedule

Day	Date		8:45-10:15	10:30-12:00		13:00-14:30	14:45-16:15	16:15-	
1	5/13/2015	Wed	Arrival of UM students						
2	5/14/2015	Thu	Orientation for UM students (10:30 @ VBL Hall)		Lunch @ VBL Hall	Japanese Lang. 13:30-15:45 (UM)			
3	5/15/2015	Fri	Research at Lab			Stipend & tuition payment@ES031	Research at Lab		
4	5/16/2015	Sat							
5	5/17/2015	Sun							
6	5/18/2015	Mon	Research at Lab			28th JUACEP Seminar	Research at Lab		
7	5/19/2015	Tue	Research at Lab	29th JUACEP Seminar		Japanese Lang 13:30-15:45 (UM)			
8	5/20/2015	Wed	Research at Lab			Research at Lab	Introduction to PE 1-2	Research at Lab	
9	5/21/2015	Thu	Japanese Lang 9:40- (UM)			Research at Lab			
10	5/22/2015	Fri	Research at Lab			Research at Lab		Discussion with NU students	
11	5/23/2015	Sat							
12	5/24/2015	Sun							
13	5/25/2015	Mon	Research at Lab			Research at Lab			
14	5/26/2015	Tue	Japanese Lang 9:40- (UM)						
15	5/27/2015	Wed	Research at Lab			Research at Lab	Introduction to PE 1-3	Research at Lab	
16	5/28/2015	Thu	Japanese Lang 9:40- (UM)			Research at Lab	Research at Lab	Research at Lab	
17	5/29/2015	Fri	Research at Lab			Research at Lab	Research at Lab	Research at Lab	
18	5/30/2015	Sat							
19	5/31/2015	Sun							
20	6/1/2015	Mon	Research at Lab			Research at Lab			
21	6/2/2015	Tue	Japanese Lang 9:40- (UM)						
22	6/3/2015	Wed	Research at Lab			Research at Lab	Introduction to PE 2-1	Research at Lab	
23	6/4/2015	Thu	Japanese Lang 9:40- (UM)			University Festival			
24	6/5/2015	Fri	University Festival						
25	6/6/2015	Sat	University Festival						
26	6/7/2015	Sun	University Festival						
27	6/8/2015	Mon	Research at Lab			Research at Lab			
28	6/9/2015	Tue	Japanese Lang 9:40- (UM)						
29	6/10/2015	Wed	Research at Lab			Research at Lab	Introduction to PE 2-2	Research at Lab	
30	6/11/2015	Thu	Japanese Lang 9:40- (UM)			Research at Lab			
31	6/12/2015	Fri	Research at Lab			Research at Lab			
32	6/13/2015	Sat							
33	6/14/2015	Sun							
34	6/15/2015	Mon	Research at Lab			Research at Lab			
35	6/16/2015	Tue	Japanese Lang 9:40- (UM)			Arrival of UCLA students			
36	6/17/2015	Wed	Orientation for UCLA students (10:30 @VBL Hall)		Lunch @ Chez Jiroud	Stipend & tuition payment@ES031	Introduction to PE 3-1	Research at Lab	
37	6/18/2015	Thu	Japanese Lang 9:40- (UCLA)			Research at Lab			
38	6/19/2015	Fri	Research at Lab			Research at Lab			
39	6/20/2015	Sat							
40	6/21/2015	Sun							
41	6/22/2015	Mon	Research at Lab			Research at Lab			
42	6/23/2015	Tue	Japanese Lang 9:40- (UCLA)			Research at Lab			
43	6/24/2015	Wed	Research at Lab			Research at Lab	Introduction to PE 3-2	Research at Lab	
44	6/25/2015	Thu	Japanese Lang 9:40- (UCLA)			Research at Lab			
45	6/26/2015	Fri	Research at Lab			Research at Lab			
46	6/27/2015	Sat							
47	6/28/2015	Sun							
48	6/29/2015	Mon	Research at Lab			Research at Lab			
49	6/30/2015	Tue	Japanese Lang 9:40- (UCLA)			Handcraft Exercice (Group A)			
50	7/1/2015	Wed	Research at Lab			Research at Lab	Introduction to PE 4-1	Research at Lab	
51	7/2/2015	Thu	Japanese Lang 9:40- (UCLA)			Handcraft Exercice (Group B)			
52	7/3/2015	Fri	Field Trip (Toyota factory visit --> Seto pottery making trial --> BBQ dinner)						
53	7/4/2015	Sat							
54	7/5/2015	Sun							
55	7/6/2015	Mon	Research at Lab			Research at Lab			
56	7/7/2015	Tue	Japanese Lang 9:40- (UCLA)			Handcraft Exercice (Group C)			

57	7/8/2015	Wed	Research at Lab		Research at Lab	Introduction to PE 4-2	Discussion with NU students
58	7/9/2015	Thu	Japanese Lang 9:40- (UCLA)		Research at Lab	30th JUACEP Seminar	
59	7/10/2015	Fri	Research at Lab				
60	7/11/2015	Sat					
61	7/12/2015	Sun					
62	7/13/2015	Mon	Research at Lab		Research at Lab		
63	7/14/2015	Tue	Japanese Lang 9:40- (UCLA)		Handcraft Excercise (Group D)		
64	7/15/2015	Wed	Research at Lab		31st JUACEP Seminar	Discussion with NU students	
65	7/16/2015	Thu	Japanese Lang 9:40- (UCLA)		Handcraft Excercise (Group E)		
66	7/17/2015	Fri	Research at Lab		Stipend payment@ES031	Research at Lab	
67	7/18/2015	Sat					
68	7/19/2015	Sun					
69	7/20/2015	Mon	Marine Day				
70	7/21/2015	Tue	Japanese Lang 9:40- (UCLA)				
71	7/22/2015	Wed			Research at Lab		
72	7/23/2015	Thu	Research at Lab				
73	7/24/2015	Fri					
74	7/25/2015	Sat					
75	7/26/2015	Sun					
76	7/27/2015	Mon			Research at Lab		
77	7/28/2015	Tue					
78	7/29/2015	Wed	Research at Lab				
79	7/30/2015	Thu					
80	7/31/2015	Fri					
81	8/1/2015	Sat					
82	8/2/2015	Sun					
83	8/3/2015	Mon			Research at Lab		
84	8/4/2015	Tue	Research at Lab				
85	8/5/2015	Wed					
86	8/6/2015	Thu	13th Workshop and Farewell Party @ VBL Hall for UM students				
87	8/7/2015	Fri	Departure of UM students				
88	8/8/2015	Sat					
89	8/9/2015	Sun					
90	8/10/2015	Mon			Research at Lab		
91	8/11/2015	Tue	Research at Lab				
92	8/12/2015	Wed			Stipend payment@ES031	Research at Lab	
93	8/13/2015	Thu					
94	8/14/2015	Fri	Bon Holidays				
95	8/15/2015	Sat					
96	8/16/2015	Sun					
97	8/17/2015	Mon					
98	8/18/2015	Tue			Research at Lab		
99	8/19/2015	Wed	Research at Lab				
100	8/20/2015	Thu					
101	8/21/2015	Fri					
102	8/22/2015	Sat					
103	8/23/2015	Sun					
104	8/24/2015	Mon			Research at Lab		
105	8/25/2015	Tue					
106	8/26/2015	Wed	Research at Lab				
107	8/27/2015	Thu					
108	8/28/2015	Fri					
109	8/29/2015	Sat					
110	8/30/2015	Sun					
111	8/31/2015	Mon			Research at Lab		
112	9/1/2015	Tue	Research at Lab				
113	9/2/2015	Wed	14th Workshop and Farewell Party @ VBL Hall for UCLA students				
114	9/3/2015	Thu			Research at Lab		
115	9/4/2015	Fri	Research at Lab				
116	9/5/2015	Sat	Departure of UCLA students				

	Japanese Language Class		Field Trip
	Introduction to Production Engineering (PE)		Workshop
	Handcraft Exercise		Holidays
	JUACEP Seminar		

<2>

Classes & Events

2-a. Japanese Class

Course name	Japanese Language		
Teaching staff	Ms. YASUI Sumie		
Teaching assistants	Tuesdays: Mr. YAMADA Kohei, Ms. HANADA Moemi Thursdays: Mr. IMAEDA Kodai, Mr. MATSUI Shintaro		
Course period	① May 14 - June 16, 2015 for University of Michigan students ② June 18- July 21, 2014 for UCLA students		
Weekly timetable	Tuesday & Thursday, 1st (45 min) & 2nd period (90 min) (9 : 40-12 : 00) * May 14(Thursday) & 19 (Tuesday) (13 : 30-15 : 50)		
Classroom	#3 Engineering Building, room 441 (4 th floor, B3-①)		
Textbook	<p>“GENKI An Integrated Course in Elementary Japanese” I (The Japan Times)</p> <p>This textbook is a comprehensive approach to developing the four basic language skills (listening, speaking, reading and writing) in order to cultivate overall Japanese-language ability.</p> <p>*Some teaching material will be given in class.</p>		
Course Contents	<p>Course outline</p> <p>The purpose of this course is to introduce the most essential Japanese words and expressions for everyday life. Students will learn writing system (Hiragana & Katakana), the basic grammar, expressions of Japanese.</p> <p>Classroom activities</p> <p>Basic communication skills required in everyday life will be taught by introducing new vocabulary, new grammar, and practicing listening, conversation and role-playings.</p> <p>Homework and Quiz</p> <p>You are expected to submit your homework by the deadline. Quizzes will be given every day in class.</p> <p>1. Hiragana 2. Katakana 3. Dictation 4. Conjugation</p>		
Evaluation	1. Homework	20%	S=100-90
	2. Quizzes	30%	A=89-80
	3. Oral exam.	50%	B=79-70
		100%	C=69-60
	More than 80% attendance is required.		F(fail)=59-0
	You will be officially awarded 1 credit of Nagoya University.		

Course
schedule

1. ① 5/14(Thu) ② 6/18(Thu)
Greeting Expressions, Hiragana 1
Introducing yourself , Noun sentences 1, Occupation, Nationality, Age,
Numbers 1-100
2. ① 5/19(Tue) ② 6/23(Tue)
Classroom expressions, Hiragana 2
Shopping, Noun sentences 2, Price, Numbers 101-1,000,000
3. ① 5/21(Thu) ② 6/25(Thu)
Hiragana 3
Describing where things are, Locations
Placing an order at a restaurant
4. ① 5/26(Tue) ② 6/30(Tue)
Hiragana 4
Talking about your daily life
Verbal sentences 1, Time reference, Adverbs
5. ① 5/28(Thu) ② 7/2(Thu)
Hiragana 5
Invitations, Suggestions, Desires
Verbal sentences 2, Days/Weeks/Months/Years, Counting
6. ① 6/2(Tue) ② 7/7(Tue)
Katakana 1
Talking about your family
Adjectives, Likes or Dislikes, Degree expressions, Family terms
7. ① 6/4(Thu) ② 7/9(Thu)
Katakana 2
Talking about your week-end, Past tense, Time words
8. ① 6/9(Tue) ② 7/14(Tue)
Katakana 3
Making a request (Verb-Te-form), Progressive actions,
Describing your status
9. ① 6/11(Thu) ② 7/16Thu)
Asking permission, Prohibition, Negative request
Describing two things
Talking about your interests
Plain form
10. ① 6/16(Tue) ② 7/21(Tue)
The Final Examination (speaking)

2-b. Handicraft Exercise

“Demonstration of the Internal Combustion Engine”

Date: Group A – June 30 (Tue)
 Group B - July 2 (Thu)
 Group C - July 7 (Tue)
 Group D - July 14 (Tue)
 Group E – July 16 (Thu)

Time: 13:00-16:00

Place: Creation Plaza (10th floor, IB Building)

Staff: Yasuhiko Sakai, Professor, Director of Creation Plaza
 Kazue Kaneko, Asst. Professor, Creation Plaza
 Koji Yamamoto, Technical staff
 Masafumi Nakakimura, Technical staff
 Shintaro Goto, Technical staff
 Kiyonori Saito, Technical staff



Schedule

--13:00~13:30--

- (1) Opening remarks: By Professor Yasuhiko Sakai
- (2) Self-introduction of Staffs
- (3) Self-introduction of Students: Department, Grade, Name, Motivation
- (4) Lecture of the basis of the Internal Combustion Engine by Teaching Assistants
 - ①History ②Characteristic ③Operation principle ④Practice engine



--13:30~14:30--

- (5) Assembling practice
 - ①Disassembling ②Assembling ③Adjustment

--14:30~15:30--

- (6) Performance test

--15:30~15:50--

- (7) Discussion
 - ①Comment ②Discussion ③Questionnaire



--15:50~16:00--

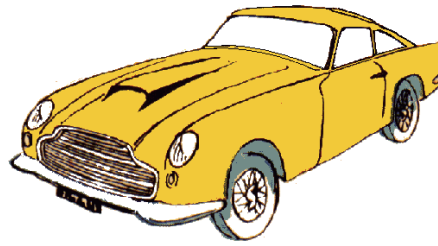
- (8) Closing with taking a memorial photograph

Groups

A	Emanuel Antony	Ulka Dandekar	Hongyang Li	Xu Li	
B	Yuting Gao	Chadwick Harvey	Yalim Yildirim	Yifan Jiang	Jimmy Ng
C	Xudong Hao	Andrea Manoppo	Chen Wang	Douglas Chen	Antonio Martinez
D	Fang Dai	Haodong Shen	Hanyi Xie	Lindsey Perry	Jacob Stremfel
E	Jiahong Ju	Goutham Thangaraj	Austin Kuo	Haroula Kyriacou	

2-c. Field Trip

Date: July 3 (Fri)



Visiting Places:

Toyota Motor Factory

http://www.toyota.co.jp/en/about_toyota/facility/toyota_kaikan/index.html

Seto Shinano Pottery Museum

<http://www.toujiki.or.jp/>

BBQ (dinner)



Schedule:

Time	Event
08:30	Departure from Nagoya University
09:30	Arrival at Toyota Motor Factory
09:30	Bus tour of the factory
11:40	Departure from Toyota Motor Factory
12:30	Arrival at Seto Shinano Pottery Museum
12:30	Lunch
14:00	Pottery making activity
16:00	Departure from Seto Shinano Pottery Museum
17:30	Arrival at Sakae
18:00	BBQ dinner



2-d. Research Reports

- Participants from University of Michigan -
Internship duration: May 14 – August 6, 2015

Student(s)	Research topic
Supervisor at Nagoya Univ.	
Emanuel A. Chirayath and Chadwick Harvey Prof. Jiro Kasahara Aerospace Engineering	Design and Development of a Rotating Detonation Gas-turbine Engine (p.18)
Fang Dai Prof. Tatsuya Suzuki Mechanical Science and Engineering	Implementation and Parameters Identification of Wiedemann Vehicle Following Model (p.19)
Ulka Dandekar Prof. Hiroyuki Asanuma Molecular Design and Engineering	Suppression of Off-target Effect by Insertion of Artificial Base-surrogate into Sense Strand of siRNA (p.20)
Yuting Gao Prof. Ichiro Naruse Mechanical Science and Engineering	Analytical Study on Combustion Kinetics of Various Solid Fuels/Waste Products (p.21)
Xudong Hao Prof. Yoji Yamada Mechanical Science and Engineering	Evaluation of Contact States Using a Wound Testing System with Slip and Force Sensors for Estimating Skin Scratch Risks (p.28)
Jiahong Ju Prof. Toshiro Matsumura Electrical Engineering and Computer Science	Investigation of Performance of the Modified MCCB with a New-developed Fault Current Limiter in Low Voltage DC Distribution System (p.29)
Andrea Manoppo Prof. Fumihito Arai Micro-Nano Systems Engineering	The Fabrication of Tissue Engineered Small Blood Vessels via 3-dimensional Cellular Self-assembly and Organization in Vitro (p.36)
Haodong Shen Prof. Norihiko Nishizawa Quantum Engineering	All-polarization-maintaining Er-doped Ultrashort-pulse Fiber Laser Using Carbon Nanotube Saturable Absorber (p.43)
Goutham Thangaraj Prof. Kazuo Shiokawa Solar-Terrestrial Environment Laboratory	Extraction and Analysis of Trigger Rate and Pedestal Data from SciCRT (p.48)
Chen Wang Prof. Toshiro Matsumoto Mechanical Science and Engineering	A Study on Topology Optimization with Fem Based on Level Set Method (p.57)
Hanyi Xie Prof. Noritsugu Umehara Mechanical Science and Engineering	Effect of Surface Treatment on Mechanical Properties of DLC Coating (p.61)
Yalim Yildirim Prof. Yasuhisa Hasegawa Micro-Nano Systems Engineering	Quasi-Passive Elastic Exoskeleton Control Based on Mechanical Joint Kinematics (p.66)

- Participants from UCLA -
Internship duration: June 17 – September 4, 2015

Student(s)	Research topic
Supervisor at Nagoya Univ.	
Douglas Chen	Direct Production of Highly Pressurized Pure Hydrogen (p.67)
Assoc. Prof. Seiichi Deguchi Energy Engineering and Science	
Yifan Jiang	An Investigation of the Top-down Approach for Gallium Nitride Nanowires Using Metal Mask and Simple Device Fabrication Using Gallium Nitride Nanowires Grown in HVPE (p.70)
Prof. Hiroshi Amano Electrical Engineering and Computer Science	
Austin Kuo	Investigation of the Control of Table Tennis Robots (p.78)
Prof. Yoshikazu Hayakawa Mechanical Science and Engineering	
Haroula Kyriacou and Lindsey Perry	Catalytic Cracking of Polyolefins for Fuel Consumption (p.87)
Prof. Masahiro Hirasawa Molecular Design and Engineering	
Hongyang Li	Deep Discharge and Elevated Temperature Performance of Solid-state Thin Film LiCoMnO ₄ Batteries (p.95)
Prof. Yasutoshi Iriyama Materials Science and Engineering	
Xu Li	Design and Optimization of Microfluidic Chip (p.96)
Prof. Fumihito Arai Micro-Nano Systems Engineering	
Antonio Martinez	Design and Implementation of Algorithm for Estimation of Elevator Travel Distance Using Smartphone Accelerometer (p.102)
Prof. Nobuo Kawaguchi Computational Science and Engineering	
Jimmy Ng	Electron Field Emission of Graphene and Zirconium Coated Graphene (p.103)
Prof. Yahachi Saito Quantum Engineering	
Jacob Stremfel	Fatigue Crack Healing via High-density Electropulsing (p.113)
Prof. Yang Ju Mechanical Science and Engineering	

DESIGN AND DEVELOPMENT OF A ROTATING DETONATION GAS-TURBINE ENGINE

Chadwick Harvey & Emanuel Antony Chirayath

Department of Aerospace Engineering, University of Michigan – Ann Arbor
chadharv@umich.edu | emanuelc@umich.edu

Supervisor: Prof. Jiro Kasahara

Graduate School of Engineering, Nagoya University
kasahara@nuae.nagoya-u.ac.jp

ABSTRACT

The thermodynamic benefits of pressure gain combustion have been sought through the addition of jet turbomachinery to a Rotational Detonation Engine (RDE). Here, the use of pre-compression and temperature rise have been added to a more traditional RDE core to decrease detonation cell size and maintain scalability of the engine. Novel techniques of water-injection and exhaust purge have been designed and incorporated in the engine to extend its operating time and lifespan. The current research focus is to first prove the concept by experiment before seeking to optimize its operation. The engine has been designed to take two configurations: one RDE-only mode to analyze the detonation properties, as well as the full gas-turbine mode including all turbomachinery. Engine experimentation is currently underway and is expected to continue over the coming months.

Undisclosed

IMPLEMENTATION AND PARAMETERS IDENTIFICATION OF WIEDEMANN VEHICLE FOLLOWING MODEL

Fang Dai

Department of Mechanical Engineering, College of Engineering, University of Michigan
davephon@umich.edu

Supervisor: Professor Tatsuya Suzuki

Graduate School of Engineering, Department of Mechanical Science and Engineering, Nagoya University
t_suzuki@nuem.nagoya-u.ac.jp

ABSTRACT

The primary idea of this research project is to use Wiedmann Vehicle Following Model to reproduce the driver's behaviour and then estimate the fuel consumption for individual person. In this research, the Wiedemann Model, as a microscopic traffic flow model, is constructed to simulate single vehicle-driver unit using relative distance and velocity difference between a leading vehicle and itself. Then both boundary and output parameters taken from source paper are identified and optimized in terms of actual field test results. By comparing the error of original and optimized parameters, the identification process is verified. Finally by implementing optimal velocity profile of the following car, fuel consumption estimation based on individual driver is generated. This value greatly represents the actual fuel consumption and it could be used for various purposes, such as evaluating the energy consumption of a customer for different vehicle models, or to encourage low energy consumption for eco-driving.

Undisclosed

SUPPRESSION OF OFF-TARGET EFFECT BY INSERTION OF ARTIFICIAL BASE- SURROGATE INTO SENSE STRAND OF siRNA

Ulka Dandekar

Department of Integrative Systems and Design, Graduate School of Engineering, University of Michigan
ubdandek@umich.edu

Professor: Hiroyuki Asanuma
Tutor: Hiroshi Kamimoto

Department of Molecular Design and Engineering, Graduate School of Engineering, Nagoya University
asanuma@nubio.nagoya-u.ac.jp

ABSTRACT

RNA interference (RNAi), specifically employing double-stranded RNA, called small-interfering RNA (siRNA), has become a common topic for biological research as it possesses potential for therapeutic applications. siRNA is capable of inducing a sequence-specific gene silencing system. Once introduced into cells, siRNA forms into the RNA-induced silencing complex (RISC) to suppress the target gene translation. However, the function of siRNA is deterred by vulnerability to nuclease-mediated degradation and off-target effects. For this study, the sense strand of siRNA was modified through the substitution of a nucleotide for, or addition of, cholesterol and D-threoninol, with the objective of inhibiting sense-strand incorporation in the formation of RISC, and thus boosting resistance to off-target effects. Results showed that addition of these artificial nucleotides into the sense strand had a greater impact of improving antisense strand selectivity than substitution into the sense strand of siRNA.

Key Words: siRNA, cholesterol, D-threoninol, luciferase, antisense strand selectivity

Undisclosed

Analytical Study on Combustion Kinetics of Various Solid Fuels/Waste Products

Yuting Gao

Chemical Engineering, University of Michigan
gyting@umich.edu

Supervisor: Ichiro Naruse

Department of Mechanical Science & Engineering, Nagoya University
Naruse@mech.nagoya-u.ac.jp

1. ABSTRACT

Nowadays, solid fuels are the main sources of energy. Meanwhile, waste disposal becomes a worldwide problem and incineration is one of the most important methods of waste treatment. The objective of this project is to study the combustion kinetics of various solid fuels and waste products and compare their reaction behavior. This report consists of the experimental data analysis and comparison of various solid fuel and waste product samples, including graphs of conversion and reaction rate, and modeling of the experimental results. Best model and the corresponding parameters, the pre-exponential factor and activation energy, for each sample was determined.

2. EQUIPMENT & METHOD

This part includes experimental equipment, theory, and setup.

2.1 Experimental Equipment

Thermo-gravimetric analyzer (TG8120, Rigaku) was used in this experiment. There are two thermocouples connecting to two Pt pans. Al_2O_3 is put in one of the pans while the sample is put in the other one. Air, or other gas used in combustion, is blown into the analyzer through a valve on one end, and is exhausted through the other end. Computer

software is used to set up the temperature profile for the heating process. The sketch diagram of this machine is shown below.

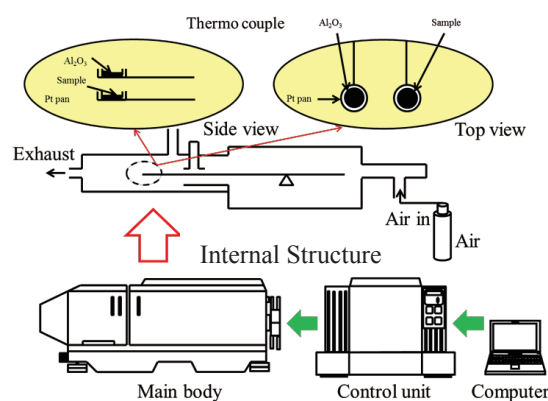


Fig. 2.1 Sketch Diagram of Thermo-gravimetric Analyzer (TG8120, Rigaku)

2.2 Experimental Theory

A thermos-gravimetric analyzer can be used as a measurement of some physical or chemical properties as a function of increasing temperature or time. In this experiment, thermo-gravimetric analyzer was used to provide analysis data of the sample mass loss as a function of time for a given temperature profile. Then differentiation method was used to analyze the experimental data to obtain the reaction rate. Finally, different reaction models were applied to the conversion and reaction rate data to calculate the parameters, such as pre-exponential factor,

activation energy, and etc., to describe the combustion behavior of different samples.

2.3 Experimental Setup

Air was used as the gas supply for all the experimental trials. Temperature profile was shown in the following table.

Room temperature → 107 °C @ 10 °C / min
107 °C for 10 min
107 °C → 900 °C @ 10 °C / min
900 °C for 10 min

Table 2.1 Temperature Profile for Combustion

3. SAMPLE PROPERTIES

In this project, five samples were used for the experiment, including Coal U, WA-8, Coal K, Coal I, and P.E. Among these five samples, the first four were used in modeling.

The table for sample properties, including composition, mass used in experiment, photo, proximate analysis, and ultimate analysis, could be found in Appendix A.

For Coal U and WA-8, 5.00 ± 0.05 mg were used in the experiment, while for Coal K and Coal I, 2.00 ± 0.05 mg was used. It was because that Coal K and Coal I were more reactive than Coal U and WA-8. If 5 mg was used, it would generate too much heat and thus be ignited. This would cause a sudden increase in temperature, resulting in a hump in the temperature profile diagram, and thus infect the modeling results. By decreasing the sample mass, the heat generated during combustion could be reduced and the temperature profile would not be disrupted.

P.E. was provided in pellets of around 17 mg. In the experiment, 17 mg, 5 mg, and 2 mg were used in three different trials. However, none of the results were good enough for modeling. P.E. would melt during the heating process, which would disrupt the

temperature profile. Thus the experimental data for P.E. was not used for modeling. The following were the temperature profile graphs of P.E.

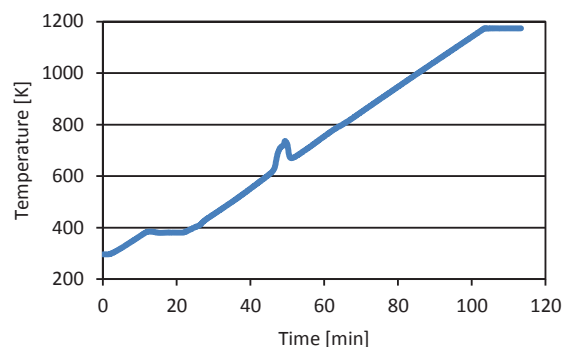


Fig. 3.1 Temperature Profile, P.E. 17 mg

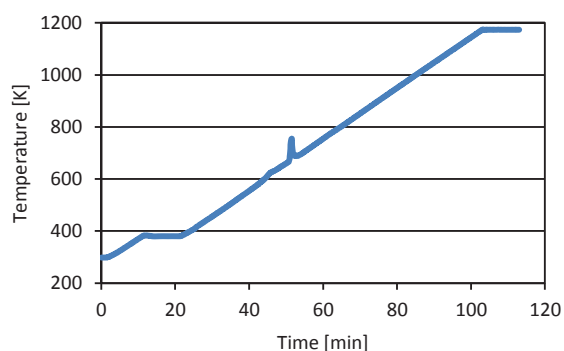


Fig. 3.2 Temperature Profile, P.E. 5 mg

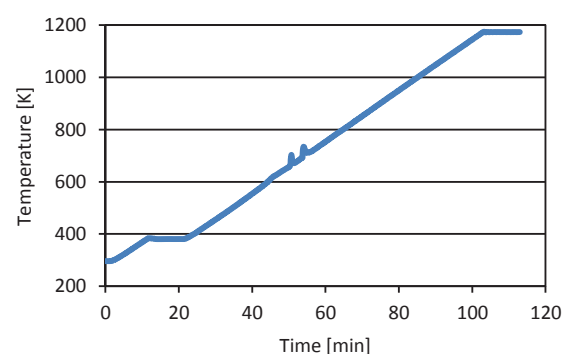


Fig. 3.3 Temperature Profile, P.E. 2 mg

As can be seen in the graphs, no matter 17 mg, 5 mg, or 2 mg were used, the hump in the temperature profile could not be removed. Thus experimental data for P.E. was not used for modeling.

4. DATA ANALYSIS

This part consists of the plots of conversion and reaction rate, detailed proximate analysis, and the comparison of Coal K and Coal I.

4.1 Plot of Conversion and Reaction Rate

The thermo-gravimetric analyzer provided data and graph of temperature, TG (mg), DTG (mg/s), and DTA (μV) as a function of time. Temperature was in Celsius. TG was the mass loss measured by the analyzer, which started from 0 and decreased with time. DTG was the differential of TG, showing the mass decreasing rate. DTA was the heat flow, but was not used in this experiment.

For each experimental trial, conversion of combustible component, X , was defined as (mass loss of combustible components) / (total mass of combustible components), which was based on the basic proximate analysis. The following graph showed a sample of basic proximate analysis.

V.M. stands for volatile matter and F.C. stands for fixed carbon.

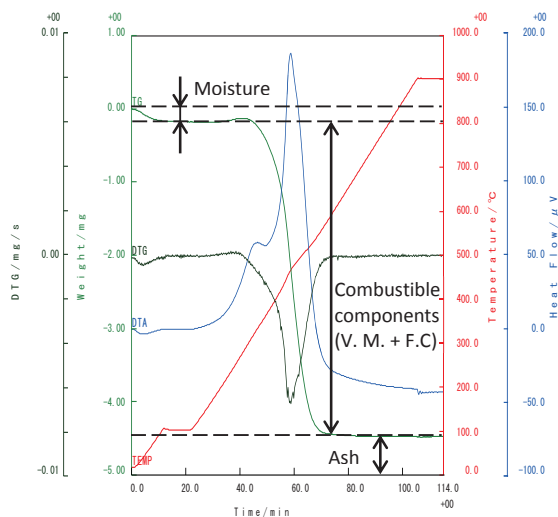


Fig. 4.1 Sample of Basic Proximate Analysis
(Coal U, Trial 2)

Conversion could be calculated based on the basic proximate analysis. After calculating X at each point, a graph of $1 - X$ as a function of time was plot.

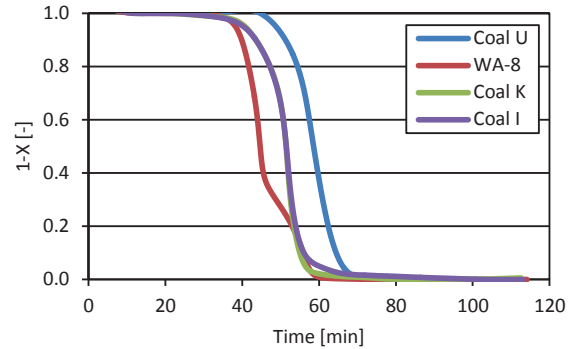


Fig. 4.2 Conversion of Combustible Components

The above graph showed the conversion of all samples as a function of time. WA-8 was the first one to start the combustion, while Coal U was the last one to start. The plots for Coal K and Coal I were in the middle. They were really close on this graph, but could be distinguished on the following graph of reaction rate.

The rate of combustion was calculated by doing differentiation on conversion X over time. Since information from the thermo-gravimetric analyzer was not continuous, data points of $(X_2 - X_1)/(t_2 - t_1)$ was calculated to simulate dX/dt curve. However, due to systematic error of the experimental equipment, the rate graph was not a smooth line. Thus the average of 20 data points of X value was used to cancel the noise. The following graph showed the plots of reaction rate of different samples after noise cancellation.

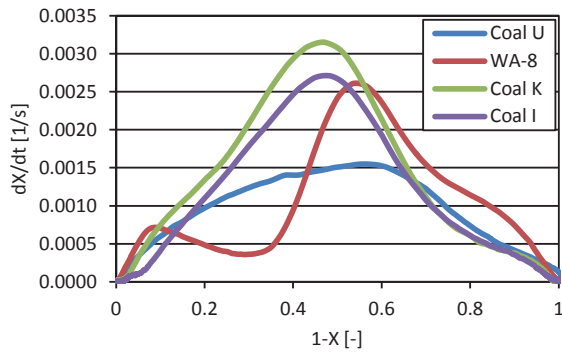


Fig. 4.3 Reaction rate

Coal K had the largest reaction rate; Coal U had the smallest reaction rate; while Coal I was in the middle. There were two humps on the curve of WA-8. This was because that the V.M. and F.C. were reacted nearly one by one. The large hump near $1 - X = 1.0$ represented V.M. and the small one stood for F.C.

There were nine trials of experiment in total. Each trial had a graph of general information from the thermos-gravimetric analyzer, including temperature, TG, DTG, and DTA, a plot of conversion of combustible components, and a plot of reaction rate after noise cancellation. All the individual figures could be found in Appendix B.

4.2 Detailed Proximate Analysis

For each experimental trial, the weight of pan, net weight of sample before combustion, and weight of pan with residue after combustion were measured; mass and mass fraction of moisture, ash, and combustible components were calculated and compared with the information of sample properties. A sample calculation (Coal U, Trial 2) was shown below.

Pan weight: 121.73 mg
 Net weight of Coal U: 5.05 mg
 Pan & residue Weight: 122.33 mg
 Moisture mass: 0.19 mg
 Moisture fraction:
 $0.19/5.05 = 3.76\%$

Dry mass:

$$5.05 - 0.19 = 4.86 \text{ mg}$$

Mass of ash:

$$122.33 - 121.73 = 0.60 \text{ mg}$$

Mass fraction of ash (dry-based):

$$0.60/4.86 = 12.35\%$$

Mass of combustible components (V.M.+F.C.):

$$4.86 - 0.60 = 4.26 \text{ mg}$$

Mass fraction of combustible components (dry-based):

$$4.26/4.86 = 87.65\%$$

The following tables showed a data summary and comparison

Coal U	Moisture %	Ash % dry-based	Combustible components (V.M.+F.C.) % dry-based
Trial 1	2.78	11.84	88.16
Trial 2	3.76	12.35	87.65
Average	3.27	12.10	87.91
Sample property	0.5	11.91	88.09

Table 4.1 Proximate Analysis of Coal U

WA-8	Moisture %	Ash % dry-based	Combustible components (V.M.+F.C.) % dry-based
Trial 1	5.58	1.69	98.31
Trial 2	6.37	2.13	97.87
Average	5.98	1.91	98.09
Sample property	5.77	2.21	97.79

Table 4.2 Proximate Analysis of WA-8

Coal K	Moisture %	Ash % dry-based	Combustible components (V.M.+F.C.) % dry-based
Trial 1	4.48	11.46	88.54
Trial 2	5.00	13.68	85.79
Average	4.74	12.57	87.17
Sample property	4.60	14.50	85.50

Table 4.3 Proximate Analysis of Coal K

Coal I	Moisture %	Ash % dry-based	Combustible components (V.M.+F.C.) % dry-based
Trial 1	7.88	5.35	94.65
Trial 2	7.96	4.32	95.68
Trial 3	9.74	4.55	95.45
Average	8.53	4.74	95.26
Sample property	3.3	8.9	91.1

Table 4.4 Proximate Analysis of Coal I

Usually moisture fraction from experimental results was higher than given value. This was because that sample would absorb moisture in the air. Coal U was an old sample thus it had absorbed a lot of moisture. For Coal U, Coal K, and WA-8, the dry-based ash and combustible components fraction values were similar to the given values.

For Coal I, however, none of the experimental calculation results could confirm with the given properties. Maybe it was the wrong sample or the given sample properties were wrong. Further experiments would be needed to study this sample.

4.3 Comparison of Coal K and Coal I

Proximate properties, maximum reaction rate, maximum DTA value, combustion period, and starting temperature of combustion were considered in the comparison. The following figure showed a sample of determining the combustion time and the starting temperature of the combustion.

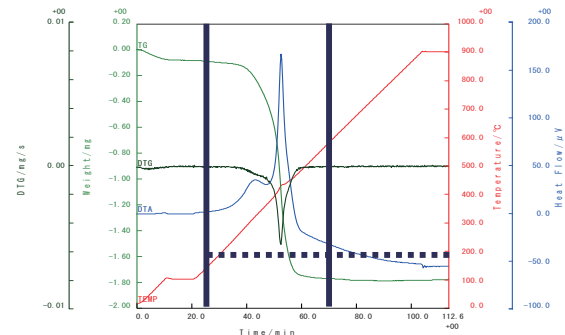


Fig. 4.4 Sample of Combustion Period and Starting Temperature determination (Coal K, Trial 1)

As can be seen in the graph, the first vertical solid line indicated the starting of combustion, while the second vertical line indicated the end of combustion. The intersection points on the time axis showed that the combustion period was about $70 - 25 = 45 \text{ min}$. The horizontal dashed line showed the starting temperature of combustion was about $150 \text{ }^\circ\text{C}$. Analysis graphs of other trials were in Appendix C.

The following table showed a summary of the comparison results. All properties were evaluated based on the average of all the trials from a sample. For the maximum reaction rate, maximum DTA, and starting temperature, the values were read from the graphs, thus had limited accuracy. However it was enough to show the difference between these two samples.

Exp. results (Avg.)	Coal K	Coal I
Combustible components (Dry-based)	87.17%	95.26%
Ash (Dry-based)	12.57%	4.74%
Moisture	4.74%	8.53%
Max. reaction rate	0.0030 [1/s]	0.0025 [1/s]
Max. DTA	170 μV	120 μV
Combustion period	50 min	57 min
Starting temperature	150 $^\circ\text{C}$	200 $^\circ\text{C}$

Table 4.5 Comparison of Coal K & Coal I

From the comparison results, it could be concluded that Coal K was more reactive while Coal I was relatively stable. For a stable sample, the maximum reaction rate and DTA would be small, but it would need a higher temperature to start the combustion and a longer period to finish the reaction. In contrast, a reactive sample performed in an opposite way.

5. MODELING & DISCUSSION

This part includes theoretical analysis and modeling results.

5.1 Theoretical Analysis

For simple model, the reaction rate can be described by equation

$$\frac{dX}{dt} = kf(x) \quad (1)$$

where

k – Overall reaction rate coefficient

X – Mass fraction of reacted combustible

components

t – Time

$$k = A \exp\left(-\frac{E}{RT}\right) \quad (2)$$

where

A – Pre-exponential factor

E – Activation energy

R – Gas constant

T – Temperature in Kelvin

For n-th order model,

$$f(x) = (1 - X)^n \quad (3)$$

For volumetric reaction model, $n = 1$,

$$f(x) = (1 - X)^1 = 1 - X \quad (4)$$

For shrinking core model, $n = 2/3$,

$$f(x) = (1 - X)^{2/3} \quad (5)$$

For a complex reaction, the rate can be described by parallel model

$$\frac{dX}{dt} = \sum R_i A_i \exp\left(-\frac{E_i}{RT}\right) \times f_i(X_i) \quad (6)$$

where

$$\sum R_i = 1 \quad (7)$$

$$\sum R_i X_i = X \quad (8)$$

5.2 Modeling Results

Due to time limit problem, only the first trial of each sample was used in modeling. For each trial, four different models were applied: one-step model with $n=1$ (volumetric reaction model), one-step model with $n=2/3$ (shrinking core model), two-step model with $n=1$ for both steps, and two-step model with $n=1$ & $n=2/3$.

The graphic results of one-step model with $n=1$ for WA-8 were shown below.

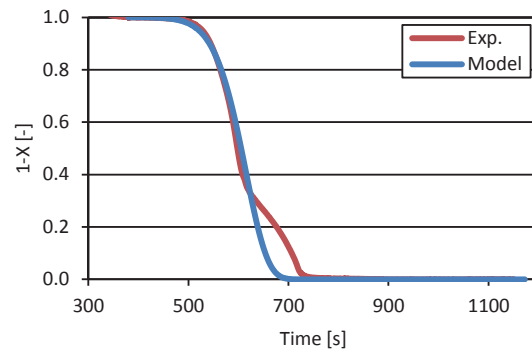


Fig. 5.1 One-Step Modeling Results for WA-8, $n=1$, Conversion

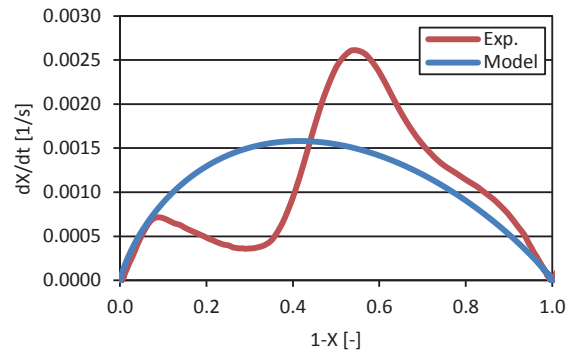


Fig. 5.2 One-Step Modeling Results for WA-8, $n=1$, Reaction Rate

The red line indicated experimental data while the blue line was plot by the model equation. Parameters and R-square values were shown in the following table.

A	E	n
5000	72	1.0
R_c^2	R_r^2	$R^2 = R_c^2 + R_r^2$
0.0221	0.2071	0.22923

Table 5.1 One-Step Modeling Parameters for WA-8, n=1

R_c^2 showed the goodness of the 1-X graph and R_r^2 showed that of the reaction rate graph. The total R^2 was the sum, showing the total goodness of the model. In this case, $R^2 = 0.22923$, indicating that the fitness was not good enough. Thus two-step model was needed to give out better results.

For two-step modeling, the first model was close to $X = 0$ or $1 - X = 1$, while the second part was close to $X = 1$ or $1 - X = 0$. The following graphs and table showed one of the Two-step modeling results for WA-8.

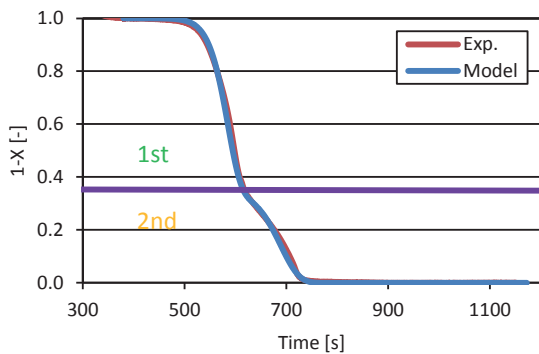


Fig. 5.3 Two-Step Modeling Results for WA-8, n=1 & n=1, Conversion

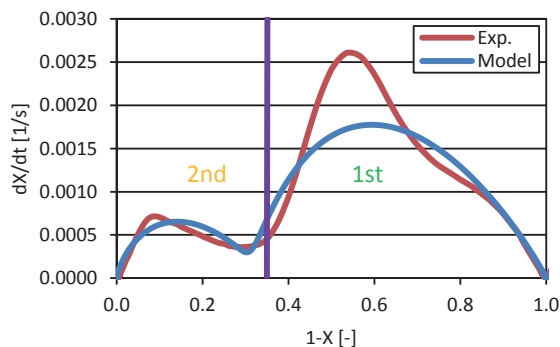


Fig. 5.4 Two-Step Modeling Results for WA-8, n=1 & n=1, Reaction Rate

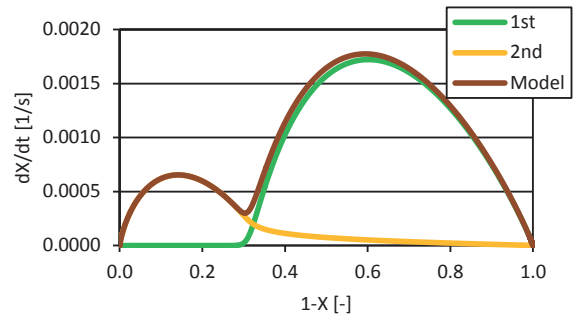


Fig. 5.5 Two-Step Modeling Results for WA-8, n=1 & n=1, Combination of Reaction Rates

A1	E1	n1	R1
1×10^8	114	1.0	0.65
A2	E2	n2	R2
1×10^6	110	1.0	0.35
R_c^2	R_r^2	$R^2 = R_c^2 + R_r^2$	
0.0087	0.0778	0.08656	

Table 5.2 Two-Step Modeling Parameters for WA-8, n=1 & n=1

Results of both parameters and curve fitting graphs of other trials could be found in Appendix D.

For both one-step and two-step modeling, Coal U gave out the best results. In general, two-step model results were much better than one-step results for all the samples.

6. CONCLUSION

In this project, I have studied the combustion behavior of Coal U, WA-8, Coal K, and Coal I. Comparison showed that Coal K was more reactive than Coal I. Different models were applied to the experimental data and the combustion parameters for the best models were calculated.

The best modeling results are: two-step model with n=1 & n=1 for Coal U; two-step model with n1=1 & n2=2/3 for WA-8; two-step model with n1=1 & n2=2/3 for Coal K; two-step model with n=1 & n=1 for Coal I.

EVALUATION OF CONTACT STATES USING A WOUND TESTING SYSTEM WITH SLIP AND FORCE SENSORS FOR ESTIMATING SKIN SCRATCH RISKS

Xudong Hao

Department of Mechanical Engineering, Graduate School of Engineering, University of Michigan
xdhao@umich.edu

Supervisor: Yoji Yamada

Graduate School of Engineering, Nagoya University
Yamada-yoji@mech.nagoya-u.ac.jp

ABSTRACT

Using wearable robots can bring a lot of benefits and convenience for us, but also can cause some injuries, such as scratches, to human skin. The skin friction and deformation behaviour both in-plane and perpendicular to the sliding direction have been measured simultaneously during sliding of a cuff against dummy skin. Two theoretical models, namely probe & skin model and rigid flat punch model, are used to analyse the experiment results. We mainly focus on the edge of cuff, where has the stress concentration. This may increase the risks of skin injuries. These analyses are intended to understand how scratches are caused and how to avoid them when wearing wearable robots.

Undisclosed

Investigation of Performance of the Modified MCCB with A New-Developed Fault Current Limiter in Low Voltage DC Distribution System

Jiahong Ju

Department of Electrical Engineering, University of Michigan
jiahong@umich.edu

Prof. Toshiro Matsumura

matumura@nuee.nagoya-u.ac.jp
Graduate School of Engineering, Nagoya University

Associate Prof. Yasunobu Yokomizu

yokomizu@nuee.nagoya-u.ac.jp
Graduate School of Engineering, Nagoya University

ABSTRACT

With increasingly more distributed generation and renewable energy added to the existing power system, the electricity demand boosts and also increases the fault current level, especially in the low voltage direct current (DC) distribution system. Hence fault current limiters (FCLs) are used to assist the circuit breaker to suppress the fault current before circuit breaker interrupts it. However, most DC FCLs used nowadays are expensive because of the materials used. Thus a new configuration of the FCL circuit consisting of only passive components is developed and the effect of fault current suppression and interruption is evaluated when the FCL is added to assist the Molded Case Circuit Breaker (MCCB). It has been proven that this new FCL has good DC current suppression performance. By appropriately choosing the inductance value in the FCL, the FCL also improves the performance of the fault current interruption for the MCCB.

I. INTRODUCTION

As the energy and environmental considerations encourages the wide spread use of the renewable energy, more distributed generations (DG) such as solar energy are added to the existing power system to meet the increased electricity demand. Thus, increasingly more low voltage DC distribution systems act as an intermediate media before the power from DG is injected to the AC grid. Normally, DC circuit breakers are employed to interrupt the fault current caused by ground fault or short circuit. However, with a higher level of DC fault current in distribution systems, the FCL is introduced to suppress the current and to assist the circuit breaker for a quicker and safer fault current interruption.

However, unlike the AC current which can be easily interrupted when it goes across 0A in each cycle, the DC current interruption is more difficult as the DC circuit breakers have to reduce the current to 0A themselves[1].

Thus, FCLs are introduced to assist the DC circuit breaker to suppress the fault current to a lower value where it can be easily interrupted by circuit breakers.

To ensure a good performance, FCL must have the low impedance under normal current for lower power losses and high impedance under fault current to suppress fault current. Thus, most of the FCLs nowadays are made by superconductors and other peripheral devices for the arc control. [2] However, all these are expensive and need to be implemented properly to work well.

The newly developed L-R type FCL consists of only passive elements with a resistor and an inductor connected in parallel and its current suppression performance has been already proven theoretically by simulation with a simply molded switch as the circuit breaker in previous research. [3] However, the circuit breaker cannot be simply molded as a switch in reality and it is much more complicated when it work together with the FCL in real circuit. So in the present research, experiments were conducted to investigate the effect of the current suppression of the new FCL and also to evaluate the performance of current interruption when after the FCL is added to assist MCCB.

This report is divided into two sections. The first part describes the reason and process of the MCCB's modification and how the fault circuit interrupt circuit in experiments is designed and built based on the modified MCCB. In the second part, experiments on the MCCB are conducted with and without FCL. By varying the resistor and inductance values in the FCL, the waveforms of the fault current and voltage across MCCB are compared and analyzed to investigate the performance of current suppression of the FCL and its effect on current interruption with the MCCB. In the end, conclusion are summarized and advices on the further improvements for this research are given.

II. Mechanism of the MCCB

Table 1 Specification of the MCCB

Rated DC Voltage (V)	Highest Interrupting DC Current (A)	Rated DC current (A)	Internal Impedance (Ω)	Voltage Drop (V)
48	750	0.3	15	4.5

The specification of Panasonic DC circuit breaker used in this research is shown in the table above.

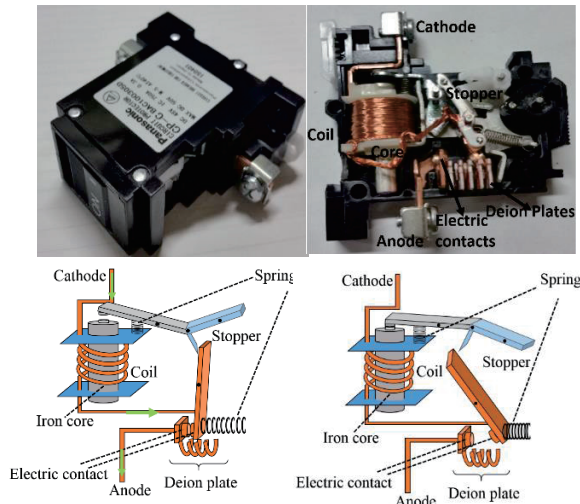


Figure 1 Inner structure of MCCB and its operation mechanism

The mechanism of MCCB shown in Figure1 can be summarized as follows:

- Under normal condition, current goes through the coil from the cathode to anode with two electric contacts connected.
- When fault current appears, the core wrapped in the coil will be magnetized and induced electromagnetic force will pull down the spring and the stopper separates two contacts.

Once two electric contacts are separated, an electric arc will be bridged between two contacts to provide a conductive path in the air for electricity to go and the current through them cannot be interrupted directly, which is shown in Figure2.

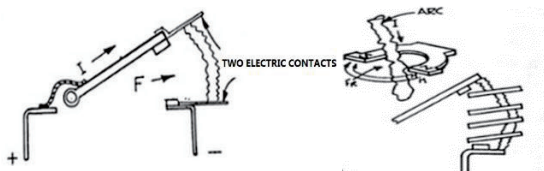


Figure 2 Initiation of the arc and the Deion plates during arc extinguishing. [4]

The fault current is not interrupted completely until the arc is removed. To ensure a quick and safe current

interruption, Deion plates are inserted between two contacts to deionize the air and to break down the arc into several shorter and weaker arcs, which makes the arc easily interrupted. Once two contacts are separated far enough, the electric arc is completely deionized and the fault current is interrupted. This process is called the arc extinguishing or arc quenching.

III. Modification of the MCCB

There are two reasons of the modification of the MCCB.

1. It is noticed in Section2 that the coil is always connected in the circuit under the normal condition with an internal impedance as 15Ω . Thus the circuit will produce unexpected extra power losses in the resistor. The large internal resistance also makes it difficult to get the high fault current from 50A to 150A.
2. The MCCB will trip automatically and cannot be controlled if it is directly connected into the circuit, which is not convenient to observe the FCL's effect for MCCB. MCCB's interruption behaviors can be controlled appropriately by relays after modification.

For these two reasons, the MCCB is modified into two parts manually as follows:

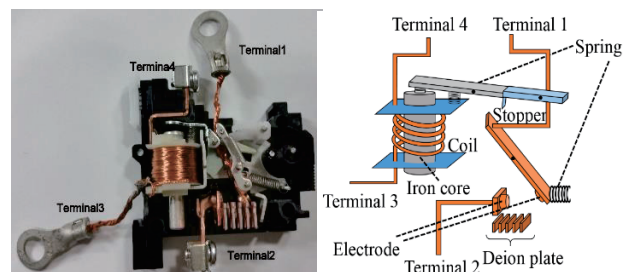


Figure 3 Internal structure of the modified MCCB

In addition to the cathode (Terminal4) and anode (Terminal2), two more terminals: Terminal1 and Terminal3 are added. Instead of flowing through the coil between Cathode (Terminal4) and Anode (Terminal2), the current now flows from Terminal1 to Terminal2 with no power losses.

IV Fault Current Interruption Circuit

To generate and interrupt the fault current in this experiment, the fault current interruption circuit is built based on the modified MCCB with two circuits: Main Circuit and Switching Circuit. They are shown as follows:

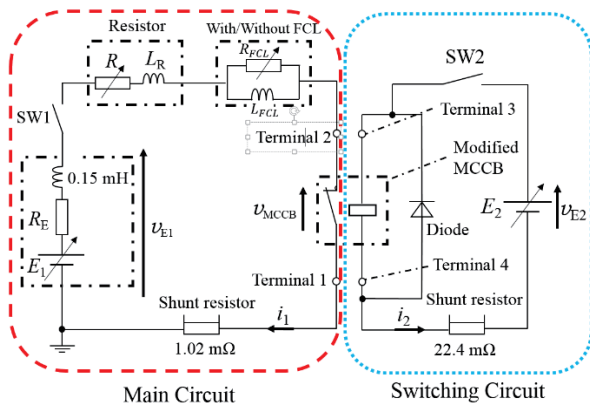


Figure 4 Fault Current Interruption Circuit for Experiment

Main Circuit

The main circuit consists a switch SW₁, a variable voltage source V_{E1} with an internal resistor R_E (0.06Ω) and an internal inductor (0.15mH), a variable resistor R, an L-R type FCL and a shunt resistor (1.02mΩ). Terminal1 and Terminal2 are connected in the main circuit with no internal resistance between them.

The main circuit is the circuit where the fault current is generated and interrupted. SW₁ is controlled by the relay. Variable resistor is changed to get various fault current. The FCL can suppress the fault current and the current is measured in the shunt resistor.

Switching Circuit

The switching circuit on the right has a voltage source V_{E2}, a switch SW₂, a shunt resistor (22.4mΩ) and a diode. The coil of the MCCB is connected between Terminal3 and Terminal4 which provides current for the coil to pull down the spring to trigger the current interruption. In other word, the switching circuit gives the interruption command to the main circuit to interrupt the fault current, which make the switching circuit acts as the gate in IGBT. Similarly, SW₂ is configured by relay to control when the circuit is closed to give the interruption command. The diode is used to pass the current across the coil when SW₂ is opened to end each experiment.

Choice of V_{E2} in the Switching Circuit

As it takes time for the core to be magnetized by the current, so there are time delay from the moment SW₂ is closed to the moment the spring is pull down and two electric contacts start to be separated. This time interval is defined as switching time and it is determined by how large the current going through, it is necessary to know that how the time delay varies with the current i₂ (or V_{E2})

and an appropriate value for V_{E2} need to be chosen for a constant switching time.

By applying different voltage values for V_{E2}, the characteristic between the switching time and V_{E2} is shown in the figure below.

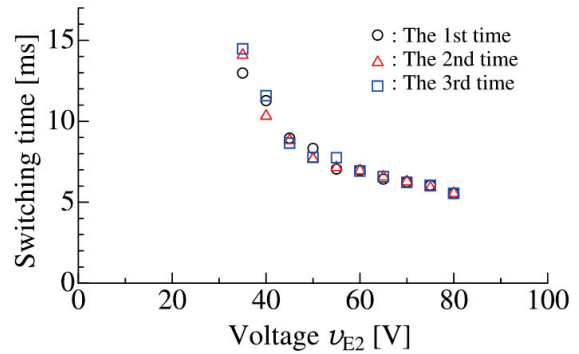


Figure 5 characteristic between the switching time and VE2

Each voltage is tested for three times. The figure shows that the switching time decreases as VE2 goes up. The larger the VE2 is, the more stable of the switching time. It also suggests that 48V is the most appropriate value for V_{E2} which has a stable switching time at 9ms. Besides, it is also same as the rated voltage of MCCB shown in Table1.

Mechanism of the Fault Current Interruption Circuit

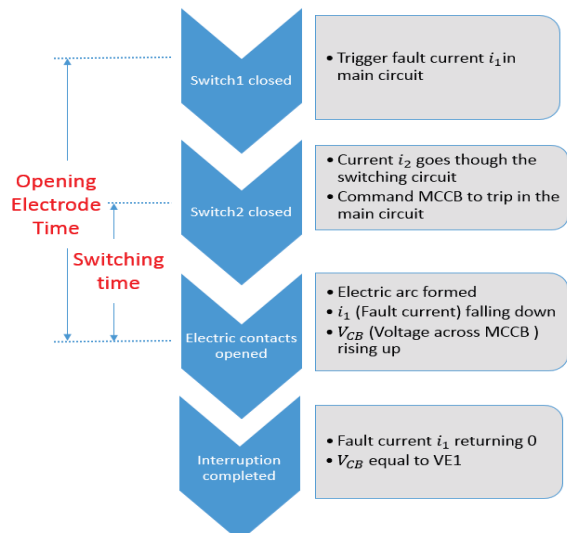


Figure 6 Flow chart of fault current generation and interruption

The flow chart above describes the process of the fault current generation and interruption. To make it clearer, the process is also illustrated in the waveforms in Fig. 4.

In Fig.6 and Fig.7, it shows that fault current in the main circuit emerges once SW₁ is closed. Then the fault current instantaneously increases to a high value. Then

the SW₂ in the switching circuit is closed at desired time to command the main circuit to trip. After the switching time, two electric contacts start to be separated and the arc is formed. Then the fault current will fall down and the voltage across the circuit breaker V_{CB} (arc voltage) will rise up. Once the arc is extinguished, the fault current will be completely interrupted to be 0. And V_{CB} will rise up to be equal to the source voltage V_{E1} and remain this value in the open circuit.

Opening electrodes time is defined as the time duration from SW₁ is closed to two electric contacts separates.

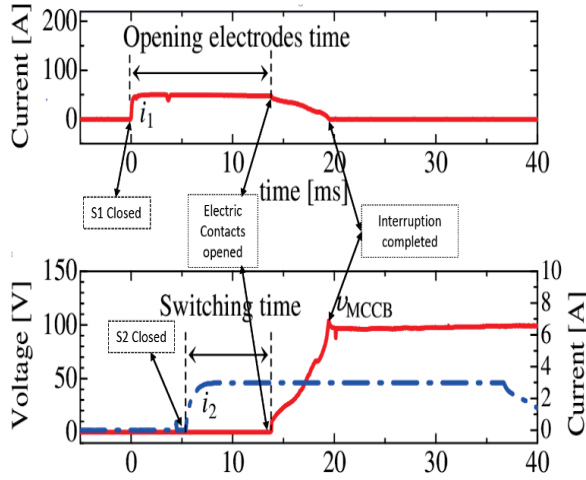


Figure 7 Waveforms of i_1 , i_2 and V_{MCCB} from fault current formation to interruption

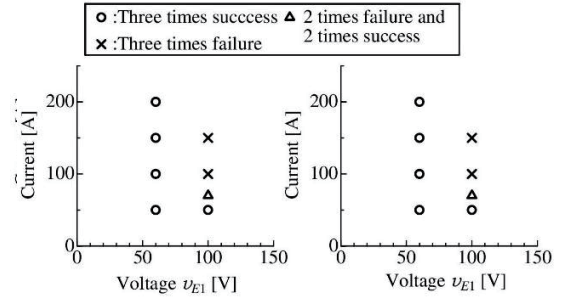
V. EXPERIMENT RESULTS

1. Experiment without L-R type FCL

To investigate the current limitation effect of FCL, the experiments was done without the FCL first. The table below summarizes different circuit configuration with different source voltage V_{E1} and variable resistance to get various fault current.

Table 2 Circuit specification under different fault current

$V_{E2}=48V$ $V_{E1}(V)=60V$		
Rush Current $i_1(A)$	Resistance $R(\Omega)$	Inductance L_R (mH)
50	0.99	0.08
100	0.51	0.04
150	0.34	0.02
200	0.23	0.01
$V_{E2}=48V$ $V_{E1}(V)=60V$		
Rush Current $i_1(A)$	Resistance $R(\Omega)$	Inductance L_R (mH)
50	1.94	0.17
70	1.36	0.11
100	0.99	0.08
150	0.60	0.05



(a) Opening electrodes time:5 ms (b) Opening electrodes time:15 ms

Figure 8 Results of the DC current interruption without FCL

Fig. 8 shows the results of the DC current interruption without FCL. It is found that there are no difference in term of the test results with opening electrode time at 5ms and 15ms. When V_{E1} is 60V, the MCCB can easily interrupt all the fault currents from 50A to 200A. When V_{E1} is increased to 100V, the MCCB can still interrupted the fault current at 50A successfully but it failed the interruption as the current is above 100A. To find the threshold current value between the success and failure, current from 50A to 100A are tested and the 70A is found to be the threshold current, which has 2 times success and 2 times failure in the current interruption.

The Fig. 9 shows the waveforms with the fault current at 70A with the successful and failed tests.

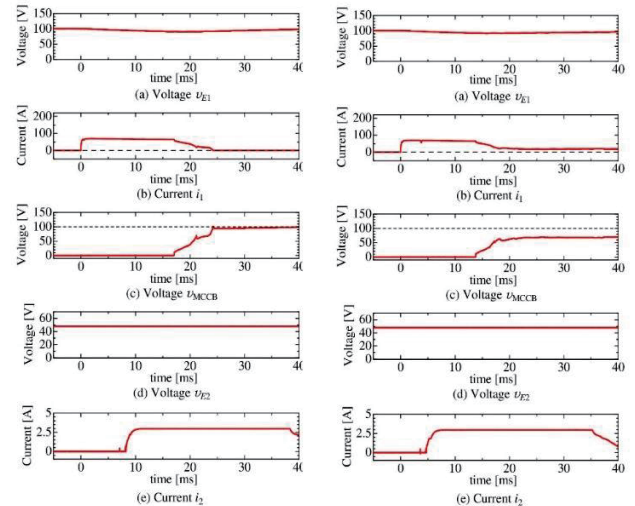


Figure 9 Waveforms of V_{E1} , i_1 , V_{MCCB} , V_{E2} and i_2 with fault current at 70A with successful (left) and failed (right) current interruption.

No matter it is successful or failed, the fault current rises instantaneously to a higher value and maintain it without the FCL. After 15ms of the fault current emergence, the arc is formed and the current starts to fall down and the V_{MCCB} rises to V_{E1} . But in the failed interruption experiment, the current cannot return 0 even after the two electric contacts were separated completely at 18ms.

Because of the non-zero current, the V_{MCCB} cannot rise to equal to the source voltage.

So a newly designed fault current limiter called L-R type FCL is expected to add and to check its effects on the fault current suppression and whether it could improve the performance of the current interruption.

2. Experiment with L-R type FCL

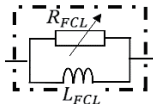


Figure 10 the Circuit of the L-R type fault current

The L-R type FCL is shown as above. It consists only passive elements with a variable resistor and an inductor connected in parallel.

Current Suppression

Firstly, the inductance L_{FCL} is kept at 2.8mH and the R_{FCL} is varied from 0.3 Ω to 5 Ω . The waveforms of the fault current with different R_{FCL} is shown as below.

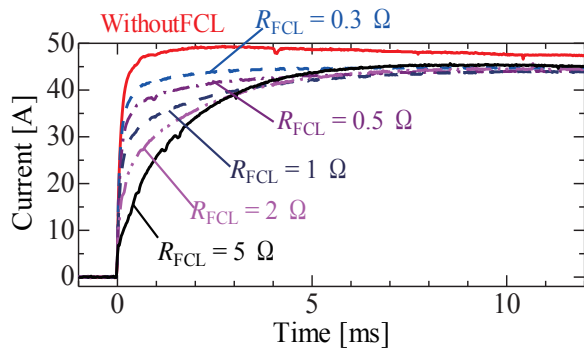


Figure 11 Waveforms of the fault current with various R_{FCL} .

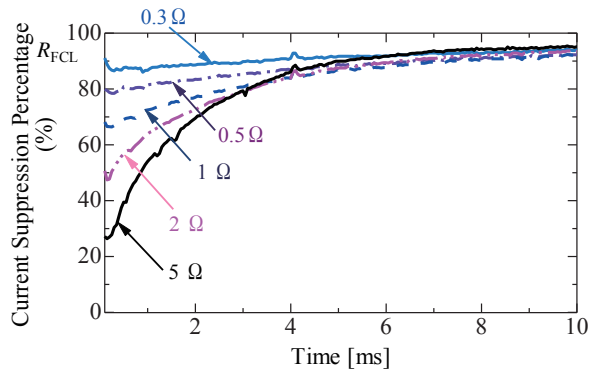


Figure 12 Current suppression percentage with various R_{FCL}

In Fig11, the current go instantaneously to 50A without FCL. When the L-R type FCL is introduced, it is obvious that the rising rate of the fault current decreases. The larger the R_{FCL} is, the slower the fault current increases. For a clearer illustration of the current suppression effect, the instantaneous current

suppression percentage (CSP) is calculated as follows and shown in Fig. 12.

$$CSP = \frac{\text{Fault current with FCL}}{\text{Fault current without FCL}} \quad (1)$$

When the fault current just emerges, it indicates that the current is reduced to 28%, 50%, 68%, 80% and 90% with R_{FCL} at 5 Ω , 2 Ω , 1 Ω , 0.5 Ω and 0.3 Ω respectively. After 6ms, all the current rise to the same maximum value. The larger the resistance in the FCL is, the more remarkably the fault current can be reduced, which proved the efficient current limitation effect for the L-R type FCL. Taking advantage of this property, the MCCB can interrupt the fault current at a lower magnitude which makes the current interruption easier and faster.

Current Interruption

When the fault current interruption is concerned, it is unexpected that no matter how resistance varied, all the interruption failed with the inductance value as 2.8mH.

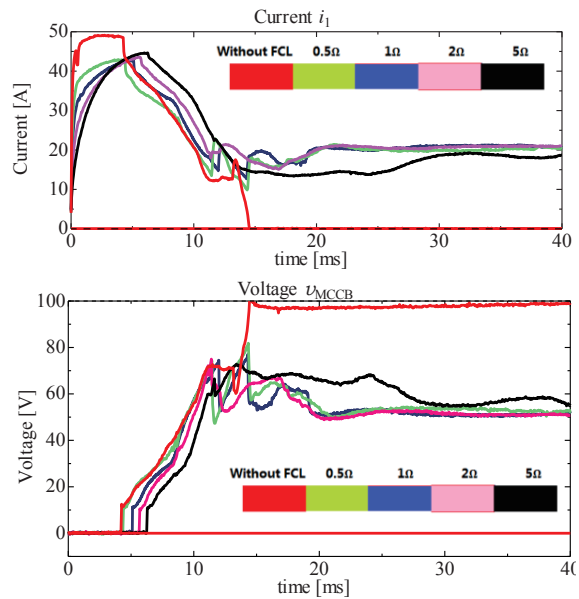


Figure 13&14 Waveforms of the current i_1 and V_{MCCB} with various R_{FCL}

The red line in Fig1 indicates that the MCCB can interrupt the fault current at 50A without the FCL. After interruption, the fault current returned 0 and the voltage across MCCB raised to equal to V_{EI} . When the FCL is added with 2.8mH, however, all the fault currents decreased and were kept at about 20A after 12ms. The voltage across MCCB cannot increase more after 12ms and remain at about 50V. Since the inductance is kept at 2.8mH all the time during this experiment, how the inductance value in FCL affect the current interruption is investigated.

To investigate the effect of L_{FCL} on the fault current suppression and interruption, experiments are conducted with various L_{FCL} and without R_{FCL} . To make it clearer for current suppression effect, the circuit is configured to interrupt at 5ms when the fault current all increased to their maximum.

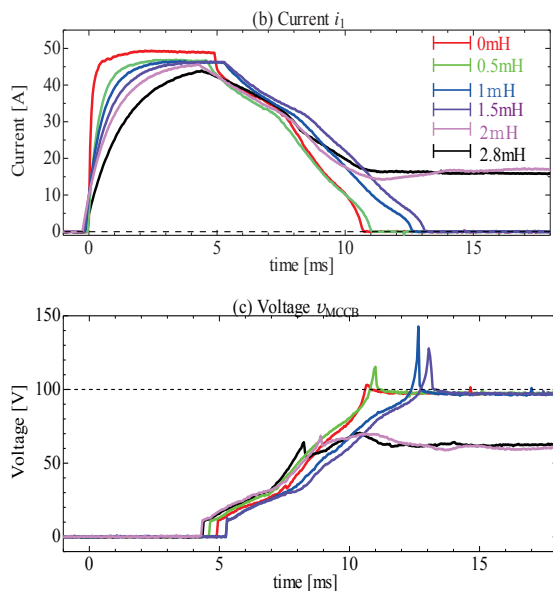


Figure 15&16 waveforms of the current i_1 and V_{MCCB} with various L_{FCL} when current is interrupted at 5ms

Although the inductance value is varied, the resistance of the inductance is almost constant at 0.13Ω . As shown in Fig. 15, during the current rising period, it is found that the waveforms shows the same tendency as those when only R_{FCL} is varied. As L_{FCL} increases from 0 to 2.8mH, the current suppression effect is getting more remarkable. For the current interruption, it shows that when L_{FCL} is smaller than 2mH, the circuit can interrupt the current successfully. Once L_{FCL} gets larger than 2mH, as the Lenz's law, the large inductance will keep the fault current going [3], which make the MCCB fail the interruption, which suggests that the added FCL not only didn't assist the MCCB in current interruption as expected, but also make the MCCB's current interruption performance worse. It also proved that why all the tests failed the interruption in Fig13&14 with L_{FCL} as 2.8mH.

However, the added L-R FCL also introduced some side effects. It is found that without FCL, the current is completely interrupted and return to 0 at 10ms, when the FCL is added, all the interruption end at about 13ms. So FCL could extend the period for the MCCB to interrupt the current, which might be a concern for the circuit with strict command of the fault current interruption speed.

In terms of V_{MCCB} , comparing with the case without FCL, it is found that the FCL will generate an overshoot in the voltage after the V_{MCCB} has already increased to be equal to source voltage V_{E1} . Although the i_1 is 0 and V_{MCCB} is equal to V_{E1} , as the Lenz's law of the inductance, there are still loop current in the FCL loop circuit. As the current fades away gradually in FCL loop circuit, the voltage across the FCL is induced that has the same direction with V_{E1} , which results in a voltage overshoot for the V_{MCCB} .

VI CONCLUSION

This report investigated the current suppression and interruption effect of the newly-developed L-R FCL when it is employed to assist the modified MCCB in DC low voltage distribution systems. In order to easily control the behavior of MCCB and avoid power losses, the MCCB is modified first. Based on the modified MCCB, the fault current interruption circuit is designed and built. By comparing the waveforms of the fault current and voltage across the MCCB with and without FCL, it is found that the both the resistor and inductor in L-R FCL can significantly limit the fault current. The larger the resistance and the inductance are, the more remarkable the fault current is suppressed. The inductance in FCL also play an important role during the fault current interruption period. In order to ensure the success of the current interruption, the inductance must be smaller than 2mH. Large inductance will keep the fault current going and make the MCCB fail the interruption. Besides, the side effect of the L-R type FCL is that it will extend the current interruption period and produce a voltage overshoot across the MCCB as the inductance and it will also produce extra power losses because of the resistance. By appropriate selection of the values of L_{FCL} and R_{FCL} , the L-R type FCL will significantly improve the current suppression and interruption performance of MCCB, which makes the L-R type FCL a promising protection device with simpler circuit configurations and lower cost in the DC distribution systems.

In the future, more efforts will be put into testing the L-R FCL with various combinations of the inductance and resistance values and find the best combination with the best performance. Also, voltage across the FCL will be measured to explore more about the inductance effect on the current interruption. As the resistance of FCL, it is also interesting to investigate how the power limit of the circuit changes after adding the FCL.

VII ACKNOWLEDGE

I would like to thank Tamao Kazuma to work together with me on this research and Ohashi Ryosake being my

teaching assistant. I am also very grateful to Prof. Yokomizu and Prof Masumura for the helpful advice on this project throughout this whole 80 days.

REFERENCES

- [1 Y. Yokomizu , T. Matsumura, Y. Taniguchi,
] “Direct-current breaking performance of molded-case circuit breaker and its dependence on source voltage and principal components,” *Frontier of Applied Plasma Technology*, vol. 3, no. 1, pp. 5-10, Jan. 2010

- [2 B.W. Lee, J.Sim, K. B. Park, and I. S. Oh:"Practical
] application issues of superconducting fault current limiters for electric power systems", *IEEE Trans. Appl. Supercond.*, Vol, 198, No. 2, pp. 620-623 (2008).

- [3 Y. Yokomizu, K. Namba, T. Matsumura,
] “Contrivance of Circuit Configuration of Fault Limiter for Low-Voltage DC System and Discussion on Its Current-Limiting Effect” IEEEJapan, *Internatinal Workshop on High Voltage Engineering.*, SP-14-70, 2014

- 4] Arc picture from the internet
“ <http://www.mechprod.com/blog/bid/323693/Arcs-in-Circuit-Breakers> ”

THE FABRICATION OF TISSUE ENGINEERED SMALL BLOOD VESSELS VIA 3-DIMENSIONAL CELLULAR SELF-ASSEMBLY AND ORGANIZATION IN VITRO

Andrea Manoppo

Department of Biomedical Engineering, College of Engineering, University of Michigan
manoppo@umich.edu

Supervisors: Dr. Fumihito Arai, Dr. Taisuke Masuda, Ukiki Mitsuhiro

Department of Micro-Nano Systems Engineering, Graduate School of Engineering, Nagoya University
arai@mech.nagoya-u.ac.jp

ABSTRACT

Although there is a great need for suitable vascular replacements in clinical practice, there is much progress to be made toward the development of a fully functional tissue-engineered construct. We propose a fabrication method of artificial small blood vessel constructs via a layer-by-layer cellular assembly technique using *M. musculus* aortic smooth muscle derived cell lines (MOVAS 7), the construction of a PLCL (poly-(L-lactide-co- ϵ -caprolactone)) scaffold, and integration in a microfluidic perfusion culture system. Laminated cell layers form a tubular structure as the result of residual stresses imposed by the PLCL scaffold. The perfusion culture system allows simulation of static, laminar, and pulsatile flow conditions. Cellular response to hemodynamic stress imposed by the dynamic culture system is monitored through expression analysis of FBN1, FBN2, and SM1 factors, which play an important role in tissue elastogenesis.

KEYWORDS

Mechanical stress culture, High Elasticity fiber, Poly-L-lactide-co- ϵ -caprolactone (PLCL), Smooth muscle cells (SMCs), Extracellular matrix (ECM), Fibronectin.

1. INTRODUCTION

Reports recently published by the World Health Organization indicated cardiovascular disease as the leading cause of human mortality, responsible for 17.5 million deaths and 46.2% of global noncommunicable disease deaths in 2012 [1]. In clinical application, the most widely used material for vascular replacement in coronary artery or peripheral bypass surgery is the patient's own native blood vessel [2, 3]. However, clinical treatments for vascular disease are limited by availability of autologous patient/donor replacements. Complications from the vein grafting process pose further risks. The use of larger-scale prosthetic grafts, such as Dacron[®] (PET, polyethylene terephthalate) and Goretex[®] (poly-tetrafluoroethylene), in

medium to large diameter vessels (ranging above 6 mm) have performed well largely in part to higher blood flow and lower resistance. Extensive research efforts have been directed toward smaller caliber diameter blood vessel replacements, such as that of the coronary and infrainguinal vascular regions, where thrombogenicity and stenosis poses greater risks [2, 4]. The development of a biomimetic model for vascularization is a crucial step toward developing more sophisticated diagnostic tools and novel therapeutics for highly prevalent diseases, such as atherosclerosis, ischemic heart disease, hypertension, cardiac arrest, diabetes, aging and cancer [4, 5]. Thus, there is incentive toward developing methods of small blood vessel construction *in vitro*.

In earlier approaches to vascular engineering, synthetic models, (such as PET, silicon, and Pyrex[®]-based models) have shown sub-optimal results due to lack of biocompatibility, deformation from hemodynamic stress, and poor cellular adhesion that result in low patency rates [2, 4]. Neointimal hyperplasia, immune response, and incompatibilities between graft/artery compliance and diameter present substantial limitations to implementation [6]. Over time, the use of biocompatible and biodegradable materials garnered more attention, such as the use of PCL (poly-caprolactone), PLGA (poly(lactic-co-glycolic)), and silk fibroin-based models. However, the need for the constructed vascular models to facilitate nutrient exchange, cellular signaling, and uphold cell viability rendered the use of these biomaterials as a replacement alone to be unsuitable as a biological conduit system [5, 7].

As research focuses shift away from synthetics and toward increasingly biology-driven approaches, such as hydrogels, interdisciplinary tissue-engineering methods have been a promising field for fabricating artificial vessels [2 - 7]. The main objectives of vascular tissue engineering are generally two-fold: 1) to create functional tissue microenvironments that facilitate proper oxygen, nutrient exchange, and waste removal and 2) to provide an *ex vivo* model for drug diagnostics and pathological studies or a vascular replacement for non-functional blood vessels in clinical practice. The earliest applications of vascular tissue

engineering are endothelial cell (EC)-seeded synthetic grafts, though research in this field has since expanded to a multitude of different approaches [5, 7]. In a subtractive pre-vascularization approach, Yoshida et al. utilized a cell accumulation technique involving alternative cellular depositions. A conduit composed of hierarchical structures of smooth muscle cells (SMC) and EC layers was successfully constructed. The method demonstrated the ability to manipulate SMC tissue thickness and rapid production of multi-layered tissue possessing native-like barrier functions [8]. We propose a method that also involves rapid fabrication of 3-dimensional and multi-layered blood vessel constructs of small blood vessel diameters ranging from 2 - 6mm [9, 10]. In addition to the use of a PLCL scaffold, a dynamic culture system has also been developed in order to create a microenvironment simulating distinctive flow conditions.

2. EXPERIMENTAL DESIGN

Fig. 1 illustrates the general process of the fabrication in a step-by-step sequence. The process involves the development of 3-dimensional cellular multilayers using protein nano-films that are deposited onto single-cell surfaces [9 - 11]. This Layer-by-Layer (LbL) method immerses cells in solutions of fibronectin and gelatin (FN-G) in an alternating fashion, permitting control of tissue thickness levels (Fig.1 Step 1). A biocompatible scaffold of PLCL is constructed and SMC cell lines are seeded onto the scaffold, as facilitated by the layer-by-layer culture process [10]. Fibronectin plays an important role in both cellular adhesion as well as ECM assembly. On pericellular surfaces, it has been shown to develop into fibrillin-type microfibrils and organize into complex structures that contribute to the elasticity of whole tissue [11]. In other studies, fibronectin was found to interact with lysyl oxidase (LOX), an enzyme functioning in the cross-linkage of elastic fiber, and contribute to its enzymatic activation [12]. Fibronectin-gelatin layering is not only useful for fabricating layered tissue constructs by enhancing cellular adhesive properties, but also by the ability to protect single cells from multiple rounds of centrifugation. Cell viability is preserved as a result.

Using a dip-coating process, a PLCL tubular structure embedded with NaCl particles is constructed. The scaffold is submerged in distilled, deionized H₂O overnight. The NaCl

crystals dissolve until a porous structure in the PLCL walls remains. The advantages of this salt-leaching process are the controllability of scaffold porosity and the optimization of growth factor diffusion to the innermost layer of cells within the finished construct. Fig. 2 provides images of the tubular PLCL scaffold. The scaffold is incised, expanded, and fashioned between two jigs (Fig. 1, Steps 2-3). The FN-G coated cells are seeded onto one surface of the scaffold and incubated before the PLCL scaffold is removed from the jigs. Once the scaffold is released from the jig configuration, the construct conforms into tubular structures due to residual stress imposed by the cylindrical PLCL scaffold (Fig. 1, Steps 4-5). The free edges of the scaffold are sealed with a biodegradable adhesive around the glass capillaries, allowing controlled media flow-through in the intra-luminal space of the constructs (Fig. 1, Step 7).

A perfusion system has been developed in order to imitate *in vivo* conditions as well as test different flow type effects on elastogenesis of the cellular constructs. Important conditions that are controlled and maintained in the microfluidic perfusion process are temperature, pH level, flow rate, and intraluminal pressure. Standard culture media (pH 7.4) is flowed through the tubular device while housed within a 37°C incubator. The constructs are placed in a dynamic culture system that is able simulate static, laminar, and pulsatile flow conditions. The final product of this culturing system is a tissue-engineered 3-dimensional conduit, composed of multiple cell layers that remain well adhered to the PLCL scaffold (Fig. 1, Step 8).

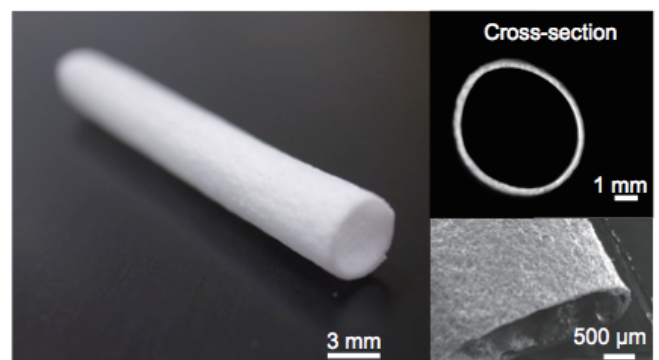


Fig. 2 Images of the fabricated PLCL scaffold are provided. A cross-sectional view measured at a 3mm diameter and thickness of 380 μm. Scanning electron microscopy (Hitachi, Japan) imaging was conducted to examine the porous structure and dimensions.

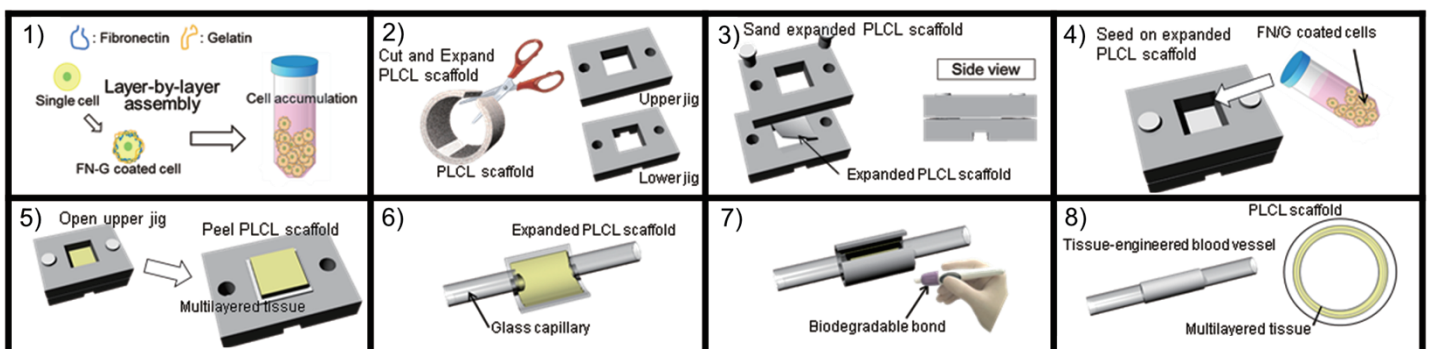


Fig.1 An illustrated sequence of the fabrication process of artificial small blood vessels using a PLCL scaffold.

3. MATERIALS AND METHODS

3.1 Construction of the PLCL Scaffold

In constructing the scaffold, 3wt. % or 5wt.% of PLCL (BMG Inc., Kyoto, Japan) are dissolved in liquid chloroform (Wako Pure Chemical Industries, Ltd., Osaka, Japan) for 24 hours. Table 1 lists the particular conditions used in constructing the PLCL. Using a ceramic mortar and pestle, NaCl is pulverized into particles (with diameters ranging no less than 53 μm), that are sorted by size, and added to the PLCL-chloroform solution at ratios of 20 wt. %, 40 wt. %, and 60 wt. % for experimental purposes. Thin, close-ended glass tubes are dipped in PLCL by an automated process using a uniaxial electric stage.

The glass tube is fixed to the stage during the dipping process, the speed of which influences the thickness of the scaffold walls. A faster speed results in a thicker coating, while the converse is true. The speed used to coat the glass tubes in the PLCL-NaCl-Chloroform solution is 30 mm/sec. The construct is then left to dry in a fume hood for 1 minute. This dipping process is repeated 6 times for the purposes of the perfusion experiment, before inverting the construct on a stand to completely dry for 24 hours. The number of coatings was varied in the case of characterizing the elastic properties of the scaffold. After removal of the construct from the glass tube, it is sterilized with an EtOH solution for 30 minutes.

A ring-type tensiometer (JIS K6251 Compliant) is used to measure the mechano-elastic properties of the PLCL scaffold. The model by which measurements of the Young's Modulus of each scaffold are analyzed using:

$$E = \frac{\sigma}{\varepsilon} = \frac{P/A}{\frac{L - L_0}{L_0}}$$

Rearranged to,

$$= \frac{P * L_0}{(2 \Delta l + L_1 - L_0) * 2 * t * d} \quad (1)$$

Where P : force, t : scaffold thickness, d : width, A : cross-sectional area, L : circumference of test-piece, L_1 : circumference of jig, and Δl : displacement.

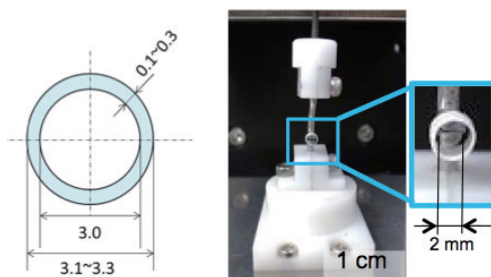


Fig. 3. Approximate measurements of the PLCL scaffold dimensions are measured with microscopy. The configuration of the ring-type tensiometer is shown on the right.

Table 1: The Conditions for Fabrication of the PLCL Scaffold

Chloroform : PLCL	95 : 5
NaCl : PLCL	4 : 6
Particle Diameter of NaCl	53 -100 μm
Number of Coatings	6
Pull-Up Velocity	3.0 mm/s

3.2 Cell Culture and Layer-by-Layer Method

All cultures are performed in an aseptic environment and incubated in 60 mm plates within a standard cell incubator at 37°C, 5% CO₂ – 95% ambient mixed air levels. When not in use, all reagents and media used for experimentation are stored in -4 °C environments.

The project was conducted using MOVAS 7 (*M. musculus* aortic smooth muscle derived cell line, Yokohama City University). Layer-by-Layer (LbL) method is used to fabricate multi-layered tissue [14,15]. LbL methods involve deposition of nano-scale thin layers of fibronectin and gelatin on single cell surfaces in order to optimize cell-to-cell interactions and cellular adhesion. In this technique, the cells are alternatively immersed in three distinct solutions: fibronectin solution (0.04 mg/ml dilution in Tris-HCl, bovine plasma-derived, F1141-5MG; Sigma-Aldrich Corp., MO, USA) dissolved in Tris-HCl buffer solution (50mm, pH 7.4), gelatin solution (0.04 mg/ml in Tris-HCl, 077-3155; Wako Pure Chemical Industries, ltd. Osaka, japan) dissolved in Tris-HCl (50mm, pH 7.4), and a separate wash of Tris-HCl (50 mm, pH 7.4) is used between each protein immersion to remove non-adhering polymers. After immersion in each solution, the cells undergo automated rotation (1 minute, 25°C) and are then centrifuged (1000 rpm, 2 minutes). The solution is aspirated and the cells are re-suspended in the following solution, before undergoing another rotation in the same manner. Although these continual cycles of immersion, centrifugation, re-suspension, and washing with Tris-HCl are repeated multiple times, high cell viability is maintained.

Following the LbL technique, an NIH3T3 fibroblast solution (1.6 x 10⁶ cells/well) is deposited onto the entire surface area of a well formed by the PLCL-jig configuration. The PLCL scaffold tube, as fabricated as in Section 3.1, is cut open down the length using surgical grade shears. Plastic screws hold the two components of the jig together. As shown in (Fig. 1, Step 3), the PLCL sheet forms a flat surface. When fixed between two plastic jigs, a well is formed. The protein solution is aspirated and the well is washed with Tris-HCl before left to dry inside the laminar flow hood. The fibronectin-gelatin coated MOVAS 7 cell solution (2.2 x 10⁶ cells/well for 10 cell layers, note: concentration may vary depending on desired experimental layer number) is seeded onto the PLCL surface of the well created by the stacked jigs. The PLCL scaffold is submerged with about 2.5 ml of media that is added to the outside space of the well formed by the PLCL-jig complex, where the non-laminated side of the PLCL scaffold is also exposed. The system is allowed to incubate for 2-3 hours. Without disturbing the cells, DMEM with 10% FBS is added. After 24 hours of incubation, cells can be laminated. Cell counts,

including dead and viable cells, were conducted using Trypan Blue solution (10 μ l) in an automated cell counter system (Luna™, Logos Biosystems). The PLCL-scaffolded constructs are cultured in the incubator (37°C, 5% CO₂) for approximately three days.

3.3 Tubular Assembly

The following procedures are performed in an aseptic environment, in which the jigs are soaked in EtOH (30 min) and sterilized with UV radiation (20 min). The solution is then aspirated and washed with Tris-HCl. Fibronectin solution (0.2 mg/ml per 50mM Tris-HCl buffer) is deposited in the center of the expansion jig and incubated for 15 minutes to promote cellular adhesion.

To disassemble the jigs containing the PLCL-scaffolded cell construct, tweezers are used to unscrew the plastic screws embedded in the mold. The PLCL gel at the bottom surface is also removed. The PLCL scaffold is released from the jig complex and autonomously conforms to a tubular structure due to residual stress (Fig. 4). The PLCL-cell construct is fixated onto a semi-circular channeled mold of polydimethylsiloxane (PDMS; diameter = 4mm), with two glass capillary tubes inserted at either side. DERMA BOND® (Johnson-Johnson, NJ, USA), an adhesive biocompatible substance, is used to bond the edges of the PLCL-scaffold housing the cell construct around the glass tubes. The edges of the cellular construct are also bonded to the glass capillaries at either side, around the circumference. The scaffolded construct is removed from the PDMS mold. The obtained construct is a tubular structure composed of multiple layers of SMCs adhered to the PLCL scaffold. Dulbecco's Modified Eagle Medium (DMEM, Sigma Aldrich, MO, USA) with 10% Fetal Bovine Serum (FBS, Thermo Scientific, MA, USA), 1% penicillin (100 U/ml) and streptomycin (100 mg/ml) media solution is injected into one side of the glass capillary to rid of trapped air. The construct is inverted and cultured in cell media for 24 hours to allow the gap in the cellular construct to be closed by migrating and dividing MOVAS 7 cells.

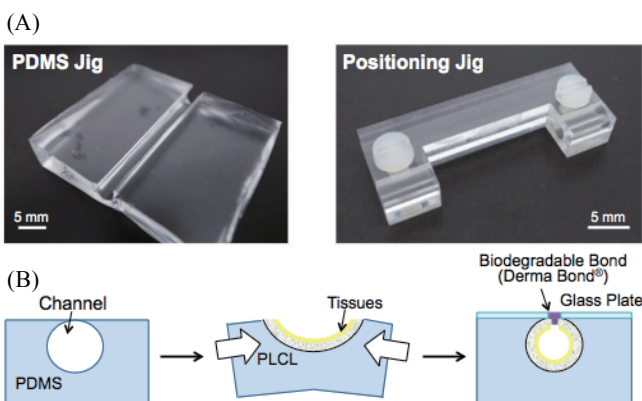


Fig. 4 (A) The left image is of the PDMS mold while the right image shows the positioning jig (B) The sequence of cross-sections illustrates how the PDMS mold houses the scaffold/cellular construct in position. The PLCL scaffold is laminated with FN-G coated cells and held in place by the PDMS mold.

3.4 Microfluidic Perfusion Testing

The constructs are cultured in a microfluidic perfusion system (Fig. 5) [16]. All culture testing is conducted in aseptic conditions at 37°C, atmospheric CO₂ levels of 5% - 95% mixed ambient air. Both ends of the glass capillaries inserted at each terminus of the construct, as described in Section 3.3, are connected to a pump system. Thus, three conditions of flow can be performed: static, laminar, and pulsatile flow with adjustable flow-rates and pressure oscillations. For laminar perfusion, the constructs are perfused at a flow rate that is comparable to native conditions (165 mL/min). In pulsatile flow conditions, amplitude and frequency of pressure fluctuations maintained by the pump system are remotely controlled. To mimic *in vivo* physiological environments, pressure fluctuations are performed (110/80 mmHg, 1 Hz). In testing the static flow condition as a control group, the constructs are submerged in media (DMEM + 10% FBS + 1% penicillin/streptomycin) within a 60 mm plate. All constructs are allowed to incubate in their respective flow conditions for 24-72 hours.

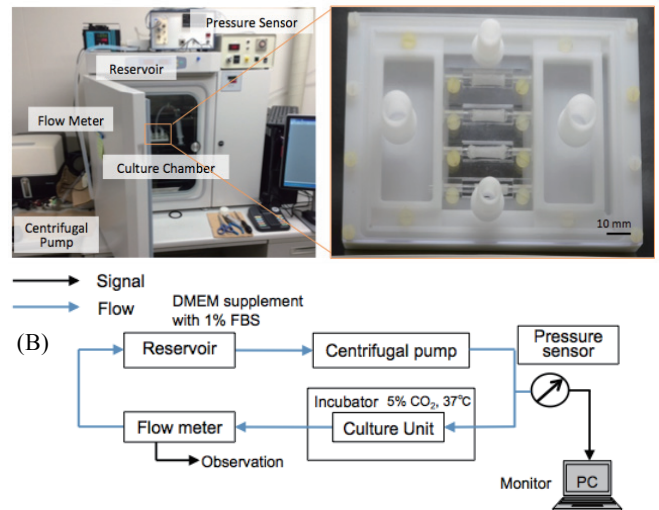


Fig. 5 (A) The left image shows the experimental setup of the perfusion culture system, the right image shows the configuration of the blood vessel constructs within the device. (B) A flow-chart depicts the basic process of this automated system: consists of a centrifugal pump, a culture chamber, pressure sensor, flow meter, and a reservoir of cell medium.

3.5 Immunohistochemistry and RNA analysis

RNA expression analysis is conducted for SM1, Fibrillin1, and Fibrillin2. These proteins are three transcription factors implicated in elastic fibers development. RNeasy® Mini Kit (cat. Nos. 74104 and 74106, QIAGEN) was used to perform expression analysis. All resulting statistical data was processed using Eco Software V5.0. For immunohistology assays, Hoechst 33342 (blue) was used to stain cell lines NIH3T3 (fibroblasts) and UV2 (endothelial cells). Calcein AM (green) stains were used for the MOVAS 7 (smooth muscle) cell lines. Images were observed using confocal fluorescence microscopy. Actin stains (Alexa Fluor 488, green) and nuclear stains (Hoechst 33342, blue) were performed. Analysis of fluorescence was performed using ANDOR iQ2 software.

4. RESULTS AND DISCUSSION

4.1 Mechanical Characterization of the Scaffold

One of the main objectives in constructing a vessel model is the replication of the micro-environmental conditions and properties of native tissue. Fig. 6(A) shows the material testing results of the mechanical properties of the PLCL scaffold as constructed through the dip-coating method. The thickness of the scaffold walls increases in a linear fashion ($0.87 < R^2 < 0.99$) in relation to increasing the number of times the glass capillary tube is dip-coated in the PLCL-chloroform solution while holding dip-velocity constant. Since the increase in thickness with number of coatings was found to be consistent, this attests to the ability to precisely control the level of scaffold thickness. Manipulation of thickness levels are important, as vessel models must be able to vary in diameter when considering the immense variation in native wall thickness, diameter, and composition. When dipped 6 times, for the purposes of experimentation, the thickness of the scaffold was consistently found to be 380 μm . The speeds and conditions used are as in Section 3.1. Fig. 6(B) shows the characterization of the elastic properties (Young's Modulus) of the scaffold when the PLCL wt% is varied, as well as PLCL ratio compared to the amount of NaCl added. In the conditions used for experimentation (a 5 wt% of PLCL, with a 4:6 ratio of NaCl to PLCL), Young's Modulus is found to be .8 MPa. The reference blood vessel modulus has been characterized as .8 MPa. Conditions that match the reference are more optimized for imitating *in vivo* properties.

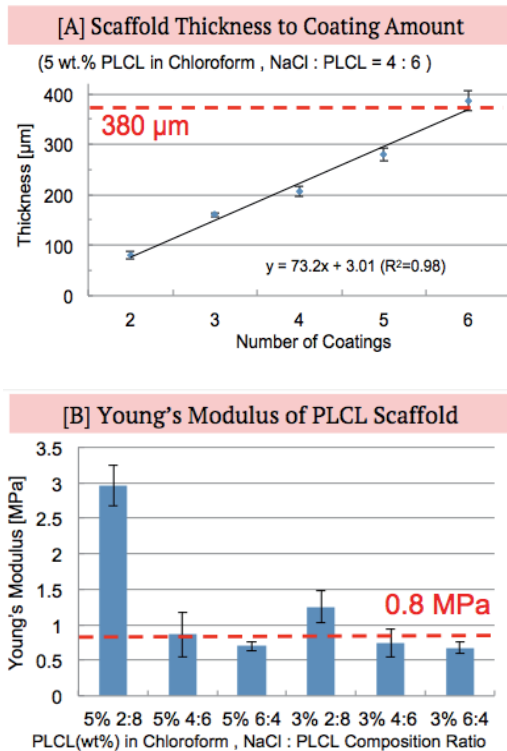


Fig. 6 (A) Measure of PLCL-scaffold thickness (in μm) is taken relative to the number of dip-coating rounds. Dip coating 6 times results in a thickness of 680 μm . (B) The Young's Modulus of the PLCL-scaffold is measured relative to percent dilution in chloroform as well as ratios of NAACL to PLCL.

4.2 Expression Analysis of Factors in Elastogenesis

Elastic fibers are comprised of elastin, microfibrils, and fibrilins. Microfibrils, such as Fibrillin-1 (FBN1) and Fibrillin-2 (FBN2), play a role in elastin assembly and organization of developing elastic fibers [11]. FBN1 is crucial in particular, as previous studies have reported that FBN1 knockout mice (FBN1 $-/-$) have underdeveloped and disjointed arterial elastic fibers. FBN2 knockout mice (FBN2 $-/-$) developed syndactyly [17]. FBN1 deficient mice tended to be prone to aortic dilation, rupture, increased aortic stiffness, and increased pulse pressure. We evaluated FBN1 and FBN2 mRNA expression levels as a marker of elastogenesis in the newly developed constructs after culturing in dynamic culture conditions (Fig. 7).

In addition, we examined SMC differentiation, also as influenced by hemodynamic stress imposed by the culture system, by monitoring the expression of various SMC markers. Other studies have reported that the expression levels of differentiation SMC markers, such as SM1 (a smooth muscle myosin heavy chain isoform), are highly expressed in the medial layer of SMCs while it is reduced in human intima of atherosclerotic lesions [11]. Importantly, SM1 is consistently expressed by any type of vascular SMCs [18]. SM1 is constitutively expressed from early development and is expressed exclusively in smooth muscle cells [19], thus it is used as a marker of SMC development. In our experiments, mRNA expressions of SM1 are evaluated, as well as that of FBN1 and FBN2.

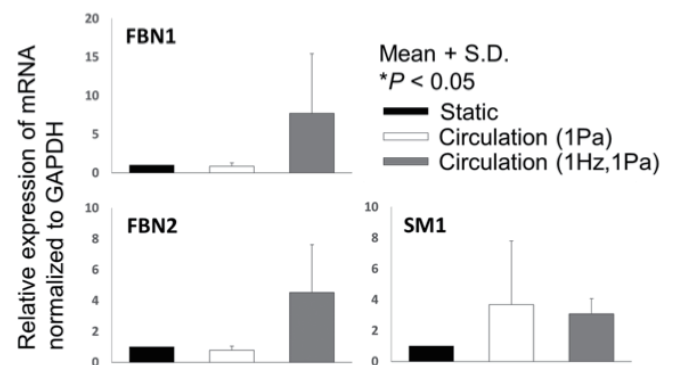
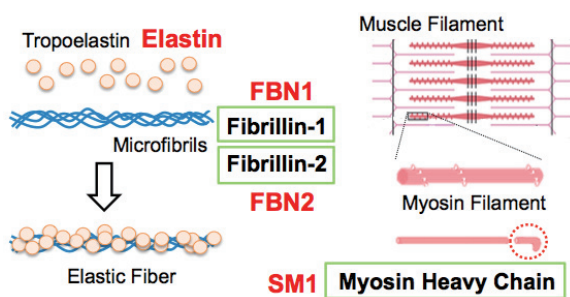


Fig. 7 (upper left) The results of an RNA expression analysis of FBN1 and (lower left) FBN2 transcription factor, all normalized relative to GAPDH expression, suggest that pulsatile flow circulated in the perfusion induces a higher expression of both transcription proteins. SM1 (lower right) shows stimulation in both flow types, but expression is minimal under static conditions devoid of mechanical stress ($n = 1$, $n = 4$, $n = 3$, respectively).

Fig. 7 displays the effects of the dynamic perfusion culture system on the constructs, as measured by gene expression analysis of transcription factors that play important roles in generation of cellular elasticity. RNA analyses for expression of SM1, Fibrillin 1 (FBN1), and Fibrillin 2 (FBN2) proteins were obtained from the construct tissue samples. The pulsatile flow conditions (165 ml/min, 110/80 mmHg, 1 Hz) showed significantly higher expression of FBN1 and FBN2 in comparison to the static and laminar flow conditions. There is also a marked increase in SM1 expression in both laminar and pulsatile

experimental groups normalized to metabolic enzyme Glyceraldehyde 3-Phosphate Dehydrogenase (GAPDH) expression. These initial results suggest that the development of elastic fibers through the activation of FBN1 and FBN2 is most responsive to mechanical stress from pulsatile pressure. Mechanical stress imposed by both laminar and pulsatile flow forms resulted in higher SM1 expression. SMCs are highly sensitive to strain through integrin-mediated connections to the ECM; dynamic culture studies have shown changes in orientation and cell proliferation under controlled strain [5]. In contrast, fibrillin has a distinct function regarding contribution to vascular compliance. While elastin contributes to elastic recoil, FBN-1 provides tensile strength and compensates aortic diameter for blood flow in physiological pressures [20]. The finding that FBN-1 and FBN-2 levels exhibited response to pulsatile pressures while SM1 responded more general mechanical stress is consistent with the known functions of these factors. However, more experimentation must be conducted in order to obtain more conclusive evidence.

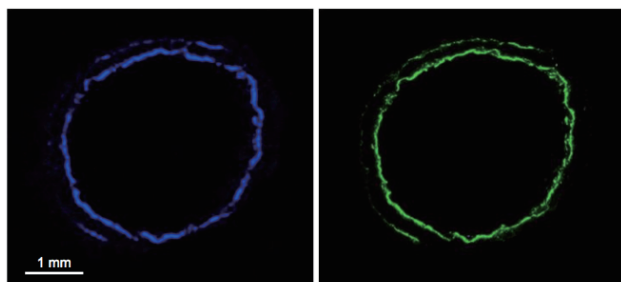
Fig. 9 A conceptual diagram of the role of FBN1, FBN2, and SM1



factors in their respective roles in the development of elastic fibers.

4.3 Results of Immunohistochemistry Assays

One of the hurdles in successfully constructing a tissue-engineered conduit using this fabrication method is the longitudinal gap of the laminated cellular construct adhered to the PLCL scaffold. Immunohistology reports of the construct *post* incubation with pulsatile flow incubation showed that migrating and dividing MOVAS 7 cells filled the unsealed gap of the cellular construct when the construct is inverted and incubated for 24 hours in pulsatile conditions.



Blue : Hoechst 33342

Green : Alexa 488 Phalloidin

Fig. 8 The immunohistochemical results of the construct post incubation in pulsatile conditions are displayed. A nuclear staining (Hoeschst 33342, blue) and an actin staining (Alexa 488 Phalloidin, green) indicate successful sealing of the gap and adherence to the PLCL scaffold.

Fig. 8 shows fluorescence microscopy images of the resulting tissue cross-section. The cells remained well adhered to the scaffold and a continuous cylindrical wall of multi-layered tissue was successfully constructed. Another important feature for any vessel construct is the retention of a hollow intraluminal space. A prevalent issue in biological conduits are low patency rates due to intimal thickening or clot formation [2]. However, it is evident from analysis of the cross-sections that a conduit structure was retained during incubation in the microfluidic perfusion system.

CONCLUSION

Principles of vascular tissue engineering entail the integration of cells into functional tissue and the developing tissue to reproduce mechanical and biological properties of native vessels. Such methods involve an interdisciplinary approach of biomechanical, materials, and cellular engineering. We have proposed a system that incorporates these principles via the usage of a 3-dimensional LbL cellular assembly technique, the development of a PLCL scaffold with a controllable thickness and porosity, and a microfluidic perfusion culture system that simulates different flow conditions. Through the use of this dynamic culture system, it is possible to analyze the progression of elastic fiber growth in the engineered constructs at the cellular level. One main objective of the proposed vessel fabrication method is the production of multi-layered structures, considering that native blood vessels are composed of distinctive layers with a varying composition of fibroblasts, smooth muscle cells, and an innermost layer of endothelial cells. The immunohistology results showed progress in that distinctive layers of cells were successfully constructed and maintained. Importantly, the marked changes in mRNA expression of factors implicated in elastic development (Fig. 9.) in response to different forms of mechanical stress applied to the intraluminal space of the construct are a promising result.

While progress toward successful fabrication of tissue-engineered small blood vessels is being made at large, there are far many more challenges to be addressed. Further directions are concerned with simulating *in vivo* biological and chemical conditions, as proper cellular function depends heavily on vast signalling networks and sensitivity to a multitude of biochemical cues. Future directions for this project may involve incorporation of vascular endothelial growth factors in the system to stimulate endothelial growth, the development of branched constructs in order to surpass limitations imposed by the use of uniaxial subtractive methods, and testing the constructs in animal models. The use of an animal model for implantation testing of constructs will require many considerations such as suturability of constructs, compliance matching, and the use of animals of comparable blood pressure levels. Among the available materials for small blood vessel construction, hybrid vascular scaffolds hold much potential due to controllability of the mechanical properties of synthetic polymers and biocompatibility of integrated cellular components.

ACKNOWLEDGEMENT

This project was conducted at Arai Laboratories, Department of Micro-Nano Systems Engineering, Graduate College of Engineering, Nagoya University. I would like to sincerely like to thank Dr. Fumihito Arai, Dr. Taisuke Masuda, Ukiki Mitsuhiro and Ayaka Sato. I am also grateful to the members of Arai Laboratories for hosting me, and to the Japan-US Advanced Collaborative Education Program (JUACEP) and staff for their support at Nagoya University. At the University of Michigan, I would like to express my appreciation to the International Program in Engineering (IPE) and to Dr. Katsuo Kurabayashi.

REFERENCES

- [1] World health organization, Global Status Report on Noncommunicable Diseases, pp. 28 (2014).
- [2] Chlupáč J., Filová E., Bacáková L. Blood Vessel Replacement: 50 Years of Development and Tissue Engineering Paradigms in Vascular Surgery. *Physiological Research*. 58 (2): pp. 119-39 (2009).
- [3] Cleary A., Geiger E., Grady C., et al. Vascular Tissue Engineering: The Next Generation. *Trends in Molecular Medicine*. 18 (7): pp. 394-404 (2012).
- [4] Peck M., Gebhart D., Dusserre N., McAllister T., L'Heureux N. The Evolution of Vascular Tissue Engineering and Current State of the Art. *Cells Tissues Organs*. 195, pp. 144-158 (2012).
- [5] Hasan A., Paul A., Vrana N., et al. Microfluidic Techniques For Development Of 3D Vascularized Tissue. *Biomaterials*. 35 (26): pp. 7308-7325 (2014).
- [6] Valentina Catto, Silvia Farè, Giuliano Freddi, And Maria Cristina Tanzi, "Vascular Tissue Engineering: Recent Advances In Small Diameter Blood Vessel Regeneration," *ISRN Vascular Medicine*, Vol. 2014, Article Id 923030, 27 Pages, 2014.
- [7] Nerem R., Seliktar D. Vascular Tissue Engineering. *Annual Review of Biomedical Engineering*. 3, pp. 225 - 243 (2001).
- [8] Yoshida H., Matsusaki M., Akashi M., Multilayered Blood Capillary Analogs n Biodegradable Hydrogels for In Vitro Drug Permeability Assays. *Advanced Functional Materials*. 23, pp. 1736 - 1742 (2012).
- [9] Y. Yamagishi, et al., Microfluidic Perfusion Cultivation System For Artery-Like Tubular Tissues With PLCL Scaffolds. *The 17th International Conference On Miniaturized Systems and Chemistry and Life Sciences*.
- [10] Yoshida, M. Matsusaki, Et Al., "Rapid Construction Of Three-Dimensional Multilayered Tissues With Endothelial Tube Networks By The Cell-Accumulation Technique," *Adv Mater*, Vol. 23, Pp. 3506-3510 (2011).
- [11] R. Ishiwata, U. Yokoyama, M. Matsusaki Et Al., Three Dimensional Multilayers Of Smooth Muscle Cells As A New Experimental Model For Vascular Elastic Fiber Formation Studies, *Atherosclerosis*, 233 : 590-600 (2014).
- [12] Fogelgren B., Polgar N., Szauter Km., Et Al. Cellular Fibronectin Binds To Lysyl Oxidase With High Affinity And Is Critical For Its Proteolytic Activation. *J Biol Chem*. 280:24690e7 (2005).
- [13] Y. Yamagishi, Et Al., Microfluidic Perfusion Cultivation System For Multilayer Structured Tubular Tissues. *The 17th International Conference On Miniaturized Systems For Chemistry And Life Sciences*, No. 1213 (2013).
- [14] M. Matsusaki, H. Ajiro, T Kida Et Al., Layer-By-Layer Assembly Through Weak Interactions And Their Biomedical Applications, *Advanced Materials*, 24 (4): pp. 454-474 (2012).
- [15] Nishiguchi A., Yoshida H., Matsusaki M. et al., Rapid Construction Of Three-Dimensional Multilayered Tissues With Endothelial Tube Networks By The Cell Accumulation Technique. *Advanced Materials*. 23 (31): pp. 3506-3510 (2011).
- [16] Yamagishi Y., Masuda T., Matsusaki M., Microfluidic Perfusion Culture System For Multilayer Artery Tissue Models. *Biomicrofluidics*. 8, 064113 (2014).
- [17] Wagenseil J., Mecham R. Vascular Extracellular Matrix and Arterial Mechanics. *Physiological Reviews*. 89 (3): pp. 957-989 (2009).
- [18] Aikawa M., Sivam PN, Kuro-o M et al., Human Smooth Muscle Myosin Heavy Chain Isoforms as Molecular Markers for Vascular Development and Atherosclerosis. *Circ Res*. 73: 1000e12 (1993).
- [19] Watanabe M., Sakomura Y., Kurabayashi M. et a. Structure and Characterization of the 5'-Flanking Region of the Mouse Smooth Muscle Myosin Heavy Chain (SM1/2) Gene. *Circulation Research*. 78 (6): pp. 978 - 89, (1996).
- [20] Carta L., Wagenseil, J., Knutsen R., et al. Discrete Contributions of Elastic Fiber Components to Arteriolar Development and Mechanical Compliance. *Arteriosclerosis, Thrombosis, and Vascular Biology*. 29 (12) pp. 2083-2089, (2009).

All-polarization-maintaining Er-doped ultrashort-pulse fiber laser using carbon nanotube saturable absorber

Haodong Shen

(Optics) Department of Electrical Engineering and computer science, Graduate School of, University of Michigan
haodong@umich.edu

Supervisor: Norihiko Nishizawa

Graduate School of Engineering, Nagoya University
nishizawa@nuee.nagoya-u.ac.jp

ABSTRACT

This report will present an all-polarization maintaining Er-doped ultrashort-pulse fiber laser using a single-wall carbon nanotube polyimide nanocomposite saturable absorber. This laser is built by fiber fusion. The maximum power for continuous output is 3.5mW, and the repetition frequency is 29.3MHz. Self-start and stable mode-locking is achieved. The output pulse has a FWHM of 452fs.

Introduction

Passively mode-locked ultrashort-pulse fiber lasers are stable, compact, maintenance-free, practical ultrashort-pulse light sources, and they have attracted a great deal of attention lately. Ultrashort-pulse fiber lasers are promising practical pump sources for ultrashort-pulse applications, such as optical frequency combs, 3D optical memory, and supercontinuum sources. The figure-eight scheme, nonlinear polarization rotation, and semiconductor saturable absorption mirrors (SESAMs) have been used in ultrashort-pulse fiber lasers for passive mode-locking. Environmental stability is one of the key issues for fiber lasers. The sigma cavity configuration and a Faraday rotator have been used in the demonstration of an environmentally stable fiber laser. A few studies of all-polarization-maintaining (PM) fiber lasers have been reported, such as a figure-eight laser, an Yb laser with a SESAM, and so on. Since the linear polarization state is always maintained in these PM fiber lasers, they are robust against environmental variations and have excellent long-term stability.

It was discovered that a single-wall carbon nano-tube (SWNT) has saturable absorption properties. The recovery time is ~ 1 ps, and a transparent saturable absorber can be formed so that it works as a useful mode-locker. SWNT saturable absorbers are divided into three types: direct deposition, evanescent, and film. The film type is a useful device because one can obtain passive mode-locking merely by setting the film between the fiber connectors. In a PM fiber laser, generally it is necessary to align the birefringent axes of PM fibers precisely. However, if we use a film-type SWNT device in the fiber connector, the birefringent axes of

the PM fibers are automatically aligned at the fiber connector, and passive mode-locking is achieved in a simple all-fiber ring cavity configuration without any polarization devices. Thus, the film type SWNT device is attractive for PM fiber lasers.

With the instruction of professor Nishizawa, I have demonstrated an all-PM SWNT Er-doped ultrashort-pulse fiber laser. It was demonstrated by professor Nishizawa and his group before. A polyimide film in which SWNTs are dispersed is used as a transparent saturable absorber, and stable passive mode-locking operation is achieved merely by setting the polyimide film between the fiber connectors in the cavity.

All-polarization-maintaining Er-doped ultrashort-pulse fiber laser using SWNTs

In figure 1, it shows the configuration of the all-PM passively mode-locked Er-doped ultrashort-pulse fiber laser using SWNTs.

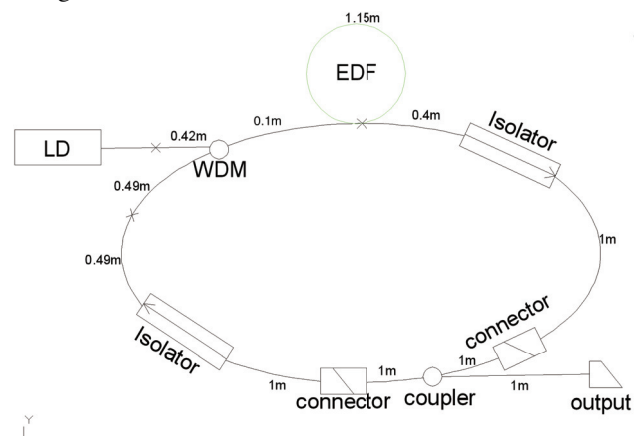


Fig.1 Configuration of all-PM passively mode-locked Er-doped ultrashort-pulse fiber laser using SWNTs.

A high-power laser diode (LD) with a input wavelength of 980 nm was used as a pump source. It is control by two parts: temperature control and current control. It was well

adjusted. Before the cavity was built, the amplification function of Er-doped fiber was examined. I used 1550nm as source whose output energy is 1mW. Then increased the LD current. It is shown in figure 2. And I set the LD current to 1140mA. Then increased the 1550nm laser source. It is shown in figure. 3. It has a good amplification profile.

Er-doped fiber amplification while input power is determined

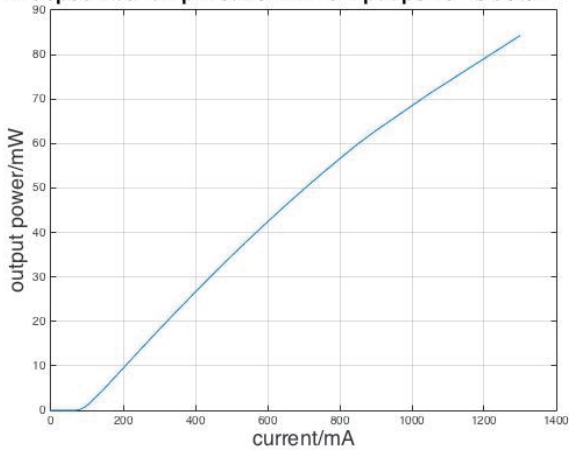


Fig. 2 The output power while changing the current

Er-doped fiber amplification while current is determined

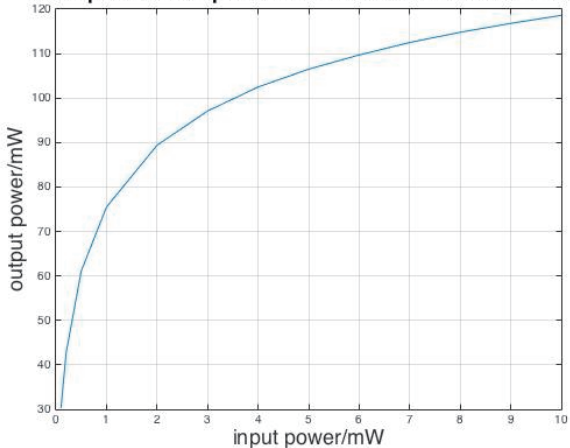


Fig. 3 The output power while changing the input power

The WDM was connected to the 1.15m long PM Er-doped fiber (EDF). Then the beam was introduced into this EDF. The peak absorption of this PM-EDF is 55dB at a wavelength of 1550nm. The PM-EDF was fusion spliced with a PM isolator and then to a 1:1 coupler to construct an all-PM fiber ring laser cavity. The isolator and fiber coupler were connected mechanically using an angled polished FC/APC fiber Connector. The total length of this laser cavity is 6.63m.

After the cavity is built, I measured the output power of the cavity. It is shown in figure 4. It increased linearly and reaches 95mW when the LD current is the maximum. If the cavity energy reaches about 10mW, it will damage the fiber on the connector when the SWNT film is inserted. So we need to carefully increase the LD current and make sure it is lower than 250mA.

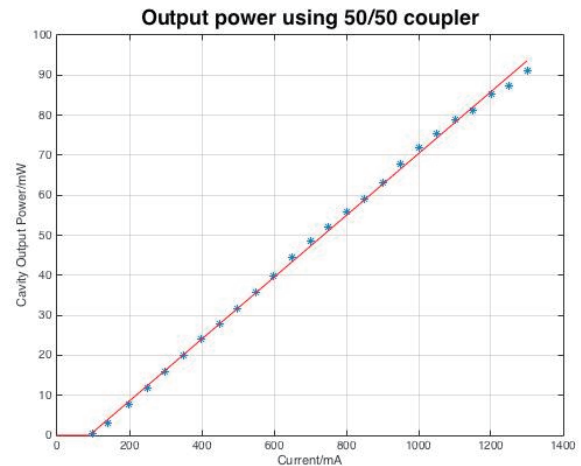


Fig. 4 Output power of the cavity before the SWNT film was inserted

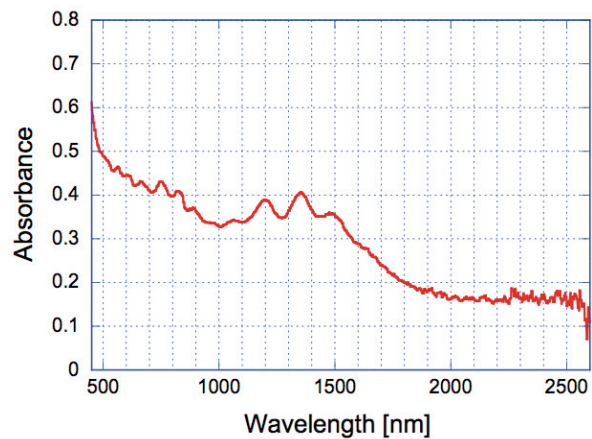


Fig. 5 Absorption spectrum of SWNT polyimide film.

A freestanding SWNT polyimide nanocomposite film saturable absorber has been demonstrated as a mode-locker. In this experiment, I used a polyimide film containing SWNTs synthesized by the high pressure CO (HiPco) method. Figure 5 shows the absorption spectrum of the film. The film thickness is 32 μm . The film had a broad absorption spectrum, and the absorbance at a wavelength of 1.55 μm is about 0.3. The refractive index of the polyimide film was about 1.58. A small film with dimension of 2mm*2mm was used as the saturable absorber.

The SWNT polyimide film was inserted in left connector in the figure 1. It is flexible and robust, so it was easily inserted between a pair of angled-polished FC/APC fiber connectors. Since the FC/APC connector were use to suppress the effect of reflection, the index matching fluid was not used. The total insertion loss of SWNT film was about 33% at a wavelength of 1.55 μ m. The cavity length was adjusted to obtain high-power single-pulse operation. The net dispersion of the cavity was estimated to be -0.1378ps². Because the cavity exhibited anomalous dispersion, stable soliton mode-locking operation was achieved.

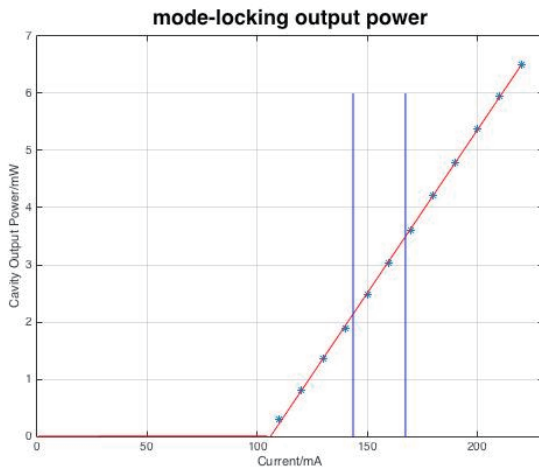


Fig. 6 Cavity output power as a function of LD current

Figure 6 shows the cavity output power as a function of the LD current. As the current increased, the output power increased linearly, and laser operation changed from cw lasing, to self-Q switching, and then single-pulse mode-locking, self-start mode-locking operation was achieved. As the LD current increased to more than 166mA, additional pulses appeared, resulting in multiple-pulse oscillation. The maximum average power in the single-pulse operation was 3.5mW. The zone between the non-zone output power and purple line is Q-switching zone, and the zone between the purple line and blue line is the single-pulse oscillation. The zone after the blue line is the multiple-pulse oscillation.

I used the autocorrelation trace method to measure the full-width at half-maximum (FWHM). I used FR-103XL which utilizes the SHG method of 1st kind in the conventional Michelson Interferometer set-up of pulsewidth measurement. In the standard configuration, noncollinear beams lead to the background-free autocorrelation. Repetitive linear delay generation in one arm of the Michelson arrangement is introduced by a pair of parallel mirror centered about a rotating axis. In the geometry of figure 7, the rotation of the parallel mirror assembly leads to an increase (or decrease) of path length for a traversing beam. Thus, the transmitted pulse train is delayed(or advanced) about the reference(zero delay) position. This delay varies with time as a function of the shaft's rotation. For small angular changes, the delay as a function of time is linear and given by

$$T = \frac{4\pi f D}{c} t \quad (1)$$

where D is the distance between the parallel mirrors, f is the frequency of rotation, and c is the speed of light.

Rotation of the parallel mirror assembly leads to a repetitive generation of linear delay which, used in the described SHG configuration, provides a continuous display of the autocorrelation function of the pulses on a conventional high impedance oscillation synchronized to this rotation.

The total scan range is given by

$$T_t = \frac{\sqrt{2}d}{c} \quad (2)$$

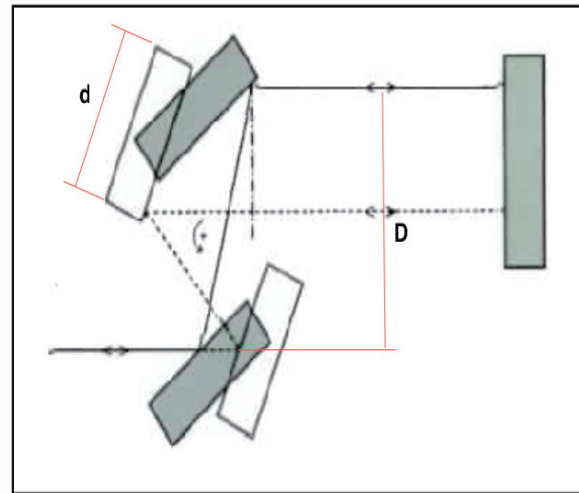


Fig. 7 Rotating parallel mirrors

In the standard configuration of the FR-103XL, the scan mirror has a size of d=1.7" and the mirror are separated by a distance of D=3". The rotation frequency is f = 5Hz(in this case). Hence we can calculate T/t = 15.5psec/msec and T_t=200psec.

However, there is a weak dependence of the calibration factor on the position of the pulse peak within the scan window. Therefore, the exact experimental calibration factor must be determined by the translation of the corner-mirror forward and backward about a given measurement position and the mean value of the two corresponding calibration factors determined must be used.

The conversion from FWHM auto correlation trace width(Δt) to the FWHM pulsewidth(ΔT) is a function of the assumed pulse shape. In Table 1, $\Delta t / \Delta T$ is given for commonly used pulse shapes.

Table 1 Relation between autocorrelation width and pulsewidth for various pulse shapes

Pulse Shape	$\Delta t / \Delta T$
Hyperbolic Secant	0.648
Gaussian	0.707
Single-Sided Exponential	0.5

After using the autocorrelation method to measure the temporal shape of the output, the can have a temporal spectrum on the oscilloscope shown in figure 8.

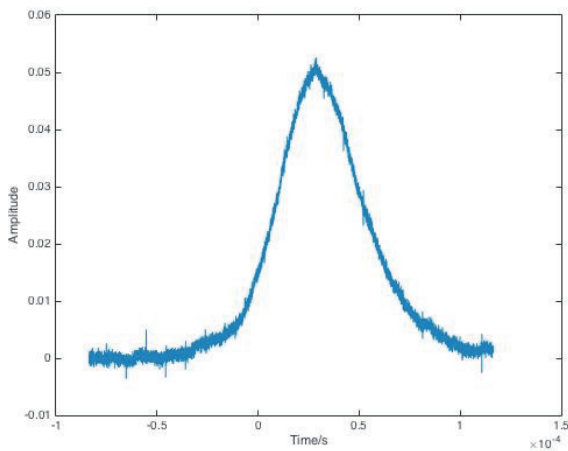


Fig. 8 Temporal spectrum of the mode-locking output

The FWHM of the temporal spectrum is about 0.045msec. Thus we can calculate the actual FWHM of the mode-locking pulse. It's 452fsec.

I also confirmed the spectrum of the all-PM passively mode-locked Er-doped ultrashort-pulse fiber laser using SWNTs. It is shown in figure 9. The spectral width was 5.2nm full-width at half-maximum which corresponding to 0.672THz. The time-bandwidth product was about 0.3038, which is almost equal to that of the transformation limited sech^2 pulse.

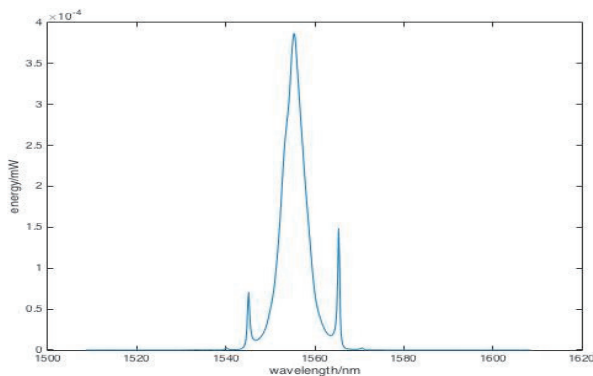


Fig. 9 Spectrum of mode-locking

I put the SWNT-polyimide saturable absorption film in the connector which is on the left of the coupler in figure 1(connector 1). Laser beam passes through the film after power division at the output fiber coupler. I also set the SWNT-polyimide in the connector which is on the right of the coupler in figure 1(connector 2) and examined the effect. For Connector 2, since the connector is before the coupler, so all of the energy passed through SWNT-polyimide film, mode-locking is also achieved. However the achieved pump energy is lower, and the threshold power of multiple-pulse operation is also lower. Moreover, the output power is larger when we put the SWMT-polyimide film in the connector 1 to achieved mode-locking.

When I removed and reinserted the SWNT-polyimide film at the fiber connector, the performance of the fiber laser was almost the same as before and showed good repeatability. This shows that SWNT-polyimide nano-composite film has good uniformity, stability, and robustness. In this work, the polyimide film containing SWNTs prepared by the laser ablation(LA) was also examined. However, it failed. So I used HiPco film in this work.

Conclusion

I demonstrated an all polarization-maintaining (PM) passively mode-locked Er-doped ultrashort-pulse fiber laser using a polyimide film with dispersed single wall carbon nanotubes. A 452fs ultrashort soliton pulse was stably generated from the fiber laser at a repetition frequency of 29.3MHz, and the maximum output power was 3.5 mW for single-pulse operation. Since this soliton fiber laser consisted of all PM type fiber devices and a robust SWNT-polyimide film, it shows stable and self-start operation.

Future Work

I haven't tried the HiPco 17um SWNT in this experiment, because it was lost. It has a smaller absorb index. I might obtain a higher power if I used that film. In this experiment, I used EDF which the dispersion is negative, the output energy of this kind fiber is relatively small compared to a EDF with a positive dispersion. So, it could generate a higher energy output if I could change the fiber. Also I need to cut some fiber or change a higher percentage output coupler to control the dispersion and increase the output power.

Acknowledgements

This research is done in Nishizawa Lab, Nagoya University. It is fully supported by Professor Nishizawa.

REFERENCES

- [1] Nishizawa, N., et al. "All-polarization-maintaining Er-doped ultrashort-pulse fiber laser using carbon nanotube saturable absorber." *Optics express* 16.13 (2008): 9429-9435.
- [2] Fermann, Martin E. *Ultrafast fiber oscillators*. Marcel Dekker, 2002.

- [3] Nishizawa, Norihiko. "Ultrashort pulse fiber lasers and their applications." *Japanese Journal of Applied Physics* 53.9 (2014): 090101.
- [4] Weiner, Andrew M. "Ultrafast Optics." *Chapter 3*: 85-146.
- [5] Nozaki, Y., N. Nishizawa, E. Omoda, H. Kataura, and Y. Sakakibara. "Power scaling of dispersion-managed Er-doped ultrashort pulse fiber laser with single wall carbon nanotubes." *Optics letters* 37, no. 24 (2012): 5079-5081.
- [6] Agrawal, Govind P. *Nonlinear fiber optics*. Academic press, 2007.

Extraction and Analysis of Trigger Rate and Pedestal Data from SciCRT

Goutham Thangaraj

Atmospheric Oceanic and Space Sciences, College of Engineering, University of Michigan
gtmth@umich.edu

Supervisors

Professor Yoshitaka Itow, Professor Matsubara,
Solar-Terrestrial Environment Laboratory, Division of Particle Area Astrophysical Science, Graduate
School of Science, Nagoya University
itow@stelab.nagoya-u.ac.jp

Professor Kazuo Shiokawa
Solar Terrestrial Environment Laboratory, Department of Electrical Engineering and Computer Science,
Graduate School of Engineering, Nagoya University

1. Abstract

This paper analyzes neutron trigger data over a period of ten seconds and sixty seconds and provides the combined trigger rate for a single data file that contains information for a period of an hour. Then, the data files are combined to obtain a month by month database. This database is used to obtain the pedestal data over the course of the operation of the SciCRT. The mean pedestal data for each month was then analyzed and variations in the data were scrutinized and studied.

2. Introduction

The study of solar flares is crucial to understanding not only how the Sun functions but also its effects on the Earth's atmosphere. Solar flares also have the ability to disrupt long distance radio signals and disturb orbiting satellites by increasing the drag experienced by the same. Worst of all, they can cause errors in satellite circuitry resulting in damage of components aboard a spacecraft. This provides sufficient reason to study the solar flare phenomenon. As of now, the acceleration mechanism in the creation of solar flares is not yet fully understood and is the topic under research in this paper.

Currently, it is known that during a solar flare, two kinds of particles are ejected out, ions and electrons. In order to understand the mechanism of a solar flare,

both particles accelerations must be observed and studied. Electron acceleration information is collected through hard X-Ray, radio wave and H α bright line observations. Proton (Ion) observations, however, are much more difficult as only the very high-energy protons reach the Earth's surface while the remaining protons get deflected from their path because of interplanetary and geomagnetic fields. In order to successfully obtain the necessary data, the gamma rays and neutrons produced by the interaction between the accelerated ions and the solar atmosphere are studied as they remain unperturbed by magnetic fields. The need for studying solar neutron observations so that the ion acceleration mechanism could be analyzed was the main cause for the implementation of the SciCRT project.

3. SciCRT Instrument

The detector consists of 14,848 plastic scintillator bars piled on top of each other to be used as a particle tracker. The instrument has a total of 64 layers. A combination of an 'X' and 'Y' plane with 116 bars on each side make up one layer. Apart from the top and bottom layers, the instrument is divided longitudinally into eight components each of which is called a superblock. Currently, there are three super blocks that are operational for solar neutron detection.

Each superblock consists of 7 Back End Boards (BEB). In turn, each BEB is connected to 4 Front End Boards (FEB) resulting in a total of 32 FEBs. Each FEB is connected to a Multi-Anode Photo Multiplier Tube (MAPMT) which consists of 64 channels. ADC values are obtained for each channel as neutrons are detected. For more information regarding the Data Acquisition System check references [1] and [2].

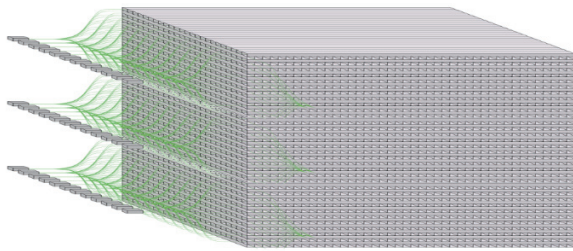


Figure 1: SciCRT Instrument

4. Raw Data File Format and Coding Platform

Each data file represents an hour data and provides ADC data for each channel of each FEB in that period. The name of each file gives us the Superblock the file originates from, the year, month, day and hour in which the data was recorded. For example, a typical data filename would be SN.1.15042414. This means that the data contained in the text file is from superblock 1 and the data is from 2 p.m. Sierra Negra Time (location of the SciCRT instrument) on the 24th of April 2015. Fig.2 shows an event in a typical data file.

```

17 1974 1980 1982 2000 1980 1967 1969 1984 2104 1855 1987 1986 1982 1973 1977 1974 1965 1983 1954 1980 1966 1980 1955 1953 1959 1976 1969 1968 1969 1981
1965 1981 1962 1969 1962 1968 1975 1963 1954 1956 1946 1970 1979 1963 1961 1967 1970 1953 1967 1986 1956 1969 1963 1964 1955 1940 1948 1943 1935 1956 1947
1962 1959 1960 20 1862 1877 1902 1891 1868 1875 1868 1867 1869 1880 1875 1878 1874 1867 1873 1869 1876 1870 1873 1887 1870 1893 1879 1890 1878 1881 1887
1898 1877 1889 1895 2019 1901 1907 1901 1908 1903 1899 1894 1899 1899 1898 1903 1896 1906 1881 1899 1902 1907 1898 1908 1901 1900 1918 1903 1888 1913 1896
1910 1888 1916 1900 1900 1913 -999
One Event Data Set
0 0 18 0 9 14 00 00
9 2009 2013 2036 1994 2013 1987 2015 2057 2032 1994 2005 2018 2008 2022 2006 2008 2019 1989 1990 2004 2004 2022 1981 2002 2001 1988 1982 2004 1998 2024
2082 2015 2004 2008 2061 2123 1989 2000 2014 2015 2022 2014 2006 2003 2026 2011 1974 1990 1981 2003 2014 2015 2008 1996 2018 2013 1989 2001 2004 2000 2019
2005 2007 1992 19 1977 2001 1984 1984 1984 1976 1970 1975 1972 1976 1986 1982 1952 1971 1968 1968 1976 1957 1959 1994 1979 1968 1985 1970 1986 1969 1977
2002 1992 1975 1991 1985 2234 2052 2023 2039 2048 2034 2035 2436 2051 2028 2025 2023 2033 2021 2034 2035 2028 2029 2026 2025 2020 2026 2015 2017 1999 2021
2034 2018 2006 2018 2022 2040 -999
0 2 8 0 10 14 00 00
11 1944 1960 1952 1947 1949 1943 1958 1954 1959 1950 1938 1950 1942 1939 1942 1958 1924 1923 1953 1944 1952 1945 1938 1954 1951 1944 1948 1949 1945 1953
1948 1961 1961 1969 1971 1981 1965 2116 2086 1960 1968 1981 1965 1960 1965 1938 1975 1958 1960 1952 1961 1973 1948 1948 1952 1945 1942 1954 1941 1950 1939
1963 1951 1949 19 1964 1992 1983 1982 1980 1976 1964 1972 1964 1972 1984 1980 1968 1970 1970 1967 1975 1955 1956 1991 1976 1966 1985 1971 1983 1969 1976
2003 1990 1973 1991 1987 2034 2039 2022 2037 2031 2030 2030 2012 2032 2024 2011 2019 2032 2017 2031 2032 2027 2016 2023 2019 2018 2024 2019 2020 2000 2143
2061 2017 2008 2018 2020 2044 -999

```

Figure 2: Event in a Data File

The coding was done on a CPU operating on Scientific Linux. ROOT was the software used to run all the described codes and obtain the necessary histograms and plots. It is an object oriented programming and library developed by CERN and is based on C++. All data stored on the database are initially in compressed form. The data for each month was then downloaded onto a hard drive and extracted to obtain the complete text files as described previously.

5. Trigger Rate

Trigger Rate is defined as the number of successful events obtained during the same time interval. The neutron data is obtained when the event satisfies a certain hardware condition, called the trigger condition. The trigger rate describes whether the data collecting hardware is functioning optimally.

A requirement in studying the solar neutrons is to know the sum total of all events that occur within a given hour in certain intervals of time. Code previously written by Nagai San displays the trend in the event number for every ten seconds for a certain data file. Modifying this code, the variation can now be obtained per minute. In order to prevent cluttering, only eight Front End Boards were processed at any given execution of the program. However, the code can be modified to show any of the four event blocks (BEBs) consisting of eight FEBs numbering from 0-31 with ranges of 0-7, 8-15, 16-23, 24-31.

Apart from the individual trigger rates, the cumulative trigger rate was also plotted along with a 5-sample running average curve to better illustrate the change in the number of events over the hour. The code can only be used for a certain superblock at any

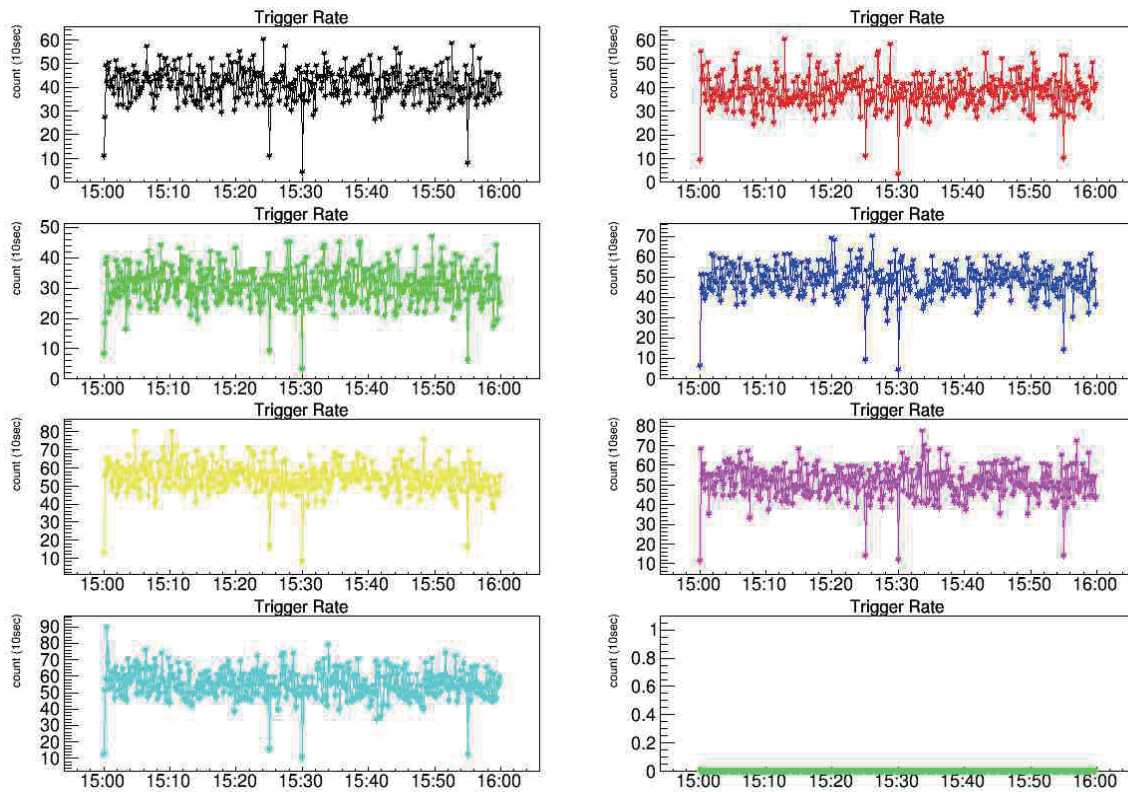


Figure 3: 10 Second Count Distribution

execution of the program although this can be varied before the program is made to run. Details of the graphs obtained and their analysis will now be further explained for data file SN.1.15042414.

Fig. 3 consists of neutron data accumulated over a period of 10 seconds for 8 FEBs of BEB 1 and of Superblock 1. This was done previously by Nagai-san, a previous member of the STEL in Nagoya University. It can be seen that the distribution of the counts is very irregular throughout the time period of one hour. An important thing to note is the flat line in the graph on the bottom right. This occurred because the final FEB on each BEB is non-operational and thus no data was recorded. The remaining 7 graphs represent the FEBs 1-7 from top to bottom, left to right. As can be observed from the graphs, the maximum count for a ten second interval is around 80. Larger dips in the count occur almost simultaneously in all the FEBs but the occurrence of peaks is more arbitrary. These graphs provide greater insight into the average number of events that can be expected at any given time for an FEB. The largest peak can be observed in FEB 7 where the count reaches a maximum of 90 while the lowest value can be found in FEB 4 with count of just 2.

Fig.4 is similar to Fig.3 in that they both show the count variation over a period of 1 hour. However, the difference lies in the fact that the count is now represented over a period of one minute rather than ten seconds. This, not only significantly reduces the number of points to be studied but also provides a clearer trend in terms of the number of events occurring by providing a smoother graph with low loss in data. As expected, as the counts occurring per minute are higher than that for every ten seconds, the graph scale has also risen to reflect a higher count rate. The highest peak still occurs in FEB 7, however, the time location of the peak has shifted because the graphs represent a minute time frame meaning that the count was consistently high for a period of minute in this timeframe rather than just a short burst of activity for ten seconds as represented by the Fig. 3. Contrary to the result of Fig. 3, the graph with the largest dip occurs in FEB 3 with a count of only 160. The results of Fig.4 were then summed together for all the FEBs of a certain BEB to bring Fig.5. Figure 5 is the cumulative trigger rate over the period of a single data file. It gives us the most accurate image of the number of solar neutron events any certain superblock experiences over a period of one hour. The figure also shows a five

element running average to provide a better picture of the curve and show the overall trend of the solar neutron flux over time.

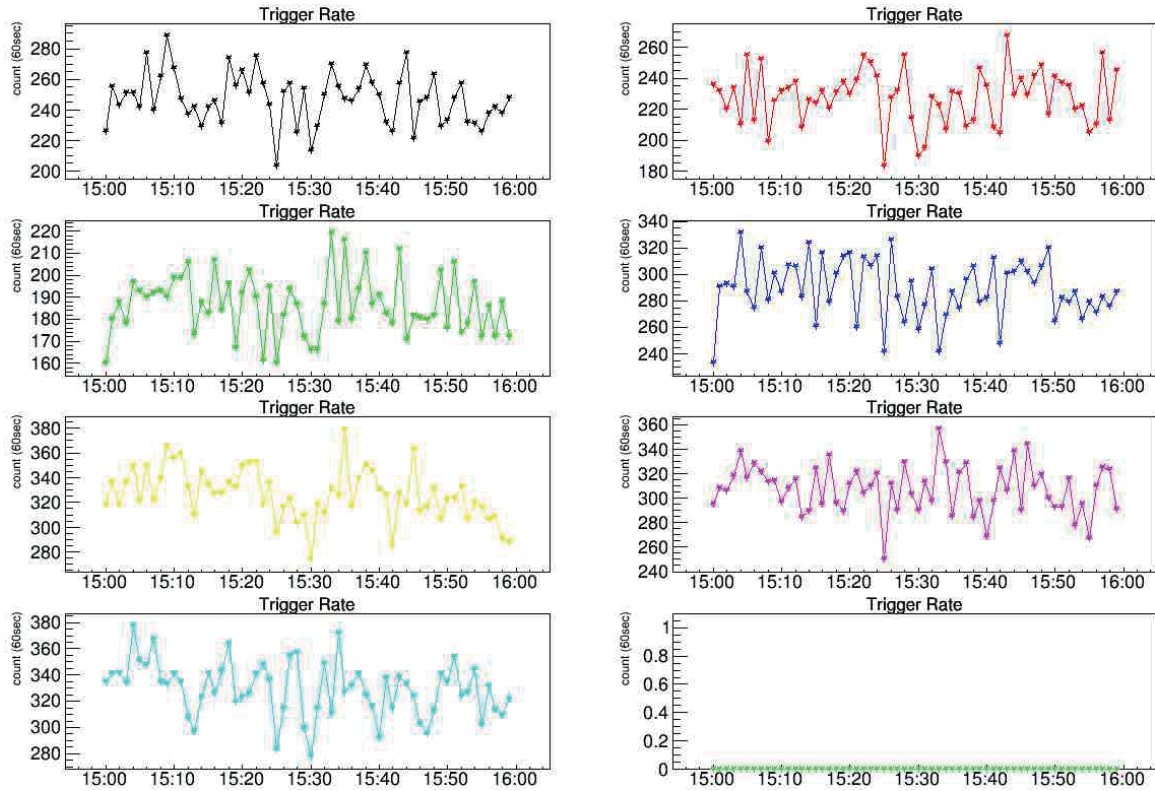


Figure 4: 1 Minute Count Distribution

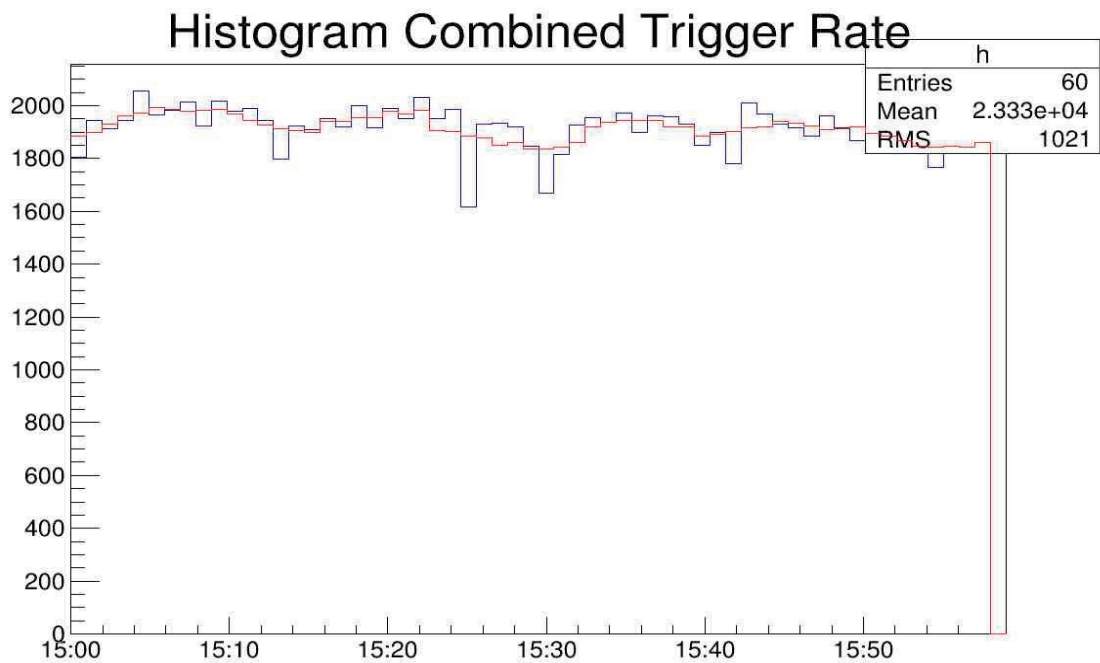


Figure 5: Cumulative Trigger Rate

```

2016 2038 2055 2032 2024 2042 2029 2024 2047 2036 2031 2051 2043 2048 2038 2033 2027 2027 2032 2026 2043 2027 2023 2035 2034 2031 2027 2031 2043 2043 2033
2036 2087 2078 2097 2103 2076 2086 2089 2089 2087 2080 2101 2098 2081 2082 2095 2099 2082 2079 2074 2089 2091 2077 2076 2096 2088 2081 2096 2086 2091 2092
2091 2083 -999
Pedestal Data of a Single File
2058 2053 2049 2062 2063 2074 2046 2024 2041 2036 2060 2074 2039 2038 2042 2034 2037 2029 2060 2043 2039 2048 2038 2043 2034 2035 2038 2045 2050 2038 2029
2026 2039 2047 2043 2025 2010 2033 2024 2018 2036 2030 2038 2042 2015 2028 2018 2029 2023 2021 2023 2027 2017 2009 2014 2007 2020 2010 2014 2024 2015 2023
2013 2027 -999
2009 1999 1997 2011 1999 2024 2004 2003 1996 2009 2015 1997 1986 1983 2000 1987 1981 1988 1977 2007 2003 1996 2008 1997 2001 2008 1980 1995 2005 1987 1993
2004 1996 2010 1994 1997 1998 2001 1988 1996 1994 1979 1989 1975 1987 2005 1993 1988 1981 1990 1980 1978 1989 1990 1980 1978 1969 1973 1977 1965 1982 1983
1971 1995 -999

```

Figure 6: Sample Pedestal Data

6. Pedestal Data

Every instrument, including the instruments aboard the SciCRT, have pedestal data that needs to be obtained in order to get the real value of the quantity being measured. Pedestal data is the obtained by turning on the instrument while not exposed to cosmic rays (although some might still appear). It is the default state of the sensor and can be considered as its zero value. Usually, the difference between observed data and the pedestal value of a particular channel will provide the actual reading of the sensor for that specific channel. The pedestal value of any instrument can be obtained by finding the highest peak in the ADC data as the ADC value with the highest count is the pedestal data for a channel. The variation in the pedestal data across months needs to be studied as variation in the temperature as well as problems with the instrument can change the pedestal data values and gives us better insight on how the pedestal data changes and how the observed data needs to be manipulated in order to obtain the actual data. This will require combining the hourly data files and plotting the data over several months. The overall process includes obtaining pedestal data for each file and storing them month-wise in text files. This month-wise pedestal data is then read and the mean pedestal and standard deviation are stored. The mean pedestal data is the plotted over a certain period of months from which the variation in pedestal data can be seen.

6.1 Combining Pedestal Data

As data is only available for each hour, the first step should be to extract the pedestal from each file and conglomerate them into another text file for easier access. This was done using pedestal data extraction for one file as written previously by Nagai San. By writing code that would access each file in a month, the pedestal data for each hour of each day for a certain month was extracted and stored in a file having the name of the month and

year the data was extracted from. This was also repeated for each superblock containing solar neutron data which, as of now, is a total of three superblocks. The data extracted was from August 2014 to April 2015. Each month can be accessed as when the data is made available and the relevant code is executed.

As shown in Fig. 6, the pedestal data for each month consists of 64 pedestal data values (one for each channel) terminated by a buffer value of -999 in order to segregate each file data and provide an easier form to read the data when the file is accessed by any other program.

6.2 Obtaining Mean Pedestal Data

Plotting all the pedestal data directly would result in long processing times and unnecessary use of computer resources. Thus, in order to get a quick yet accurate reading of the pedestal data, the mean pedestal value was calculated along with the standard deviation. This gives a simple and smooth representation of the data while simultaneously showing regions of error or variation in the values of the pedestal data over the period of months. This was done by accessing the output files of any one superblock as described in the previous section. Once the all the pedestal values were extracted, they were stored temporarily and then each channel's data was individually summed and divided by the total number of valid data taken from the file. This means that the times when the sensor was switched and had values of zero were ignored. The standard deviation was then calculated by again going through the files and measuring them against the mean value of the particular channel using the respective formula for calculating S.D. The program also places the monthly data one after another so that as each month is read, it is copied into the same file. This means that each file could contain anywhere

between one month's data to all the available months' data and is dependent on the user and the region under study. By generating all the output onto just one file, clutter formation was reduced with just one file creation being sufficient for each superblock.

6.3 Plotting Pedestal Data

Using the Mean Pedestal Data, the data was then plotted using the histogram function located in the ROOT library. As the plotting period depends on the size of the input file and the months for which the data was extracted, an integer scale was used in the X-axis to depict the each month in the data file with the first month being depicted in the range from 0-1, the second one being 1-2 and so on. This means that those analyzing the graphs must have access to the Readable Mean Pedestal Data File that was created in the previous section while obtaining mean pedestal data.

7 Analysis of Pedestal Data

As can be seen from Figures 7 and 8, the mean pedestal data was plotted for the months of August'14 to April'15. These two graphs show minimal change in pedestal data with variations lying within the margin of speculation. This is applicable to all of the 64 channels aboard the each of the Front End Boards. This shows the consistency of the pedestal data and the functioning of the SciCRT for these particular boards. There are other FEBs however that show larger variation in the counts. This can be observed in Figure 9, where there is a sharp drop in the counts in the month of January. This could be explained by the fact that the Superblock 1 of the Sci CRT was not fully functional during that period which is what resulted in the abnormal dip in the graph.

In Figure 10, we observe that there is a jump in the reading in February. There are a couple of reasons that can explain the step increase. First, the change in temperature during this period affected the SciCRT and has caused a change in the Pedestal Data Values.

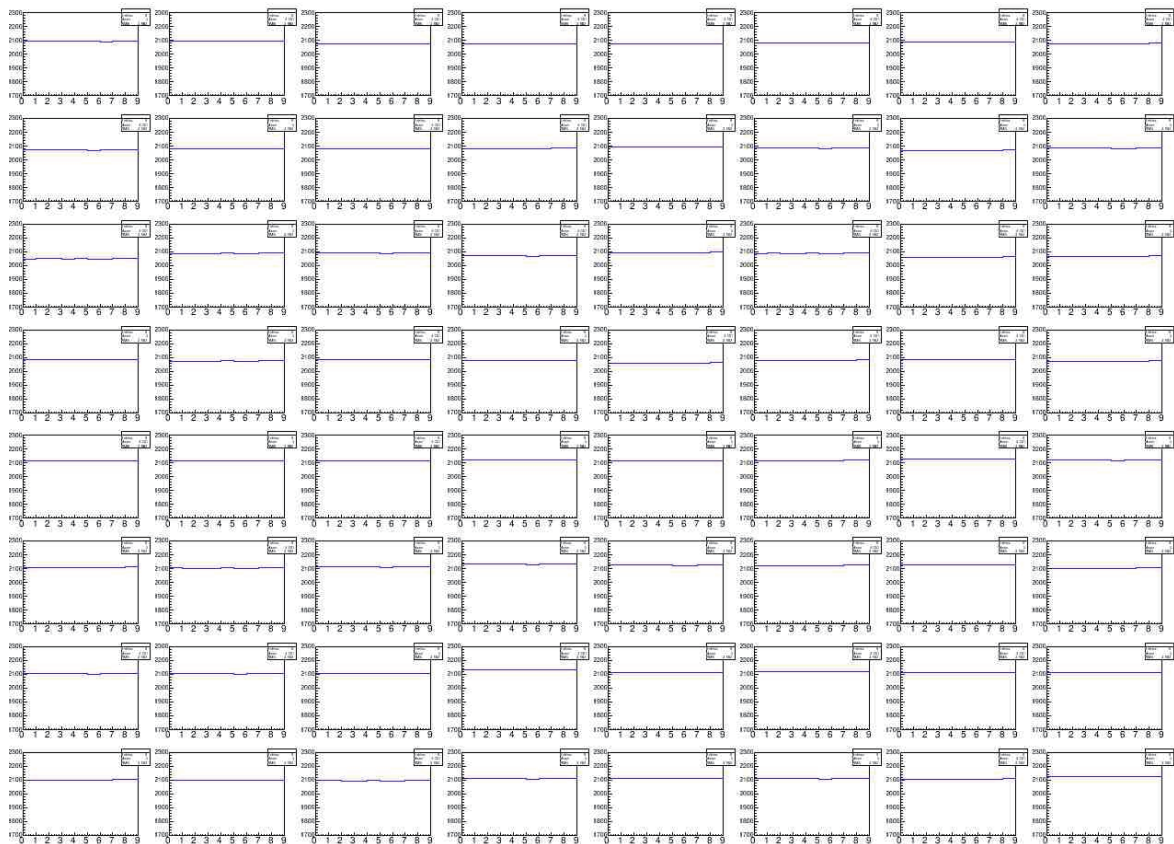


Figure 7: Superblock 1, Event Block 2, Connector 0

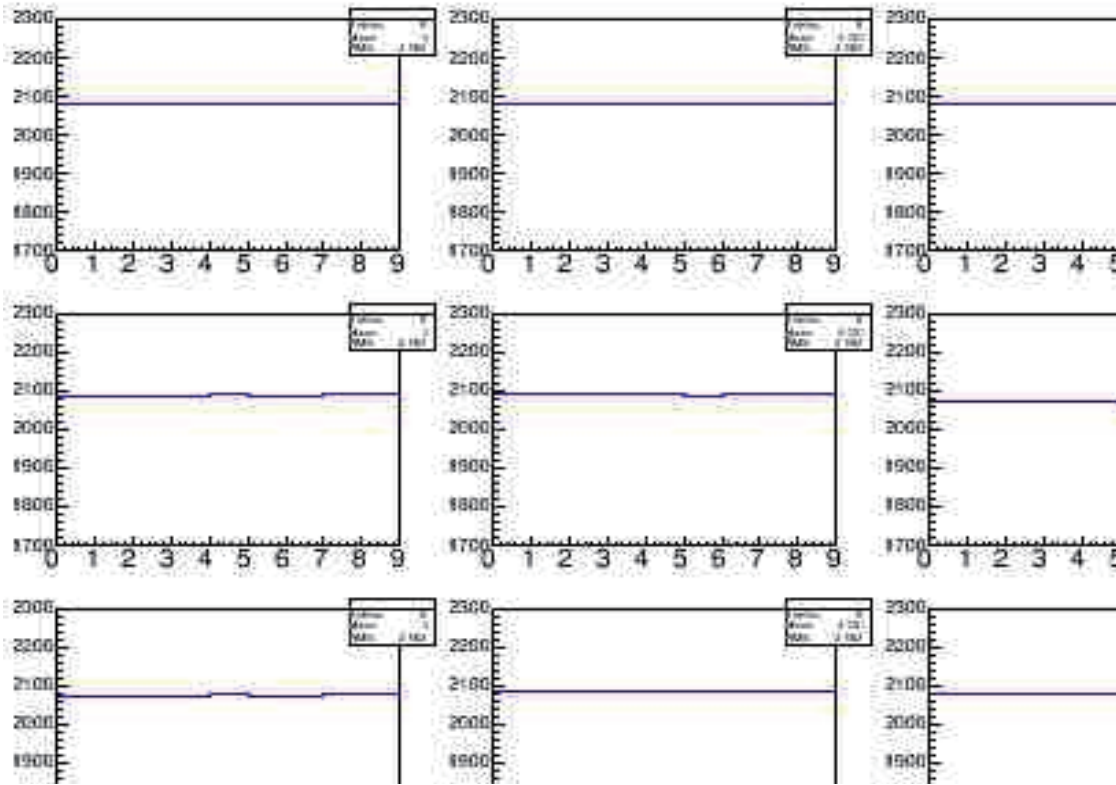


Figure 8: Zoom up of Figure 7

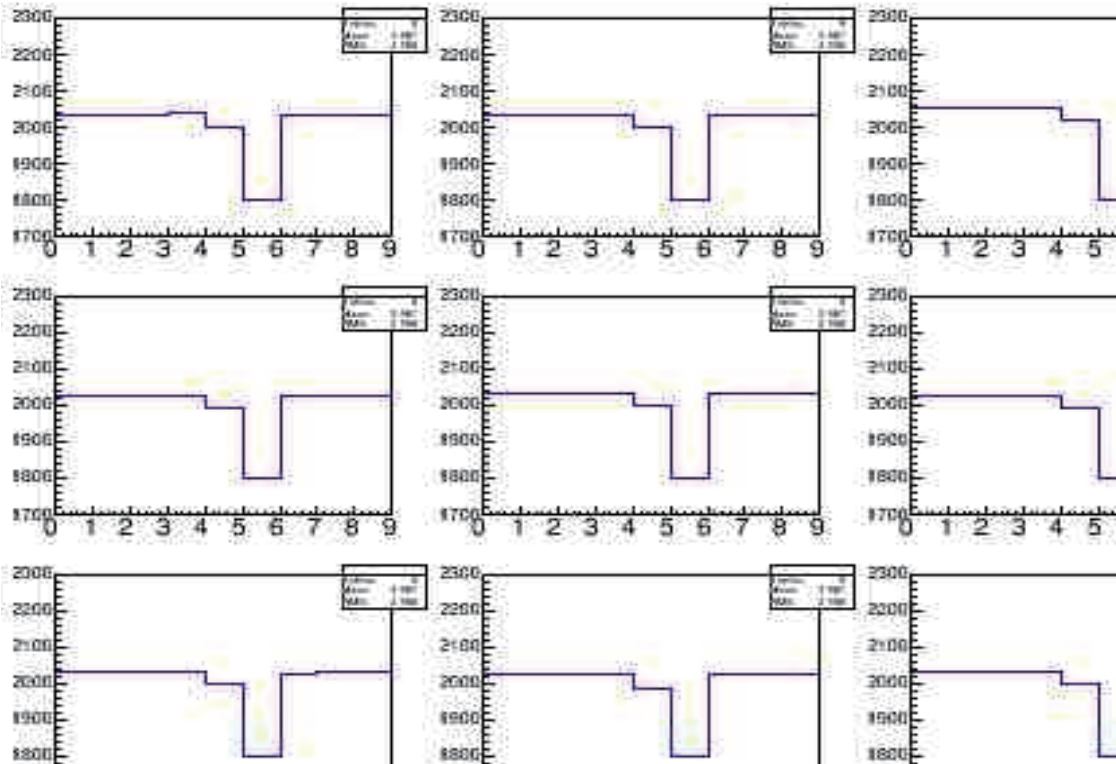


Figure 9: Zoom up of Superblock 1, Eventblock 2, Connector 1

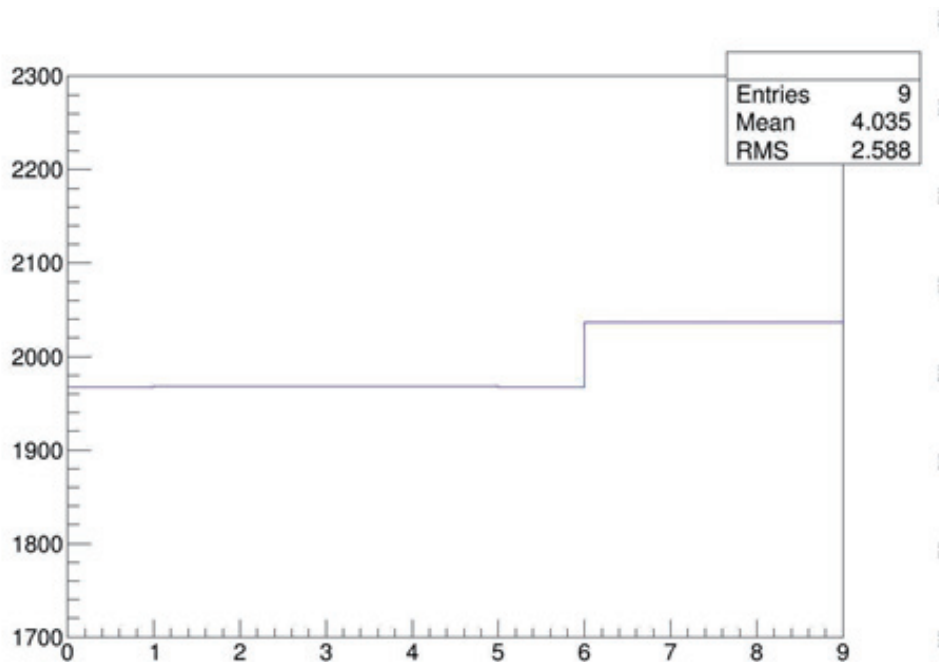


Figure 10: Pedestal Data for Channel 1 of Superblock 1 of Back End Board 4 Front End Board 2

Alternatively, re-calibration of the SciCRT may have affected the pedestal value for certain FEBs this one being one of them. For the most part, the pedestal data does not show any significant change in value during the operation of the SciCRT. This provides us with the information required towards eventually calculating the neutron flux.

8 Future Work

Next, the calculation of the gain data is crucial. This will require an understanding of the physics behind the incoming solar neutrons and application of relevant formulas to solve the gain. This, along with the pedestal and ADC data, will be used to calculate the neutron flux and associate it back to the ions produced on the Sun to study the acceleration mechanism which is the final goal of the project. Apart from this, a user friendly interface that utilizes the concept of classes and objects that can smoothly obtain the required pedestal, gain and ADC data along with other time stamp information, from a certain time period needs to be implemented.

Also, the variation in the pedestal data needs to be studied in further detail to confirm the reasons as to

why there is a sudden change in some FEBs. This will give us a better picture of how the SciCRT is affected by certain events and the protective as well as risk mitigation measures that can be implemented to prevent such disturbances from happening in the future.

9 Conclusion

Thus, the neutron trigger data was analyzed for a period of ten seconds as well as sixty seconds. The pedestal data was also obtained from the raw data files and plotted to be used in further calculations. Certain discrepancies in the pedestal data were explained but needs further looking into.

10 Acknowledgements

I would like to thank Professor Itow and Professor Matsubara for providing well needed guidance throughout the project and providing opportunities to learn the Japanese work culture. I would also like to thank Professor Shiokawa for becoming my mentor for this program. Finally, I would like to thank all the JUACEP staff who made this program, and hence, this paper possible.

11 References

[1] *Y. Nagai, Y. Matsubara, Y. Itow, T. Sako, D. Lopez, Y. Sasai, T. Itow, K. Munakata, C. Kato, M. Kozai, T. Miyazaki, S. Shibata, H. Takamaru, H. Kojima, H. Tsuchiya, K. Watanabe, T. Koi, J.F. Valdés-Galicia, A. Hurtado, O. Musalem, E. Ortiz, L.X. González, M. Anzorena, R. Garcia*, First cosmic-ray measurements by the SciCRT solar neutron experiment in Mexico

[2] *Sasai et al.*: Performance of the SciBar cosmic ray telescope (SciCRT) toward the detection of high-energy solar neutrons in solar cycle 24. *Earth, Planets and Space* 2014 66:130.

A STUDY ON TOPOLOGY OPTIMIZATION WITH FEM BASED ON LEVEL SET METHOD

Chen Wang

Department of Mechanical Engineering, University of Michigan, Ann Arbor
chnwang@umich.edu

Supervisor: Toshiro Matsumoto

Department of Mechanical Science and Engineering, Nagoya University
t.matsumoto@nuem.nagoya-u.ac.jp

ABSTRACT

This report studies on topology optimization of the linear elastic problem formulated by level set method. Based on the formulation, the design sensitivities are derived using adjoint variable method. With the derived sensitivities, topology optimization algorithm is constructed, in which the Finite Element Method (FEM) is used to solve the equilibrium equations and to update the level set functions. A numerical implementation for generating finite element mesh based on level set method is proposed. A three-dimensional practical example is given to demonstrate the validity and utility of the proposed implementation.

1. INTRODUCTION

Structural optimization has been intensively studied in few decades and successfully utilized in some industrial areas. Structural optimization is classified into sizing optimization, shaping optimization and topology optimization (Fig.1 [1]). The topology optimization is first proposed by Bendsøe and Kikuchi in 1988 [2], which is considered as the most powerful design method amongst the three methods. In the field of topology optimization, certain methods are essentially mature and very effective in a variety of industrial settings such as automotive and aeronautical industries.

The basic ideas of topology optimization consist of (1) the extension of a design domain to a fixed design domain, and (2) replacement of the optimization problem with a material distribution problem using the characteristic function that requires a value of 0 or 1 in the fixed design domain. Since the characteristic function can be very discontinuous, some regularization techniques are used. However, there are still some limitations of these conventional topology methods. On the other hand, new types of optimization methods based on level set method have been proposed so as to overcome the limitations of conventional methods.

In this report, the basic principles and derivations of topology optimization based on level set method are studied.

The equations of time evolution problem and design sensitivities are then investigated. Afterwards, general algorithm of numerical implementation is proposed. Finally, a three-dimensional example of linear elasticity problem is discussed to validate the proposed numerical implementation.

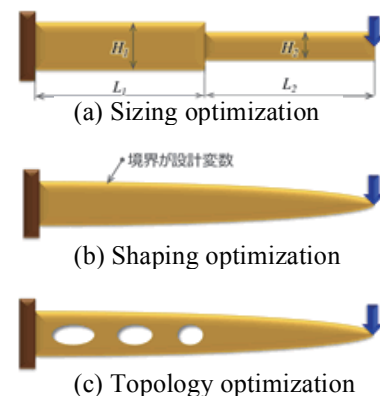


Fig.1 Structural optimization classification

2. FORMULATIONS

2.1 Level set-based topology optimization method using a fictitious interface energy model [3]

Here, we briefly discuss the basic concept of the level set-based topology optimization method using a fictitious interface energy model based on the phase field concept. Suppose that a fixed design domain D is composed of a domain filled with a solid material, i.e. a material domain Ω , and another complementary domain representing a void exists (Fig.1). Here, the level set function ϕ is introduced to represent the structural boundaries using the isosurface of the level set function ϕ as follows:

$$\begin{cases} 0 < \phi(x) \leq 1 & \text{if } \forall x \in \Omega \setminus \partial\Omega \\ \phi(x) = 0 & \text{if } \forall x \in \partial\Omega \\ -1 \leq \phi(x) < 0 & \text{if } \forall x \in D \setminus \Omega \end{cases} \quad (1)$$

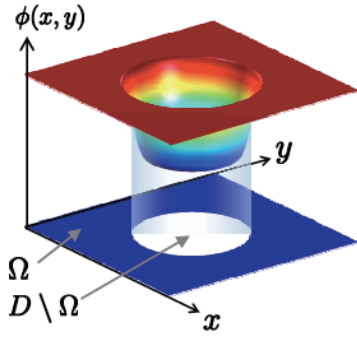


Fig.2 Fixed design domain D and level set function ϕ

In the formulation above, the level set function has upper and lower limits imposed, which are required for the representation of the fictitious interface energy that is defined using the gradient of the level set function. Therefore, as shown in Fig.2, the level set function does not have the characteristic of a signed distance function but is instead a function of which values are -1 in the void domain and 1 in the material domain with a smooth distribution in the neighborhood of the boundaries.

Based on the shape representation above, the optimization problem is formulated as follows:

$$\inf_{\phi} F = \int_D f(x)\chi_{\Omega}(\phi)d\Omega \quad (2)$$

subject to

$$G = \int_D g(x)\chi_{\Omega}(\phi)d\Omega - G_{max} \leq 0 \quad (3)$$

where F is the objective functional, G is the constraint functional, G_{max} is the upper limit value of G , and χ_{Ω} is the characteristic function defined as

$$\chi_{\Omega} = \begin{cases} 1 & \text{if } \phi \geq 0 \\ 0 & \text{if } \phi < 0 \end{cases} \quad (4)$$

The optimization problem above is an ill-posed problem since the optimal configuration expressed by the level set function is not required to be continuous, and as a result, obtained optimal solutions may be discontinuous everywhere in the fixed design domain. Although in conventional topology optimization methods the design domain is relaxed using various regularization techniques such as a homogenization method, such techniques cannot be directly applied in optimization methods that use level set boundary expressions.

In response, a new topology optimization method, based on level set boundary expressions incorporating the Tikhonov regularization method, has been proposed. In this method, the level set function is sufficiently continuous after the regularization always exists. The basic concept of this method is to embed the level set function in a fixed design domain and add a fictitious interface energy term derived from the concept of the phase field theory to the objective functional, to regularize the optimization problem, as follows:

$$\inf_{\phi} F_R = \int_D f(x)\chi_{\Omega}(\phi)d\Omega + \int_D \frac{1}{2}\tau|\nabla\phi|^2d\Omega \quad (5)$$

subject to

$$G = \int_D g(x)\chi_{\Omega}(\phi)d\Omega - G_{max} \leq 0 \quad (6)$$

where F_R is a regularized objective functional and τ is a regularization parameter. This fictitious interface energy not only relaxes the design domain but can also be used to specify the complexity of the optimal structure because controlling the fictitious interface energy is equivalent to implicitly controlling the perimeter. Exercising such control may increase the availability of useful optimal solutions from an engineering standpoint. We note that the regularization method above is called the Tikhonov regularization method and published details are available concerning its theoretical background.

2.2 Topology optimization of linear elasticity problem

The general expressions of topology optimization of linear elasticity problem are shown as follows [4]:

$$\begin{aligned} \inf_{\phi} \bar{F}_R = & \int f_1(u)dD + \int_D f_2(u, \phi)dD \\ & + \int_D \frac{1}{2}\tau|\nabla\phi|^2dD + \int tvdD \\ & + \int_D \epsilon(u):E:\epsilon(v)\chi(\phi)dD \\ & + \lambda(\int_D g(\phi)dD - G_{max}) \end{aligned} \quad (7)$$

where \bar{F}_R is the Lagrangian and λ is the Lagrange multiplier of the constraint functional G . The Karush-Kuhn-Tucker (KKT) conditions of the optimization problem above are given by

$$\frac{\delta\bar{F}_R}{\delta\phi} = 0, R = 0, \lambda G = 0, \lambda \geq 0, G \leq 0 \quad (8)$$

By solving the above KKT conditions, we obtain optimal solution candidates of the level set function ϕ , but obtaining optimal solutions directly is problematic. Therefore, an initial solution is derived by updating the level set function based on the gradient of the objective functional. Let a fictitious time t be introduced and assume that a change in value of the level set function is proportional to the gradient of the Lagrangian \bar{F}_R , as shown below:

$$\frac{\partial\phi}{\partial t} = -K \frac{d\bar{F}_R}{d\phi} \quad (9)$$

where $K > 0$ is a coefficient of proportionality. Submitting Eq. (5) into Eq. (9) and after introducing appropriate boundary conditions, we have

$$\begin{cases} \frac{\partial \phi}{\partial t} = -K \left(\frac{d\bar{F}(\chi_{\Omega}(\phi))}{d\phi} - \tau \nabla^2 \phi \right) \\ \frac{\partial \phi}{\partial n} = 0 & \text{on } \partial D \setminus \partial D_N \\ \phi = 1 & \text{on } \partial D_N \end{cases} \quad (10)$$

where ∂D_N represents non-design boundaries. These boundary conditions represent the level set function independent of the exterior of the fixed design domain.

Finally, after concern calculation, the system of time evolutionary equations (10) is as follows:

$$\begin{aligned} \frac{\partial \phi}{\partial t} &= -K \left(\frac{\partial f_2(u, \phi)}{\partial \phi} + \epsilon(u) : E : \epsilon(v) \chi(\phi) \right. \\ &\quad \left. - \lambda \frac{\partial g(\phi)}{\partial \phi} - \tau \nabla^2 \phi \right) \end{aligned} \quad (11)$$

3. NUMERICAL IMPLEMENTATION

Optimization algorithm

A flowchart of the optimization procedure is shown in Fig.3. In the first step, the level set function representing an appropriate initial shape is provided. In the second step, the mesh is generated by a three-dimensional mesh generator. In the third step, the equilibrium equation is solved using the finite element method (FEM). In the fourth step, the objective functional is calculated. If the objective functional converges, the optimization process is finished. Otherwise, the flow steps in next step. In the fifth step, the sensitivities of the objective functional with respect to the design variables are computed. In the sixth step, the level set function is updated using the finite element method (FEM) and then the optimization procedure is repeated from the second step.

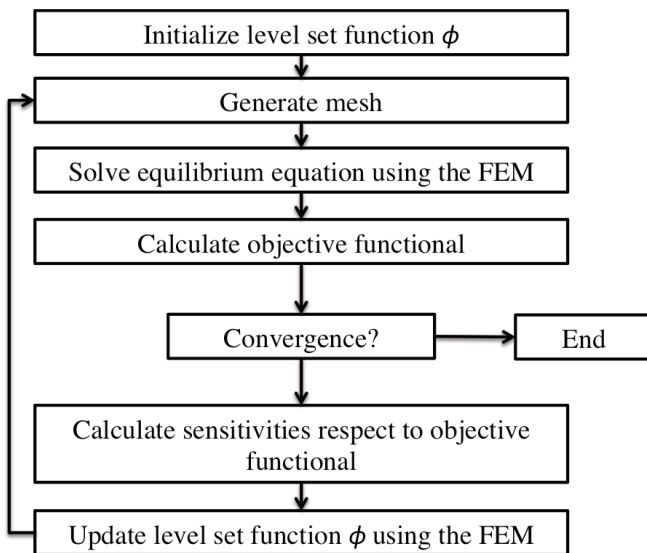


Fig.3 Algorithm flowchart of the optimization procedure

4. NUMERICAL EXAMPLES

4.1 Optimization problem description

Here, we deal with a topology optimization of a linear elasticity problem with non-design domain. As shown in Fig.4, a rectangular solid is the fixed design domain with two non-design domains of cylinder on opposite sides of the rectangular solid. It explores the possibility to extend topology optimization from design domain to design and non-design combined domain.

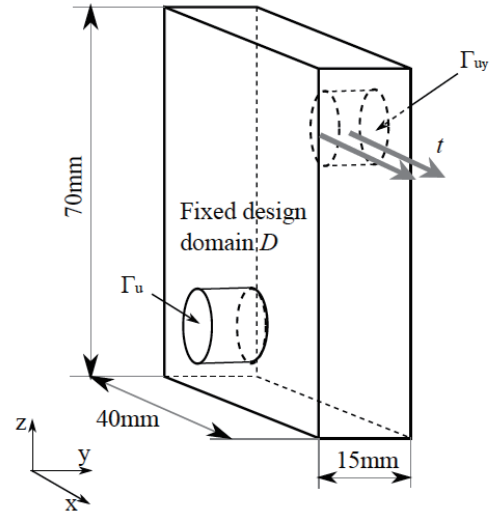


Fig.4 Optimization problem with non-design domain

4.2 Simulation results

The Fig.5 shows the initial configuration, optimizing procedure and final configuration. From the results, the configuration is gradually optimized. In practical sense, the original structure can be seen as handle which is widely used in daily life.

5. CONCLUSION

In the report, the topology optimization of linear elasticity problem is studied by level set method. The main conclusions are shown as below.

(1) Based on the formulation, the design sensitivities are derived using adjoint variable method. With the derived sensitivities, topology optimization algorithm is constructed, in which the Finite Element Method (FEM) is used to solve the equilibrium equations and to update the level set functions.

(2) A numerical implementation for generating finite element mesh based on level set method is proposed. A three-dimensional practical example is given to demonstrate the validity and utility of the proposed implementation.

Currently, more complicated configurations are tested to be optimized by the proposed numerical implementation method above in order to confirm the universal validity and utility in linear elasticity optimization problem.

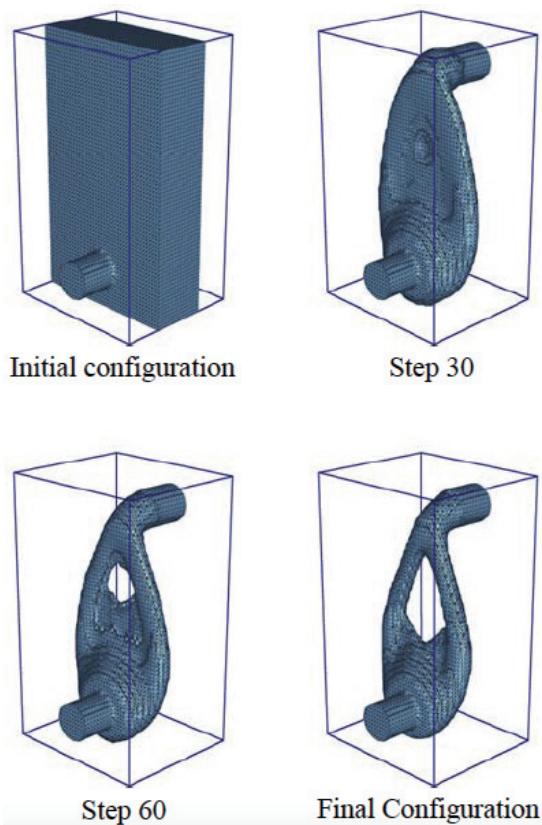


Fig.5 Configuration optimization process

ACKNOWLEDGEMENTS

All the research data and work belong to Matsumoto Lab (Computational Mechatronics Group). Thanks for the instructions of Prof. Toshiro Matsumoto, and help from the lab members with this report.

REFERENCES

- [1] Manufacturing Systems Engineering Laboratory of Kyoto University, Homepage, http://www.osdel.me.kyoto-u.ac.jp/members/overview_nishiwaki.html.
- [2] Bendsøe, M.P. and Kikuchi, N., Generating Optimal Topologies in Structural Design Using a Homogenization Method, *Computer Methods in Applied Mechanics and Engineering*, 71, pp. 197-224 (1988).
- [3] Takayuki Yamada, Kazuhiro Izui, Shinji Nishiwaki, A Level Set-Based Topology Optimization Method for Maximizing Thermal Diffusivity in Problems Including Design-Dependent Effects, *Journal of Mechanical Design*, 122, pp. 64-71 (2011).
- [4] Takayuki Yamada, Akihisa Suzuki, Toshiro Matsumoto, Toru Takahashi, A Level Set-Based Topology Optimization Method Considering Design Dependent Load Using a Three-Dimensional Mesh Generator, *Transactions of JSCEs*, Paper No.20120006 (2012).

Effect of Surface Treatment on Mechanical Properties of DLC Coating

Hanyi Xie

Department of Mechanical Engineering, University of Michigan
xiehy@umich.edu

Prof. Noritsugu Umehara

ume@mech.nagoya-u.ac.jp
Graduate School of Engineering, Nagoya University

Associate Prof. Hiroyuki Kousaka

kousaka@mech.nagoya-u.ac.jp
Graduate School of Engineering, Nagoya University

Assistant Prof. Xingrui Deng

deng@mech.nagoya-u.ac.jp
Graduate School of Engineering, Nagoya University

ABSTRACT

DLC coatings are widely applied on sliding parts due to their good wear resistance, low friction coefficient, high hardness. However, little is still known about their properties. In this research, annealing tests were carried out at temperatures from 200 °C up to 800 °C for Inconel X750 alloy disks with ta-C coating to study the mechanical properties' change of DLC film. Co, Ni and SUJ2 were used as metal catalysts contacting with ta-C film during annealing. Increasing temperatures up to 400 °C led to the increase in hardness, while increasing temperatures higher than 400 °C resulted in the hardness decreased from the peak. ta-C contacted with SUJ2 has highest hardness under all temperatures.

I. INTRODUCTION

Diamond-Like Carbon (DLC) coatings are often expected to be applied to prevent wear due to their excellent tribological properties, such as low friction, high hardness, chemical stability, etc. DLC is very resistant to abrasive and adhesive wear [1] making it possible to use in applications that experience extreme contact pressure, both in rolling and sliding contact. These properties are usually linked to the mixed presence of sp^3 bonds and sp^2 bonds. The higher, the higher the sp^3 / sp^2 ratio, the more the film structure approaches that of diamond and consequently the higher is the film hardness [2].

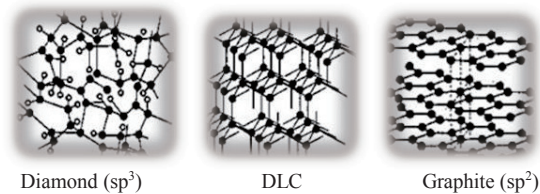


Figure 1. Bond structures of carbon allotropes

The hardening conditions and related mechanisms, however, have not been well understood. The same holds for structures of these films and the reason of hardness changes after annealing. In particular, is it caused by changes of density, or diffusion between metals and coating? Therefore, a study of investigating the explanation is a great importance.

In this study, ta-C was coated on Inconel X750 alloy disks. Co, Ni, and SUJ2 [3] were used to contact with coating for annealing [4]. Then the hardness at the contacting area was examined by Nano indentation. Vickers Hardness test was conducted to make marks in order to eliminate dispersion uncertainties.

The study first illustrates material preparation, annealing test set-up, the marking way done by Vickers hardness test, hardness measurements by Nano indentation, Nano-scratch test and analysis by using Energy-dispersive X-ray spectroscopy (EDS). Results including hardness, AFM images, and EDS analysis are then presented. Hardness results and possible explanations are discussed in the third section. And the last section provides conclusions and future works.

II. EXPERIMENTAL METHOD

In this research, Inconel X750 alloy manufactured into disks with 20mm in diameter and 2mm in thickness was coated by ta-C with thickness of 607.0 nm. Ni, Co, SUJ2 were cut into pieces in dimension of 3mm x 3mm. The hardness of disks and metal specimens was measured by Vickers hardness test and the surface roughness was detected by Profilometer.

Table 1. Material Properties

Material	Hardness (GPa)	Roughness (nm)
ta-C	52	23
Ni	6.1	25
Co	5.2	21
SUJ2	14	21

Ni, Co, SUJ2 specimens were pressed on the surface of the coated disk which were placed on the jig under 0.3kgf·m normal load. The set-up is shown in Fig. 2.

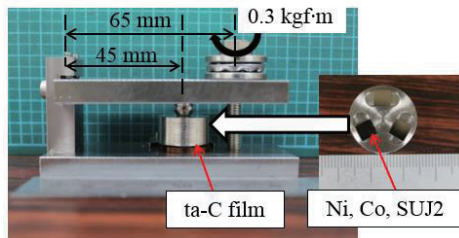


Figure 2. High temperature contacting catalysis system

The jig then was settled into a vacuum environment as shown in Fig. 3. All experiments were performed on the same set of samples. First, the original hardness and surface roughness of as-deposited film was measured and subsequently annealed for 1 hour in vacuum at 200 °C. Then the same step was repeated for the rest of as-deposited films conducted at 300 °C, 400 °C, 500 °C and 800 °C.

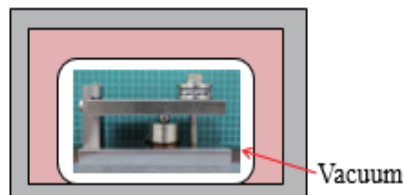


Figure 3. Annealing Test Set-up Schematic

After annealing test, in order to measure the hardness eliminating dispersion uncertainties, Vickers indentation was used to mark specific positions for Nano-indentation and Nano-scratch tests.

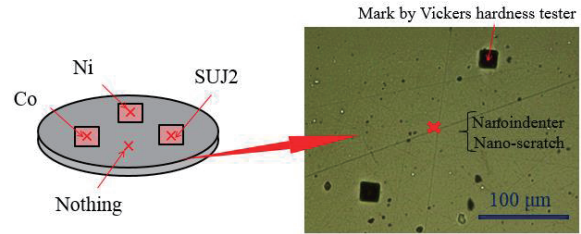


Figure 4. Making Marks by Vickers Hardness test

Nano-indentations were conducted to get the average hardness for ta-C film contacting with different metals. Nano-scratch test (the experiment condition was shown in Table 2) was carried out as well at the same position marked by Vickers test to ensure the reliability.

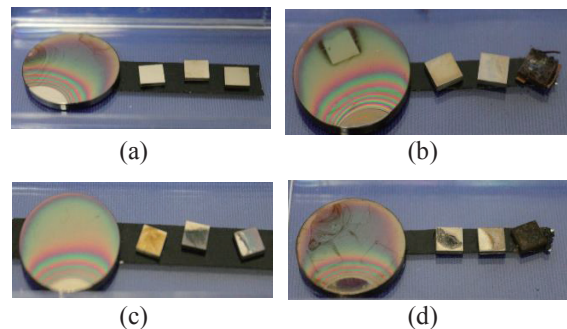
Table 2. Nano scratch test conditions

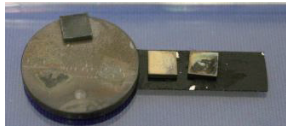
Scratch test	
Normal load	5000 nN
Number of scratch	10 times
Scratch range	1000 nm × 1000 nm
Scratch speed	1.0 μm/s

Finally, EDS was performed to detect elements' distribution due to diffusion.

III. RESULTS AND DISCUSSION

The specimens after annealing are shown in Fig. 5. According to photos, the contacting traces were more obvious with increasing the annealing temperature. In addition, under 800 °C, SUJ2 was not able to take off from the disk.





(e)

Figure 5. Photos of specimens after annealing test:

(a). 200 °C, (b). 300 °C, (c). 400 °C, (d). 500 °C, (e). 800 °C

After annealing test, Nano-indentation was conducted to measure the hardness in the contacting area of ta-C coating and metals, as well as the blank position without any metal contacted. The primary data of hardness are shown in Fig. 6.

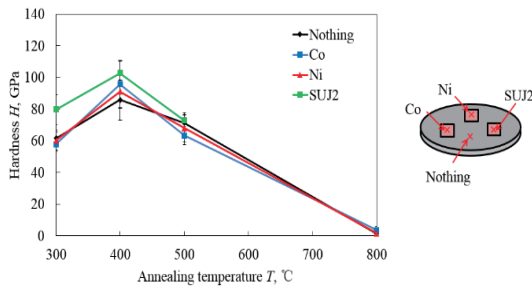


Figure 6. Primary Result of Hardness

The primary results show that the hardness increases with increasing the annealing temperature. The maximum hardness appears at 400 °C. In particular, SUJ2 reaches the value higher than 100 GPa, which is as hard as diamond. Since the hardness of the detecting needle of Nano-indentation is only 92 GPa. The value higher than 100 GPa might not be correct. A possible explanation is about Elastic Power (n_{IT}).

$$n_{IT} = \frac{W_{elast}}{W_{elast} + W_{plast}} \times 100$$

Theoretically, n_{IT} should not be larger than 100%. Since the boundary condition is that there is elastic case only. That means data with $n_{IT} > 100\%$ should not be used for calculation.

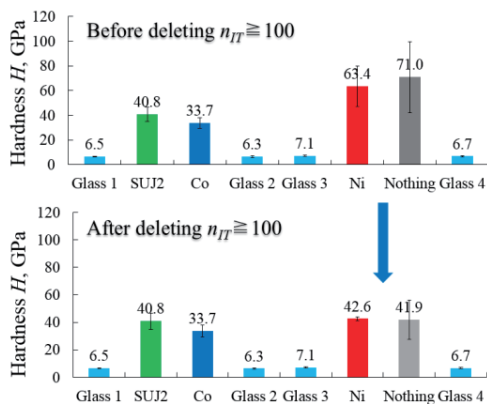


Figure 7. Comparison for deleting $n_{IT} > 100\%$ data points

Figure 7 shows the change of hardness values before and after deleting data with $n_{IT} > 100\%$ for 500 °C specimens. The hardness of Ni and blank position reduced from 63.4 GPa and 71.0 GPa to 42.6 GPa and 41.9 GPa.

By repeating the same step for specimens at other temperatures, revised hardness values are presented as shown in Fig. 8.

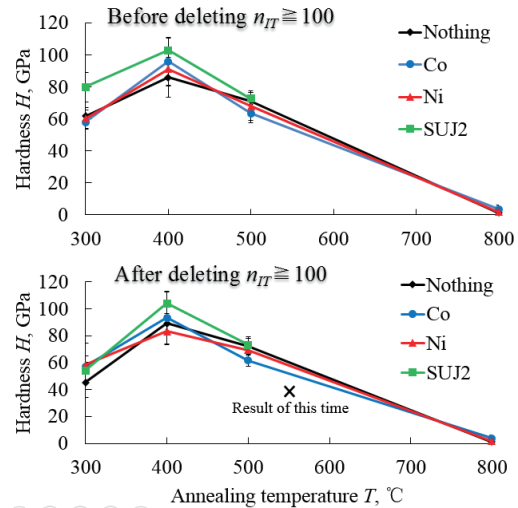


Figure 8. Comparison for deleting $n_{IT} > 100\%$ data points

According to Fig. 8, the hardness increases with raising the annealing temperature until 400 °C. The maximum hardness appears at 400 °C. Compared to Ni and Co, the hardness of ta-C contacted with SUJ2 is the highest at all temperatures. While when annealing temperature goes higher than 400 °C, hardness decreases with temperature increase.

Nano-scratch test was also conducted to ensure the hardness measurement. Figure 9 shows the AFM images after scratch test for 0, 5, 10 times.

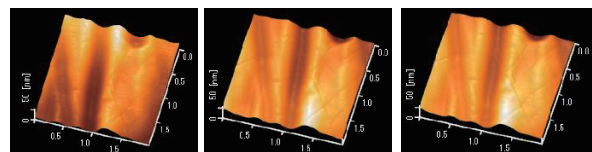


Figure 9. AFM images of scratch test

(a). number of scratch: 0, (b). number of scratch: 5, (c). number of scratch: 15

According to Fig. 9 and results in Fig. 10. The surface was not removed so much after scratch tests, which means the ta-C coating surface is very hard.

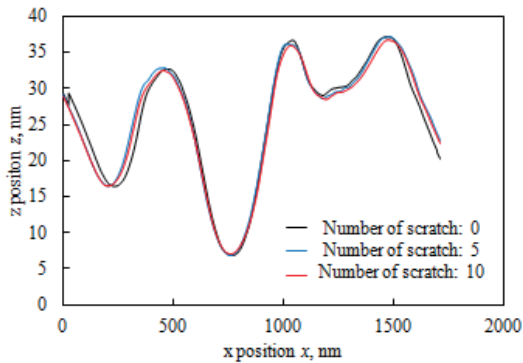
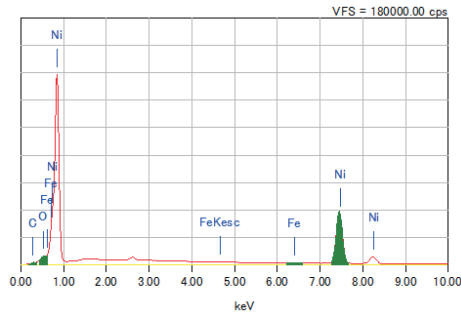
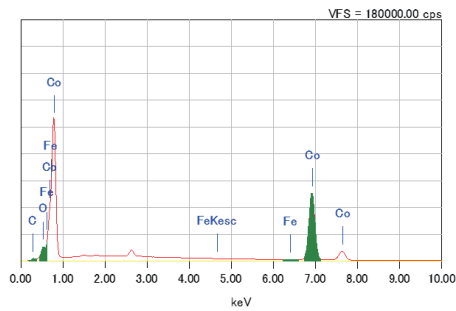


Figure 10. Cross section of ta-C Nano-scratch test

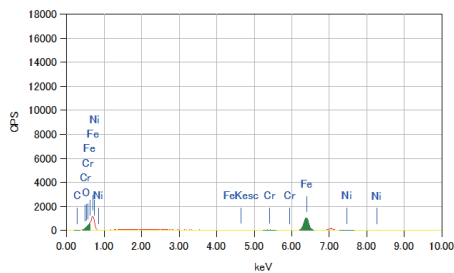
To investigate the reason for ta-C's hardening, EDS was conducted to detect elements distribution after annealing test. From Figure 11, carbon was detected, which means carbon diffusion might happen due to metal catalyst's effect.



(a)



(b)



(c)

Figure 11. EDS analysis: (a). Ni, (b). Co, (c).SUJ2

IV. CONCLUSIONS

This report has explored the characteristics that ta-C films will become harder after annealing test. Disks made of Inconel were coated by ta-C. Then three different metals were put on the top surface of coating layer under normal force in vacuum environment being heated for 1 hour at different temperatures. After annealing, the hardness of ta-C in contacting area increased with annealing temperature increasing until 400 °C. When annealing temperature goes higher than 400 °C, hardness decreases with temperature increase. Compared to Ni and Co, the hardness of ta-C contacted with SUJ2 is the highest at all temperatures.

More effort has been put into investigating possible explanations. Nano-scratch tests were conducted to ensure the hardness, which shows that even if after 10 times scratches, the surface profile hardly changed. In addition, EDS was carried out to measure the elements diffusion. Results show that carbon was detected after annealing test, which illustrates carbon diffusion might happen during the annealing.

In future work, tests can be conducted to further understand the reason why ta-C films become super hard after annealing. In addition, more thoughts can be given to develop hardness change in various conditions, such as high pressure, etc.

ACKNOWLEDGEMENTS

Foremost, I would like to express my sincere gratitude to my supervisor Prof. Umehara, Prof. Kousaka, and Prof. Deng for the continuous support of my study and research, for their patience, motivation, enthusiasm, and immense knowledge. Their guidance helped me in all the time of research and writing of this report.

Besides, I would like to express my heartfelt thanks to my TA, Eitaro Nakatani. He spent a lot time teaching and helping me in these three months. I am very appreciated working with him on this project.

My sincere thanks also go to students in Umehara's lab who helped and contributed great ideas and suggestions on this research.

And lastly, I would like to say thanks to the JUACEP program for giving me this chance to get evolved in such an excellent lab in summer 2015, which will be the precious experience in my life.

REFERENCES

- [1] Holmberg K, Matthews A, Ronkainen H. Coatings tribology—contact mechanisms and surface design[J]. Tribology International, 1998, 31(1): 107-120.
- [2] D. Schneider, C.F. Meyer, H. Mai, et al., Diamond Relat. Mater. 7 (1998) 973
- [3] M. Zheng, K. Takei, B. Hsia, H. Fang, X. Zhang, N. Ferralis, “Metal-catalyzed crystallization of amorphous carbon to graphene”, Applied Physics Letters, vol. 96, 063110 (2010)
- [4] Kulikovskiy V, Vorlí V, Boháč P, et al. Thermal stability of microhardness and internal stress of hard aC films with predominantly sp² bonds[J]. Diamond and related materials, 2003, 12(8): 1378-1384.
- [5] Z.P. Huang, D.Z. Wang, J.G. Wen, M. Sennett, H. Gibson, Z.F. Ren, Effect of nickel, iron and cobalt on growth of aligned carbon nanotubes

QUASI-PASSIVE ELASTIC EXOSKELETON CONTROL BASED ON MECHANICAL JOINT KINEMATICS

Yalim Yıldırım

Department of Mechanical Engineering, College of Engineering, University of Michigan
yalimy@umich.edu

Supervisor: Professor Yasuhisa Hasegawa

Department of Micro-Nano Systems Engineering, Graduate School of Engineering, Nagoya University
hasegawa@mein.nagoya-u.ac.jp

ABSTRACT

Many human running exoskeleton prototypes use joint angle measurement to infer the transition from swing phase to stance phase. The exoskeleton PEXER developed in our laboratory (Fig. 1) uses Bioelectric Potentials (BEP) to perform this task. Although this is a novel and promising approach, it currently does not suffice for accurate and consistent gait cycle mapping. This paper investigates the use of joint angle data readily available on the PEXER exoskeleton to infer the swing-to-stance phase transition. The hip joint of the exoskeleton that connects the hip to the ball of the foot was fitted with a potentiometer to collect angular velocity data. Pressure sensors were connected to the ball and heel region of the shoe soles to detect heel and toe strike. A 6 km/h running test showed that the angular velocity of the exoskeleton hip joint switches signs 84 ± 13 ms before heel strike for the left leg, and 91 ± 36 ms for the right leg, verifying that this switch consistently precedes heel strike and can potentially be used to predict the end of swing phase.

Undisclosed

DIRECT PRODUCTION OF HIGHLY PRESSURIZED PURE HYDROGEN

Douglas Chen

Materials Science and Engineering, University of California Los Angeles
dc14@ucla.edu

Supervisor: Professor Seiichi Deguchi

Graduate School of Engineering, Thermal Energy Engineering, Nagoya University
deguchi@nuce.nagoya-u.ac.jp

ABSTRACT

Production of gaseous hydrogen was attempted through various methods. The first method was by reacting urea aqueous solutions with aluminium powder in a metallic reaction chamber. The second method was by reacting aqueous ammonia solutions with powder TiO_2 catalysts modified to include platinum. The first method produced hydrogen, hypothesized to be caused by reaction of aluminium with water. The consumption of aluminium in the reaction resulted in attempts to find a reusable catalyst in the form of modified TiO_2 . Experiments run with this catalyst did not result in hydrogen production, although previous experiments using the same materials have been successful. The failure could be attributed to improper replication of the reactants and catalysts. The reactants used to synthesize the catalysts were past expiration date. It is hoped that with successful hydrogen production with the TiO_2 catalyst, it can then be used to react urea via a simple process.

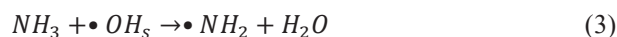
MOTIVATION

Energy is an extremely important issue in continued technological development for society. Energy production and storage are both critical issues faced in development today. Environmental friendly renewable methods to produce energy are strongly desired, as is a stable and high capacity method of storage. Electricity can be easily created by utilizing sunlight in photovoltaics or wind in wind turbines. However, storage of this electricity is currently problematic, as battery technology is currently lacking in safety and high capacity.

Another proposed method for energy creation and storage is via hydrogen storage and fuel cells. Hydrogen is high in energy density and can be safely stored in high pressure gas tanks, though alternative methods of safe storage are also being researched. Such stored hydrogen can then be fed to a fuel cell in order to create electricity, thus making hydrogen an appealing alternative to energy storage. A major factor in developing a hydrogen system is a facile

renewable method of hydrogen production. Of particular note in this paper is the creation of hydrogen from urea. It is hoped that ultimately urine could be used to create hydrogen, thus resulting in the production of hydrogen from human waste. Thus an environmentally friendly method of energy production would be possible in the stored form of hydrogen.

It has previously been proven that hydrogen can be created by the photocatalytic conversion of ammonia to hydrogen via the following reactions, following the photoexcitation of electrons from TiO_2 causing the formation of holes and surface hydroxyl radicals¹.



The catalyst used in these reactions is a modified TiO_2 catalyst that contains platinum. The catalyst is synthesized by depositing platinum upon the surface of the catalyst in solution while illuminated by UV light.

It is the ultimate goal of the experiments performed in this paper to decompose urea into natural products, specifically ammonia, in order to synthesize hydrogen. This production can be accomplished via a known photocatalytic conversion. If urea can be used to synthesize hydrogen, the next procedure to develop would be to utilize urine in order to create hydrogen, thus resulting in a sustainable hydrogen production method that consumes and reduces human waste.

EXPERIMENTAL METHODS

The experimental setup for the first method is a steel cylindrical tube in which aluminum powder and an aqueous urea solution of 40 wt% urea were mixed and placed. This

tube was evacuated of gases via vacuum pump, and then sealed and heated to a temperature of 200 or 300 °C. The reaction chamber was left at this temperature for times beyond 2 hours, at which point the reaction had totally consumed the available reactants. A gas was created, and could fill empty bags in order to achieve equilibrium. Samples of this gas were then extracted and run through gas chromatography in order to identify the hydrogen gas as well as other gases that may have been present.

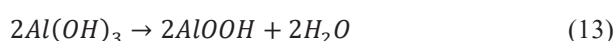
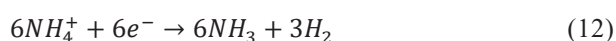
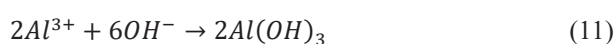
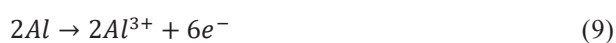
The experimental setup for the second method is a glass container with two separate sections. Catalyst preparation was performed by combining 1.990 g TiO₂ powder (Aeroxide TiO₂ P90) with 0.058 g hexachloroplatinate (Kanto Chemical Co., Inc. Hydrogen Hexachloroplatinate(IV) Hexahydrate) in a solution of 50 mL water and 50 mL methanol (Wako methanol, 99.5% assay). The reactants and solutions were stirred together by magnetic mixing bar while illuminated by UV light for approximately 12 hours. The modified catalyst powder was then washed and filtered through filter paper and dried in an oven running at 150 °C. For the photocatalytic conversion of ammonia to hydrogen, around 10 mL ammonia solution and 30 mL H₂O was mixed together with 0.4 g of the catalyst. Cooling water was run through one section in order to drive the reaction in the other section. The reaction was run for several hours and maintained at a temperature of 10 °C. Gas samples could be extracted directly from the reaction chamber and then run through gas chromatography.



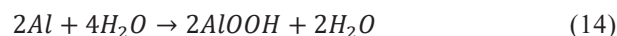
Fig. 1 Experimental setup for second method of hydrogen production.

RESULTS AND DISCUSSION

The first method of hydrogen production was found to produce a relatively pure hydrogen gas. However, it was found that this hydrogen production process was due to the reaction of aluminum with water, according to reaction equations of



As seen here, aluminum reacts with water. The water is then regenerated from the ammonia present. Thus pure aluminum is consumed, making the production method unsustainable. The overall reaction would be:



These proposed reactions were confirmed when pure water was reacted with aluminum, which resulted in the production of hydrogen. The results of these experiments can be seen in table 1.

Table 1 Urea Concentrations of Reactants and Resulting Hydrogen Concentrations for First Method

Urea Concentration (wt%)	Temp. (°C)	Equilibrium Pressure (MPa)	H ₂ Concentration
40	200	1.5	99.6
40	300	4.0	99.1
0	300	2.5	99.8

The second method of hydrogen production is the reaction of ammonia with photocatalytic TiO₂. The overall goal of the project is to decompose urea in order to produce ammonia. However, current reactions of the catalyst with ammonia have been unsuccessful, as no hydrogen has been detected. It is believed that the reaction does not occur due to improper synthesis of the catalyst. This could be due to several factors. The major issues include the condition of the reactants. The age of the reactants may be beyond the expiration date. In the case of the hexachloroplatinate (an anhydrate), it has absorbed water from the environment, making it heavier in mass compared to its original state. Thus the platinum content of the TiO₂ catalyst is unknown, leaving the possibility that the catalyst does not meet the correct conditions for photocatalytic conversion. Secondly, the TiO₂ may have changed in chemical structure over time, as evidenced by a light grey color compared to the original white. This could again lead to a catalyst that does not meet the requirements for photocatalytic conversion of ammonia. The environmental conditions of the reaction may not have been adequately met.

CONCLUSION

In the experiments listed here, direct gaseous hydrogen was produced via two methods. In the first method, aluminum reacted with water in a heated steel cylindrical reaction chamber to form hydrogen. The second method was the synthesis of hydrogen by photocatalytic conversion of ammonia to hydrogen with the presence of platinum-loaded TiO₂. The first method proved to be unsustainable due to consumption of aluminum, while the second method has so far been unsuccessful. However, after the second method has been successfully replicated, it is hoped that urea

solutions can be decomposed into ammonia which can then be converted to hydrogen. Thus a renewable and sustainable hydrogen production process may be developed by the processing of urine.

ACKNOWLEDGEMENTS

Special thanks to Professor Seiichi Deguchi for hosting me in his lab, everyone in JUACEP for accommodating me at Nagoya University, and my newfound friends in the Deguchi lab for their help and friendship.

REFERENCES

- [1] Yuzawa, H., Mori, T., Itoh, H., Yoshida, H., Reaction Mechanism of Ammonia Decomposition to Nitrogen and Hydrogen over Metal Loaded Titanium Oxide Photocatalyst, JPCC, 116, pp. 4126-4136 (2012).

AN INVESTIGATION OF THE TOP-DOWN APPROACH FOR GALLIUM NITRIDE NANOWIRES USING METAL MASK AND SIMPLE DEVICE FABRICATION USING GALLIUM NITRIDE NANOWIRES GROWN IN HVPE

Jiang, Yifan

Department of Electrical Engineering
Henry Samueli School of Engineering and Applied Science, University of California, Los Angeles
yjjiang5043@ucla.edu

Supervisor: Lekhal, Kaddour

Department of Electrical Engineering and Computer Science
Graduate School of Engineering, Nagoya University
lekhal.kaddour@yahoo.fr

Bae, Si-Young

Department of Electrical Engineering and Computer Science
Graduate School of Engineering, Nagoya University
bae@nuee.nagoya-u.ac.jp

Amano, Hiroshi

Department of Electrical Engineering and Computer Science
Graduate School of Engineering, Nagoya University
amano@nuee.nagoya-u.ac.jp

ABSTRACT

Bottom-up approach for GaN nanowire growth is introduced. A simple device with source and drain is fabricated by GaN nanowires grown in HVPE. Top-down approach using self-assembled metal mask for the GaN nanowires is also investigated. Different RIE etching power and time are tested. Moreover, Au and Ni mask are used and tested for different metal thickness, RTA temperature and time. Experiment shows that both of the two metal can be used as the mask for nanorod etching. As a mask, Ni is more durable than Au but no isolated Ni islands can form even the RTA temperature is as high as 850°C. Investigation of the two approaches with PL, TEM and EDX analysis show that nanowire/nanorod structure is available for device fabrication and implies some benefits for applications.

1. INTRODUCTION

As a large band-gap semiconductor, GaN is an important material in applications of different fields such as light emitting diode (LED), laser diode (LD) and field effect transistor (FET). Nowadays, the typical planar structure is still dominant in GaN-based devices. Those planar GaN grown on a foreign substrate has problems of dislocations

and cracks due to lattice mismatch and thermal expansion. Nevertheless, a different structure, nanowire/nanorod is developed, which may overcome the problems mentioned above by relaxation. Moreover, with the large aspect ratio, nanowire/nanorod is typically considered as a one-dimensional nano-structure. Therefore, Nanowire-based one dimensional electronics is expected. For example, high-performance graphene transistors based on highly doped GaN nanowires has been reported [1]. Furthermore, the nanowire/nanorod structure is reported to be used for LED fabrication, a method which implies possibilities for higher-efficiency and lower-cost light resources [2-6]. Nanowire/nanorod structure can also be used for overgrowth of a-plane GaN and better crystal quality is reported [7]. Nanowire/nanorod structure provides the opportunity for important development in future devices. Those devices can be from zero-dimensional to three-dimensional and new functionality to electronics, photonics, magnetic and thermal devices will be possible. For the interest of GaN nanowire/nanorod applications, two aspects naturally become attractive to study, the growth of GaN nanowire/nanorod and the device fabrication using nanowire/nanorod.

Basically, there are two methods for the growth or generation of GaN nanowire/nanorod: bottom-up approach and top-down approach. For bottom-up approach, the nanowire/nanorod is grown on a substrate in HVPE or MOCVD. Catalyst, such as Ni, Au and Pd can be used for the nucleation of GaN in HVPE. In MOCVD, Trimethylgallium (TMG) is used. For top-down approach, desired structures (for example, multi-quantum well) are grown or coated on planar GaN. Then, patterned nano-mask (typically, by rapid thermal annealing (RTA) of metal) is coated or formed on the top surface, following with etching process. For a specified GaN template, the quality of the nanowire/nanorod by this method is basically determined by the two key-steps: nano-mask formation and etching.

In this report, both of the two methods for nanowire/nanorod growth or generation are investigated. For the top-down approach, the nano-mask formation is focused. Two kinds of metal, Ni and Au are tested. The size and density distribution is studied with the influence of RTA temperature and time; with the influence of the metal thickness. Reactive-ion etching (RIE) and inductively coupled plasma (ICP) etching are used to test the result of nanowire/nanorod generation. For the bottom-up approach, HVPE is used for nanowire growth. The grown nanowire is tried to be fabricated to a simple device (only source and drain).

2. METHOD AND EXPERIMENT

2.1 BOTTOM-UP APPROACH

The bottom-up approach is capable for the growth of long GaN nanowires. In HVPE, Ni is used as a catalyst for GaN nucleation. A nickle layer is coated on a sapphire substrate and put into the reactor of HVPE. The temperature in the whole reactor is kept high and Ni will form nano-islands or nano-droplet structure. HCl and Ga are introduced into the reactor with N₂ ambient for reaction. HCl gas react with liquid Ga and form Ga-Cl at 780°C; NH₃ is also introduced and react with Ga-Cl to form GaN at 950°C. As shown in the phase diagram (Fig. 1), at this temperature, Ni is close to the melting point. However, in microscale, the melting point can be lower and Ni is liquid. The liquid phase of Ni is very important. It is easier for the Ga-Cl bond to be broken on the Ni droplet and the Ga atom is attached and collected into the Ni droplets with N atoms. N atoms has low solubility in the Ni droplets and may diffuse to the interface (between the substrate and the droplet), where Ga reacts with N atom to form GaN. In MOCVD, the process is similar. However, only the substrate is heated to high temperature and TMG, instead of Ga-Cl, is used for reaction. Other part of the reactor is kept with relatively low temperature to avoid the pyrolysis of TMG. The growth rate of nanowires in HVPE is larger than the growth rate in MOCVD. Thus, HVPE is more available to grow long GaN nanowires for single-nanowire device fabrication. However, the growth rate in HVPE is too large and introduce difficulties for the growth of hetero-structures. Therefore,

MOCVD is preferable for those devices with hetero-structures, LED for example.

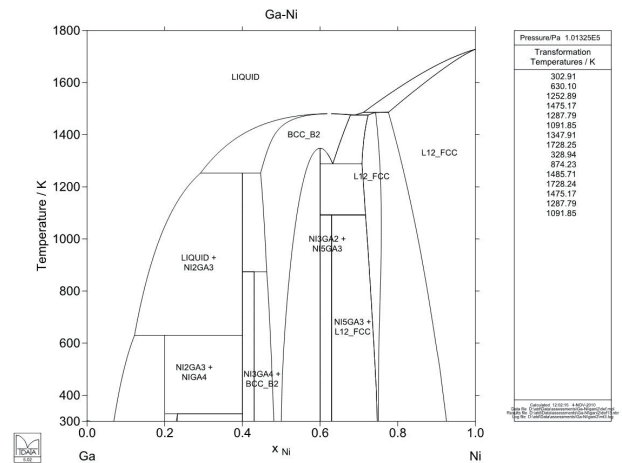


Fig. 1 Calculated Phase Diagram of Ga-Ni [8]

With the nanowires grown by HVPE (from my colleague [9]), a simple device is fabricated. A commercial 111, n-type silicon substrate is coated with 400nm SiO₂ through sputter deposition. A single nanowire is transferred mechanically to the surface of the SiO₂ layer. Photolithography is used to make source and drain patterns on the SiO₂ surface and the nanowire is connected between the source and drain pattern. Ti/Al/Ti/Au layers with thickness of 30/100/30/100nm are coated through e-beam evaporation. After lift-off, 650°C, 5min RTA is operated for the final formation of the source and drain.

2.2 TOP-DOWN APPROACH

The top-down method is straightforward. A template with GaN grown on sapphire substrate from my lab colleague [10] is coated with 200nm SiO₂ by sputter. The whole sample is then cut into two group of pieces which are coated by 10nm Au and 10nm Ni respectively by E-beam evaporation. The samples with Au is then processed by 550°C, 10min RTA and the samples with Ni is then processed by 850°C, 5min RTA. After annealing, the metal layer is expected to form self-assembled nano-islands. Those islands become masks for etching. In the optimal condition, it is expected that after RIE, the part of the SiO₂ layer not covered by the metal islands is totally etched and the part of the SiO₂ with islands covered is remained. Those remained SiO₂ become the mask for ICP to etch the GaN layer. As a result, nanorod structure should be formed. For the experiment, RIE using CF₄ and ICP using Cl₂ with different time and power is operated. Five samples of Au mask are etched using RIE RF power of 70W and etching time of 4.5min, 9.0min, 13.5min, 18.0min and 22.5min respectively. Another four samples of Au mask are etched using RF power of 150W and etching time of 2.5min, 5.0min, 10.0min and 12.5min respectively. The flow rate of CF₄ gas is 20 sccm and the pressure is 5 pa. The nine samples are then operated in ICP for 30min. The ICP etching is programmed in the etching device and the etching rate is

expected to be 60Å/s. Same process is operated to samples of Ni mask. The result is observed in SEM. Unfortunately, the thickness of the GaN sample is only about 2µm. Even in the best case for the GaN layer totally etched down to the bottom, the length of the nanorod is only 2µm. The length is too short to connect between source and drain as in the bottom-up approach.

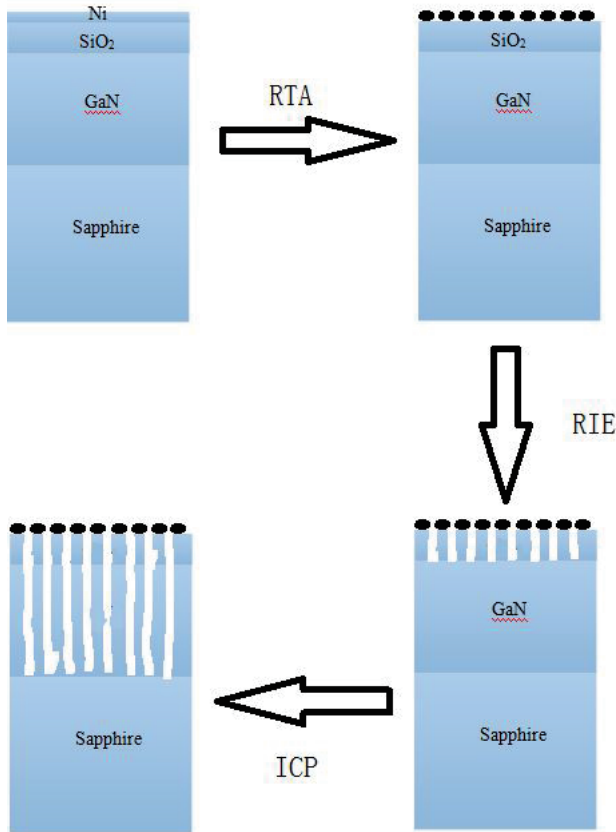


Fig. 2 Process of Top-Down Approach

Obviously, the property of the metal islands is a key factor for the approach. To investigate this point, different conditions should be tested. Because the limited amount of the material, a layer of SiO₂ is directly coated onto a sapphire substrate and then with metal coating. Since the metal is still just on the SiO₂ surface, this kind of sample is used to test the factors which influence the property of the metal islands. To test the possibility of the influence from the quality of the SiO₂ layer, E-beam and sputter are used to coat 100nm SiO₂ onto the sapphire substrate. Then, 10nm Au is coated onto the SiO₂ surface by E-beam. 30min RTA of 400°C, 450°C, 500°C and 550°C is processed to test the temperature dependence. To test the metal thickness dependence, 2nm, 6nm, 10nm and 20nm Au is coated and processed with 550°C, 30min RTA. To test the RTA time dependence, 10nm Au is coated and processed with 550°C, 5min, 10min, 30min and 60min RTA. The RTA processes all operate in N₂ ambient. The result is observed in SEM and AFM. Similar process is operated for Ni.

Unfortunately, the etching rate of the Au, Ni and SiO₂ for RIE is not clear for this experiment in my lab. The

selectivity (the ratio of the etching rate of different materials) is therefore cannot be calculated. Theoretically, the selectivity of the material to be etched and the mask material should be high for good etching performance. The condition should be optimized for the generation of the nanorod. Nevertheless, the etching results observed by SEM can provide a valuable reference for this optimization.

3. RESULTS AND DISCUSSION

3.1 BOTTOM-UP APPROACH

The nanowires grown by bottom-up approach in HVPE is shown Fig. 3 and Fig. 4. As shown in the SEM images, the nanowires grown by this approach is very long. A typical GaN nanowire can be longer than 20µm, a length which is decent for single-nanowire devices. The benefit of long nanowires is not only the relative easiness for device fabrication, but also the large aspect ratio. For some applications, for instance, sensors, the large surface area of the nanowire is expected to introduce good sensitivity for the device.



Fig. 3 Nanowires Grown by HVPE



Fig. 4 Nanowires Grown by HVPE, the Stage in SEM is Titled by 40°.

Fig. 5 presents the simple single-nanowire device. A nanowire is connected between the source and drain. Compared with the dimension of the source and drain, it is reasonable to consider this device as one-dimensional. This simplicity of degree of freedom may pose benefits for theoretical modeling and numerical simulation. Based on this simple device, other more complicated device structure can be fabricated. For example, a MOSFET can be fabricated by adding a gate.

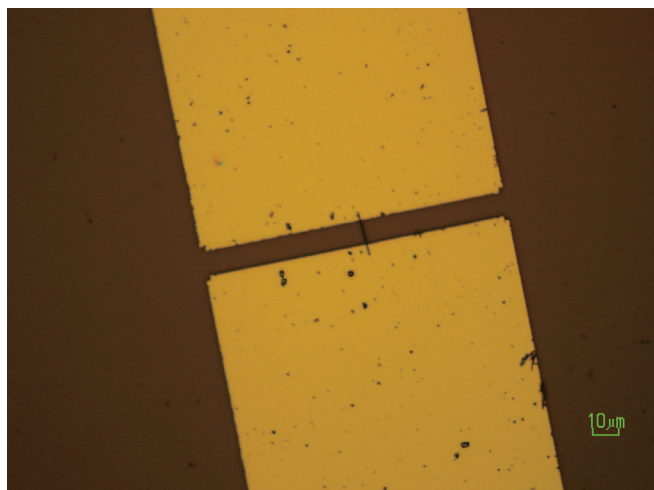


Fig. 5 A Simple Single Nanowire Device

3.2 TOP-DOWN APPROACH

3.2.1 Metal Islands Formation

Both of the Ni and Au are investigated for self-assembled mask by RTA.

A typical SEM image of the mask using Ni is shown in Fig. 6. There is no clearly isolated nano-islands or nanodroplets formed. It seems that there are still many Ni left between Ni droplets. Instead of Ni islands structure, it forms

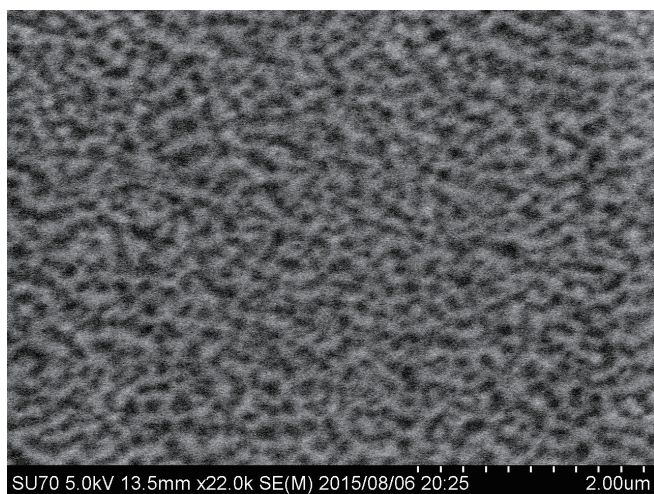


Fig. 6 A Typical SEM Image of Ni "Nano-net" Structure

a "nano-net" structure. Even though different RTA temperatures, different RTA times and different Ni thickness are tested, there is no isolated islands formed, at least under the SEM used in this experiment. The results

indicate that if the Ni thickness is under 10nm, there is even no nano-net structure can be found under SEM. For the Ni thickness under 10nm, the structure may be too small to tell. For a relatively low RTA temperature, for example, 500°C, it is still possible to find the net structure for a 10nm thick Ni. There are clues [11, 12] that for a higher RTA temperature, isolated islands can be formed. However, even 850°C RTA still cannot present isolated islands. Longer RTA time, for example, 40min also cannot help for the isolated islands formation. A higher temperature RTA may solve this problem; however, higher temperature may introduce some defects into the material, especially for some devices with hetero-structures.

This nano-net structure poses obvious difficulties for etching. The left Ni between two islands center becomes unexpected mask which will obstruct the etching of SiO₂. The etching condition is therefore difficult to control and the morphology of the nanorod is harder to study. In the worst case, if the unexpected left Ni is too thick, no nanorod structures cannot be etched.

Compared with Ni, Au is turned out to be a better material for nano-islands formation. Fig. 7 and Fig. 8 show the Au islands from 10nm Au and 30min RTA with different RTA temperatures. Different methods for SiO₂ coating are used. It can be seen that at 400°C, Au islands are

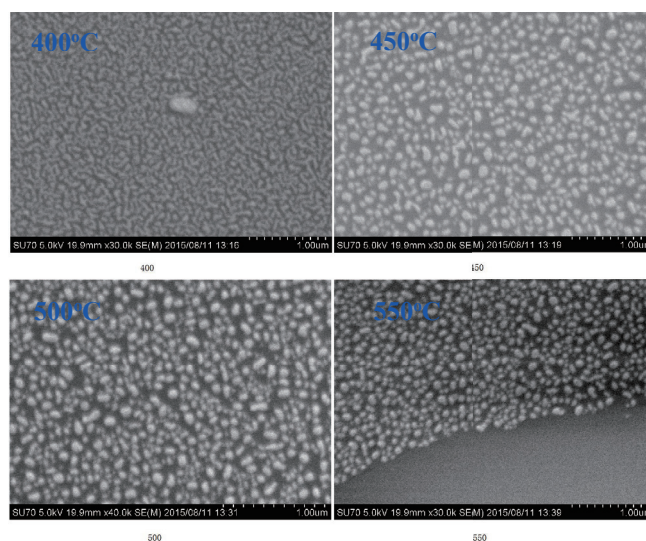


Fig. 7 Au Islands Formed by Different RTA Temperature.
SiO₂ is Coated by E-beam

not isolated and nano-net structure is formed. At 450°C, the islands start to be isolated. At higher temperatures, well isolated islands can be clearly viewed. Moreover, there is no obvious difference found between sputter coated and e-beam coated SiO₂ layer. Fig. 9 shows the Au islands formed from 30min, 550°C RTA with 2nm, 6nm, 10nm and 20nm Au. Fig. 10 shows the Au islands formed from 10nm Au, 550°C RTA with 5min, 10min, 30min and 60min RTA time. Sputter is used for SiO₂ coating. It can be seen that there is an obvious Au thickness dependence for the islands size and density distribution. For a better understanding of the different conditions for Au islands formation, AFM is used and typical images are shown in Fig. 11 and Fig. 12. Three

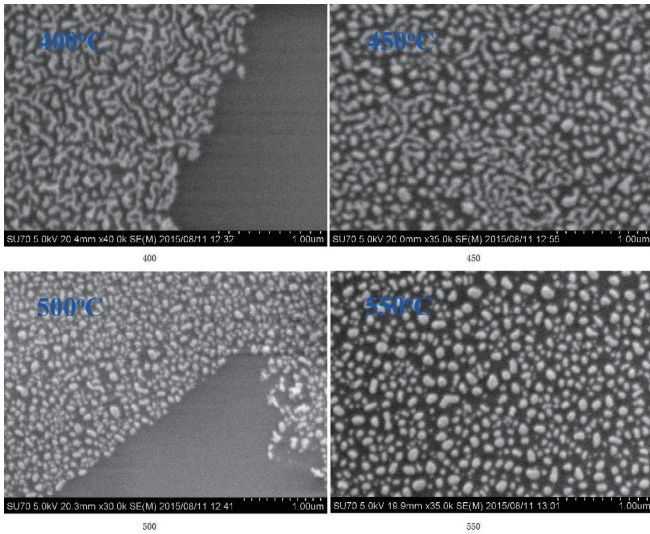


Fig. 8 Au Islands Formed by Different RTA Temperature. SiO₂ is Coated by Sputter

different places of each sample are scanned by AFM and the size and the density of the formed islands are calculated by

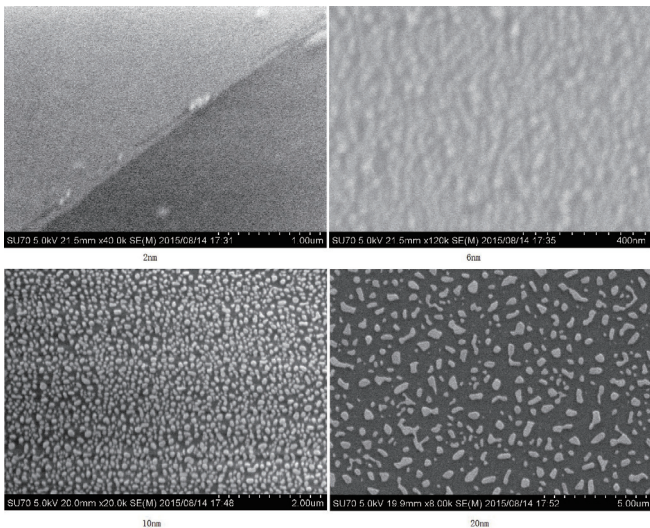


Fig. 9 Au Islands Formed by Different Au Thickness

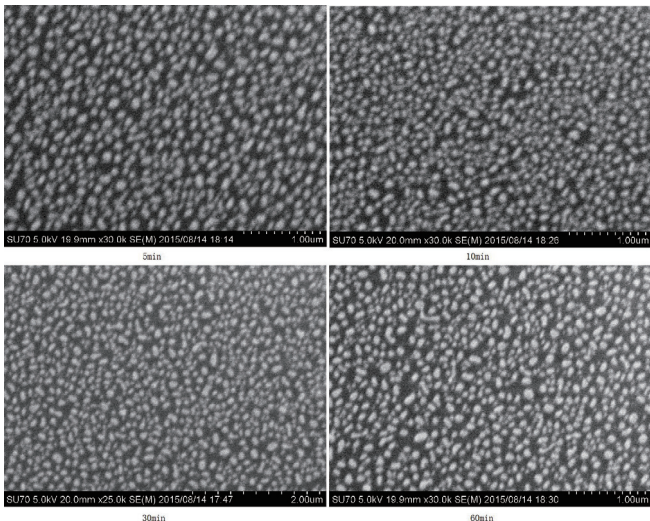


Fig. 10 Au Islands Formed by Different RTA Time

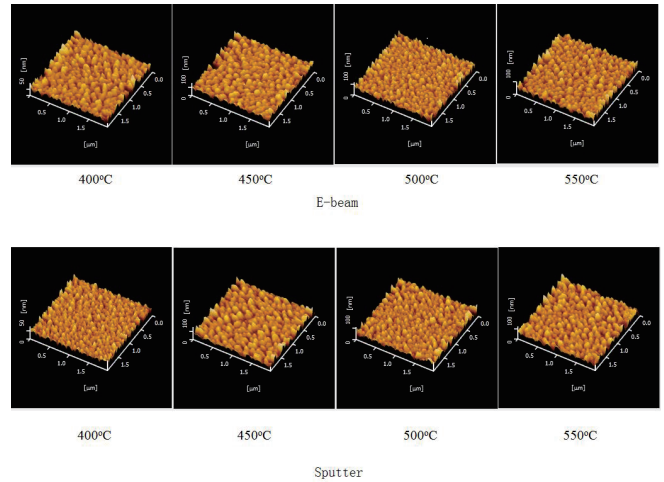


Fig. 11 AFM Image of Au Islands with Different RTA Temperature

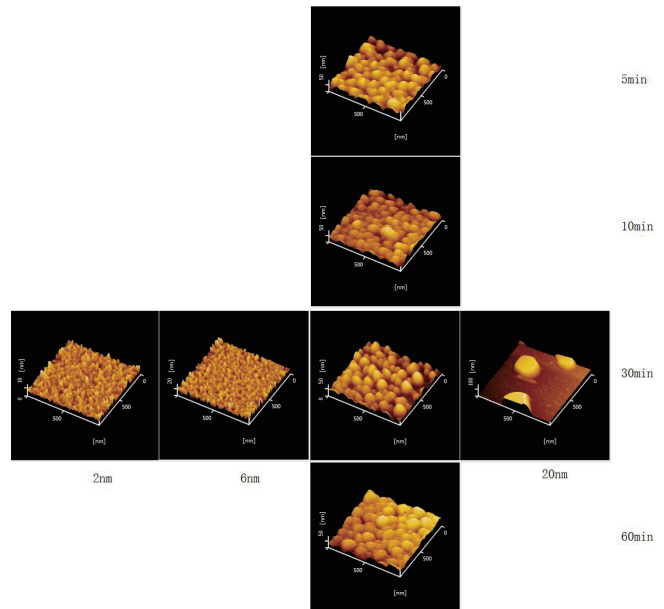


Fig. 12 AFM Image of Au Islands Formed by Different Au Thickness and RTA Time

taking account of all of the three places. Histograms are generated and shown in Fig. 13-Fig. 15. The results are also summarized in Table 1. It should be noted that the condition for 2nm is not appropriate for this measurement since the islands are too small.

Based on all of these results, there are some clues for that the islands size increases with the increasing of metal thickness, RTA temperature and RTA time; the islands density decrease with the increasing of metal thickness, RTA temperature and RTA time. However, except for Au thickness, other dependence is not obvious and even indistinct. RTA temperature and RTA time are more likely to be kind of threshold for the formation of metal islands. When the RTA temperature is high enough and the RTA time is long enough, isolated metal islands will form. If the temperature is not high enough, nano-net structures will form. The RTA time needs not to be long for islands to be isolated. At least in this experiment, time is not an important

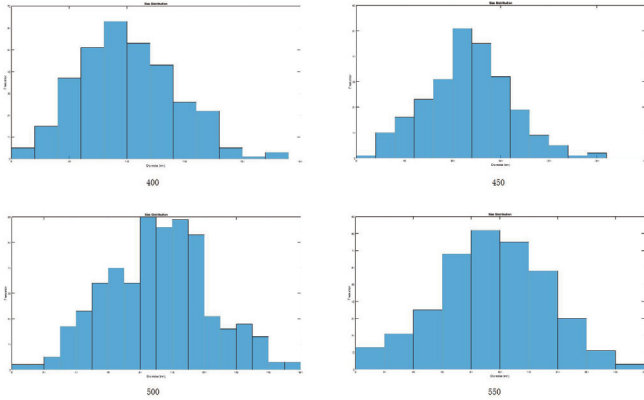


Fig. 13 The Distribution of Au Islands Formed by Different RTA Temperature. SiO₂ is Coated by E-beam

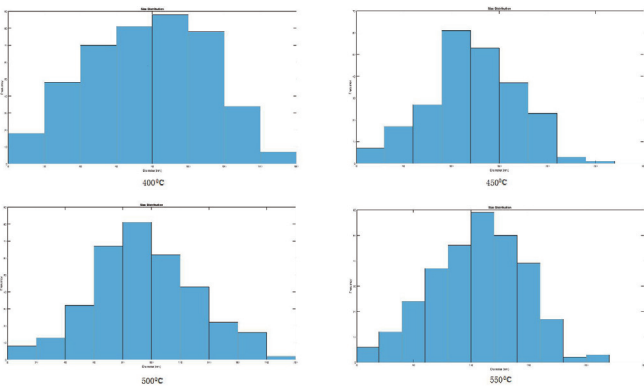


Fig. 14 The Distribution of Au Islands Formed by Different RTA Temperature. SiO₂ is Coated by Sputter

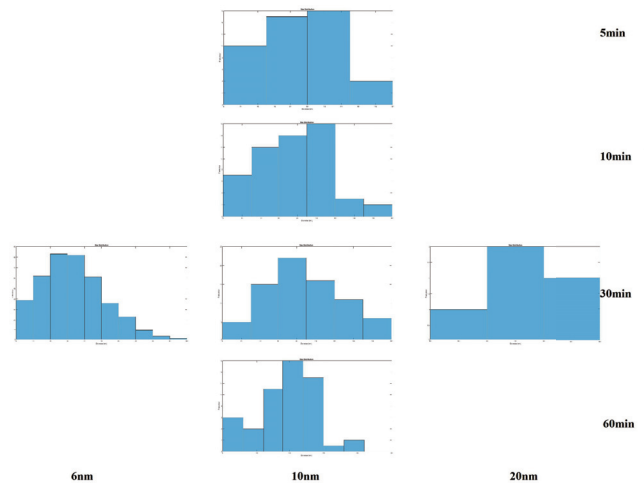


Fig. 15 The Distribution of Au Islands Formed by Different Au Thickness and RTA Time

Table 1 Summary of Metal Islands Distribution

Method for SiO ₂ Coating	SiO ₂ Thickness (nm)	Metal Thickness (nm)	RTA Temperature (°C)	RTA Time (min)	Islands Density (nm ⁻²)	Islands Size (nm, av)	Standard Deviation (nm)
Sputter	100	10	400	30	1.0197E+10	77.3655	32.6395
Sputter	100	10	450	30	5.1028E+09	122.1262	46.5145
Sputter	100	10	500	30	3.2003E+09	94.5156	36.0255
Sputter	100	10	550	30	6.4029E+09	105.238	39.7102
E-beam	100	10	400	30	6.9345E+09	100.0918	41.9377
E-beam	100	10	450	30	5.6755E+09	116.6571	45.7051
E-beam	100	10	500	30	2.9562E+09	101.364	31.3094
E-beam	100	10	550	30	7.5962E+09	94.9473	37.6551
Sputter	200	5	550	30	Cannot be measured	23.5201	18.085
Sputter	200	10	550	30	4.0354E+10	86.9214	41.0022
Sputter	200	20	550	30	3.3930E+08	295.6571	61.5187
Sputter	200	10	550	5	6.7182E+09	94.8844	42.7225
Sputter	200	10	550	10	6.7977E+09	74.4959	36.1375
Sputter	200	10	550	60	6.3915E+09	88.2573	41.1968

factor. Moreover, the standard deviation of islands size is large, which indicates that the distribution of islands is not very uniform. Since the islands are not uniform, the

distribution of the etched nanorods will be negatively influenced. Another point to be noticed is that since the Ni islands are not isolated, the accuracy of the statistics is relatively low. Moreover, no obvious difference is found between the samples with sputter coated and E-beam coated SiO₂.

If only considering about the shape and distribution of metal islands, Au is a much better mask for etching. However, we can still not jump to this conclusion since compared to Ni, Au may be not very durable for RIE. Even though not covered in this report, the etching rate of Ni and Au in RIE should be studied for a better conclusion.

3.2.2 Nanorod Etching

The result of etching for nanorods is presented in Fig. 16-Fig. 19. It can be shown that even though the Ni islands are not isolated under SEM, nanorod structure can still be formed. For 70W RF power, 18.0min and 22.5min RIE can form nanorod structure using Ni mask. The density is relatively small. For other etching time, no good nanorod structure is formed. It indicates that left Ni between islands hinder the etching process. For 150W RF power, good

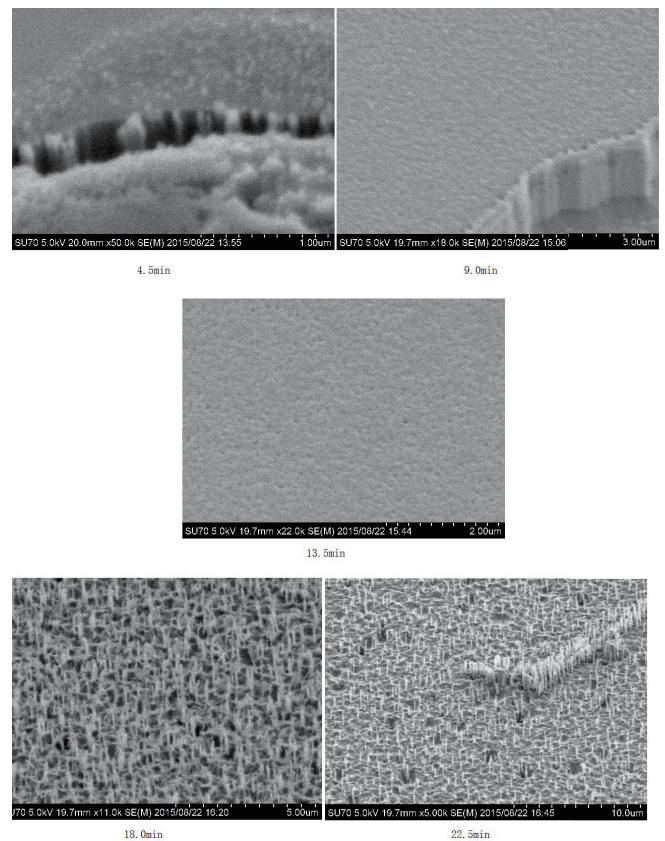


Fig. 16 Etching Result of 70W RF Power with Different RIE Time. The Mask is Ni.

nanorod structure is formed for 5min RIE. The density is much larger and the nanorods are more uniform. Thus, in this condition, the left Ni between islands is totally etched without over etching of islands. For 10min and 12.5min, the etching time is too long and Ni islands are totally etched; the SiO₂ is etched too much to form GaN nanorod pattern. For

Au mask, both of 4.5min 70W RIE and 2.5min 150W RIE are enough for good nanorods formation. The nanorods present large density and relatively uniform. The isolated Au islands become decent nano-masks and attribute well for pattern formation. For longer etching time, the effect of over etching is obvious. As a nano-mask, Au is less durable than

since higher density implies that more nanorods are stimulated in a specified region. However, because there is still flat GaN layer left, the measurements are influenced by this flat structure. A comparison between totally not etched GaN sample and the etched nanorods is expected for experiments in the future. To have a better understanding of

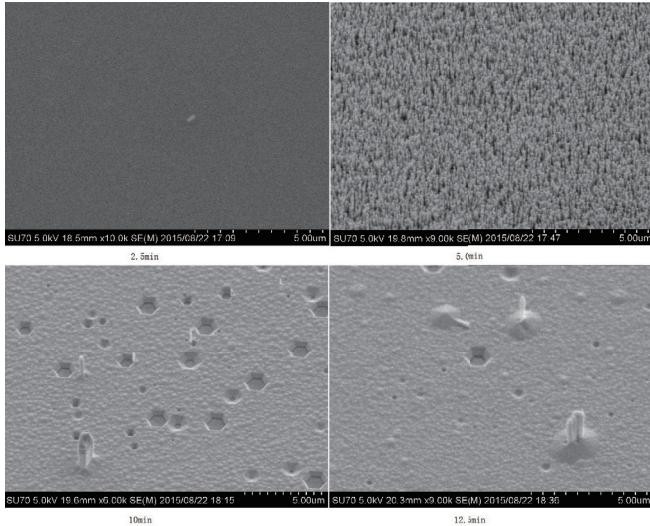


Fig. 17 Etching Result of 150W RF Power with Different RIE Time. The Mask is Ni.

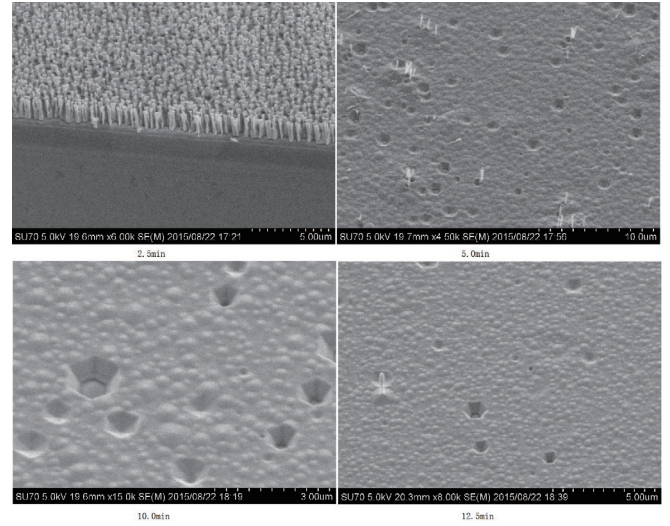


Fig. 19 Etching Result of 150W RF Power with Different RIE Time. The Mask is Au.

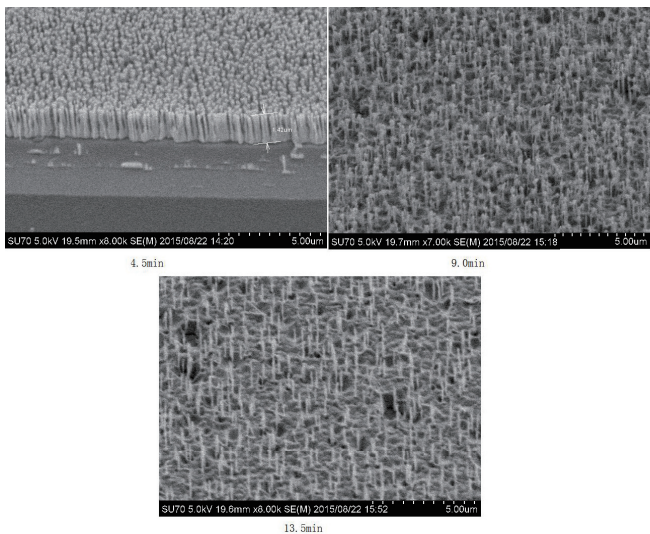


Fig. 18 Etching Result of 70W RF Power with Different RIE Time. The Mask is Au.

Ni. Lower RF power is preferred. Fig. 20 shows the PL measurement of etched nanorods. The peak indicates that the material is GaN. There is also a tendency that nanorods with higher density has larger intensity. This is reasonable

the component of the nanorod, Transmission Electron Microscopy (TEM) and Energy Dispersive X-Ray Analyser

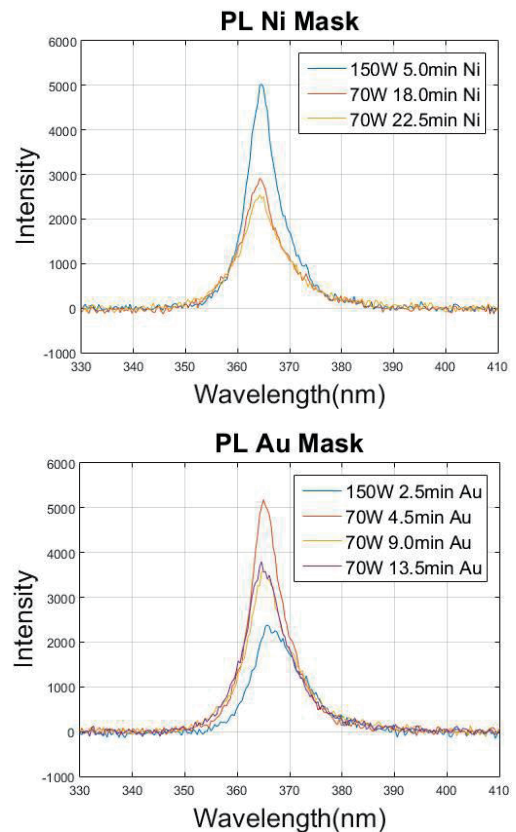


Fig. 20 PL Measurements of Nanorods

(EDX) are used. Fig. 21 shows the TEM image of three typical nanorods. There is no stacking fault or dislocation

observed; dislocation may be “healed” after etching. The side-wall of the nanorod is rough; optimization of etching may be helpful to this problem. Moreover, the EDX analysis (graphs are not shown here) shows that the nanorod is GaN except for the hemispherical structure. The hemispherical structure is shown to be composed of O and Si, which means that it is the left SiO₂ mask. This is desirable since it

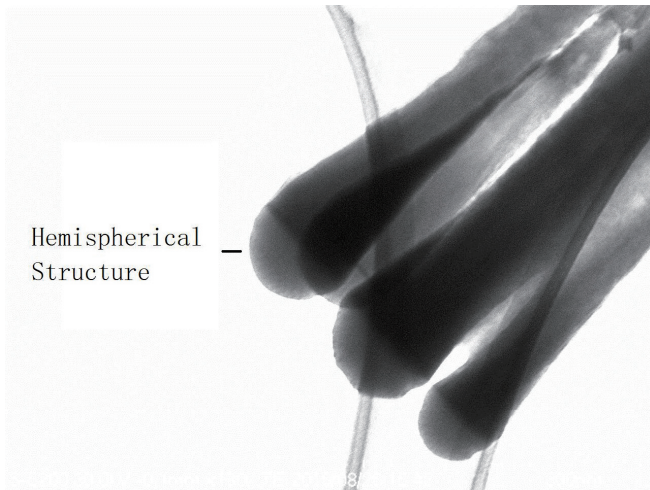


Fig. 21 TEM Image of Three Nanorods (RIE 4.5min, 50W, Au mask)

can protect other structures for device fabrication (for example, quantum-well) and the left SiO₂ mask can be easily removed by acid.

From the point of view of device fabrication, Ni and Au both have advantages. Ni is cheaper than Au and more durable under etching. This point can be important since some devices may have structures which should be prevented from etching. For instance, the fabrication of LED requires that the quantum well structure on GaN is not etched. Furthermore, higher RTA temperature may help isolate Ni islands and therefore solve the problem of Ni mask mentioned in this report. However, Au islands can be isolated in low temperature. If a device is preferred to be fabricated in low temperature, Au will be a better choice. The trade-off of using Ni or Au mask, or even using other materials is an important point to be searched in the future.

4. CONCLUSION

Both of bottom-up and top-down approaches for GaN nanowire/nanorod are investigated in this report. It shows that the long nanowires grown from bottom-up approach is decent for single-nanowire fabrication. Top-down approach can be achieved by using Ni and Au nano-mask. The nanorod by etching implies some possibilities to avoid stacking fault and dislocation. Heterostructure of nanorods can be easily formed by simply etching from normal flat structures. More measurements, including but not limited to electrical properties, thermal properties and side-wall recombination are expected for the characterization of the nanowires/nanorods in the future.

ACKNOWLEDGEMENTS

I thank JUACEP summer program and Prof. Hiroshi Amano for providing me the opportunity to get involved in his group. I would like to thank those group members who help me with my research. Special thanks to Mr. Suzuki for helping me with RIE and ICP; and to Dr. Lekhal's great help for my research.

REFERENCES

- [1] Liao, L., Bai, J., Cheng, R., Lin, Y., Jiang, S., Qu, Y., Huang, Y., Duan, X., Sub-100 nm Channel Length Graphene Transistors, *Nano Lett.*, vol. 10, pp. 3952–3956 (2010).
- [2] Wang, G., Li, Q., Wierer, J., Koleske, D., Figiel, J., Top-down fabrication and characterization of axial and radial III-nitride nanowire LEDs, *Phys. Status Solidi A*, 211, No. 4, pp. 748–751 (2014).
- [3] Bai, J., Wang, Q., and Wang, T., Characterization of InGaN-based nanorod light emitting diodes with different indium compositions, *J. Appl. Phys.*, 111, 113103 (2012).
- [4] Li, S., and Waag, A., GaN based nanorods for solid state lighting, *J. Appl. Phys.*, 111, 071101 (2012).
- [5] Kim, H., Cho, Y., Lee, H., Kim, S., Ryu, S., Kim, D., Kang, T., Chung, K., High-Brightness Light Emitting Diodes Using Dislocation-Free Indium Gallium Nitride/Gallium Nitride Multiquantum-Well Nanorod Arrays, *Nano Lett.*, vol. 4, No. 6, pp. 1059-1062 (2004).
- [6] Chiu, C., Lo, M., Lu, T., Yu, P., Huang, H., Kuo, H., Wang, S., Nano-Processing Techniques Applied in GaN-Based Light-Emitting Devices With Self-Assembly Ni Nano-Masks, *J. Lightwave Technol.*, vol. 26, No. 11, pp. 1445-1454 (2008)
- [7] Xing, K., Gong, Y., Bai, J., and Wang, T., InGaN/GaN quantum well structures with greatly enhanced performance on a-plane GaN grown using self-organized nano-masks, *Appl. Phys. Lett.*, 99, 181907 (2011).
- [8] Calculated Ga-Ni phase diagram, <http://resource.npl.co.uk/mtdata/phdiagrams/gani.htm>.
- [9] Lekhal, K., Department of Electrical Engineering and Computer Science, Nagoya University, Japan.
- [10] Usami, S., Department of Electrical Engineering and Computer Science, Nagoya University, Japan.
- [11] Carey, J., Ong, L., Silva, S., Formation of low-temperature self-organized nanoscale nickel metal islands, *Nanotechnology*, vol 14, pp. 1223-1227 (2003).
- [12] Lee, D., Li, M., Sui, M., Zhang, Q., Pandey, P., Kim, E., Lee, J., Observation of Shape, Configuration, and Density of Au Nanoparticles on Various GaAs Surfaces via Deposition Amount, Annealing Temperature, and Dwelling Time, *Nanoscale Res Lett*, 10:240, pp. 1-14 (2015).

INVESTIGATION OF THE CONTROL OF TABLE TENNIS ROBOTS

Austin Kuo

Henry Samueli School of Engineering, University of California, Los Angeles
austinkuo@ucla.edu

Supervisor: Yoshikazu Hayakawa

Mechatronics Laboratory, Graduate School of Engineering, Nagoya University
hayakawa@nuem.nagoya-u.ac.jp

Abstract - A table tennis robot necessarily operates in a dynamic, high speed environment and therefore is an excellent exercise in modern robot design. A two part problem is posed. First, a physical model that describes the ball's motion through the air and its interaction with surfaces must be created. Second, a racket control method must be devised in congruence with the physical model, such that controllable inputs (racket posture, velocity) can reach a specified output (ball position). A numerical simulation is carried out to verify the model.

Keywords: robotics, ping pong, table tennis, serving task

I. INTRODUCTION

Since their debut on the manufacturing floor in the mid-20th century, robots have gradually taken over tasks deemed too hazardous, tedious, delicate or otherwise difficult for humans to do. More recently, robots are graduating from teleoperation (remote control or pre-programmed commands by a human) to full autonomy (self-selection and execution of tasks), thus crossing at threshold that will exponentially increase their usefulness to humans.

The future success of applied robotics hinges on its ability to autonomously operate in a dynamic and unstructured environment. In this context, autonomous operation indicates minimal user input, while a dynamic environment suggests an environment with varied stimuli that the robot must detect via sensor networks and react to accordingly.

A current project undertaken at Nagoya University is concerned with development of such a robot. It employs a Mitsubishi Heavy Industries PA-10 7-axis robotic arm with a table tennis racket attached to the end effector. A high speed camera system tracks the ball and feeds the data through a physical model. A predictive trajectory is plotted and the racket moves to intercept accordingly. The entire process is transcribed in C++ code, which gives a serial output to the robotic arm.

II. NOTATION

The physical model of the table tennis robot is adequately represented by the diagram below.

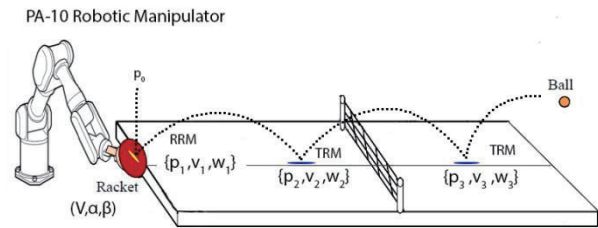


Figure 1: Table Tennis Setup

There are four points of interest. Point 0 is where the ball is dropped over the paddle. Point 1 is the ball's state when it makes contact with the paddle during the serving task. Points 2 and 3 are the ball's state when it rebounds off the table on the home side and opponent side respectively. In this paper, a '+' subscript denotes the state just after the impact, while a '-' subscript denotes the state just before the impact.

V	Racket velocity	t_i	time
α	Racket yaw	m	Mass of ball
β	Racket pitch	r	Radius of ball
$p_i(t)$	position	I	Moment of Inertia
$v_i(t)$	Translational velocity	L	Table Length (2.74m)
$w_i(t)$	Rotational velocity	W	Table Width (1.525m)

Table 1: List of Variables

Additionally, each component of the table tennis system has its own frame of reference, as illustrated below.

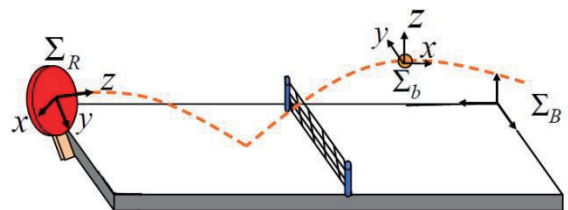


Figure 2: Coordinate System Locations

$\Sigma_R, \Sigma_B, \Sigma_b$ are the coordinate systems of the racket, table, and ball, respectively.

III. PHYSICAL MODELING

A table tennis serve and return comprises three distinct types of interaction:

- 1) Table Rebound Model, the description of the interaction between the ball and the table.
- 2) Aerodynamic Model, the description of the ball's motion through the air.
- 3) Racket Rebound Model, the description of the interaction between the ball and the table tennis racket.

III.a Table Rebound Model (TRM)

The Table rebound model describes the near instantaneous interaction between the ball and the surface of the table.

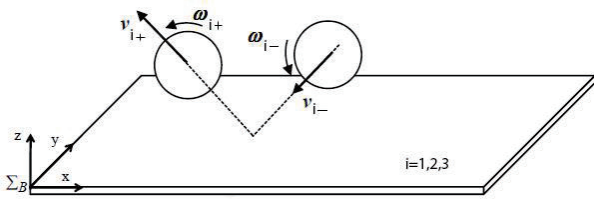


Figure 3: TRM Diagram

To develop a matrix relation between the translational and rotational velocities just before and after the impact, some assumptions must be made.

- 1) The ball makes an infinitesimally small point contact with the table. Rotation along the Z axis has no effect on the motion of the ball.
- 2) In accordance with the impulse-momentum theorem, the change in translational and rotational momentum of the ball due to impact is equal to the impulse applied to it.

$$m\mathbf{v}_+ - m\mathbf{v}_- = \mathbf{P} \quad (1)$$

$$I\mathbf{w}_+ - I\mathbf{w}_- = \mathbf{r} \times \mathbf{P} \quad (2)$$

Where \mathbf{r} is the vector $[0 \ 0 \ -r]^T$, \mathbf{P} is the impulse on the ball, and I is the inertia of a hollow sphere, $I = \frac{2}{3}mr^2$.

- 3) There are two cases concerning the motion of the ball after the impact. In the nominal case, hereinafter referred to as Case 1, the direction of the contact velocity, v_T , is the same before and after the impact, but its magnitude may be reduced. In the second case, or Case 2, the contact velocity after impact is 0 such that the ball bounces upward without spinning.

$$v_{T+} = \gamma v_{T-} \quad \gamma > 0 \text{ or } \gamma = 0 \quad (3)$$

- 4) The direction of the translational velocity along the z-axis is reversed, and its magnitude is attenuated due to the elastic collision.

$$v_{z+} = -e_t v_{z-} \quad (4)$$

Where e_t is the coefficient of restitution between the ball and the table, experimentally determined to be 0.93.

- 5) The impulse in the x and y directions is along the direction of the contact velocity, and defined as the following

$$P_{xy} = -\lambda \left(\frac{v_{T-}}{\|v_{T-}\|} \right); \quad 0 \leq \lambda \leq \mu|P_z| \quad (5)$$

The impulse in the z direction is found by simply substituting (4) into (1).

$$P_z = -m(1 + e_t)v_z \quad (6)$$

The contact velocity after impact is found by solving equations (1) and (2) for v_+ and w_+ respectively, and substituting the result into the contact velocity before using equation (5) to replace P .

$$v_{T+} = -\lambda \left(\frac{1}{m} + \frac{r^2}{I} \right) \frac{v_{T-}}{\|v_{T-}\|} + v_{T-} \quad (7)$$

Note Equation (7) is just a more explicit version of equation (3), and we can now use it to define the two cases. Let

$$\gamma(\lambda) = -\frac{\lambda}{\|v_{T-}\|} \left(\frac{1}{m} + \frac{r^2}{I} \right) + 1 \quad (8)$$

If $\lambda = \mu|P_z|$, a necessary condition for Case 1, then (8) becomes

$$\gamma(\mu|P_z|) = 1 - \frac{5}{2} \mu(1 + e_t) \frac{|v_z|}{\|v_{T-}\|} \quad (9)$$

From (3), it is clear that if $\gamma(\mu|P_z|) > 0$, the table rebound is indicative of case 1, but if $\gamma(\mu|P_z|) \leq 0$ then the rebound is indicative of case 2, and (8) must be zero in observance of assumption 3. For case 2, λ is calculated with $\gamma = 0$.

$$\lambda = \frac{2}{5} m \|v_{T-}\| \quad (10)$$

Finally we can assemble the matrix that relates pre and post impact translational and rotational velocities. For translational velocities, start from (1) and substitute in (5) and (6). The three translational components become

$$v_{x+} = (1 - a)v_{x-} + arw_{y-} \quad (11)$$

$$v_{y+} = (1 - a)v_{y-} - arw_{x-} \quad (12)$$

$$v_{z+} = -e_t v_{z-} \quad (13)$$

Where $a = \mu(1 + e_t) \frac{|v_{z-}|}{\|v_{T-}\|}$

Similarly, starting from (2), substituting (5) and (6) the three rotational velocities are given by

$$w_{x+} = \frac{3a}{2r} v_{y-} + \left(1 - \frac{3a}{2}\right) w_{x-} \quad (14)$$

$$w_{y+} = \frac{3a}{2r} v_{x-} + \left(1 - \frac{3a}{2}\right) w_{y-} \quad (15)$$

$$w_{z+} = w_{z-} \quad (16)$$

The six equations for case 2 are constant relations that are found by substituting (10) into (5). We can assemble (11)-(16) into matrix format.

$$\begin{bmatrix} \mathbf{v}_+ \\ \mathbf{w}_+ \end{bmatrix} = \begin{bmatrix} A_t & B_t \\ C_t & D_t \end{bmatrix} \begin{bmatrix} \mathbf{v}_- \\ \mathbf{w}_- \end{bmatrix} \quad (17)$$

Where $\mathbf{v}, \mathbf{w} \in R^3$ and

$$[A_t] = \begin{bmatrix} 1 - a & 0 & 0 \\ 0 & 1 - a & 0 \\ 0 & 0 & -e_t \end{bmatrix}$$

$$[B_t] = \begin{bmatrix} 0 & ar & 0 \\ -ar & 0 & 0 \\ 0 & 0 & 0 \end{bmatrix}$$

$$[C_t] = \begin{bmatrix} 0 & -\frac{3a}{2r} & 0 \\ \frac{3a}{2r} & 0 & 0 \\ 0 & 0 & 0 \end{bmatrix}$$

$$[D_t] = \begin{bmatrix} 1 - \frac{3a}{2} & 0 & 0 \\ 0 & 1 - \frac{3a}{2} & 0 \\ 0 & 0 & 0 \end{bmatrix}$$

$$a := \begin{cases} \mu(1 + e_t) \frac{|v_{z-}|}{\|v_{T-}\|} & \text{for case 1 } (v_T \neq 0) \\ \frac{2}{5} & \text{for case 2 } (v_T = 0) \end{cases}$$

III.b Aerodynamic Model (ADM)

The aerodynamic model takes into account the weight, drag, and Magnus forces acting on the ball as it travels through the air. The equation of motion for the ball is

$$\begin{aligned} \ddot{\mathbf{p}}(t) = & -\mathbf{g} - \frac{1}{2} C_D(t) \frac{\rho}{m} S_b \|\dot{\mathbf{p}}(t)\| \dot{\mathbf{p}}(t) \\ & + C_M(t) \frac{\rho}{m} V_b (\mathbf{w} \times \dot{\mathbf{p}}(t)) \end{aligned} \quad (18)$$

Where $\mathbf{p}(t) \in R^3$ is the position of the ball, \mathbf{g} is the vector $[0 \ 0 \ g]^T$ containing the gravitational constant ($9.81 \frac{m}{s^2}$), ρ is the density of air at $25^\circ C$ ($1.184 \frac{kg}{m^3}$), C_D , C_M are drag

and Magnus coefficients, respectively. Finally, $S_b = \pi r^2$ is the frontal area and $V_b = \frac{4}{3} \pi r^3$ is the volume of the ball.

The rotational velocity is assumed to be constant (i.e. not a function of time).

III.c Racket Rebound Model (RRM)

The racket rebound model describes the near instantaneous interaction between the ball and the rubber surface of the racket. Unlike the table rebound model, the ball's rotational velocity about the y axis will reverse upon impact. The translational velocity will reverse direction and may increase in magnitude if the racket is mid-swing.

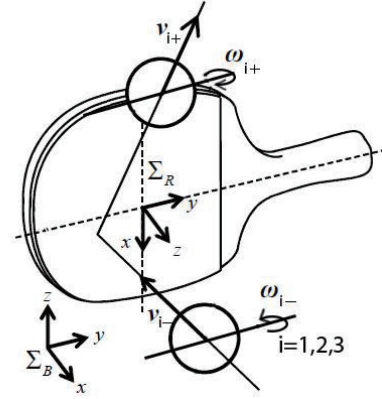


Figure 4: RRM Diagram

The rubber surface of the racket acts like an elastic spring which absorbs energy before converting back into the kinetic energy of the ball. From the TRM, assumptions 1, 2, and 4 still hold, although the equations for impulse do not. The new impulse equation for the x and y directions is found by integrating Hooke's law over the time T that the ball is in contact with the racket.

$$\mathbf{P}_{xy} = \int_0^T -k_s \mathbf{x}(t) dt \quad (19)$$

Where $\mathbf{x}(t) \in R^3$ is the displacement of the rubber surface during impact. Noting that $\mathbf{x}(t) = \mathbf{v}t$ for $0 \leq t \leq T$, then

$$\mathbf{P}_{xy} = -k_s \mathbf{v} \int_0^T t dt = -\frac{1}{2} k_s \mathbf{v} T^2 \quad (20)$$

Clearly $\mathbf{v}T = x_{max}$, the maximum displacement of the rubber due to the ball impact.

The energy equation, which balances potential and kinetic energy, yields

$$\frac{1}{2} m_{eq} \|v_T\|^2 = \int_0^{x_{max}} -k_s x dx \quad (21)$$

Where m_{eq} is the equivalent mass of the ball and the deformed rubber displaced by the ball. After taking the integral and solving for x_{max} , we get

$$x_{max} = vT = \sqrt{\frac{m_{eq}}{k_s}} vT \quad (22)$$

Substituting (22) back into (20), we can solve for impulse

$$\mathbf{P}_{xy} = -k_p \mathbf{v}_T \quad (23)$$

$$k_p := \frac{1}{2} T \sqrt{m_{eq} k_s} \quad (24)$$

Finally, substituting (23) into (1) and (2) will show the relationship between the pre and post impact translational and rotational velocities in the x and y direction. The translation velocities are

$$v_{x+} - v_{x-} = -\frac{k_p}{m} (v_{x-} - r w_{y-}) \quad (25)$$

$$v_{y+} - v_{y-} = -\frac{k_p}{m} (v_{y-} + r w_{x-}) \quad (26)$$

$$v_{z+} = -e_r v_{z-} \quad (27)$$

Where e_r is the coefficient of restitution between the ball and the rubber surface of the racket, experimentally determined to be 0.73.

Similarly, the rotational velocities are found to be

$$w_{x+} - w_{x-} = -\frac{k_p}{I} r v_{y-} - \frac{k_p}{I} r^2 w_{x-} \quad (28)$$

$$w_{y+} - w_{y-} = \frac{k_p}{I} r v_{x-} - \frac{k_p}{I} r^2 w_{y-} \quad (29)$$

$$w_{z+} = w_{z-} \quad (30)$$

Similar to the TRM, we put equations (25)-(30) into matrix format. Unlike TRM, the translational velocity of the racket must be taken into account.

$$\begin{bmatrix} \mathbf{v}_+ - \mathbf{V} \\ \mathbf{w}_+ \end{bmatrix} = \begin{bmatrix} A_r & B_r \\ C_r & D_r \end{bmatrix} \begin{bmatrix} \mathbf{v}_- - \mathbf{V} \\ \mathbf{w}_- \end{bmatrix} \quad (31)$$

$$\begin{aligned} [A_r] &= \begin{bmatrix} 1 - k_v & 0 & 0 \\ 0 & 1 - k_v & 0 \\ 0 & 0 & -e_r \end{bmatrix} \\ [B_r] &= \begin{bmatrix} 0 & r & 0 \\ -r & 0 & 0 \\ 0 & 0 & 0 \end{bmatrix} \\ [C_r] &= \begin{bmatrix} 0 & -r & 0 \\ r & 0 & 0 \\ 0 & 0 & 0 \end{bmatrix} \\ [D_r] &= \begin{bmatrix} 1 - k_w r^2 & 0 & 0 \\ 0 & 1 - k_w r^2 & 0 \\ 0 & 0 & 1 \end{bmatrix} \end{aligned}$$

Where $k_v = \frac{k_p}{m}$ and $k_w = \frac{k_p}{I}$

The RRM model has been constructed in the coordinate system frame of the racket, though it is desired to use the 'global' frame of the table. Two rotation matrices – one for pitch and one for yaw – can provide a coordinate transform from the table to the racket. Let N be the frame of the table, and B be the frame of the racket, and A be an intermediary frame.

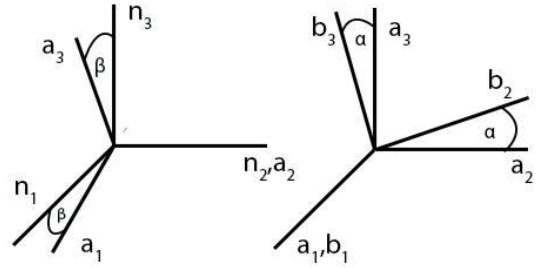


Figure 5: Coordinate Transform

$$\begin{bmatrix} n_x \\ n_y \\ n_z \end{bmatrix} = \begin{bmatrix} \cos(\beta) & 0 & \sin(\beta) \\ 0 & 1 & 0 \\ -\sin(\beta) & 0 & \cos(\beta) \end{bmatrix} \begin{bmatrix} a_x \\ a_y \\ a_z \end{bmatrix} \quad (32)$$

$$\begin{bmatrix} a_x \\ a_y \\ a_z \end{bmatrix} = \begin{bmatrix} 1 & 0 & 0 \\ 0 & \cos(\alpha) & -\sin(\alpha) \\ 0 & \sin(\alpha) & \cos(\alpha) \end{bmatrix} \begin{bmatrix} b_x \\ b_y \\ b_z \end{bmatrix} \quad (33)$$

Multiplying (32) and (33) we get a coordinate transform matrix

$$R_R = \begin{bmatrix} \cos(\beta) & \sin(\alpha) \sin(\beta) & \sin(\beta) \cos(\alpha) \\ 0 & \cos(\alpha) & -\sin(\alpha) \\ -\sin(\beta) & \cos(\beta) \cos(\alpha) & \cos(\beta) \cos(\alpha) \end{bmatrix} \quad (34)$$

The final RRM model in the table frame is

$$\begin{bmatrix} \mathbf{v}_+ - \mathbf{V} \\ \mathbf{w}_+ \end{bmatrix} = \begin{bmatrix} R_R & 0 \\ 0 & R_R \end{bmatrix} \begin{bmatrix} A_r & B_r \\ C_r & D_r \end{bmatrix} \begin{bmatrix} R_R & 0 \\ 0 & R_R \end{bmatrix}^T \begin{bmatrix} \mathbf{v}_- - \mathbf{V} \\ \mathbf{w}_- \end{bmatrix} \quad (35)$$

The combination of TRM, ADM, and RRM enable a *forward calculation*. Given the initial rotational and translational velocity and position $(\mathbf{p}_1, \mathbf{v}_{1-}, \mathbf{w}_{1-})$ and the racket state $(\mathbf{V}, \alpha, \beta)$, it is clear that (17),(18), and (31) can numerically determine the end position, rotational and translational velocity $(\mathbf{p}_3, \mathbf{v}_{3+}, \mathbf{w}_{3+})$.

IV. INVERSE CALCULATION

The physical models and forward control algorithm derived in III are helpful, but for the racket control problem, it is actually desirable to perform the *inverse calculation* that answers the question: With a specified combination of desired output variables from $\{\mathbf{p}_3, \mathbf{v}_{3+}, \mathbf{w}_{3+}, T\}$ (for a total of 9 variables, note $p_{3z} = 0$) what are the appropriate input variables for the racket $\{\mathbf{V}, \alpha, \beta\}$?

IV.a TRM Inverse Relation

The inverse relation for the TRM is similar to (17), except we wish to find the pre-impact velocities given the post-impact velocities instead of vice-versa.

Recalling case 1 ($v_{T+} \neq 0$) described in III, the inverse TRM is given by the following relation, known as Lemma 1.

$$\begin{aligned} \begin{bmatrix} \mathbf{v}_- \\ \mathbf{w}_- \end{bmatrix} &= \begin{bmatrix} \tilde{A}_t & \tilde{B}_t \\ \tilde{C}_t & \tilde{D}_t \end{bmatrix} \begin{bmatrix} \mathbf{v}_+ \\ \mathbf{w}_+ \end{bmatrix} & (36) \\ [\tilde{A}_r] &= \begin{bmatrix} 1+b & 0 & 0 \\ 0 & 1+b & 0 \\ 0 & 0 & -\frac{1}{e_t} \end{bmatrix} \\ [\tilde{B}_r] &= \begin{bmatrix} 0 & -br & 0 \\ br & 0 & 0 \\ 0 & 0 & 0 \end{bmatrix} \\ [\tilde{C}_r] &= \begin{bmatrix} 0 & \frac{3b}{2r} & 0 \\ -\frac{3b}{2r} & 0 & 0 \\ 0 & 0 & 0 \end{bmatrix} \\ [\tilde{D}_r] &= \begin{bmatrix} 1+\frac{3b}{2} & 0 & 0 \\ 0 & 1-\frac{3b}{2} & 0 \\ 0 & 0 & 1 \end{bmatrix} \end{aligned}$$

Where $b := \mu(1 + \frac{1}{e_t}) \frac{|v_{z+}|}{\|v_{T+}\|}$

For Case 2 ($v_T = 0$), pre impact rotational and translational velocities are given non uniquely as

$$\mathbf{v}_- = \left[\frac{5}{3}v_{x+} - \frac{2r}{3}w_{2+}, \frac{5}{3}v_{y+} + \frac{2r}{3}w_{1+}, -\frac{1}{e_t}v_{z+} \right]^T \quad (37)$$

$$\mathbf{w}_- = [w_{1+}, w_{2+}, w_{z+}]^T \quad (38)$$

With any $(\mathbf{w}_1, \mathbf{w}_2) \in \Omega(\mathbf{v}_+)$, where

$$\Omega(\mathbf{v}_+) := \{(\mathbf{w}_1, \mathbf{w}_2) | (rw_{1+} + v_{y+})^2 + (rw_{2+} - v_{x+})^2 \leq d^2 v_{z+}^2\} \quad (39)$$

$$\text{And } d := \frac{6}{25}\mu(1 + \frac{1}{e_t})$$

IV.b ADM Inverse Relation

To reduce the computational time (<30ms) for calculating aerodynamic trajectory, the Magnus and Drag terms are dropped from (18). The simplified ADM becomes

$$\ddot{\mathbf{p}}(t) = -\mathbf{g} \quad (40)$$

$$\dot{\mathbf{p}} = \int_{t_0}^t -\mathbf{g} dt = \dot{\mathbf{p}}_0 - \mathbf{g}(t - t_0) \quad (41)$$

$$\mathbf{p} = \iint_{t_0}^t -\mathbf{g} dt = \mathbf{p}_0 + \dot{\mathbf{p}}_0(t - t_0) + \frac{1}{2}\mathbf{g}(t - t_0)^2 \quad (42)$$

Where $\mathbf{g} = [\mathbf{0} \ \mathbf{0} \ g]^T$.

After this simplification, the inverse relation for the ADM is fairly straightforward. The kinematic equations are derived by taking the integral of (40).

From position 1 to 2, the equations are

$$\mathbf{p}_2 = \mathbf{p}_1 + \mathbf{v}_{1+}T_1 - \frac{1}{2}\mathbf{g}T_1^2 \quad (43)$$

$$\mathbf{v}_{2-} = \mathbf{v}_{1+} - \mathbf{g}T_1 \quad (44)$$

$$\mathbf{w}_{2-} = \mathbf{w}_{1+} \quad (45)$$

From position 2 to 3, the equations are

$$\mathbf{p}_3 = \mathbf{p}_2 + \mathbf{v}_{2+}T_2 - \frac{1}{2}\mathbf{g}T_2^2 \quad (46)$$

$$\mathbf{v}_{3-} = \begin{bmatrix} 1 & 0 & 0 \\ 0 & 1 & 0 \\ 0 & 0 & -1 \end{bmatrix} \mathbf{v}_{3+} \quad (47)$$

$$\mathbf{w}_{3-} = \mathbf{w}_{2+} \quad (48)$$

Where $T_1 = t_2 - t_1, T_2 = t_3 - t_2$

IV.c RRM Inverse Relation

The RRM Inverse calculation is the crux of the control problem. In this case, the pre and post impact velocities are known. It is the independently controlled racket variables, velocity \mathbf{V} , yaw α and pitch β that are to be solved for.

Starting from the RRM (31), the first three equations for translational velocity are expanded as

$$\mathbf{v}_+ - \mathbf{V} = R_R A_r R_R^T (\mathbf{v}_- - \mathbf{V}) + R_R B_r R_R^T \mathbf{w}_- \quad (49)$$

Isolating \mathbf{V} yields

$$\mathbf{V} = (I - R_R A_r R_R^T)^{-1} [\mathbf{v}_1 - R_R A_r R_R^T \mathbf{v}_- - R_R B_r R_R^T \mathbf{w}_-] \quad (50)$$

The $-R_R A_r R_R^T v_-$ term can be rewritten as $(I - R_R A_r R_R^T) v_- - v_-$. Keeping in mind that R_R is a unitary matrix, (50) reduces to

$$\mathbf{V} = R_R(1 - A_r)^{-1}[R^T(v_+ - v_-) - B_r R_R^T w_-] + v_- \quad (51)$$

We solve for w_+ with the next three equations from the RRM (31), with the goal of relating translational velocity to rotational velocity.

$$\mathbf{w}_+ = R_R C_r R_R^T (v_- - \mathbf{V}) + R_R D_r R_R^T w_- \quad (52)$$

Substituting (51) into (52) yields

$$\begin{aligned} \mathbf{w}_+ = & -R_R C_r (1 - A_r)^{-1} R_R^T (v_+ - v_-) \\ & + R_R C_r (1 - A_r)^{-1} B_r R_R^T w_- \\ & + R_R C_r R_R^T w_- \end{aligned} \quad (53)$$

Next we define

$$S := -R_R C_r (1 - A_r)^{-1} R_R^T \quad (54)$$

Note that S evaluates to

$$S = \frac{k_w r}{k_v} \begin{bmatrix} 0 & c(\alpha) c(\beta) & s(\alpha) \\ -c(\alpha) c(\beta) & 0 & c(\alpha) s(\beta) \\ -s(\alpha) & -c(\alpha) s(\beta) & 0 \end{bmatrix} \quad (55)$$

Where c, s denote $\cos(), \sin()$ respectively. Let S_s represent the matrix portion of (55)

$$S_s(\alpha, \beta) = \begin{bmatrix} 0 & c(\alpha) c(\beta) & s(\alpha) \\ -c(\alpha) c(\beta) & 0 & c(\alpha) s(\beta) \\ -s(\alpha) & -c(\alpha) s(\beta) & 0 \end{bmatrix} \quad (56)$$

Equation (53) is simplified to

$$\mathbf{w}_+ = S(v_+ - v_-) + R_R(C_r(1 - A_r)^{-1} B_r + D_r) R_R^T w_- \quad (57)$$

$C_r(1 - A_r)^{-1} B_r + D_r$ evaluates to a 3x3 identity, and R_R is unitary, so (56) simplifies to

$$\mathbf{w}_+ = S(v_+ - v_-) + \mathbf{w}_- \quad (58)$$

We now introduce two variables

$$\boldsymbol{\xi} = \frac{k_w r}{k_v} (v_+ - v_-) \quad (59)$$

$$\boldsymbol{\eta} = (\mathbf{w}_+ - \mathbf{w}_-) \quad (60)$$

With these variables, we rewrite (57) as

$$\boldsymbol{\eta} = S_s(\alpha, \beta) \boldsymbol{\xi} \quad (61)$$

$$\boldsymbol{\xi}^T \boldsymbol{\eta} = \boldsymbol{\xi}^T S_s(\alpha, \beta) \boldsymbol{\xi} \quad (62)$$

The right hand term evaluates to zero

$$\frac{k_w r}{k_v} \begin{bmatrix} v_{x+} - v_{x-} \\ v_{y+} - v_{y-} \\ v_{z+} - v_{z-} \end{bmatrix}^T [S_s(\alpha, \beta)] \frac{k_w r}{k_v} \begin{bmatrix} v_{x+} - v_{x-} \\ v_{y+} - v_{y-} \\ v_{z+} - v_{z-} \end{bmatrix} = 0 \quad (63)$$

Thus $\boldsymbol{\xi}^T \boldsymbol{\eta} = 0$ is the first of three necessary conditions for a solution of $(\mathbf{V}, \boldsymbol{\alpha}, \boldsymbol{\beta})$ to exist.

Writing out (61) yields

$$\eta_x = \xi_y \cos(\alpha) \cos(\beta) + \xi_z \sin(\alpha) \quad (64)$$

$$\eta_y = -\xi_x \cos(\alpha) \cos(\beta) + \xi_z \cos(\alpha) \sin(\beta) \quad (65)$$

$$\eta_z = -\xi_x \sin(\alpha) - \xi_y \cos(\alpha) \sin(\beta) \quad (66)$$

(64) and (66) have a common term $\xi_y \cos(\alpha) \cos(\beta)$. We square both equations and add them together to lose the β term, resulting in

$$\begin{aligned} \xi_y^2 (1 - \sin(\alpha)^2) = & \eta_x^2 - 2\eta_x \xi_z \sin(\alpha) + \xi_z^2 \sin(\alpha)^2 \\ & + \eta_z^2 + 2\eta_z \xi_x \sin(\alpha) + \xi_x^2 \sin(\alpha)^2 \end{aligned} \quad (67)$$

Combining like terms in (67) reveals that the equation has the form of a quadratic equation

$$0 = ax^2 + bx + c \quad (68)$$

Where

$$\begin{aligned} x &= \sin(\alpha) \\ a &= \xi_y^2 + \xi_x^2 + \xi_z^2 \\ b &= 2(\eta_z \xi_x - \eta_x \xi_z) \\ c &= \eta_z^2 + \eta_x^2 - \xi_y^2 \end{aligned}$$

We can solve for α by using the quadratic formula

$$\sin(\alpha) = \frac{-b \pm \sqrt{b^2 - 4ac}}{2a} \quad (69)$$

To ensure that (69) has a solution, the discriminant must be greater than zero. This condition implies that $\|\boldsymbol{\eta}\|^2 \leq \|\boldsymbol{\xi}\|^2$, which is the second of three conditions for the solution to exist.

With α solved, β can be found by rearranging (65)

$$\frac{\eta_y}{\cos(\alpha)} = -\xi_x \cos(\beta) + \xi_z \sin(\beta) \quad (70)$$

Note (70) only has a solution if

$$|\eta_y| \leq \sqrt{\xi_x^2 + \xi_z^2} \cos(\alpha) \quad (71)$$

(71) can be rewritten as

$$\frac{\eta_y^2}{\xi_x^2 + \xi_z^2} \leq 1 - \left(\frac{-b \pm \sqrt{b^2 - 4ac}}{2a} \right)^2 \quad (72)$$

(72), is the third and final condition for a solution of $(\mathbf{V}, \boldsymbol{\alpha}, \boldsymbol{\beta})$ to exist.

The three conditions comprise Lemma 2. They are reiterated below.

- 1) $\boldsymbol{\xi}^T \boldsymbol{\eta} = 0$
- 2) $\|\boldsymbol{\eta}\|^2 \leq \|\boldsymbol{\xi}\|^2$
- 3) $\frac{\eta_y^2}{\xi_x^2 + \xi_z^2} \leq 1 - \left(\frac{-b \pm \sqrt{b^2 - 4ac}}{2a} \right)^2$

V. RACKET CONTROL

We now distinguish between three possible cases of ball motion in the serving task by developing Lemma 3. Notice from the TRM (17) that

$$\mathbf{v}_{T+} = \left(1 - \frac{5a}{2}\right) \mathbf{v}_{T-} \quad (73)$$

And from case 1 in the inverse TRM

$$\mathbf{v}_{T-} = \left(1 + \frac{5b}{2}\right) \mathbf{v}_{T+} \quad (74)$$

(73) and (74), combined with (47) show that if $\mathbf{v}_{3T+} \neq \mathbf{0}$, then $\mathbf{v}_{3T-} = \mathbf{v}_{2T+} \neq \mathbf{0}$ as well, hereinafter known as Case 1. But if $\mathbf{v}_{3T+} = \mathbf{0}$, then either $\mathbf{v}_{3T-} = \mathbf{v}_{2T+} \neq \mathbf{0}$ (Case 2) or $\mathbf{v}_{3T-} = \mathbf{v}_{2T+} = \mathbf{0}$ (Case 3).

With three distinct cases and equations from ADM (43)-(48) and the TRM (17), the relation between initial and final positions, translational, and rotational velocities can be determined.

$$p_{3x} - p_{1x} = v_{3x+}(T_1 + T_2) + (v_{3x+} - rw_2)(\delta T_1 + \gamma T_2) \quad (75)$$

$$p_{3y} - p_{1y} = v_{3y+}(T_1 + T_2) + (v_{3y+} + rw_1)(\delta T_1 + \gamma T_2) \quad (76)$$

$$p_{3z} = 0 = \frac{1}{e_t} v_{3z+} T_2 - \frac{1}{2} g T_2^2 \quad (77)$$

$$-p_{1z} = -\frac{1}{e_t^2} v_{3z+} T_1 + \frac{1}{2} g T_1^2 \quad (78)$$

$$v_{1x+} = v_{3x+} + \delta(v_{3x+} - rw_2) \quad (79)$$

$$v_{1y+} = v_{3y+} + \delta(v_{3y+} + rw_1) \quad (80)$$

$$v_{1z+} = -\frac{1}{e_t} v_{3z+} + g T_1 \quad (81)$$

$$w_{1x+} = w_1 + \theta(v_{3y+} + rw_1) \quad (82)$$

$$w_{1y+} = w_2 - \theta(v_{3x+} - rw_2) \quad (83)$$

$$w_{1z+} = w_{3z+} \quad (84)$$

$$(w_1, w_2) \begin{cases} := (w_{3x+}, w_{ry+}) \text{ for Case 1} \\ \in \frac{\Omega(\mathbf{v}_{3+})}{-\frac{v_{3y+}}{r}, \frac{v_{3x+}}{r}} \text{ for Case 2} \\ \in \Omega\left(\left[v_{3x+}, v_{3y+}, \frac{v_{3z+}}{e_t}\right]\right) \text{ for Case 3} \end{cases} \quad (85)$$

$$\gamma := \begin{cases} b_3 \text{ for Case 1} \\ \frac{2}{3} \text{ for Case 2} \\ 0 \text{ for Case 3} \end{cases} \quad (86)$$

$$\delta := \begin{cases} \left(1 + \frac{1}{e_t}\right) b_3 \text{ for Case 1} \\ \frac{2 + 5b_2}{3} \text{ for Case 2} \\ \frac{2}{3} \text{ for Case 3} \end{cases} \quad (87)$$

$$\theta := \begin{cases} \frac{3\left(1 + \frac{1}{e_t}\right) b_3}{2r} \text{ for Case 1} \\ \frac{5b_2}{2r} \text{ for Case 2} \\ 0 \text{ for Case 3} \end{cases} \quad (88)$$

$$b_3 := \frac{\mu\left(1 + \frac{1}{e_t}\right) |v_{3z+}|}{\sqrt{(v_{3x+} - rw_{3y+})^2 + (v_{3y+} + rw_{3x+})^2}} \quad (89)$$

$$b_2 := \frac{3\mu\left(1 + \frac{1}{e_t}\right) |v_{3z+}|}{5e_t \sqrt{(v_{3x+} - rw_2)^2 + (v_{3y+} + rw_1)^2}} \quad (90)$$

For serving, it is often desired to choose where the ball will land on the opponent's side, i.e. $\{p_{3x}, p_{3y}\}$. From (77) and (78), the variable v_{3z+} determines how quickly it gets there, i.e. $\{T_1, T_2\}$.

$$T_2 = \frac{2}{ge_t} v_{3z+} \quad (91)$$

$$T_1 = \frac{1}{ge_t^2} \left(v_{3z+} \pm \sqrt{v_{3z+}^2 - 2gp_{1z}e_t^4} \right) \quad (92)$$

Thus p_{3x}, p_{3y}, v_{3z+} are ideal candidates for independently controlled variables. Since there are five input variables, $\{\mathbf{V} \in \mathbb{R}^3, \alpha, \beta\}$, there can be two more variables that are independently controlled.

Theorem 1 posits that given $\{\mathbf{p}_1, \mathbf{v}_{1-}, \mathbf{w}_{1-}\}$ and a specified output $\{p_{3x}, p_{3y}, v_{3z+}\}$, the following pairs of variables can also be controlled, depending on the case.

For Case 1:

$$\{v_{3x+}, w_{3x+}\}, \{v_{3x+}, w_{3y+}\}, \{v_{3y+}, w_{3x+}\}, \{v_{3y+}, w_{3y+}\}$$

For Case 2 and 3:

$$\{v_{3x+}, v_{3y+}\}, \{v_{3x+}, w_{3x+}\}, \{v_{3y+}, w_{3y+}\}, \{w_{3x+}, w_{3x+}\}$$

VI. NUMERICAL SIMULATION

A numerical simulation verifies the proposed model by performing the following steps.

- 1) Assign output variables. The three recommended variables $\{p_{3x}, p_{3y}, v_{3z+}\}$, plus an additional two.

- 2) Perform inverse calculation to find the input variables $\{\mathbf{V} \in \mathbb{R}^3, \alpha, \beta\}$ as well as T_1, T_2 .
- 3) Perform forward calculation to find output variables $\{\mathbf{p}_3, \mathbf{v}_{3+}, \mathbf{w}_{3+}\}$ as well as intermediate variables $\{\mathbf{p}_3, \mathbf{v}_{3+}, \mathbf{w}_{3+}\}$ using both complex and simple ADMs.
- 4) Compare the assigned outputs to the calculated output.

VI.a Initial Conditions

For the complex ADM, the Magnus and drag coefficients are found by referencing experimental data.

Referencing figure 2, the ball is dropped at $(L, W/2, 0.8 m)$. $\mathbf{p}_1 = (L, \frac{W}{2}, 0.3m)$. From the aerodynamic model, $\mathbf{v}_{1-} = (0, 0, -3.043 m/s)$ and $\mathbf{w}_{1-} = (0, 0, 0)$.

VI.b Tabulated Results

In each table, the top sub-table lists the five variables that are chosen for step (1). The next sub-tables show the calculated input variables and the time variables in step (2). The bottom two sub-tables show the intermediate and final output variables in the forward calculation. The complex ADM (ADM With) is compared to the simplified ADM (ADM W/O).

Case 1, $V_{3T+} \neq 0$

	p_{3x}, p_{3y}	$v_{3x+}, v_{3y+}, v_{3z+}$	$\omega_{3x+}, \omega_{3y+}, \omega_{3z+}$
Ass.	0.342, 0.381	-4, -0.5, 2.15	***, ***, ***

V	α [deg]	β [deg]	T_1	T_2
-3.48, -1.25, 1.59	5.3	120.0	With 0.196	0.433
			W/O 0.199	0.471

	p_{2x}, p_{2y}	v_{2Tx+}, v_{2Ty+}	v_{3Tx+}, v_{3Ty+}
With	2.209, 0.627	0.24, -0.04	0.00, 0.00
W/O	2.195, 0.622	0.18, -0.03	0.00, 0.00

	p_{3x}, p_{3y}	$v_{3x+}, v_{3y+}, v_{3z+}$	$\omega_{3x+}, \omega_{3y+}, \omega_{3z+}$
With	0.624, 0.449	-3.69, -0.38, 2.08	19.1, -184.7, -72.4
W/O	0.343, 0.381	-4.00, -0.50, 2.15	25.0, -200.0, -72.4

Table 2: Numerical Results for Case 1

Case 2, $V_{3T+} = 0, V_{2T+} \neq 0$

	p_{3x}, p_{3y}	$v_{3x+}, v_{3y+}, v_{3z+}$	$\omega_{3x+}, \omega_{3y+}, \omega_{3z+}$
Ass.	0.342, 0.381	-4, -0.5, 2.15	***, ***, ***

V	α [deg]	β [deg]	T_1	T_2
-3.48, -1.25, 1.59	5.3	120.0	With 0.196	0.433
			W/O 0.199	0.471

	p_{2x}, p_{2y}	v_{2Tx+}, v_{2Ty+}	v_{3Tx+}, v_{3Ty+}
With	2.209, 0.627	0.24, -0.04	0.00, 0.00
W/O	2.195, 0.622	0.18, -0.03	0.00, 0.00

	p_{3x}, p_{3y}	$v_{3x+}, v_{3y+}, v_{3z+}$	$\omega_{3x+}, \omega_{3y+}, \omega_{3z+}$
With	0.624, 0.449	-3.69, -0.38, 2.08	19.1, -184.7, -72.4
W/O	0.343, 0.381	-4.00, -0.50, 2.15	25.0, -200.0, -72.4

Table 3: Numerical Results for Case 2

Case 3, $V_{3T+} = 0, V_{2T+} = 0$

	p_{3x}, p_{3y}	$v_{3x+}, v_{3y+}, v_{3z+}$	$\omega_{3x+}, \omega_{3y+}, \omega_{3z+}$
Ass.	0.342, 0.381	-3.6, -0.55, 2.15	***, ***, ***

V	α [deg]	β [deg]	T_1	T_2
-1.85, -0.50, 0.74	-7.3	85.7	With 0.196	0.437
			W/O 0.199	0.471

	p_{2x}, p_{2y}	v_{2Tx+}, v_{2Ty+}	v_{3Tx+}, v_{3Ty+}
With	2.071, 0.647	0.00, 0.00	0.00, 0.00
W/O	2.039, 0.641	0.00, 0.00	0.00, 0.00

	p_{3x}, p_{3y}	$v_{3x+}, v_{3y+}, v_{3z+}$	$\omega_{3x+}, \omega_{3y+}, \omega_{3z+}$
With	0.632, 0.434	-3.23, -0.48, 2.07	23.8, -161.7, -13.5
W/O	0.343, 0.381	-3.60, -0.55, 2.15	27.5, -180.0, -13.5

Table 4: Numerical Results for Case 3

VI.c Graphical Results

To show the results graphically, the trajectory as calculated by the forward prediction is plotted. The dotted line is the trajectory calculated with the simple ADM, the solid line uses the complex ADM.

Case 1:

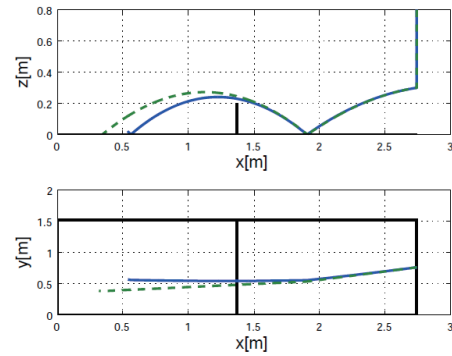


Figure 6: Graphical Results for Case 1

Case 2:

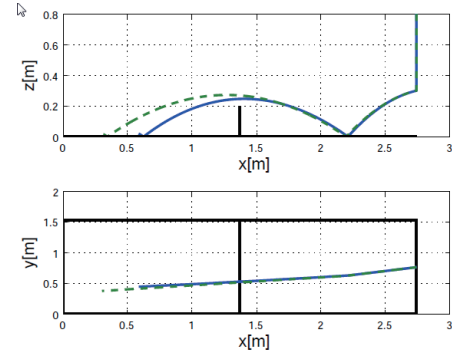


Figure 7: Graphical Results for Case 2

Case 3:

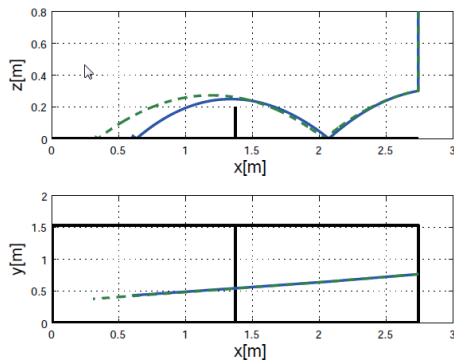


Figure 8: Graphical Results for Case 3

VII. CONCLUSION

In this paper, the process for developing a table tennis robot was elucidated. Equations were derived from physics principles to describe the motion of the ball as it travels through the air and collides with the surface of the racket and the table. These equations formed the basis of relationships (ADM, TRM, RRM) that allow for the ball's trajectory to be predicted. Then the control problem was introduced. An algorithm was proposed to determine the racket's striking posture and velocity given the desired output variables via inverse calculation of the forward prediction problem.

The results were verified by numerical simulation.

VIII. ACKNOWLEDGEMENTS

Professor Yoshikazu Hayakawa has furnished me with a once in a lifetime opportunity to work in an academic environment in Japan. I am extremely grateful for his cordiality and accommodating demeanor.

Chunfang Liu was a graduate student at Nagoya University. Her dissertation was an invaluable resource to me, and referenced countless times. Though I never met her, I thank her profusely for her efforts.

The JUACEP office initiated the exchange program to make all of this possible. They receive my thanks and praise for facilitating such a worthy program. I hope the experience was as delightful to them as it was for me.

IX. REFERENCES

Hayakawa, Yoshikazu, Satoshi Itoh, and Akira Nakashima. "Ball's

Trajectory Planning in Serving Task for Table Tennis

Robot." *SICE Journal of Control* (2015): n. pag. Web.

Liu, Chunfang. *Racket Control and Spinning Ball Measurement for Table*

Tennis Robot. Diss. Nagoya U, 2013. N.p.: n.p., n.d. Print.

Liu, Chunfang, Yoshikazu Hayakawa, and Akira Nakashima. "Racket Control for a Table Tennis Robot to Return a Ball." *SICE Journal of Control* 6.4 (2013): 259-66. Web.

Nakashima, A., Y. Ogawa, Y. Kobayashi, and Y. Hayakawa. "Modeling of Rebound Phenomenon of a Rigid Ball with Friction and Elastic Effects." *Proceedings of the 2010 American Control Conference* (2010): n. pag. Web.

CATALYTIC CRACKING OF POLYOLEFINS FOR FUEL CONSUMPTION

Haroula Kyriacou and Lindsey Perry

Department of Materials Science and Engineering, Henry Samueli School of Engineering, UCLA
haroulahoop@ucla.edu, lindsey.perry@ucla.edu

Supervisor: Masahiro Hirasawa

Department of Molecular Design and Engineering, Graduate School of Engineering, Nagoya University
hirasawa@numse.nagoya-u.ac.jp

ABSTRACT

The catalytic cracking of common polymers to create oil for fuel usage resulted in petrochemical products of varying composition. Two types of polyethylene (HDPE, LDPE), polypropylene (PP), and polystyrene (PS) were tested for their gas and liquid production yields. The objective was to identify the expected advantages of using a spent FCC catalyst and to compare the results of the polyolefin samples to the products of a waste plastic packaging. The quality of the oil and gas products was analyzed for its expected octane number and is shown to have improved with catalytic usage. Additionally, the fuel was tested for its functionality in a motorized scooter.

1. INTRODUCTION

Polymer cracking is a popular and necessary action to create hydrocarbons of higher quality for fuel consumption. Though thermal cracking is the current widespread method, catalytic cracking shows potential due to its higher production of aromatic and branched hydrocarbons. This is a necessary action to aid plastic recycling efforts as the growing population has exponentially increased its waste [1].

In order to promote the highest yield, in both volume and gasoline quality, a FCC catalyst is chosen for its zeolite Y structure. The hydrated

aluminosilicate's crystal structure and porosity allows for entrapment of elements to occur, aiding the reaction. However, the catalyst is a solid acid which can cause overcracking, or the formation of numerous small carbon chains which are then mainly collected as gas, decreasing liquid fuel production yields [2]. The acidic nature of the catalyst is overcome by use of a previously used sample provided by a petrochemical company, while any water present is evaporated through a preheat treatment.

In addition, different polyolefins show varying reactivity depending on their chemical structure. A definite trend is apparent when comparing liquid product yield of the polymers. A polymer containing a phenyl group, such as polystyrene, would theoretically create the highest amount of aromatics and therefore, the highest quality of gasoline. An octane number is the best qualifier for gas products but is hard to quantify. Therefore, information about octane number classification is necessary. Octane numbers are high for alkanes, aromatics and short carbon chains and increase with an increase in carbon chain branching [3].

2. EXPERIMENTAL

2.1 APPARATUS AND RAW MATERIALS

Gas and liquid samples were obtained using the experimental set-up shown in Figure 1. The primary component of the apparatus was an agitated semi-batch reactor with an inner volume of 500 mL. The experiment was performed for five different samples: four polymers- HDPE, LDPE, PP, PS- existing in virgin pellet form and a plastic waste soda packaging thought to be composed of HDPE. Each polymer was run twice in order to compare cracking methods. The first run consisted of preheated FCC catalyst (Catalyst 1) and was followed with a thermal cracking (no catalyst) trial. In addition, HDPE was cracked using a second catalyst of a different composition (Catalyst 2), giving a total of 11 experimental runs.

The polymer and catalyst, if used, were weighed and loaded into the reactor before it was sealed. 75 grams of polymer and 10 grams of catalyst (if applicable) were used in each run except LDPE, which was scaled to original parameters and consisted of 50 grams of polymer and 6.6667 grams of catalyst. The reactor was placed in a heater and sealed. A stir bar, thermocouple, and carrier gas tube were added and adjusted. Argon was used as the carrier gas due to its inert properties.

In addition, a cooler with its own thermocouple for measuring gas temperature were added as well as a flask to collect the liquid and aluminum bags to collect the gas. A heat wrap was also placed around the connecting glassware between the reactor and cooler in order to insulate the gas and prevent premature condensation. The Ar gas flowed through the apparatus at a rate of 100 mL/minute and water at 5.7°C flowed through the cooler to condense the vapor. The aluminum bags were changed at 10 to 15 minute intervals, at which time the temperatures were also recorded. The reactor reached temperatures as high as 783 K. In addition, the gas flow rate was periodically

measured in order to approximate the volume of gas in the bags.

2.2 ANALYSIS

Organic Elemental Analysis (OEA) was performed on the packaging waste sample to identify its components.

The morphology of the catalyst was analyzed using a Scanning Electron Microscope (SEM) coupled with energy dispersive spectroscopy (EDS). The catalysts were also analyzed using X-Ray Diffraction (XRD) to determine their crystal structures and X-Ray Fluorescence (XRF) to determine their elemental compositions. Finally, Inductively Coupled Plasma Mass Spectrometry (ICP-MS) was used to find trace elements in the catalysts' compositions.

Liquid and gas samples were analyzed using Gas Chromatography (GC-MS) to determine the type and carbon number of hydrocarbon products in order to compare both liquid and gas phase products with and without catalyst. Argon was again used as the carrier gas.

The solid coke product from catalyst trials was also kept for examination. SEM and XRD aided analysis for waste packaging coke.

3. RESULTS

The experiment resulted in both liquid and gas products. The solid coke residue found in the reactor after catalytic trials was considered to be the transformed catalyst and not considered a product of the reaction.

3.1 MATERIALS - CATALYST AND PACKAGING

Catalyst analysis proved imperative to identify elements present and confirm crystal structure. XRD analysis of Catalyst 1 correctly

classified the structure as a zeolite Y, aluminosilicate structure as well as tridymite and andalusite, variations of silica and aluminosilicate structures. Depending on the framework of synthetic catalyst, zeolite X or Y classifications can be made. Their silica-to-alumina ratios determine their activity and stability at high temperatures. Zeolite Y, with a ratio over 3, is preferred to Zeolite X whose ratio is between 2 to 3, as it functions at higher temperatures.

EDS, XRF and ICP identified the following expected elements in Catalyst 1: aluminum, silicon, iron, nickel, manganese, vanadium and lanthanum. The zeolite Y structure is an aluminosilicate capable of elemental exchange. For catalytic cracking, it is often used in a rare-earth hydrogen exchanged form, which is confirmed with the presence of lanthanum [4]. Other possible elements include calcium and rhodium (XRF and ICP only), sodium and carbon (EDS and ICP only) and nitrogen and oxygen from EDS only.

Catalyst 2 also contained a zeolite structure but differed from Catalyst 1 in that its structure did not contain aluminum but instead titanium. This was confirmed through XRD, which reported a Ti-exchanged silicalite structure. However, through elemental analysis, aluminum and silicon were found by all three techniques-EDS, XRF and ICP. However, titanium was only found through ICP and XRF as were manganese, iron and rhodium. Additionally, carbon and calcium were identified by ICP and EDS while nitrogen was only found through EDS.

The waste packaging sample, thought to contain high-density polyethylene, underwent OEA to test for its organic components. Though it had high component percentages of H, C and N, it was not identical to that of HDPE or LDPE, with its carbon content more than a whole percent below either polymer sample. Therefore, it can be

assumed that other additive elements are present in the packaging label.

Additionally, XRD and SEM-EDS were analyzed on the coke residue from the packaging trial. XRD analysis indicated that the packaging coke contained quartz, or SiO_2 , as well as calcium and magnesioferrite. EDS was performed on the packaging coke a total of five times, on different particles. The elements aluminum, silicon, and oxygen were present in all five runs, confirming that the coke is the transformed aluminosilicate catalyst. In addition, four of the runs showed that carbon and titanium were present and three of the runs showed that calcium was present. In one EDS run, the following elements were also identified in the packaging coke: chlorine, vanadium, manganese, iron, nickel, copper, zinc, and lanthanum.

3.2 PRODUCT

Liquid oil and gas samples underwent extensive GC-MS analysis. Each presented spectra of components varying in both carbon number and type with seemingly various trends. Components were subcategorized into bond type (paraffin, olefin, aromatic) and geometry (n vs. iso). Gas GC-MS required the removal of Ar from spectra data, as it was the carrier gas for both the experiment and chromatograph column. In addition, any peaks from water, as a result of catalyst hydration, or carbon dioxide from the atmosphere, were removed from the spectrum.

3.3 DISCUSSION

There are many limitations to the various analysis equipment used for this experiment. ICP required a diluted solution with use of NaOH. This may have affected the detection of Na in the catalyst samples. XRF has a lower limitation of elemental capability- it does not detect elements

with atomic numbers lower than 10 (sodium). It also uses rhodium as a target material for creation of x-rays, which could inaccurately be identified in sample spectrum.

Additionally, organic materials usually required specialized analysis (such as OEA) to identify their presence. However, as a synthetic compound, the catalyst did not require extra organic analysis. Catalyst 2 showed discrepancies in elemental analysis. It was thought to not contain any aluminum but instead only titanium. Though XRD confirmed a Ti-exchanged structure, Al was found in the various analyses. This may be explained through a zeolite structure where some Al was still present in addition to the Ti, as both exist as 3+ ions [5].

The analysis on the coke residue from the packaging gave expected results. Analysis on Catalyst 1 showed that it contained high amounts of silicon, in addition to trace magnesium, iron, and oxygen. Therefore, the XRD results of quartz, calcium, and magnesioferrite confirm that coke was the spent catalyst. The calcium in the coke was shown to be present in the form of wollastonite, or CaSiO_3 , which is appropriate due to silicon and oxygen also being found in the coke.

EDS confirmed that several elements found in Catalyst 1 were again present in the coke, such as silicon and oxygen. Titanium was also shown to be present in Catalyst 1 through three different methods of analysis, supporting that the EDS on the packaging coke was correct in identifying Ti. The same methodology applies to calcium being found in the coke. EDS also identified carbon as being present in the packaging coke. This was expected because EDS and ICP showed carbon in Catalyst 1; however it is also possible that the carbon was introduced to the coke, or increased its amount, through interactions with the primarily HDPE packaging.

One interesting result was that only a single run showed the presence of several elements that had been identified to be in Catalyst 1, such as iron, nickel, manganese, vanadium and lanthanum. These elements were expected to appear based on the catalyst analysis, but it is difficult to determine if their appearance in one EDS run was due to error or simply because they were not present on the other particles used for the other four runs. In addition, this run showed that chlorine was present in the coke. GC analysis on the gas produced from the packaging indicated that chloromethane was produced. Therefore, it is likely that the chlorine in the coke was introduced by the packaging since none of the analysis on Catalyst 1 showed any chlorine. Chlorine in the packaging could be due to an impurity in the HDPE or the pigments used for labeling.

As discussed, vehicular fuel oil requires high-octane values. This includes low carbon number components, as the oil GC-MS presented (Figure 2). It also improves with increased branching (iso) and alkanes (paraffins) as the gas data reports (Table 2). Aromatics also increase octane number; however, the use of a catalyst did not increase the amount of aromatics in the gaseous products. This could be due to machine or human error in the experimental and analytical steps. An overall comparison of catalytic to thermal cracking for each polymer type is also presented (Figures 6 and 7). From the figures, it can be seen that more five and six carbon compounds are produced from catalyst use, which are both more stable cyclic compounds and around the minimum carbon number for aromatic compounds.

Catalytic trials did not always show improvement over thermal cracking. In oil analysis, there seemed to be no improvement in any of the important octane ranking compounds (iso-paraffins, aromatics). This task was

problematic as the software had much difficulty discerning between the numerous peaks and identifying exact compounds with carbon numbers above than 8. Additionally, polystyrene produced liquid products that all contained benzene, as expected from its phenyl side group. As the carbon numbers increased, bibenzyl and naphthalene were created but their identification proved challenging. Their production also created a trend in the liquid products as there were two distinct peaks, one for the benzyl derivatives and another for the bibenzyl compounds.

Trends in individual trial data as well as overall comparison were identified. In individual polymer liquid samples, there were distinct peak groupings that easily corresponded to carbon number with the trailing peak always identified as the straight chain (n) paraffin. The gas analysis showed that all samples except for PP produced a significant increase in branched paraffins with the use of Catalyst 1. This provides information of catalyst success with the creation of compounds that contribute to a higher octane number.

However, with both PE samples, there seems to be aromatic production without catalyst use that is muted with use of catalyst (Catalyst 1 for LDPE, Catalyst 2 for HDPE). An interesting finding is that Catalyst 1 seems to have slightly increased the number of aromatic compounds for HDPE. Catalyst 1 also gave a better aromatic yield for PS. Lastly, HDPE and waste packaging show similar trends in that both showed a decrease in n-type yield with an increase in branched products with Catalyst 1 use. Again, this is in agreement with the idea of an increased octane value as branched hydrocarbons contribute to a higher octane rating. We compare HDPE and the packaging specifically as we expect the packaging to be made of HDPE.

Lastly, the functionality of the liquid fuel was tested. It first needed to be distilled to

eliminate heavy hydrocarbons. This required an additional few runs of the apparatus with carrier gas, thermocouples and cooler to reheat the liquid fuel and condense only the lighter hydrocarbons by keeping the gas temperature around 323 K, the boiling point of the lighter compounds. Though over 1000 mL of liquid was produced in the initial experimental runs, only about 500 mL was created through the distillation. This is less than 50% for fuel yield consumption, a rather low and surprising number. While it may not be efficient to produce fuel through catalytic cracking of waste plastics, the oil can be reused for other tasks such as plastic production.

In order to test the fuel, a motorized scooter was purchased. The scooter required gasoline siphoning as well as cleansing of the carburetor for old fuel. The newly distilled fuel was then placed in the scooter and after multiple attempts, the scooter started. The scooter was ridden by various lab members who attested to an increase in engine power they experienced as opposed to normal gasoline.

4. CONCLUSION

The comparison of catalytic and thermal cracking as well as sample polymer versus waste packaging gave the expected outcomes. The use of a used FCC catalyst correctly mitigated the hydrated and solid acid aspects of the zeolite structure and resulted in products whose compositions would lead to higher-octane values. The cracking of the waste plastic was comparable in both product yield and components to the polyethylene sample (HDPE). Moreover, visible trends in both liquid and gas products were observed. Lastly, the liquid product was shown to properly function as fuel for a motorized scooter.

4.1 FUTURE WORK

Thermo gravimetric analysis (TGA) for the coke byproduct would prove helpful to further classify elemental presence from both polymer and packaging sample. In addition, the chlorine found in the gas samples of the plastic waste packaging should be further studied with Chlorine Analysis on the packaging film. For the distilled liquid fuel, efficiency and power capabilities should be calculated through motorized scooter trials. Overall, it seems that PS created fuel with the highest octane number but is not widely used as a main component in the plastic packaging world. An ideal future would see the widespread use of polystyrene in plastic packaging instead of polyethylene to aid plastic recycling.

ACKNOWLEDGEMENTS

We would like to acknowledge JUACEP and JASSO for the support to conduct this research. We would also like to thank Professor Hirasawa for the opportunity to work on this research topic and for providing all the necessary materials and equipment. We want to give a special thank you to Professor Tani for the assistance on the analysis and testing of oil product (scooter) and our mentors, Takashi Shirao and Shiori Saino, for the endless help and support.

REFERENCES

- (1) Tani, H., et al. "Liquefaction of Waste Plastics- Catalytic Cracking of Polyolefins in the Molten Phase." *Fuel Processing Technology*. (2015). (Submitted for Publication)
- (2) Gobin, Karishma, and George Manos. "Polymer degradation to fuels over microporous catalysts as a novel tertiary plastic recycling method." *Polymer Degradation and Stability* 83.2 (2004): 267-279.
- (3) Miskolczi, N., et al. "Thermal degradation of municipal plastic waste for production of fuel-like hydrocarbons." *Polymer Degradation and Stability* 86.2 (2004): 357-366.
- (4) Lee, Kyong-Hwan, et al. "Comparison of plastic types for catalytic degradation of waste plastics into liquid product with spent FCC catalyst." *Polymer Degradation and Stability* 78.3 (2002): 539-544.
- (5) Achilias, D. S., et al. "Chemical recycling of plastic wastes made from polyethylene (LDPE and HDPE) and polypropylene (PP)." *Journal of Hazardous Materials* 149.3 (2007): 536-542.

5. TABLES AND FIGURES

Table 1. Experimental Summary

Catalyst	Sample	Temperature [K]		Time [min]	Percent Yield Oil
		T _i **	T _{max}	t _i ***	
FCC(2)	HDPE	642	768	33.2	61
FCC(1)	HDPE	721	763	31.4	83
FCC(1)	LDPE*	688	764	33.15	77
FCC(1)	PP	438	775	20.3	86
FCC(1)	PS	613	782	23	88
FCC(1)	Packaging	715	723	38.05	70

* LDPE - 50 grams
** T_i: temperature at first liquid drop
*** t_i: time at first liquid drop

Table 2. Percent Yield (Gaseous Products)

Product	Catalytic	Thermal
n-paraffin	13.3	21
i-paraffin	20.9	10.6
n-olefin	29.4	36.7
i-olefin	35.8	30.9
aromatics	0.6	0.8
other	0.02	0.06

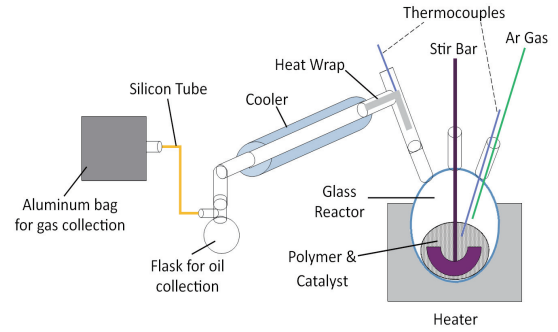


Figure 1. Reaction Apparatus

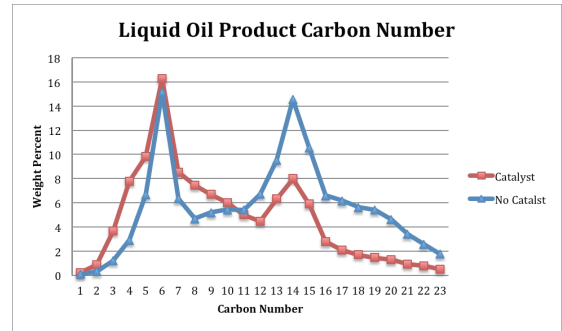


Figure 2. Carbon Number Yield (Liquid Product)

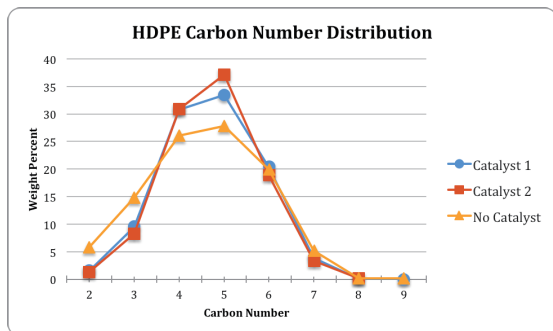


Figure 3A. Carbon Number Yield (Gaseous Product) of High-Density Polyethylene.

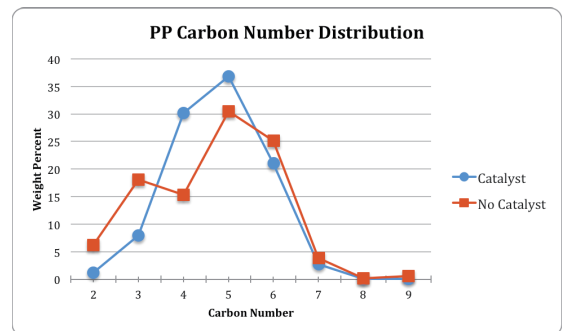


Figure 4A. Carbon Number Yield (Gaseous Product) of Polypropylene.

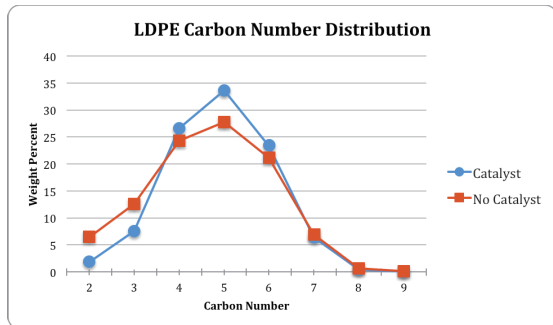


Figure 3B. Carbon Number Yield (Gaseous Product) of Low-Density Polyethylene.

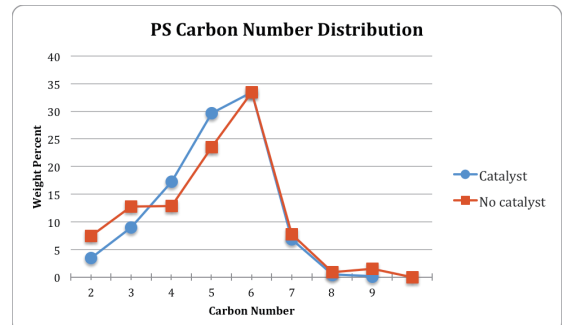


Figure 4B. Carbon Number Yield (Gaseous Product) of Polystyrene.

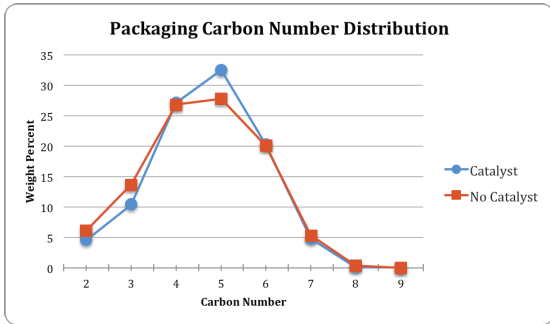


Figure 5. Carbon Number Yield (Gaseous Product) Waste Packaging.

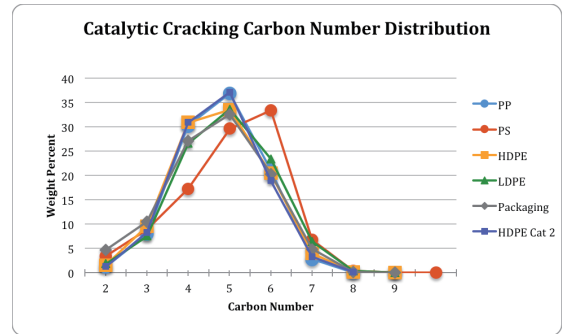


Figure 6. Carbon Number Distribution (Gaseous Products) for all Catalytic Runs.

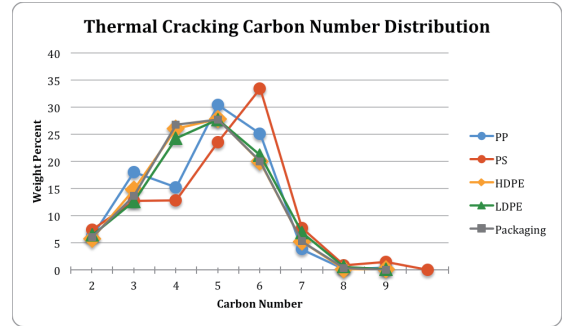


Figure 7. Carbon Number Distribution (Gaseous Products) for all Trials Without Catalyst.

Deep Discharge and Elevated Temperature Performance of Solid-state Thin Film LiCoMnO_4 Batteries

Hongyang Li

Department of Materials Science and Engineering, UCLA
hongyangli@ucla.edu

Supervisor: Prof. Yasutoshi Iriyama
Prof. William West

Department of Materials, Physics, and Energy Engineering Graduate School of Engineering, Nagoya University
iriya@numse.nagoya-u.ac.jp
william.west@numse.nagoya-u.ac.jp

ABSTRACT

LiCoMnO_4 (LCM) is one of the most important members of 5V spinel cathode material family, which is capable of offering high working voltage [1]. Most of the work on liquid electrolyte LCM batteries has been focused on the working performance above 3V. And some researchers believe that the Jahn-Teller distortion, which happens when Mn^{4+} is reduced to Mn^{3+} , would introduce rapid capacity fade. In this work, we found that in solid-state thin film batteries, there is considerable available capacity under 3V associated with the phase transition. And unlike in liquid electrolyte cell, the cycling performance between 5V to 2V at room temperature is desirable and at elevated temperature, the capacity below 3V get enlarged without compromising the capacity retention. This work suggests that by using solid-state thin film techniques, we could utilize the considerable capacity below 3V in spite of Jahn-Teller distortion.

Undisclosed

DESIGN AND OPTIMIZATION OF MICROFLUIDIC CHIP

Xu Li

Department of Mechanical and Aerospace, UCLA
Xuli9302@ucla.edu

Supervisor: Fumihito Arai

Graduate School of Engineering, Nagoya University
Arai@mech.nagoya-u.ac.jp

ABSTRACT

This work proposed a magnetically driven microfluidic chip for single cell manipulation which is based on micropillar vibration induced local whirling flow. Basically three magnetic tips are used to generate alternating magnetic fields which remotely control the magnetic beads embedded in the micropillar array. With alternating magnetic force exerting on the magnetic beads, micropillar arrays are thus subject to circular vibration which induced local whirling flow around micropillars. Based on fluidics dynamics, the target cell are then transported along the designed route until reaching the center of micropillar array, which is also the final destination. This technology has wide applications, such as single cell catcher, target cell 3D rotation and cell's mechanical properties measurement which makes this proposed microfluidic chip a competitive candidate for single cell manipulation.

1. INTRODUCTION

Single cell analysis has been a research hotspot for the last decades because of its significance in regenerative therapy and antibody medicines. In order to analyze single cell characteristics without influence from its neighboring cells or conduct a surgery to single cell, it is necessary to isolate a single cell out of a cell pool. Moreover, single cell 3D rotation is also a necessity technique in target cell 3D examination and observation for inhomogeneous cell surface textures. Until now, many techniques have been well developed by researchers, such as fluorescent-activated cell sorters (FACS) and optical tweezers, etc. The most accepted one is FACS, which is, however, consisted of many components and thus results in a rather complex system which is unfavorable in fabrication process. This disadvantage leads to an increasing interest in microfluidic chip which is able to shrink the whole system size down to a desirable range, and allows mass production of such chips. Furthermore, on-chip rotation studies have reported the use of electric, magnetic and optical forces⁵⁻⁹. However the majority of those systems either requires complicated

measurement and control system configuration or has relative low success rate, which can be overcome by microfluidics system.

Recently, a piezoelectric actuator based vibration induced whirling flow has been introduced by Hayakawa^{1,2}, who used piezoelectric material to generate circular vibration in PDMS substrate by altering electrical signals applied to piezoelectric material. This technology provides an option for single-cell on-chip manipulation, including trapping, alignment and movement. This work proposed an alternate driven force: magnetic force which has following advantages compared to PZT driven vibration: 1. Applied force is independent of bead position which means the drift in the sample position doesn't give appreciable changes in applied force, which thus gets rid of a complex feedback system. 2. Magnetically driven systems can control the target cell remotely without directly connecting the substrate, which removes the necessity of sample precise position control during fabrication process. 3. Magnetically driven system are in general insensitive to low-frequency noise (<1Hz) and thus provides ultrastable operation⁴.

This work firstly introduces the basic design of magnetically driven microfluidic chip based on vibration-induced whirling flow. Then corresponding theoretical model has been introduced, based on which finite element simulation is performed in order to optimize system parameter. Finally the fabrication process of this microfluidic chip is described. This work has been demonstrated as a competitive candidate for on-chip single cell manipulation.

2. 1. SYSTEM DESIGN AND THEORETICAL MODEL

2.1 System design

In our magnetic tips set up shown in Fig1(a), three NiFe alloy magnetic tips are used to produce uniform magnetic field gradient in the operational area. The scheme for micro-fluidic chips are shown in Fig 1(b), which was

previously done by Hayakawa, etc¹. Micropillar arrays are fabricated on the downside of PDMS roof with a distance from PDMS substrate, where magnetic beads are embedded in micropillar arrays. The size for micropillar is determined so that a local and global whirling flow can be generated to transport a single cell from outside into the center of micropillar array, the destination pot. Figure 2 depicts the basic concept of the single cell extraction chip. Cell transport is achieved by the local whirling flow which properties depending on micropillar array and a circular vibration magnitude and frequency. A local whirling flow can be induced in the vicinity of each micropillar under circular vibration. *If the micropillar pitch is shorter than the flow-induced area thickness, “global” whirling flow can be generated along the micropillar array*¹.

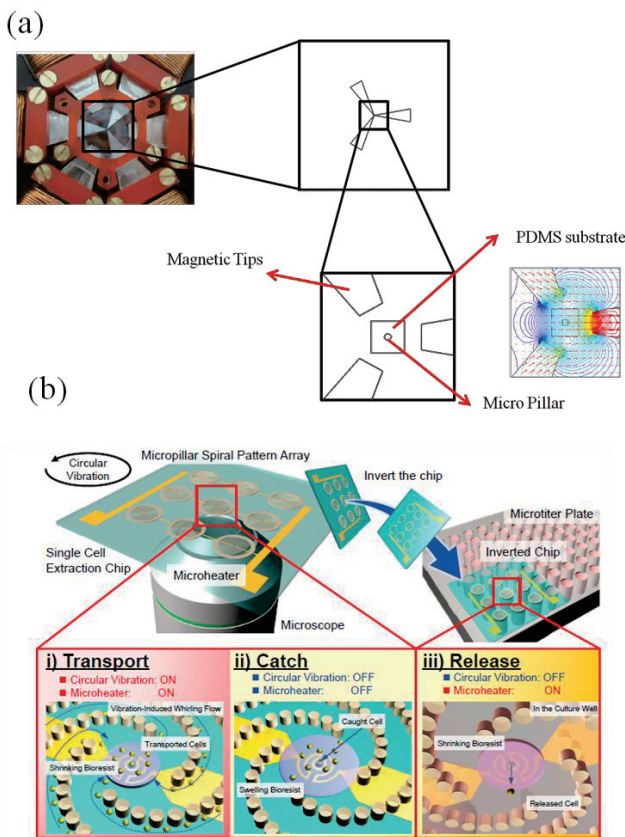


Fig 1. Proposed system scheme¹. (a) Six Magnetic Yoke with material PERMENORMR, 5000 H2, Vacuum schmelze GmbH & Co. KG, Germany and three NiFe alloy magnetic tips which distributed equally around the working area.(b) Proposed micropillar array on microfluidic chips¹.

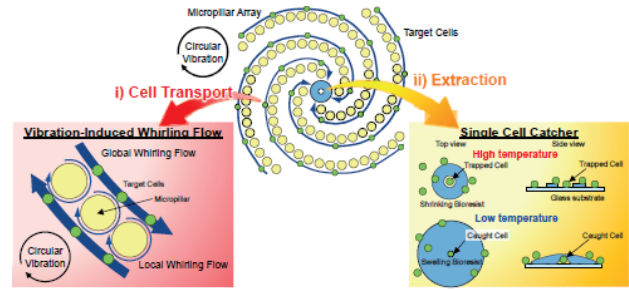


Fig 2 Basic concept of the single cell extraction chip¹.

With the ensuing magnetic field gradient, an actuation force can be applied on the magnetic beads. This magnetic force obeys¹⁰

$$F = \nabla (m \cdot B) \quad (1)$$

Where B is the magnetic flux density and m is magnetic moment of the bead. From Eq.1, it can be seen that the magnetic force is proportional to the magnetic field gradient. Therefore one of the goals in magnetic tips design and optimization is to obtain as large as magnetic field gradient as possible without damaging target cell.

A ferromagnetic bead, pure iron, is chosen in this work for its large saturation magnetization 1.4T. Ferromagnetic material has a high susceptibility to magnetization, the strength of which depends on that of the applied magnetizing field, and which may persist after removal of the applied field¹¹. Therefore when a ferromagnetic material is magnetized in one direction under external field, it will not relax back to zero magnetization when the imposed magnetizing field is removed. A field in the opposite direction is required for ferromagnetic material in order to be driven back to zero. *If an alternating magnetic field is applied to the material, its magnetization will trace out a loop called a hysteresis loop*¹³. The hysteresis loop for iron¹² is shown in Fig3(a).

In our proposed system, the magnetic beads are equally distributed with angle 120° between each other. When the magnetic beads experience an external force, it will cause the deformation on micropillar tip, and thus circular vibration can be achieved by alternating external magnetic field. This solid mechanical model is simplified as cantilever beam, whose basic structure is shown in Fig 3(b).

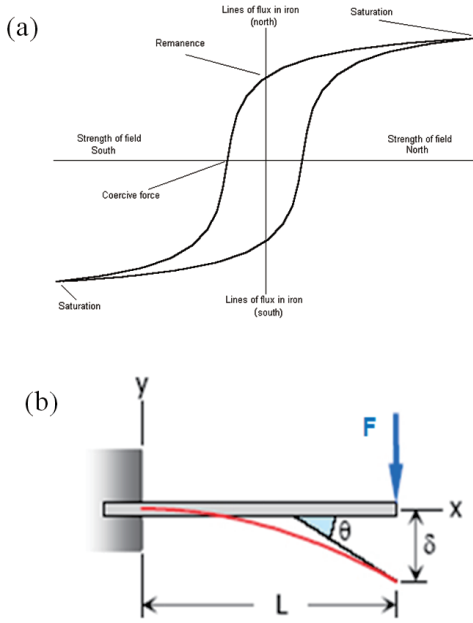


Fig 3(a) Hysteresis loop for iron. (b) Cantilever beam module

If force F is applied at the end of beam, the beam tip displacement is given by

$$\delta = F L^3 / 6EI \quad (2)$$

Where F is magnetic force, L is the pillar height, E is young's modulus and δ is tip deflection. The deflection equation now reads as

$$EI y = F x^2 / (6EI) \quad (3)$$

Where coordinate x, y is shown in Fig3(b).

In Ref[1], Hayakawa etc introduced the method to calculate vibration induced whirling flow. Though it's one of the essential parts for microfluidic design, it's not the focus for now in this work. Therefore a brief introduction has been given below.

The differential equations for the motion of an incompressible viscous fluid in 2D can be given by Eq4

$$\begin{aligned} \nabla^4 \psi - \frac{1}{\eta} \frac{\partial}{\partial t} \psi &= \frac{u}{\eta} \frac{\partial}{\partial x} \nabla^2 \psi + \frac{v}{\eta} \frac{\partial}{\partial y} \nabla^2 \psi \\ \frac{\partial u}{\partial x} + \frac{\partial v}{\partial y} &= 0 \end{aligned} \quad (4)$$

Where ψ is a stream function, η is the kinematic viscosity, and u and v are the velocity components along x and y direction. This equation was solved under such consumption that the convection term in the right hand side is much smaller than the others. And then the following boundary condition is applied

$$v_r|_{r=a} = v_\theta|_{r=a} = 0$$

$$v_r|_{r \rightarrow \infty} = \omega A_0 [\cos \theta \cos \omega t + \sin \theta \cos(\omega t \pm \pi)] \quad (5)$$

$$v_\theta|_{r \rightarrow \infty} = -\omega A_0 [\sin \theta \cos \omega t - \cos \theta \cos(\omega t \pm \pi)]$$

Where A_0 is the amplitude of vibration and ω is the vibration frequency. By solving the above equation, zero order solution can be obtained, which is given below

$$\psi^{(0)} = \omega A_0 [\sin \theta e^{-i\omega t} - \cos \theta e^{-i(\omega t \pm \pi)}] \left(\frac{2Y}{\varepsilon} - \frac{r}{a} - \frac{a}{r} C \right) \quad (6)$$

Where X, Y, Z and C are abbreviations of radial functions expressed by first kind Hankel functions.

After obtained zero order solution, the first order solution can such be calculated by the method of successive approximation to treat the nonlinear convection term in Eq4¹. More details in calculation can be found in Ref.1

3.2 SIMULATION RESULTS

Though the basic theoretical model is quite simple, it is extremely difficult to describe the microfluidic system by analytical solution in our design. Therefore in order to precisely optimize the system size, the finite element simulation has been performed with Comsol 4.4.

One of the major goals of magnetic tips design is to achieve a strong magnetic force on the magnetic beads embedded in micropillar arrays and produce relative uniform force within working area. Parameters used in this simulation are micropillar height $h=300\mu\text{m}$, pillar diameter $d=100\mu\text{m}$, the angle between two micropillars are 120° . PDMS substrate length $l=0.8\text{mm}$. Magnetic bead is pure iron with saturation magnetization 1.4T , magnetic tips is NiFe alloy with saturation magnetization 1.55T . The adjustable parameter is magnetic tip number, position, tip width w and space d . In the previous work done by Hayakaw¹, the micropillar array has been precisely designed and therefore this work mainly focuses on magnetic tips part.

Fig 4 shows magnetic flux density norm contour and flux density vector for two magnetic tips with three different configurations. Two magnetic tips can only generate uniform magnetic flux gradient in a relatively small area near tips. Except for that, magnetic flux density tends to be highly nonuniform as shown in the second configuration, which is clearly not an ideal working environment for microfluidic chips.

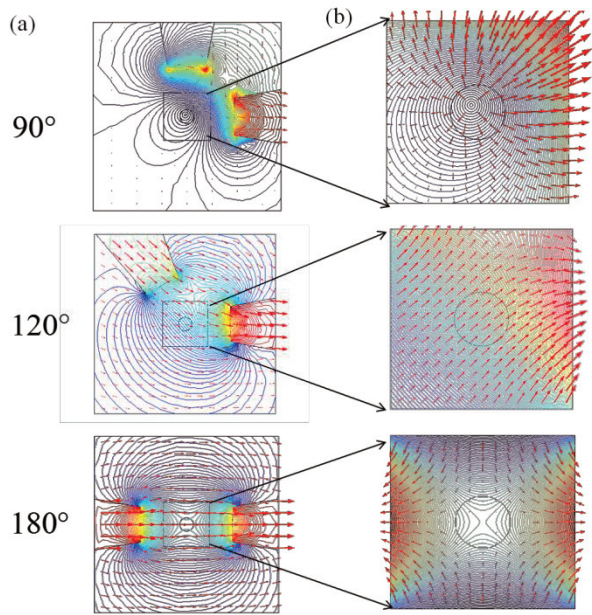


Fig.4 Two magnetic tips configuration with angle 90° , 120° and 180° respectively. Contour: magnetic flux density norm contour (a) Arrow: magnetic flux density.(b) Arrow: Magnetic force in the working area

On the contrary, three magnetic tips which are equally distributed around circle are able to generate a relatively uniform magnetic force in the working area, as shown in Fig 5(a)(b). Therefore in this work three magnetic tips configuration is accepted.

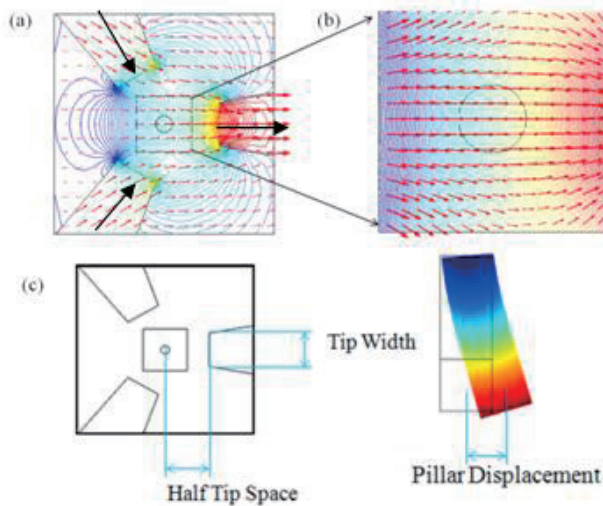


Fig.5 Magnetic tips configuration. Contour: magnetic flux density norm contour. (a) Red Arrow: magnetic flux density and black arrows show the default magnetic flux directions.(b) Arrow: Magnetic force in the working area. (c) Adjustable parameters

Next step is to optimize the magnetic tip width and tip space, which are shown in Fig.5(c). Fig.6 shows the dependence of magnetic force on tip width and tip space respectively. The magnetic force exerted on the micropillar is shown in Eq1.

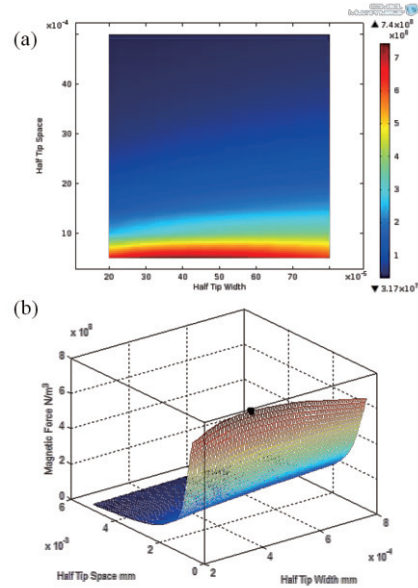


Fig.6 The dependence of magnetic force on tip width and tip space respectively. Colorbar shows the magnitude of magnetic force. (a) 2D (b)3D. The black point indicates the maximum value of magnetic force, which happens at 0.4mm half tip width and 0.5mm half tip space.

From optimization, the maximum force $7.4e8 \text{ N/m}^3$ occurs at 0.8mm magnetic width and 0.5mm half magnetic space. Under this condition, the micropillar tip displacement with diameter 100um and height 300um is 1um.

In order to generate circular vibration, the current must be applied in a sequence and magnetude of current should be determined carefully to ensure a uniform magnetic force in the working area. Since three magnetic tips are totally identical to each other, thus dividing the circular vibration into three identical parts, 120 polar angle degree for each one. Therefore for the following study we only focus the magnetic flux sequence on the first part (120 degree), and then periodic sequence can be applied in order to achieve circular vibration. Table1 shows the sequence of normalized magnetic flux in three tips.

Table 1 Sequence of normalized magnetic flux in three magnetic tips

	0	30	60	90	120
fLU	0.5	0.7	1	1	1
fLD	0.5	0.3	0	-0.3	-0.5
fR	1	1	1	0.7	0.5

Here fLU represents the normalization factor of magnetic tip on the left upper side, fLD is for left down side one and fR means the factor for right hand side magnetic tip. 1 represents the saturation magnetic flux density. The default magnetic flux directions (+) for three tips are shown in Fig4(a) respectively. Negative sign simply means the opposite of default direction. Fig.7 shows the magnetic force

within the working area under five angles 0,30,60,90 and 120, respectively.

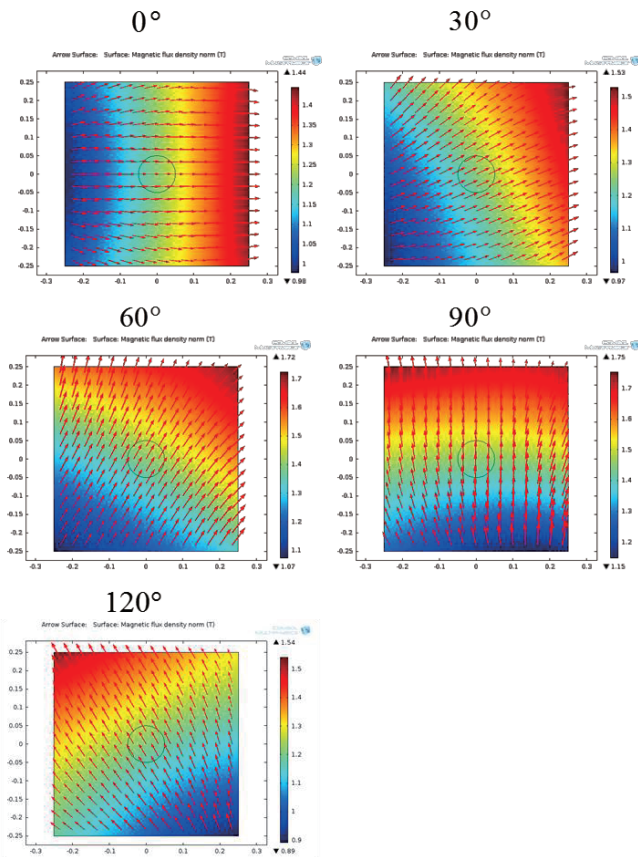


Fig.7 Red arrows show the magnetic force in the operational area. Color indicates the magnetic density norm. Five different force directions are obtained by following the magnetic flux applying sequence corresponding to Table 1.

From Fig.7 it can be seen that by varying magnetic flux magnitude and direction, different magnetic force direction can be achieved, which thus demonstrates the feasibility of the magnetic tips systems.

Fig.8 shows the sequence of normalized magnetic flux density in three magnetic tips corresponding to table 1. The top part sinoid curve in Fig.8 represents the magnetic tip vibration phase.

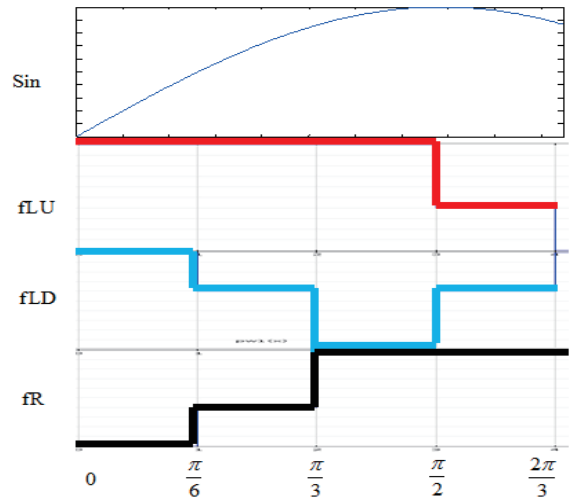


Fig.8 The sequence of normalized magnetic flux density. The top part sinoid curve represents the magnetic tip vibration phase.

Further optimization can be done to smooth the vibration phase.

4 . FABRICATION PROCESS

After finishing system design and optimizing system parameter, the next step is to fabricate the whole system. The main fabrication process is shown below¹:

1. Sputtering of Cr/Au on a glass substrate.
2. Spin coating of OFPR (Tokyo Ohka Kogyo Co. Ltd., Tokyo, Japan) on the sputtered Cr/Au layer.
3. Exposure and development of the OFPR as an etching mask of the microheater.
4. Etching Cr/Au and removal of the OFPR.
5. Spin coating the bioresist on the patterned microheater.
6. Exposure and development of the bioresist as a single cell catcher.
7. Spin coating SU-8.
8. Exposure and development of SU-8 as a micropillar array.

Fig.9 shows the real image in the fabrication process¹.

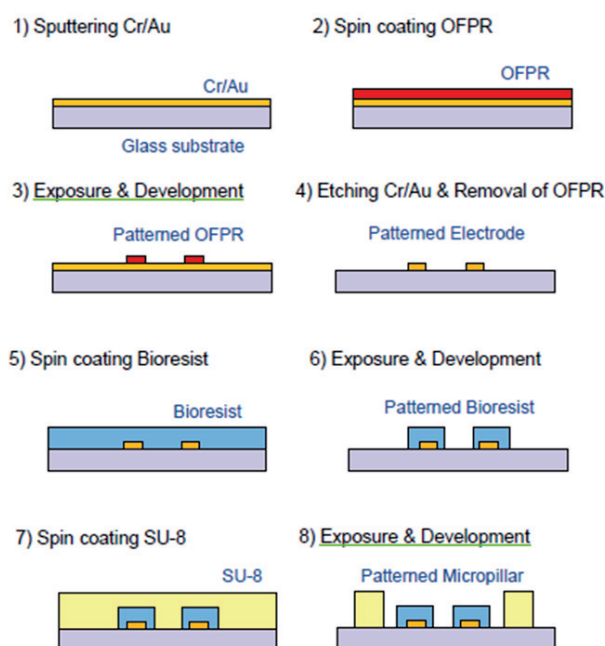


Fig.9 Fabrication Process¹

Until now, the fabrication process is still going which may require another month to fabricate the whole system and at least two more months to test and optimize system experimentally. So far all the optimization work has been done which provides the necessary theoretical base for the experimental set up.

5. CONCLUSION AND FUTURE WORK

This work proposed a new magnetically driven microfluidic chip. This kind of chip is based on micropillar vibration induced local whirling flow and magnetic tips were used to remotely control micropillar vibration by exerting the force on the magnetic beads which are uniformly embedded in the micropillars. Furthermore FEM simulation has been performed to optimize the system parameters for desired vibration.

For the future work, micropillar array will continue to be fabricated and magnetic tips system will be established based on optimization results. This system can be further optimized to reduce the energy consumption and increase working efficiency. The microfluidic chip proposed in this work provides a competitive candidate for the next generation single cell manipulation microchip.

ACKNOWLEDGEMENTS

The author would like to thank Arai sensei for providing such a valuable opportunity studying in this lab, Takeshi Hayakawa san for being such an amazing tutor and Maki Kikukawa san who has been a wonderful TA. The author also would like to express special thanks to JUACEP, who is the one making all these happen.

REFERENCES

- [1] Hayakawa, Takeshi, et al. "A single cell extraction chip using vibration-induced whirling flow and a thermo-responsive gel pattern." *Micromachines* 5.3 (2014): 681-696.
- [2] Hayakawa, Takeshi, Shina Sakuma, and Fumihito Arai. "On-chip 3D rotation of oocyte based on a vibration-induced local whirling flow." *Microsystems & Nanoengineering* 1 (2015).
- [3] Nakahara, Kou, et al. "On-Chip Transportation and Measurement of Mechanical Characteristics of Oocytes in an Open Environment." *Micromachines* 6.5 (2015): 648-659.
- [4] De Vlaminck, Iwijn, and Cees Dekker. "Recent advances in magnetic tweezers." *Annual review of biophysics* 41 (2012): 453-472.
- [5] Turcu I, Lucaciuc CM. Electrorotation: a spherical shell model. *Journal of Physics A: Mathematical and General* 1989; 22: 995-1003.
- [6]. Hölzel R, Lamprecht I. Dielectric properties of yeast cells as determined by electrorotation. *Biochimica et Biophysica Acta (BBA)-Biomembranes* 1992; 1104: 195-200.
- [7].Huang Y, Wang XB, Holzel R, et al. Electrorotational studies of the cytoplasmic dielectric properties of murine erythroleukaemia cells. *Physics in Medicine and Biology* 1995; 40: 1789-1806.
- [8].Jones TB. Basic theory of dielectrophoresis and electrorotation. *IEEE Engineering in Medicine and Biology Magazine* 2003; 22: 33-42.
- [9].Pethig R, Jakubek LM, Sanger RH, et al. Electrokinetic measurements of membrane capacitance and conductance for pancreatic β -cells. *IEE Proceedings-Nanobiotechnology* 2005; 152: 189-193.
- [10]. Chen, La, Andreas Offenhäusser, and Hans-Joachim Krause. "Magnetic tweezers with high permeability electromagnets for fast actuation of magnetic beads." *Review of Scientific Instruments* 86.4 (2015): 044701.
- [11]. <https://en.wikipedia.org/wiki/Ferromagnetism>
- [12].<http://www.energeticforum.com/eric-dollard-official-forum/11855-eric-dollard-3.html>
- [13]. https://en.wikipedia.org/wiki/Magnetic_hysteresis

**DESIGN AND IMPLEMENTATION OF
ALGORITHM FOR ESTIMATION OF ELEVATOR
TRAVEL DISTANCE USING SMARTPHONE
ACCELEROMETER**

Antonio Martinez

Department of Electrical Engineering, Graduate School of Engineering, UCLA
anmarti@ucla.edu

Supervisor: Nobuo Kawaguchi

Graduate School of Engineering, Nagoya University
kawaguti@nagoya-u.jp

Undisclosed

Electron Field Emission of Graphene and Zirconium coated Graphene

Jimmy Ng

Department of Materials Science and Engineering, Graduate School of Engineering, UCLA

ngjimmy310@ucla.edu

Supervisor: Yahachi Saito

Department of Quantum Engineering, Graduate School of Engineering, Nagoya University

ysaito@nagoya-u.jp

ABSTRACT:

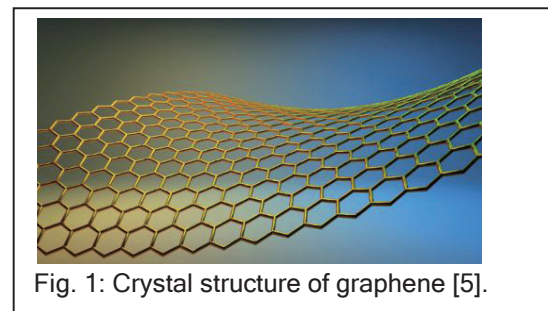
The electron field emission properties of graphene and the effects of Zirconium (Zr) deposition were investigated to achieve emitters with low threshold voltage and a stable emission pattern. The Fowler-Nordheim tunneling model and equation was used as an approximation to model the graphene-based nano-emitters. Field emission microscopy was conducted on graphene with none, 4Å, and 19Å Zr deposited and current vs time curves, I-V curves, and FEM videos were taken. It appears a dragonfly-like FEM pattern, predicted to be characteristic of graphene, was achieved for the bare graphene emitter. However, frequent current fluctuations in the bare graphene emitter and current decay over time for all emitters were found. Finally, it was found that although deposition of Zr significantly lowered the threshold voltage, it also altered the graphene's characteristic FEM pattern. The causes of and solutions to these problems are discussed in the discussion and conclusion.

INTRODUCTION:

Field emission is the emission of electrons, generally from a solid surface into vacuum, using an applied electric field. Electron emitters have been used for a number of applications, such as high resolution electron microscopes [1]. Furthermore, field emission is the primary source of vacuum breakdown and electrical discharge phenomena, something undesirable that engineers often try to

prevent [2]. Therefore, the understanding and study of field emission is important for many high technology electronic applications.

More recently, nanostructures of various materials have been explored to make atomically sharp emitters, with the end goal of constructing a practical microelectronic vacuum electron source that can be used in flat-panel displays, electron holography, and parallel electron beam lithography systems. So far, emission properties of one-dimensional structures have been well studied [3, 4]. My project investigates the emission properties of graphene, a two dimensional nanostructure of carbon atoms arranged in a honeycomb lattice, is shown in Figure 1 [5].



Winning the Physics Nobel Prize in 2010, it has attracted lots of attention recently due to its extraordinary electrical and mechanical properties and has been named the “new wonder material.” It conducts electricity better than copper, is 200 times stronger than steel but six times lighter, is almost perfectly transparent (absorbing only 2% of light), is

impermeable to gases (even those as light as hydrogen or helium), and can have its electronic properties altered with the addition of chemical components onto its surface [6]. Furthermore, it consists only of carbon, which is abundant and cheap. The carbon nanotube, its one dimensional counterpart, is known to have excellent characteristics that make it an ideal electron field emitter. For the reasons mentioned above, graphene's field emission properties and the effects from deposition of Zirconium (Zr) were investigated and are presented in this paper. The goal of the project is to obtain a graphene-based emitter with a stable emission pattern that can be turned on at a low threshold voltage.

This report first introduces the underlying physics necessary to understand field emission in the background knowledge section, namely quantum mechanical tunneling. Then it builds upon that to explain field emission, also known as Fowler-Nordheim tunneling. Then, the experimental procedures of making graphene electron field emitters, depositing Zr, and measuring emission properties is explained. After that, experimental data is presented and then interpreted in the results and discussion. Lastly, the conclusion summarizes the report.

BACKGROUND KNOWLEDGE:

Field emission was explained by quantum tunneling in the 1920s and became one of the triumphs of quantum mechanics. This builds on the idea that particles on the quantum scale, such as electrons, have particle-wave duality and can be described by the Schrodinger equation:

$$-\frac{\hbar^2}{2m^*} \frac{d^2\Psi}{dx^2} + V(x)\Psi = E\Psi \quad (1)$$

Where V is the potential energy of the particle and Ψ is the particle's wavefunction. The amplitude of the wavefunction squared is related to its probability of being found in a particular location in space and time.

Quantum tunneling is the quantum mechanical phenomenon where a particle "tunnels" through a potential barrier it would normally be unable to surmount in the classical world. To understand this,

consider a ball trying to roll over a hill as shown in Figure 2 top [7]. Classical mechanics and quantum mechanics has a different explanation of the scenario. In classical mechanics, if the ball does not have enough energy, it will be unable to roll over and would roll back down. In quantum mechanics, even without enough energy, the ball has a very small probability to tunnel to the other side, thus effectively crossing the barrier.

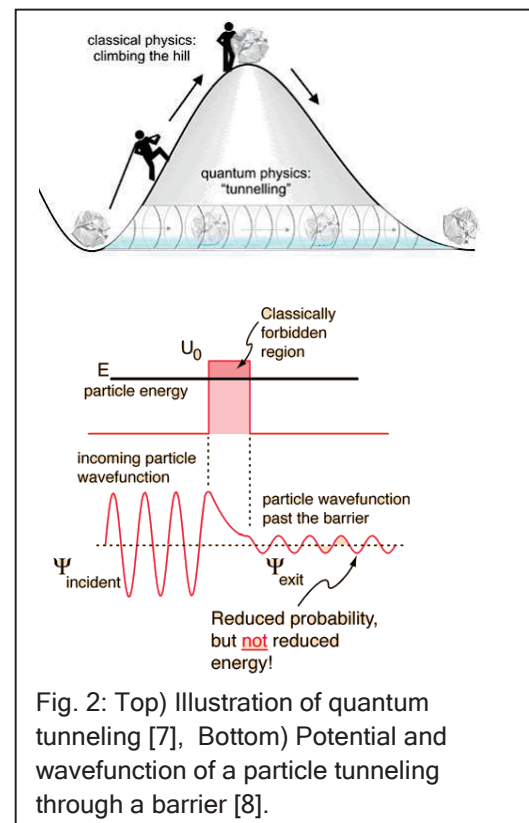


Fig. 2: Top) Illustration of quantum tunneling [7], Bottom) Potential and wavefunction of a particle tunneling through a barrier [8].

Quantum tunneling can be understood quantitatively by solving the Schrodinger equation (Equation 1). Consider the situation illustrated by Figure 2 right, where a particle is traveling to the right with energy lower than the energy of the potential barrier [8]. Using Equation 1, the wavefunction of the electron appearing to the right of the barrier can be solved for and is given by [8]:

$$\Psi = Ae^{-\alpha x} \text{ where } \alpha = \sqrt{\frac{2m^*(U_0 - E)}{\hbar^2}} \quad (2)$$

A is a normalization constant and α is a constant which characterizes wavefunction decay. The

wavefunction shows an exponential decay inside the barrier, which has a strong exponential dependence on the height and thickness of the barrier. Therefore, decreasing the height and thickness of the barrier slightly can lead to great increases in the amount of electrons that can tunnel through the barrier.

Electron field emission builds upon quantum tunneling. Field emission, also known as Fowler-Nordheim tunneling, is the process in which electrons tunnel through a barrier in the presence of a high electric field. It was named after Ralph H. Fowler and Lothar Wolfgang Nordheim, who first proposed the theory of electron field emission from bulk metals [9]. I investigated the electron properties of graphene using Fowler-Nordheim tunneling as the physical model explaining the phenomenon. The rest of the section explains the model and derives the Fowler-Nordheim equation.

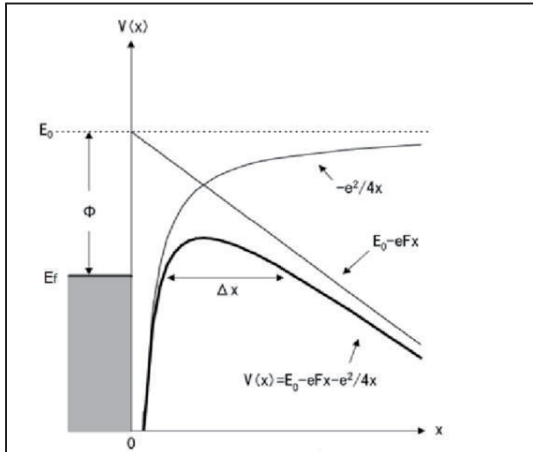


Fig. 3: Potential felt by electrons in a metal under Fowler-Nordheim emission [10]. Electrons in the metal have quantized energies, ranging from 0 to the E_f , the energy of the most weakly bound electrons. The potential consists of contributions from the work function, image charge, and applied electric field.

Figure 3 illustrates the potential felt by electrons to be emitted from a metal [10], which is a bit more complicated than the potential from Figure 2. The total potential is made up of three components:

- The work function, ϕ . This is the energy required to pull the most weakly bounded electrons to vacuum.
- The potential due to the image charge, $-e^2/4x$. Without going into unnecessarily complicated details, the image charge is an imaginary charge used to replicate boundary conditions of problems in electrostatics. This is the image charge potential for a flat conducting surface next to vacuum, which is the approximation used in the derivation of the Fowler-Nordheim equation [11].
- Potential from the applied electric field, $-eFx$.

Electrons in the metal have quantized energy levels, ranging from 0 to Fermi energy, E_f . E_f is the energy of the most weakly bounded electrons and it is these electrons which have the greatest probability of escape. The presence of an electric field bends the potential energy barrier so that the height and thickness of the barrier to be tunneled decreases. Again, to quantitatively describe it, we solve the Schrodinger equation (Equation 1). This time, the potential is:

$$V(F, x) = E_0 - \frac{e^2}{4x} - eFx \quad (3)$$

Unfortunately, the Schrodinger equation cannot be solved analytically for this potential. For an analytical solution, a semiclassical approach called the JWKB (Jeffreys-Wentzel-Kramers-Brillouin) approximation is used [12]. For the case of field emission, assuming electrons will be emitted out in the x -direction, the probability of an electron with x -direction energy, E_x , tunneling through the barrier and emitting from the metal with an applied electric field, F , with this approximation is:

$$D(E_x, F) = \exp \left\{ -\frac{8\pi(2m)^{\frac{1}{2}}}{3heF} (E_0 - E_x)^{\frac{3}{2}} \right\} \quad (4)$$

The general definition for current is the flow of electric charge, which is the amount of passing charge multiplied by the rate at which they are traveling. Therefore, to calculate the emission current, we must know the number of electrons that escape (which is the amount of electrons that can escape multiplied by its escape probability) and then the velocity at which those electrons are traveling at.

To obtain the energy distribution of electrons in the material, quantum statistical mechanics must be understood. But without going into too much technical detail, we can compare electrons moving inside a metal to a collection of gas molecules inside a container. Inside the container, there is an energy distribution of gas molecules. Most gas molecules will travel near the average velocity with some average energy, with very fast and slow molecules at the ends of the distribution. Increasing the temperature of the container would increase the average energy of the molecules, shifting the energy distribution. Therefore, there is a temperature dependent energy distribution of gas molecules. Similarly, there is a temperature dependent energy distribution of electrons in a metal given by quantum statistical mechanics [12] and is:

$$n(E_x)dE_x = \frac{4\pi mkT}{h^3} \ln \left[1 + \exp \left[-\frac{E_x - E_f}{kT} \right] \right] dE_x \quad (5)$$

With Equation 4 and Equation 5, we can calculate the current density, J , by multiplying the electron energy distribution by the escape probability and then integrating over all energies:

$$J = \frac{4\pi emkT^3}{h^3} \int_0^\infty \exp \left\{ -\frac{8\pi(2m)^{\frac{1}{2}}}{3heF} (E_0 - E_x)^{\frac{3}{2}} \right\} \ln \left[1 + \exp \left[-\frac{E_x - E_f}{kT} \right] \right] dE_x \quad (6)$$

With some approximation techniques to simplify the calculation, the current density is:

$$J = \frac{e^3 F^2}{8\pi h \phi} \exp \left[-\frac{(8\pi(2m)^{\frac{1}{2}})}{3heF} \phi^{\frac{3}{2}} \right] \quad (7)$$

And the current, I , given in SI units is:

$$I = 1.54 \times \frac{10^{-6} A (\beta V)^2}{\phi} \exp \left[-\frac{6.83 \times 10^7 \phi^{\frac{3}{2}}}{\beta V} \right] \quad (8)$$

Where A is the cross section area electrons are emitting from in units of cm^2 , ϕ is the work function in units of eV, and F is the applied electric field which is $F = \beta V$ where β is a proportionality constant with units $1/\text{cm}$ and V is the applied voltage.

This is necessary because applying voltage does not create an electric field landscape that is not uniformly distributed. The electric field is highly dependent on the surface morphology of the emitter and tends to greatly increase in areas on the surface with the greatest curvature (ie. Sharp edges), which is where electron emission is mostly likely to occur [13]. Therefore, F in the above equations is actually the effective electric field related to the voltage through proportionality constant β .

We can also qualitatively analyze the graphene's electron emission. Due to the wave-particle duality, emitted electrons' wavefunctions interfere in such a way that produces an observable emission pattern characteristic to graphene. Using a general approach to coherent field electron emission of nanoemitters applied to graphene, Zibing Li and Ningsheng Xu from the State Key Laboratory of Optoelectronic Materials and Technologies at Sun Yat-Sen University in China predicted a dragonfly like emission pattern with a dark body and two pairs of wings (see Figure 4) [14]. Emission patterns taken from my experiments are compared to those predicted by Li and Xu.

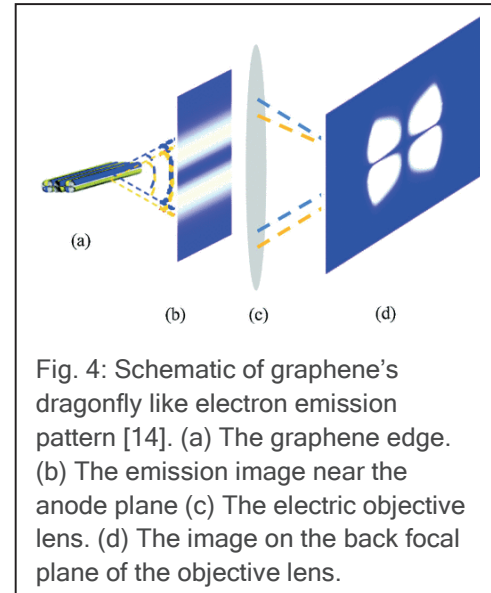


Fig. 4: Schematic of graphene's dragonfly like electron emission pattern [14]. (a) The graphene edge. (b) The emission image near the anode plane (c) The electric objective lens. (d) The image on the back focal plane of the objective lens.

EXPERIMENTAL PROCEDURE:

The experimental procedures consists of 4 steps: 1) making tungsten (W) needles, 2) using a scanning electron microscope (SEM) and microcontrollers to obtain graphene on the W needle to use as emitters, 3) characterization of graphene emitters by taking field electron microscope (FEM) images and corresponding current-voltage (I-V) and current-time curves, and 4) deposition of zirconium (Zr) onto graphene.

To make the W needles, first pieces of 0.15 mm diameter high purity W wire of about 1.5cm were cut. About 2 mm of the wire is soaked inside a NaOH solution and 4 V is applied. This procedure etches away W, creating a sharp tip. Figure 5 shows a schematic of this. After, newly made needles are cleaned with water and ethanol, and then inspected with an optical microscope and SEM to ensure they are usable.

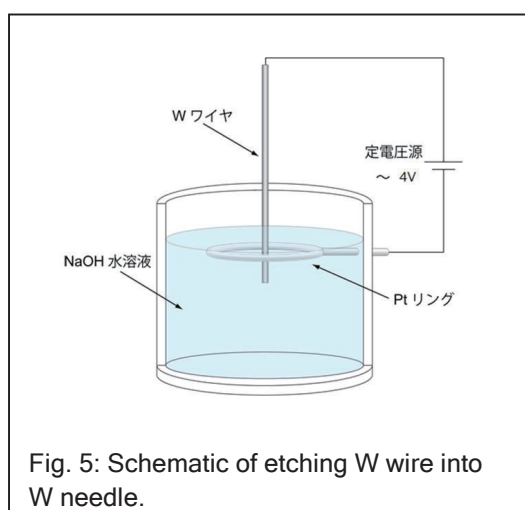


Fig. 5: Schematic of etching W wire into W needle.

Next, clean usable needles are loaded into the SEM. Using microcontrollers, a W needle is moved to graphite (bulk carbon), carefully coming in contact with the surface. The W needle is carefully scraped across carbon surface, picking up a few atomic layers of graphene. Figure 6 illustrates this process. The graphene sticks to the W needle by Van der Waals forces. This is what will be used as the emitter. The W needle part of the emitter is then spot welded onto Tantalum wire supported by an emitter holder, ready to be loaded into the FEM.

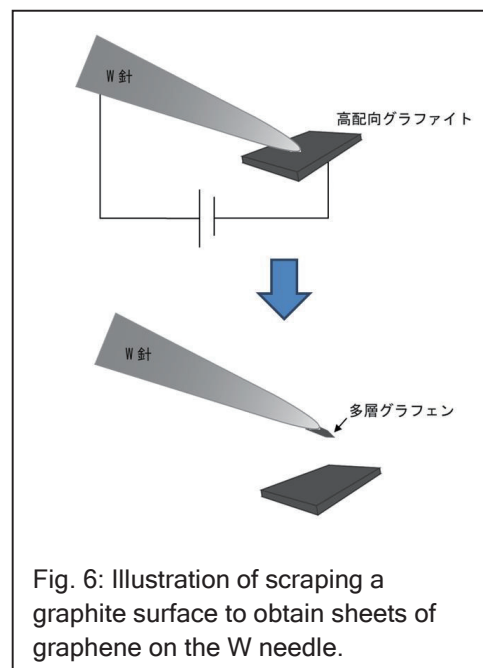


Fig. 6: Illustration of scraping a graphite surface to obtain sheets of graphene on the W needle.

About 3 emitters are made each time, and then the samples are loaded into the FEM. Figure 7 shows a schematic of the apparatus. The emitters are loaded into the emitter chamber, the right side of the apparatus, which contains multiple platforms to store emitters and has a system used to deposit Zr onto the emitter. Emitters can be moved to the main chamber, the left side, where FEM images can be taken. Inside the main chamber, the emitters can be reoriented so that graphene faces the green phosphor screen. Before doing any measurements, a high vacuum environment (pressure $\approx 10^{-7}$ Pa) is created using high vacuum pumps and the FEM chamber is heated for 1 to 2 days to remove any adsorbed molecules on the chamber walls.

To conduct FEM experiments, the screen is set to ground and a negative voltage is applied to emitter, creating an electric field in graphene that induces Fowler-Nordheim tunneling. Electrons are emitted out of graphene towards the phosphor screen. Impact with the screen produces FEM image patterns. A camera is set up to take pictures and videos of the FEM pattern. Simultaneously as images are taken, there is an ammeter that records the emission current.

With these capabilities, two kinds of measurements were taken:

- A constant voltage was applied and the emission current and FEM pattern was recorded and monitored over a fix time. This produces current-time graphs and videos.
- A voltage was applied, going from 0 V to either 600 or 700 V then back to 0 V in 1V steps. The emission current and FEM pattern was recorded with varying voltage, producing I-V curves and videos. Going forward (front sweeping) has shown to produce different results than going backwards (back sweeping), which will be discussed in the discussion section.

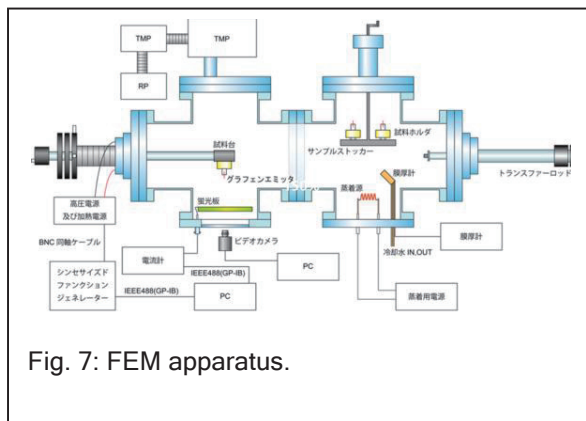


Fig. 7: FEM apparatus.

The effect of depositing Zr on the graphene was also studied. Metal deposition can be done in the FEM's emitter chamber and is illustrated in Figure 8. First, a 15 cm long Zr wire is wrapped along a 10 cm long W wire and a coil is created and loaded into the FEM. Like previously, a high vacuum environment is created and baking is done before deposition. The emitter is rotated to face the coil, and is placed about 10 cm above the coil. Then, a current is passed through the W coil, heating it up and vaporizing the Zr wrapped around it. The Zr vapor diffuses in the chamber spherically, reaching the emitter and the thickness gauge simultaneously. The thickness of deposited Zr deposited on graphene is measured using the calibrated thickness gauge. After deposition, the emitter can be moved into the main chamber for FEM measurements.

After data was collected, Mathematica programs were coded to analyze the measured I-V curves and current vs time curves and were compared to the

FEM videos taken. There was a small background current in all the data sets which were eliminated using the program. For the I-V curves, the measured data points were fitted to Equation 8 and plotted on the same graph for comparison to see how closely the graphene emitters adhered to Fowler-Nordheim emission theory.

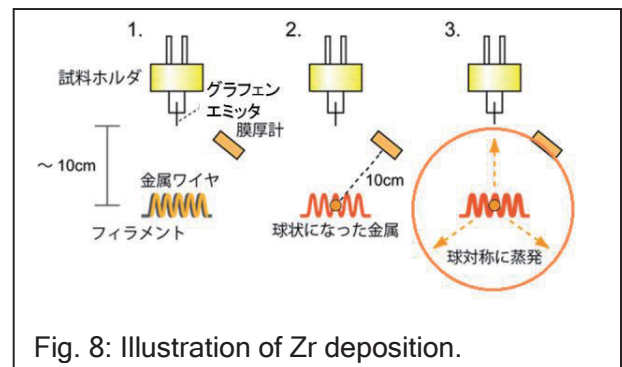


Fig. 8: Illustration of Zr deposition.

RESULTS AND DISCUSSION:

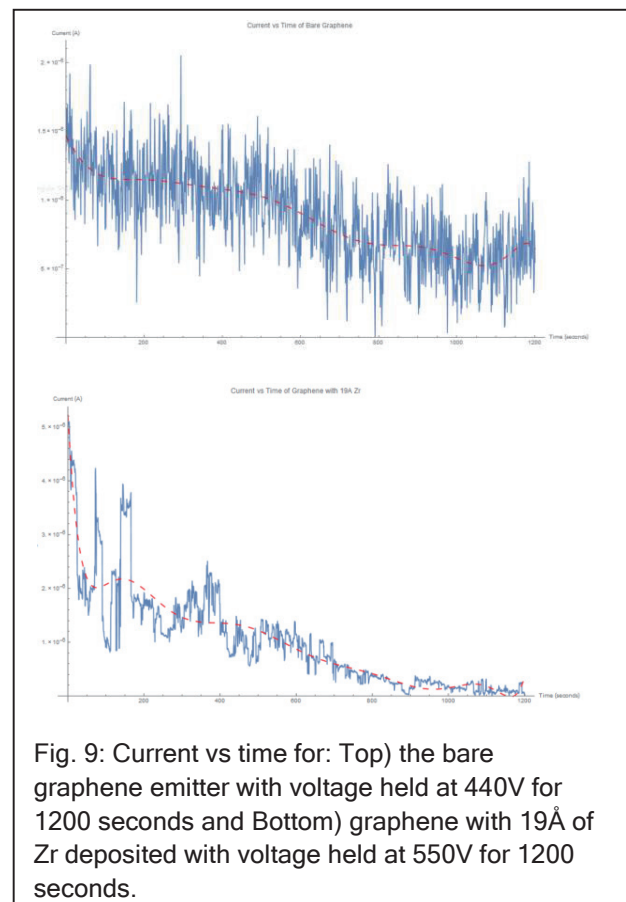


Fig. 9: Current vs time for: Top) the bare graphene emitter with voltage held at 440V for 1200 seconds and Bottom) graphene with 19Å of Zr deposited with voltage held at 550V for 1200 seconds.

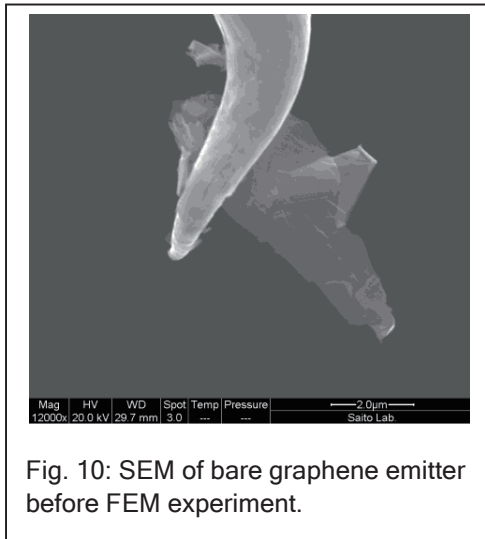


Fig. 10: SEM of bare graphene emitter before FEM experiment.

First, time vs current curves were produced for bare graphene and graphene with 19\AA of Zr deposited and is shown in Figure 10. For bare graphene, the voltage was held constant at 440V for 1200 seconds (Fig. 9 Top). Data was fitted to a 10^{th} degree polynomial and is plotted as the red dotted line to show the current behavior, which appears to decay with time. My interpretation of this is that the physical structure of graphene is changing with time. Before the FEM, the graphene emitter has many sharp edges due to obtainment from scraping (an SEM image of this is shown in Figure 10). It is well known that when a voltage is applied, the electric field is not uniformly distributed. Rather, it spikes in areas with sharp edges; thus, sharp edges on the emitter surface are areas where electron emission is most likely to occur. As time passes, the graphene emitter is heated to an elevated temperature due to the emission current, which enables diffusion processes to occur. In a progression to minimize its total free energy, the carbon atoms in graphene reconfigure themselves in such a way that the sharpness of the edges is reduced. Thus, there are fewer places that electrons can easily emit from, which explain the current decay over time.

Another thing to note is the frequent and strong fluctuations in the current. I believe this is due to the adsorption and desorption of molecules on the

surface. The electric field is known to be stronger closer to areas with adsorbed molecules, thus electrons are more likely to emit there. Thus, frequent adsorption and desorption would lead to frequent current fluctuations.

For graphene with 19\AA of Zr deposited, the voltage was held constant at 550V for 1200 seconds (Fig. 9 bottom). The data was fitted to a 10^{th} degree polynomial and is plotted as a red dotted line to show the current behavior, which appears to decay with time. Like for bare graphene, my interpretation of this is that structural changes are occurring on the surface of Zr, but in a different way. From TEM images taken, it appears that Zr does not deposit layer by layer uniformly on the graphene surface, which is common during heteroepitaxy of mismatched materials. Instead, islands are nucleating upon deposition due to the high lattice mismatch. Both graphene and Zr have hexagonal close packed crystal structures, but have lattice constants of 0.14 nm and 0.32 nm respectively, leading to a lattice mismatch of 129%! I believe that many islands are nucleated upon deposition, with a landscape of many smaller islands. During FEM, electron emission heats up the emitter and raises it to elevated temperatures. A process of diffusion and coalescence of the islands occur over time producing a landscape of fewer, bigger, and more rounded islands. The former landscape makes electron emission easier due to its large amounts of areas with high curvature, while the latter landscape makes electron emission more difficult for the opposite reason, thus explaining the decay in current over time.

Another thing to note is that current fluctuations are far less frequent for the emitter with Zr deposited than for bare graphene. I believe this is because Zr was deposited in a high vacuum environment (pressure $\sim 10^{-7}$ Pa) so there were few adsorbed molecules on the surface before FEM. Thus, there is no frequent process of adsorption and desorption like with the bare graphene emitter.

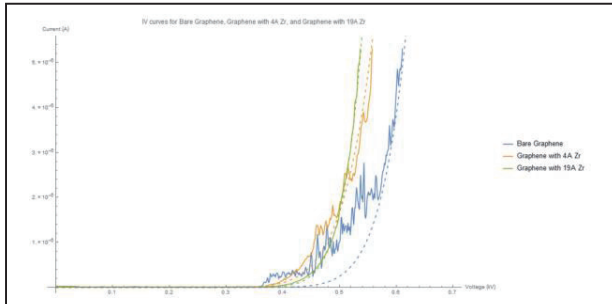


Fig. 11: Solid lines show IV curves of bare graphene, graphene with 4Å Zr deposited, and graphene with 19Å Zr deposited. Dashed lines plot Fowler-Nordheim equations fitted to the data.

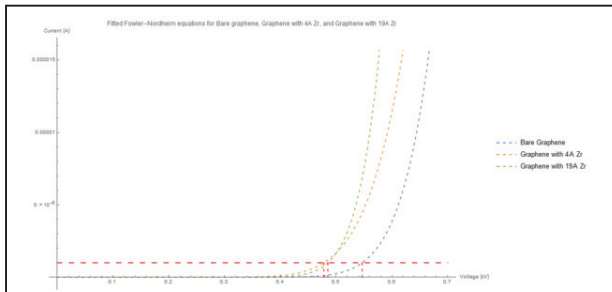


Fig. 12: Fitted Fowler-Nordheim equations and positions of threshold voltages for a threshold current defined to be 1 µA. The threshold voltages are 0.5467, 0.4781, 0.4853 kV respectively.

Next, IV curves were taken of bare graphene, graphene with 4Å Zr deposited, and graphene with 19Å Zr deposited. The Fowler-Nordheim equation, Equation 8, was fitted to the sets of data and is shown in Figure 11. The work functions assumed for graphene was 4.60 eV and for Zr deposited on graphene was 4.00 eV based on previous research done [15,16]. Because what is desirable is a stable electron emission pattern that can be activated at a low voltage, I defined the threshold current to be 1 µA then using the fitted Fowler-Nordheim equations, the corresponding voltages were found and defined as the threshold voltages. They are 0.5467, 0.4781, 0.4853 kV for bare graphene, graphene with 4Å Zr deposited, and graphene with 19Å Zr deposited respectively. Figure 12 shows the fitted Fowler-

Nordheim equations and the positions of the threshold voltages.

From Figure 11, we can see that the data does not fit smoothly with the Fowler-Nordheim equation. I believe there are two significant reasons for this. First, the Fowler-Nordheim equations must only be used as an approximation to our nano-scale emitters because it was derived assuming electron emission from a uniform bulk metal. Second, I believe that the structure of the emitter changes with each IV curve acquisition. Acquisition elevates the temperature of the emitter, possibly enabling diffusion and rearrangement of atoms, which explains “roughness” of the data.

There are a couple trends that must be noted from the data. First, as more Zr is deposited, the better the data fits the Nordheim-Fowler equation. This makes sense because depositing Zr brings the emitter closer to the assumptions made when deriving Fowler-Nordheim. Second, we see a notable decrease in the threshold voltage when Zr is deposited onto bare graphene. This also makes sense because the work function of Zr is lower than that of graphene, thus we should expect electron emission to be easier with Zr deposition.

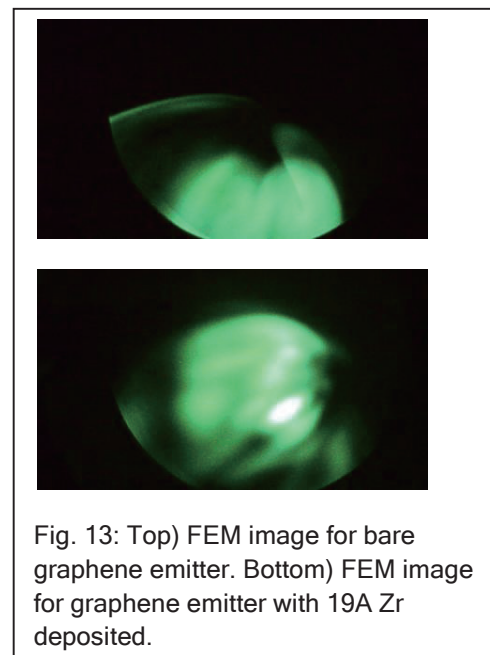


Fig. 13: Top) FEM image for bare graphene emitter. Bottom) FEM image for graphene emitter with 19Å Zr deposited.

Figure 13 Top and Bottom show the FEM pattern for bare graphene and graphene with 19 Å Zr deposited respectively. From Figure 13 Top, we can make out a dragonfly like pattern predicted by Li and Xu mentioned in the background knowledge. However, the pattern seems to drastically change when Zr is deposited. I believe that depositing Zr changes the emitter's surface and thus the way electron waves interact and interfere after being emitted, which leads to a change in the FEM pattern. Because a stable dragonfly emission pattern with a low threshold voltage is desired, what can be further investigated is the effect of lower thickness of Zr deposited onto graphene on the FEM pattern.

CONCLUSION:

For my project, the electron field emission properties of graphene were investigated. The effects of deposition of Zr on graphene were also investigated in an attempt to achieve a graphene-based emitter with a stable emission pattern that can be activated with a low threshold voltage. Graphene emitters were made by scraping W needles across a carbon surface with microcontrollers in a SEM. FEM was conducted on emitters of bare graphene and graphene with deposited Zr and current vs time and I-V curves were taken for quantitative analysis. The Fowler-Nordheim model and equation was used as an approximation to describe emission behavior of the graphene-based emitters. FEM patterns were recorded on camera and compared to the dragonfly-like FEM pattern predicted by Li and Xu for qualitative analysis.

The current vs time curves for bare graphene and graphene with 19 Å Zr deposited both show decay in current over time. I believe this is due to the atoms on the surface diffusing at elevated temperatures during FEM and creating surface landscapes that make electron emission less favorable. In bare graphene, I believe C atoms are reorienting themselves in a way that round out sharp edges on the surface. In graphene with 19 Å Zr, I believe that the landscape of many small nucleated Zr islands that formed upon deposition is transformed into a landscape of fewer larger islands via diffusion. The current vs time curve

for bare graphene also exhibits much more frequent current fluctuations than the 19 Å Zr curve. I believe this is due to the frequent adsorption and desorption of molecules on bare graphene. This is undesirable in the goal towards a stable FEM pattern and a proposed solution would simply to heat the emitter to desorb all adsorbed molecules before doing FEM.

I-V curves of bare graphene, graphene with 4 Å Zr deposited, and graphene with 19 Å Zr deposited was taken. The data sets were fitted to the Fowler-Nordheim equation for quantitative analysis. It was found that the data does not fit the equation smoothly, which we believe is due to two reasons: 1) the Fowler-Nordheim equation can only be used as a rough approximation for nano-emitters, and 2) there are structural changes on the emitter surface that affect the emission properties during I-V curve acquisition. Then, with the fitted equations and with a threshold current defined to be 1 μA, the corresponding threshold voltages were found. Threshold voltages are 0.5467, 0.4781, and 0.4853 kV for bare graphene, graphene with 4 Å Zr, and graphene with 19 Å Zr respectively. Deposition of Zr, even a low thickness layer, produces significant reduction of the threshold voltage. This is expected because the work function of Zr (4 eV) is significantly lower than the work function of graphene (~ 4.60 eV) and is desirable towards our goal of a graphene-based emitter with a lower threshold.

The FEM pattern of bare graphene showed resemblance to the dragonfly-like pattern predicted by Li and Xu. However, a video taken of the of FEM show that the pattern is not stable, which I believe is due to the frequent adsorption and desorption of surface molecules. Deposition of Zr alters the FEM pattern. I believe this is due to a change in the surface morphology, which in turn changes the way matter-waves of emitted electrons interfere.

More research must be done on the topic if a graphene-based emitter with a stable emission pattern and low threshold voltage is to be achieved. It appears that a dragonfly-like FEM pattern is achieved with bare graphene, but the pattern is unstable. To see

if a stable pattern from is achievable; we should desorb surface molecules before doing FEM. Also, it appears that deposition of Zr leads to both desirable and undesirable effects. It significantly lowers the threshold voltage, but also alters the FEM pattern. From the data, it appears as if depositing 4Å of Zr yields about the same threshold voltage reduction as 19Å of Zr. Depositing even lower thickness of Zr and analyzing its effect on the emission properties should be considered. Finally, the method of obtaining graphene by scraping a carbon surface leaves little controllability over the structure of graphene emitter. Furthermore, Zr and graphene both have hexagonal close packed crystal structures but have a large lattice mismatch, which leads to nonuniform island growth during deposition. Generally, both of the above is undesirable because it leads to less predictable emitter surface morphology and emission patterns. Different processes to produce graphene emitters and deposition metals should be considered. In conclusion, more research must be done if graphene-based emitters are to be used in the future as practical microelectronic vacuum electron sources.

REFERENCES:

1. Charbonnier F., Developing and using field emitter as a high intensity electron source, *Applied Surface Science*, vol. 94-95, pp. 26-43 (1996).
2. Miller, H.C., Electrical discharges in vacuum: 1980-90, *IEEE Transactions on Electrical Insulation*, vol. 26 no. 5, pp. 949-1043 (1991).
3. Oshima C., Mastuda K., Kona T., Mogami Y., Komaki M., Murata Y., Yamashita T., Kuzumaki T., and Horiike Y., Young's interferences of electrons in field emission patterns, *Physical Review Letters*, Vol. 8 Issue 3, pp. 83-84 (2002).
4. Hasselbach F., Progress in electron and ion-interferometry, *Reports on Progress in Physics*, Vol. 73 Issue 1, pp.1-43 (2010).
5. Hruska, J., New graphene displays create LEDs at an atomic level, *Extreme Tech Magazine* (2015).
<http://www.extremetech.com/computing/198773-new-graphene-display-creates-leds-at-an-atomic-level>
6. Larousserie, D., Graphene: the new wonder material, *The Guardian: Science* (2013).
<http://www.theguardian.com/science/2013/nov/26/graphene-molecule-potential-wonder-material>
7. Simko T., *Quantumianiac* (2015).
<http://quantumianiac.com/post/10373804268/quantum-tunneling-according-to-quantum-mechanics>
8. Barrier Penetration, *HyperPhysics Website* (2015). <http://hyperphysics.phy-astr.gsu.edu/hbase/quantum/barr.html>
9. Fowler, R. H., Nordheim, L. Electron emission in intense electric fields, *Proceedings of the Royal Society A*, Vol. 111 No. 781, pp. 173-181 (1928).
10. Fursey G., *Field Emission in Vacuum Microelectronics*, Kluwer Academic/Plenum Publishers, New York, Chap.1 (2005).
11. Griffiths, D. J., *Introduction to Electrodynamics* (4th Ed.), p. 121 (2015).
12. Froman, N., Froman P. O., *JWKB approximations to the theory* (1st Ed.), (1965).
13. Wheeler, C.B., Influence on space charge of field emission of electrons from sharp edges, *IEEE Proceedings A*, Vol. 139 No. 4, pp. 169-173 (1992).
14. Li Z., Ningsheng X., Kreuzer H. J., Coherent field emission image of graphene predicted with a microscopic theory, *Physical Review B*, Vol. 85 Issue 11, pp. 1-9 (2012).
15. Garg R., Naba D., Coudhury N. R., Work function engineering of graphene, *Nanomaterials*, Vol. 4, pp. 267-300 (2014).
16. Speight, J., *Lange's Handbook of Chemistry* (16th ed) p. 132 (2004).

FATIGUE CRACK HEALING VIA HIGH-DENSITY ELECTROPULSING

Jacob W. Stremfel

Department of Materials Science and Engineering, University of California, Los Angeles
jstremfel@ucla.edu

Supervisor: Yang Ju

Department of Mechanical Science and Engineering, Nagoya University
ju@mech.nagoya-u.ac.jp

ABSTRACT

A technique to prolong the fatigue life of Aluminum 6061-T6 was studied. High-density electropulses were administered to two fatigue samples with one sample only receiving once electropulse and the other sample receiving electropulses periodically, both beginning at 70% of their traditional fatigue lives. From the experimental results, it was found that both samples exhibited an extended fatigue life, but that the sample receiving periodic electropulses had a significantly higher gain in fatigue life compared to the sample that only received one electropulse.

Undisclosed

2-e. Workshop

The 13th JUACEP Workshop

Date: August 6 (Thu), 2015

Venue: VBL Hall, Nagoya University

Timetable:

13:40	Opening Address
13:45 - 17:30	Presentations by UM students (10 mins. presentation + 4 mins. Q&A each)
17:30 - 17:40	Completion Ceremony
18:00 -	Farewell Banquet

~Presentation Titles~

1: Fang Dai

“Implementation and Parameters Identification of Wiedemann Vehicle Following Model” (N/A)

2: Ulka Dandekar

“Suppression of Off-Target Effect by Chemically Modified siRNA” (N/A)

3: Haodong Shen, Nishizawa Lab, Quantum Engineering

“All-Polarization-Maintaining Er-Doped Ultrashort-Pulse Fiber Laser Using Carbon Nanotube Saturable Absorber” (p.115)

4: Hanyi Xie

“Effect of Surface Treatment on Mechanical Properties of DLC Coating” (p.118)

5: Goutham Thangaraj

“Extraction and Analysis of Trigger Rate and Pedestal Data from SciCRT” (p.122)

6: Emanuel Chirayath and Chadwick Harvey

“Design, Development, and Testing of a Rotating Detonation Gas-Turbine Engine” (N/A)

7: Jiahong Ju

“Investigation on the Performance of the L-R Type Fault Current Limiter in Low Voltage DC Distribution System” (p.125)

8: Chen Wang

“A Study on Topology Optimization with FEM Based on Level Set Method” (p.127)

9: Yuting Gao

“Analytical Study on Combustion Kinetics of Various Solid Fuels/Waste Products” (p.129)

10: Yalim Yildirim

“Quasi-passive Elastic Exoskeleton Control Based on Mechanical Joint Kinematics” (N/A)

11: Xudong Hao

“Evaluation of Contact States Using a Wound Testing System with Slip and Force Sensors for Estimating Skin Scratch Risks” (N/A)

12: Andrea Manoppo

“The Fabrication of Tissue Engineered Small Blood Vessels via 3D Cell Self-Assembly and Organization in Vitro” (p.131)

All-polarization-maintaining Er-doped ultrashort-pulse fiber laser using carbon nanotube saturable absorber

Haodong Shen
Nishizawa Laboratory
Dept. Quantum Engineering
Nagoya University

Introduction (Ultrashort pulse and applications)

Advance of laser technology → Ultrashort pulse

Ultrashort pulse (High peak power kW~MW, Ultrashort pulse width fs (10^{-15}))

- Metrology**
 - 3D measurement
 - UHR-OCT
- Amplifier**
 - Laser processing
 - Nonlinear microscopy
- Optical communication**
 - THz generation, Optical memory

Background

CLEO/QECC 09

Passively mode-locked ultrashort pulse fiber laser

- Compact
- Maintenance-free
- Practical
- Stable → One of the key issues

All polarization maintaining fiber lasers → Environmentally stable performance

- SESAM + PMF (Hartl, Nielsen), Figure 8 (Nicholson)
- Saturable absorber: self-start, stable, all PM configuration

SESAM

semiconductor saturable absorption mirror

- transparent-type
- fast response
- expensive
- difficult to fabricate

SWNT

single-walled carbon nanotube

- transparent-type
- fast response
- broadband
- mass productive

Nano-carbon materials

Single wall CNT (SWNT)

Double wall CNT (DWNT)

Graphene

<http://www.surf.nuqe.nagoya-u.ac.jp>

- Single wall CNT (SWNT) -

Properties depend on chirality and diameter

Diameter of 1.2 nm corresponds to saturable absorption at 1.55 μ m wavelength

Fast response: less than 1 ps

Preparation of SWNT polyimide film

Synthesis techniques of SWNT

- Arc discharge
- CVD
- High pressure CO (HiPco)
- Mass-production is demonstrated
- Laser ablation
- High controllability of SWNT diameter

Absorption spectra

Fabrication of SWNT polyimide film

- SWNTs were carefully purified
- SWNTs were equally dispersed in polyimide varnish
- Film was formed by evaporating organic solvent

2mm×2mm×17 μ m

Saturable absorption property of SWNT

Absorption [%]

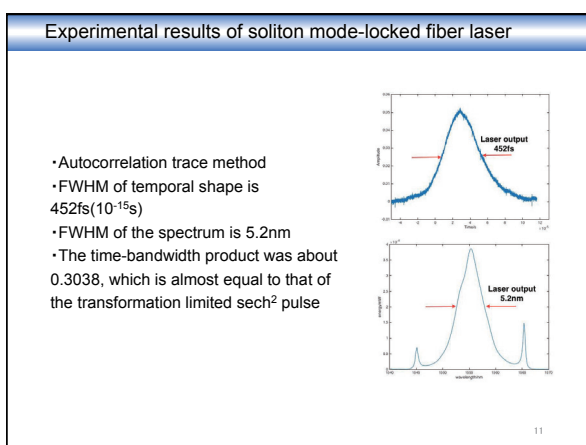
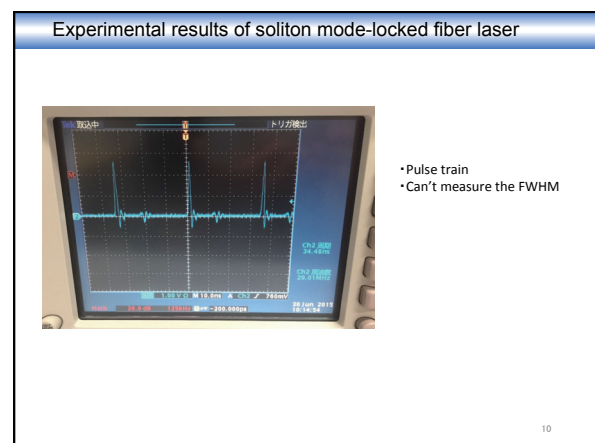
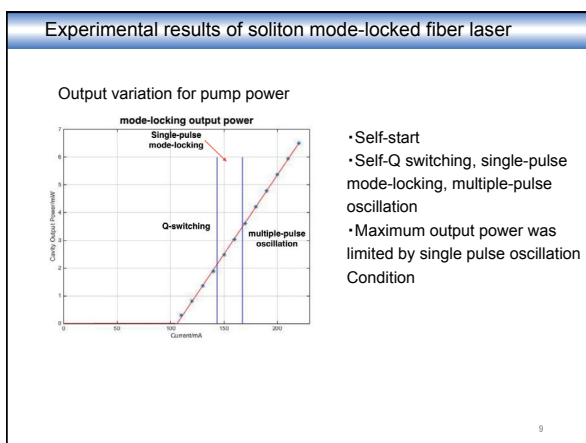
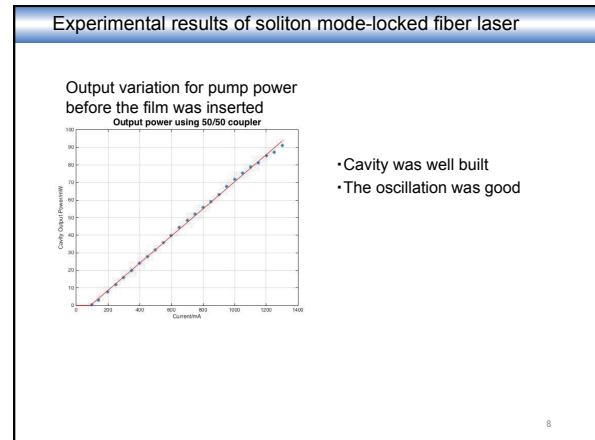
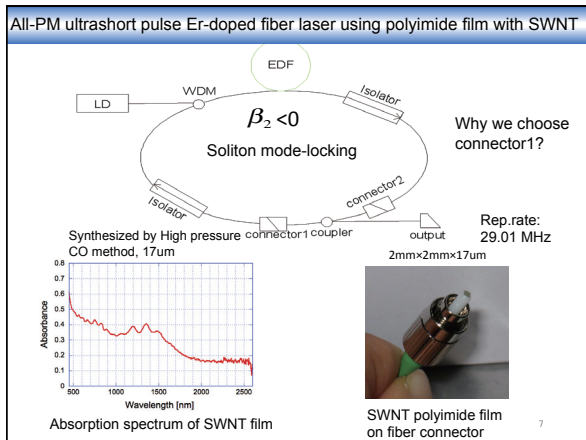
Pulse energy flux [μ J/ cm^2]

Absorption spectra

Wavelength [nm]

Modulation depth: ~20% for LA-SWNT
~10% for HiPco-SWNT

Connector with SWNT polyimide film



Conclusion

- Built the whole set-up
- Demonstrated an all polarization-maintaining (PM) passively mode-locked Er-doped ultrashort-pulse fiber laser using a polyimide film with dispersed single wall carbon nanotubes.
- A 452fs ultrashort soliton pulse was stably generated from the fiber laser at a repetition frequency of 29.3MHz, and the maximum output power was 3.5 mW for single-pulse operation.
- It shows stable and self-start operation.

Reference

- [1] Nishizawa, N., et al. "All-polarization-maintaining Er-doped ultrashort-pulse fiber laser using carbon nanotube saturable absorber." *Optics express* 16.13 (2008): 9429-9435.
- [2] Fermann, Martin E. *Ultrafast fiber oscillators*. Marcel Dekker, 2002.
- [3] Nishizawa, Norihiko. "Ultrashort pulse fiber lasers and their applications." *Japanese Journal of Applied Physics* 53.9 (2014): 090101.
- [4] Weiner, Andrew M. "Ultrafast Optics." *Chapter 3*: 85-146.
- [5] Nozaki, Y., N. Nishizawa, E. Omoda, H. Kataura, and Y. Sakakibara. "Power scaling of dispersion-managed Er-doped ultrashort pulse fiber laser with single wall carbon nanotubes." *Optics letters* 37, no. 24 (2012): 5079-5081.
- [6] Agrawal, Govind P. *Nonlinear fiber optics*. Academic press, 2007.

13

1

Effect of Surface Treatment on Mechanical Properties of DLC Coating

Hanyi Xie
TA: Eitaro Nakatani
PI: Hiroyuki Kousaka, Xingrui Deng, Noritsugu Umehara

2

Agenda

- ▶ Project Background
- ▶ Experimental Method
- ▶ Results & Discussion
- ▶ Conclusion

3

Agenda


- ▶ Project Background
- ▶ Experimental Method
- ▶ Results & Discussion
- ▶ Conclusion

4

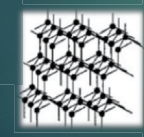
Background Information

DLC (Diamond Like Carbon) film is expected to be applied to sliding parts.

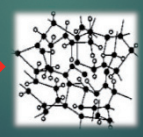
- Low Friction
- High Hardness
- Wear Resistance
- Chemical Stability



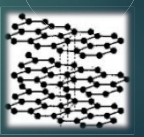
DLC application



Diamond (sp³)



DLC



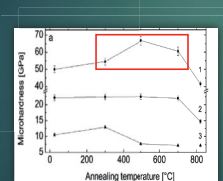
Graphite (sp²)

5

Previous Research

Hard coatings are particularly useful in abrasive environments, which is common in sliding contact [1].

▶ Purpose:
To increase the hardness of DLC coating by surface treatment.



Hardness Vs. Temperature Plot [2]

▶ The hardness of ta-C can be improved by annealing test.

6

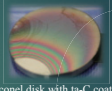
Agenda

- ▶ Project Background
- ▶ Experimental Method
- ▶ Results & Discussion
- ▶ Conclusion & Future Work

Material Preparation

7

- Properties
 - Disk material: inconel X750 Alloy
 - Coating layer: ta-C
- Dimensions
 - $\phi=20$ mm
 - $t=2$ mm
- Deposition method (FCVA)



Inconel disk with ta-C coating

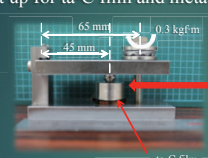
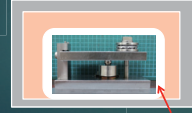
	H_c , GPa	R_a , nm	d_r , nm
ta-C	52	23	607.0
Ni	6.1	25	N/A
Co	5.2	21	N/A
SUJ2	14	21	N/A

Material Property Table

Experimental Method

8

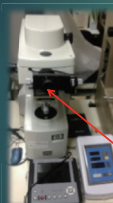

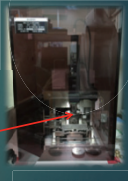
- Set up for ta-C film and metal disks on the jig
 - 65 mm
 - 45 mm
 - 0.3 kgf/m
 - ta-C film
 - Ni, Co, SUJ2
- Annealing Test in vacuum
 - Temperature (°C): 200, 300, 400, 500, 800
 - Time (hour): 1
 - Pressure (Pa): $3-5 \times 10E3$
 - Vacuum

Hardness Measurement

9

- Mark specific positions on ta-C coating for hardness test
- Measure the hardness in contacting area of ta-C and metals by Nano-indenter

Vickers Hardness Test

Hardness Measurement under Nano-indenter

Nano Indenter

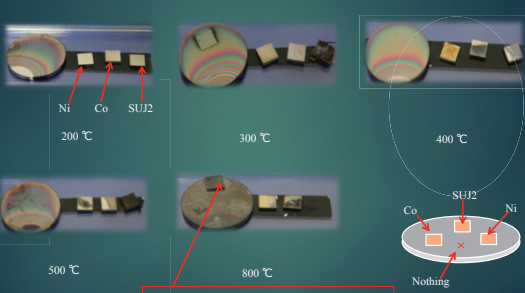
Agenda

10

- Project Background
- Experimental Method
- Results & Discussion
- Conclusion

Specimens after Annealing

11



200 °C

300 °C

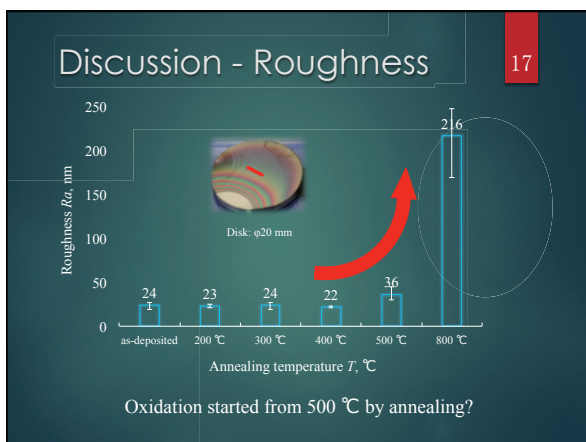
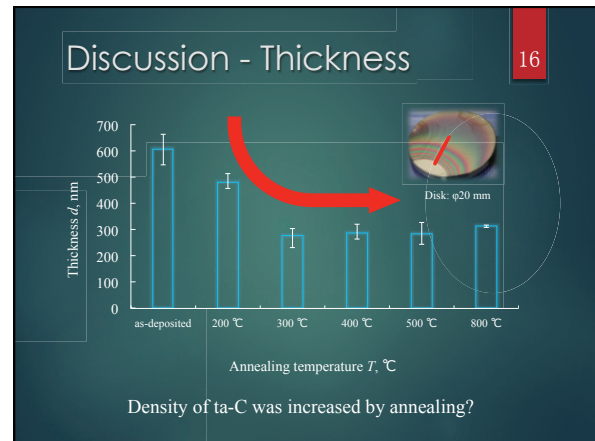
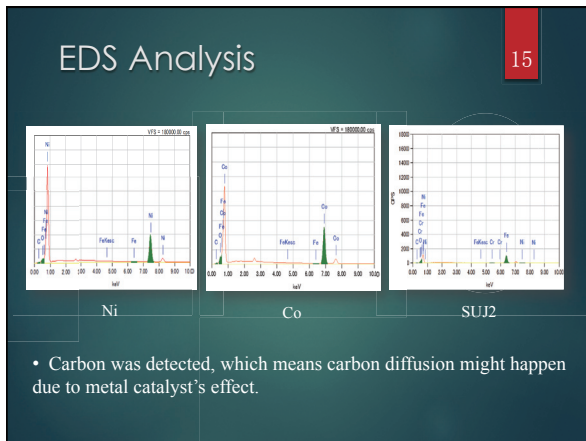
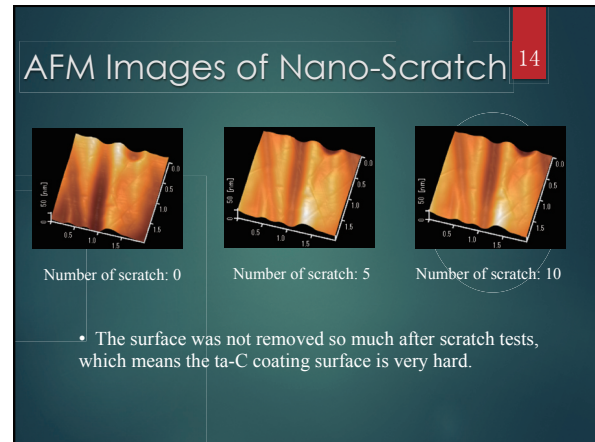
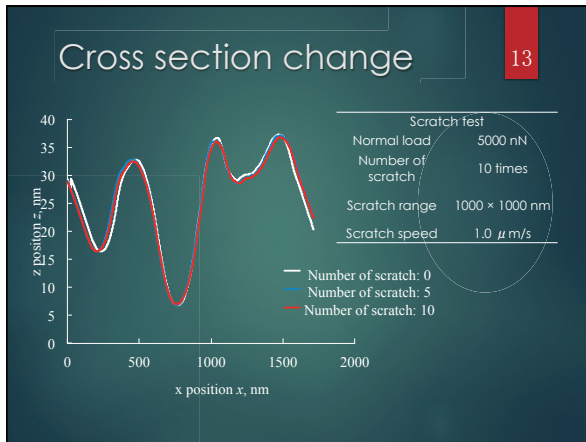
400 °C

500 °C

800 °C

Unable to detach (SUJ2)





Conclusion

19

- The hardness of ta-C in contacting area increased with annealing temperature increasing until 400 °C
- When annealing temperature goes higher than 400 °C, hardness decreases with temperature increase.
- Compared to Ni and Co, the hardness of ta-C contacted with SUJ2 is the highest at all temperatures.

Acknowledgement

20



Serendipity

21



1

Extraction and Analysis of Trigger Rate and Pedestal Data from SciCRT

MENTORS: PROFESSORS ITOW SAN, MATSUBARA SAN AND SHIOKAWA SAN

GOUTHAM THANGARAJ

2

Sun and Solar Flares

- A solar flare is an enormous release of the energy occurring at the Sun, and we believe some portion of this released energy is used to accelerate particles.
- This includes electrons, protons and gamma rays.



Image Courtesy: NASA/Reuters

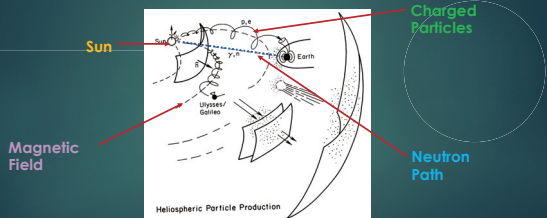
3

Why study Solar Flares?

- ▶ The study of solar flares is crucial to understanding not only how the Sun functions but also its effects on the Earth's atmosphere.
- ▶ Solar flares also have the ability to disrupt long distance radio signals and disturb orbiting satellites by increasing the drag experienced by the same.
- ▶ Worst of all, they can cause errors in satellite circuitry resulting in damage of components aboard a spacecraft.
- ▶ Neutrons pose the most danger to satellites as they cannot be easily shielded against.

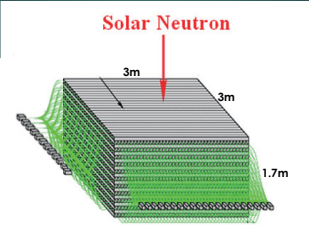
4

How to study Solar Flares?



5

SciCRT Instrument



6

Details of the Instrument

- ▶ There are currently 5 operational Superblocks. 2 for Muons and 3 for neutrons.
- ▶ In each superblock, there are 32 MAPMTs each having 44 channels. Currently, 28 are operational in each Superblock.
- ▶ The instrument can detect the path of a neutron and the energy possessed by it which is known as the ADC data.
- ▶ These MAPMTs are attached to Back-End Boards which act as the DAQ boards.
- ▶ The SciCRT Detector is located at Mt. Sierra Negra in Mexico.

Purpose of Study

7

- ▶ To develop an analysis framework based on C++ and ROOT that plots the neutron count in 1-minute interval for every data file (each one being 1 hour long).
- ▶ To study pedestal variation and determine the calibration parameter at any point during the operation of the SciCRT.

Data Collection and Coding Platform

8

- ▶ Each data file represents an hour data and provides ADC data for each channel of each FEB in that period.

```
17 1574 2000 1842 2000 2000 2007 1809 2040 2204 2003 1857 2000 1842 1973 2037 1974 1803 1843 2034 1800 1840 2000 1935 1935 2035 1976 1909 2040 1840 1840 1943
1843 1843 2002 2002 2002 2002 2075 1843 1954 1956 1940 2070 2043 2043 1843 1847 1970 1913 1847 1986 1956 1949 1840 2044 2044 1944 2044 2044 1943 1935 1936 1947
1942 1939 2040 2040 2042 2037 2042 1931 1848 1975 1848 2002 1940 1848 1975 2038 2047 1847 1973 1980 1976 1936 1975 1847 1976 1976 1976 1976 1988 1988 1987
1988 2037 2040 2041 1841 1841 1841 2040 2040 1849 1944 1939 1944 1939 1944 2039 2040 2040 2040 2040 2040 1841 1849 1942 1947 1848 1940 2041 1944 2043 1943 2044
1949 1949 2040 1949 2040 2041 -999
```

- ▶ ROOT and C++ were the software used to run all the described codes and obtain the necessary histograms and plots.

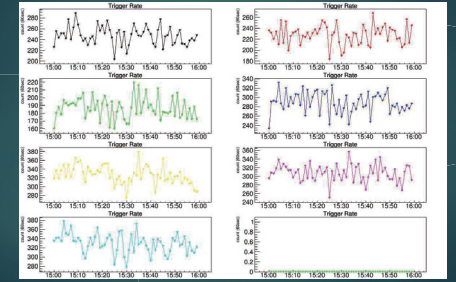
Trigger Rate

9

- ▶ Trigger Rate is defined as the number of successful events obtained during the same time interval.
- ▶ The neutron data is obtained when the event satisfies a certain hardware condition, called the trigger condition.
- ▶ The trigger rate describes whether the data collecting hardware is functioning optimally.

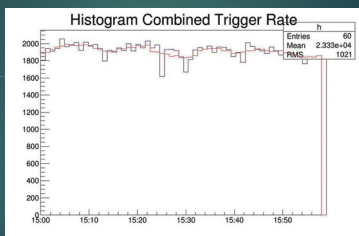
1 - Minute Count Distribution

10



Combined Trigger Rate

11



Pedestal Data – What is it?

12

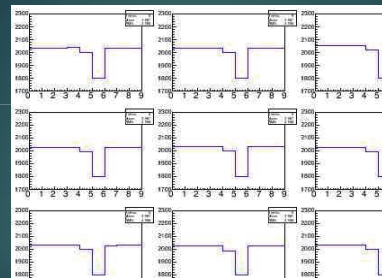
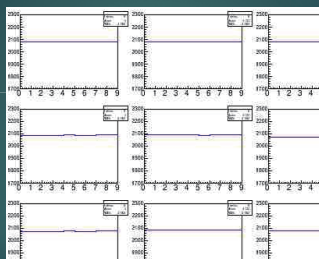
- ▶ It is the default state of the sensor and can be considered as its zero value.
- ▶ Every instrument, including the instruments aboard the SciCRT, have pedestal data that needs to be obtained in order to get the real value of the quantity being measured.

```
3016 2030 2050 2052 2024 2042 2029 2024 2047 2036 2031 2031 2043 2040 2030 2033 2027 2027 2032 2026 2043 2027 2023 2023 2033 2034 2031 2027 2031 2043 2043 2033
2030 2087 2070 2097 2103 2070 2068 2069 2069 2087 2089 2101 2098 2081 2082 2055 2059 2082 2075 2074 2069 2091 2077 2076 2090 2080 2081 2066 2068 2091 2092
2051 2051 -999
3103 2033 2049 2062 2063 2074 2040 2024 2041 2036 2060 2074 2039 2030 2042 2034 2037 2025 2060 2049 2039 2043 2030 2043 2034 2035 2038 2045 1959 2038 2039
2026 2030 2047 2043 2023 2030 2033 2024 2018 2030 2030 2038 2042 2015 2020 2018 2029 2023 2021 2023 2027 2017 2089 2014 2007 2020 2018 2014 2024 2015 2023
3112 2027 -999
3200 1950 1997 2023 2024 2004 2009 1899 2015 1997 1888 1888 2006 1997 1931 1938 1977 2007 1930 1936 1996 1997 1971 2008 1980 1997 1978 1968 1955 1865 1867 1993
2064 1996 2020 1994 1997 1990 2081 1988 1996 1994 1979 1989 1975 1987 2065 1993 1980 1981 1990 1988 1978 1988 1989 1988 1978 1969 1973 1977 1965 1882 1883
1971 1995 -999
```

Process of Obtaining Pedestal Data 13

- ▶ Combining Pedestal Data
- ▶ Obtaining Mean Pedestal Data
- ▶ Plotting Pedestal Data
- ▶ Analysis of Pedestal Data

Sample Pedestal Data Output 14



Results from Pedestal Data 17

- ▶ The pedestal data shows a variation of less than 5% over the course of nine months from August 2014 – April 2015.
- ▶ This provides us with the information required towards eventually calculating the neutron flux.
- ▶ There are certain MAPMTs however that show a plunge of 10% in a single month.
- ▶ This will not cause a problem as the instrument data can be recalibrated using the pedestal.
- ▶ However, this variation does enable indication of a problem in the hardware.

Conclusion 18

- ▶ Thus, the neutron trigger data was analyzed for a period of 10 seconds and 60 seconds.
- ▶ Neutron flux over the course of operation of the SciCRT can now be plotted and studied.
- ▶ The pedestal data was also obtained and a variation of less than 5% was observed during the period of 9 months from August 2014-April 2015 when the instrument was operational.

Investigation on the Performance of the L-R type Fault Current Limiter in Low Voltage DC Distribution System (Electrical Engineering)

JUACEP Research Presentation

Jiahong Ju
Department of Electrical Engineering, University of Michigan
Supervisors
Prof. Toshiro Matsumura
Graduate School of Engineering, Nagoya University
Associate Prof. Yasunobu Yokomizu
Graduate School of Engineering, Nagoya University



Motivation

Low Voltage DC Distribution System:

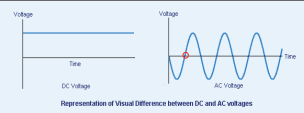
- Widely spread renewable energy and distributed generation **boosts the DC power** delivered in the low voltage DC distribution line.
- For power protection, **higher DC fault current** will exceed the capability for the existing protection equipment to interrupt the faults safely and reliably

Solution

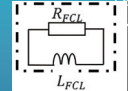
- Instead of replacing the existing equipment, DC Fault Current Limiter (FCL) introduced
- Suppress the magnitude of the fault current** to a lower value at which the circuit breaker can easily interrupt

Introduction

- Most of the researches on FLCs are for AC
- Unlike AC current that can be interrupted by utilizing the zero current in each cycle, DC fault current is much more difficult to be interrupted than AC
- Widely used FCLs usually are made with superconductive materials and consist of additional peripheral control section which make them **expensive and complex to be implemented**
- A simple circuit configuration named L-R type FCL that consists of **only passive components** is introduced.
- Investigate the **current limiting performance of FCL** and its **effect on the current interruption of circuit breaker** by experiments



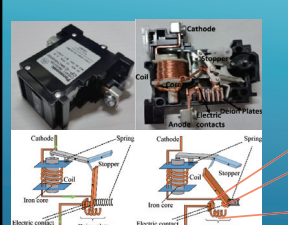
Representation of Visual Difference between DC and AC Voltages



Mechanism of MCCB

- A molded case circuit breaker (MCCB) from Panasonic is chosen.
- Normal operation: rated current flows through the coil from cathode to anode with two electric contacts connected
- Fault condition: the electromagnetic force induced by the fault current pull down the spring to separate two electric contacts and the electric arc is formed in the air to provide a conductive path for electricity to keep flowing.

Rated DC Voltage (V)	Highest Interrupting DC Current (A)	Rated DC Current (A)	Internal Impedance (Ω)	Voltage Drop (V)
48	750	0.3	15	4.5



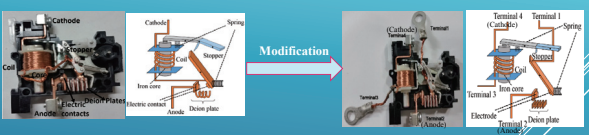
To ensure a quicker and safer interruption, **Metal Deion plates are inserted to break down the arc**.

- Once two contacts are separated far enough and arc is deionized, the fault current is interrupted completely.

Modification of MCCB

Modification to avoid the internal resistance

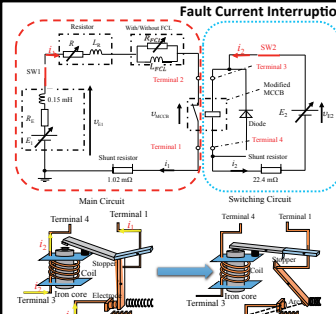
- it is **hard to get large fault current** with the equipment in our lab with internal resistance at 15Ω
- Power losses



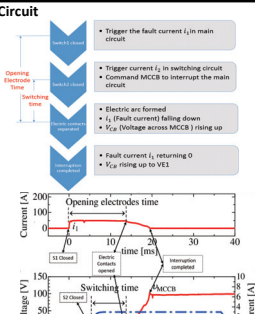
Modification

- Two more terminals: Terminal1 and Terminal3
- Rated current and fault current go through Terminal1 to Terminal2 with no power losses.
- Based on four terminals, the fault current interruption circuit is built.

Fault Current Interruption Circuit



- Trigger the fault current I_f in main circuit
- Trigger current I_s in switching circuit
- Command MCCB to interrupt the main circuit
- Electric arc formed
- I_f (Fault current) falling down
- V_{CB} (Voltage across MCCB) rising up
- Fault current I_f returning 0
- V_{CB} rising up to V_{E1}



Opening electrodes time

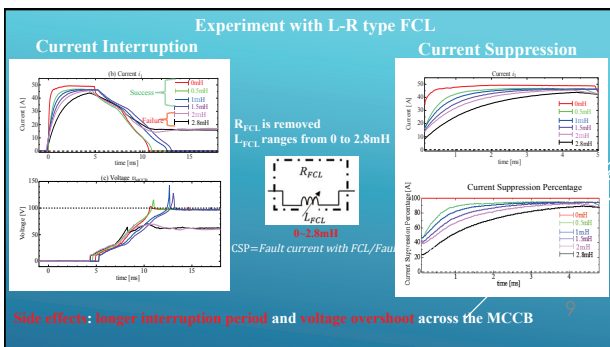
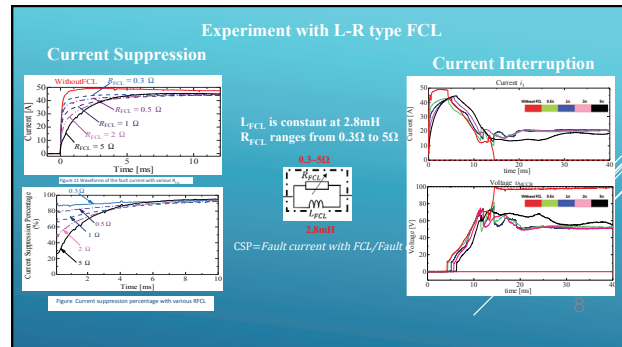
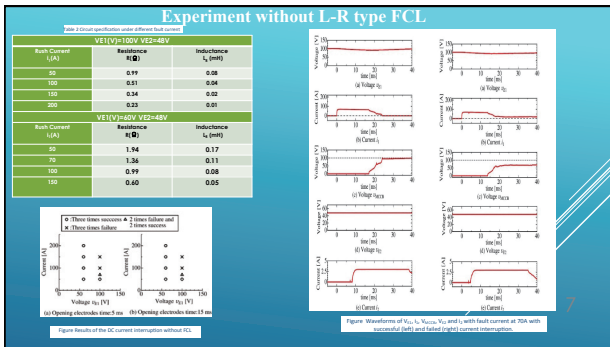
Switching time

Opening electrodes time

Switching time

Opening electrodes time

Switching time



Conclusion

- Both resistance and inductance in L-R type FCL **effectively suppress** the fault current. The larger the value is, the more remarkably the fault current is suppressed.
- Inductance play a **more important role for the current interruption**. Large inductance could fall the interruption.
- The L-R type FCL **extend the interruption period** and cause **voltage overshoot** across the MCCB.
- By appropriate selection of R_{FCL} and L_{FCL} values, the L-R type FCL will be a promising in DC current protection, which effectively suppresses the fault current to a lower value where the MCCB can interrupt
- Power during the current interruption** will be calculated and compared to find the threshold power value between success and failure of current interruption
- Modification on the circuit could be proposed to reduce the voltage overshoot and slow down rate of increase for the fault current by experiment in the future.

A STUDY ON TOPOLOGY OPTIMIZATION WITH FEM BASED ON LEVEL SET METHOD

Chen Wang
Department of Mechanical Engineering
University of Michigan, Ann Arbor

Supervisor: Prof. Toshiro Matsumoto
Department of Mechanical Science and Engineering
Nagoya University

1

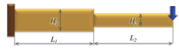


Contents

1. Introduction
2. Principles & Formulations
3. Numerical Implementation
4. Numerical Examples
5. Conclusion

2

1. Introduction

1.1 Structural optimization

- Sizing optimization 
- Shaping optimization 
- **Topology optimization** 

Original optimization problem

↓

Material distribution problem in a fixed domain

3

1. Introduction

1.2 Topology optimization

Using characteristic function (0 or 1) to distinguish material regions from non-material regions

↓

Instability Problems (Discontinuity)

↓

Regularization Methods: Homogenization Design Method
SIMP (Solid Isotropic Material with Penalization method)

↓

“Intermediate Materials” (NOT clear boundary)

↓

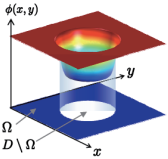
Using **Level Set Function** to represent material distribution

4

2. Principles & Formulations

Level set-based topology optimization method

- A fictitious interface energy model based on the phase field concept: Fixed domain D (Material domain Ω , Complementary domain $D \setminus \Omega$)
- Using level set functions ϕ to represent the structural boundaries:

$$\begin{cases} 0 < \phi(x) \leq 1 & \text{if } \forall x \in \Omega \setminus \partial\Omega \\ \phi(x) = 0 & \text{if } \forall x \in \partial\Omega \\ -1 \leq \phi(x) < 0 & \text{if } \forall x \in D \setminus \Omega \end{cases}$$


5

2. Principles & Formulations

Level set-based topology optimization method

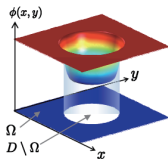
- Based on the shape representation above, the optimization problem is formulated as follows:

$$\inf_{\phi} F = \int_{\Omega} f(x)\chi_{\Omega}(\phi) d\Omega$$

subject to

$$G = \int_{\Omega} g(x)\chi_{\Omega}(\phi) d\Omega - G_{max} \leq 0$$

where F is the objective functional, G is the constraint functional, G_{max} is the upper limit of G , and χ_{Ω} is the characteristic function as

$$\chi_{\Omega} = \begin{cases} 1 & \text{if } \phi \geq 0 \\ 0 & \text{if } \phi < 0 \end{cases}$$


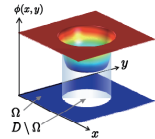
The obtained optimal solutions from above may be **DISCONTINUOUS!**

6

2. Principles & Formulations

Level set-based topology optimization method

- Based on level set boundary expressions incorporating the Tikhonov regularization method, to regularize the problem as follows:



$$\inf_{\phi} F_R = \int_D f(x)\chi_{\Omega}(\phi)d\Omega + \int_D \frac{1}{2}\tau|\nabla\phi|^2d\Omega$$

subject to

$$G = \int_D g(x)\chi_{\Omega}(\phi)d\Omega - G_{max} \leq 0$$

where F_R is a regularized objective functional, and τ is a regularization parameter.

- Time evolutionary equation of linear elasticity problem:

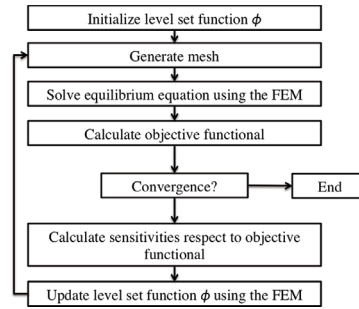
$$\frac{\partial\phi}{\partial t} = -K\left(\frac{\partial F_R(u, \phi)}{\partial\phi} + \epsilon(u); E: \epsilon(v)\chi(\phi)\right)$$

$$-\lambda\frac{\partial g(\phi)}{\partial\phi} - \tau\nabla^2\phi$$

7

3. Numerical Implementation

Algorithm Flowchart



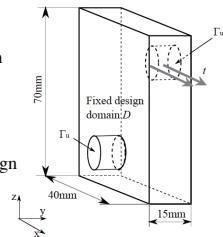
8

4. Numerical Examples

4.1 Problem Description

A topology optimization problem of a linear elasticity problem with **non-design** domain:

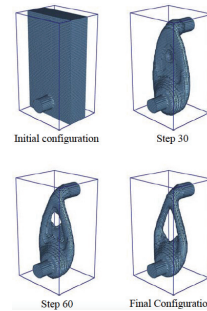
A rectangular solid is the fixed design domain with two non-design domains of cylinder on opposite sides of the rectangular solid.



9

4. Numerical Examples

4.2 Simulation Results



10

5. Conclusions

- Based on the formulation, the design sensitivities are derived using adjoint variable method. With the derived sensitivities, topology optimization algorithm is constructed, in which the Finite Element Method (FEM) is used to solve the equilibrium equations and to update the level set functions.

- A numerical implementation for generating finite element mesh based on level set method is proposed. A three-dimensional practical example is given to demonstrate the validity and utility of the proposed implementation. Currently, more complicated configurations are tested to be optimized by the method proposed above.

11

THANK YOU!

12

Analytical Study on Combustion Kinetics of Various Solid Fuels/ Waste Products

Naruse Lab
Yuting Gao
2015-08-06

1

Background and Objective

- ▶ Main energy source: solid fuels
- ▶ Waste disposal problem
 - ▶ Main method of waste treatment: incineration
- ▶ Objective: comparison of reaction behavior between solid fuels and wastes

2

Experimental Equipment & Setup

- ▶ Thermo-gravimetric analyzer
 - ▶ Given temperature profile
 - ▶ Mass loss vs. time
 - ▶ Reaction rate → Combustion parameters (A & E)

Overall reaction rate coefficient:
 $k = A \exp(-E/RT)$

A – Pre-exponential factor
E – Activation energy

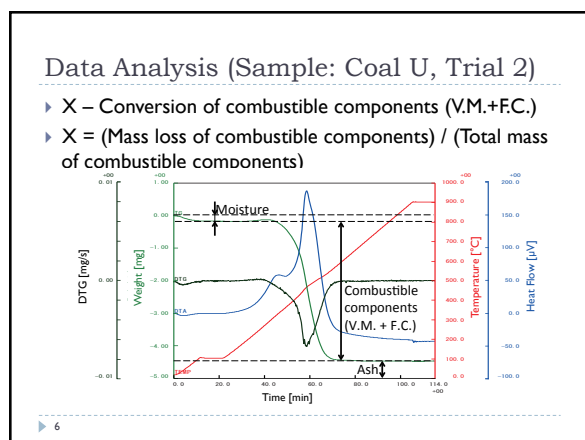
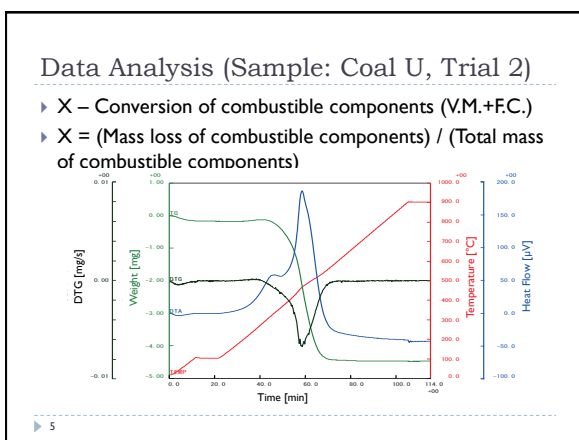
Temperature profile	RT → 107°C @ 10°C/min
	107°C for 10 min
	107°C → 900°C @ 10°C/min
	900°C for 10 min

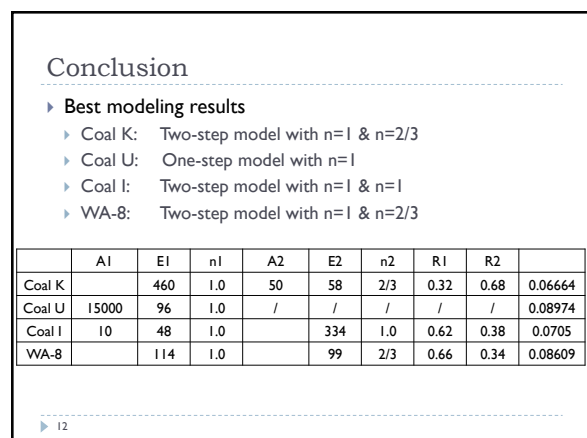
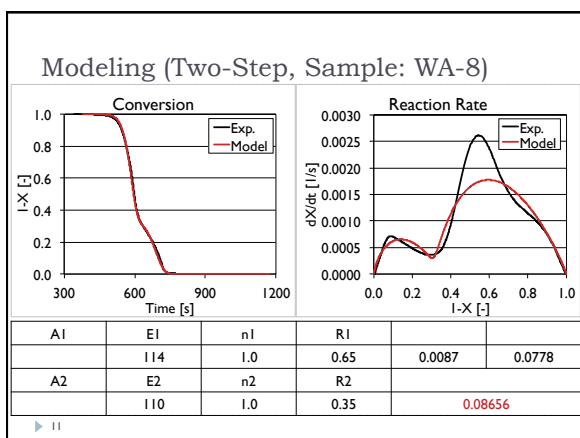
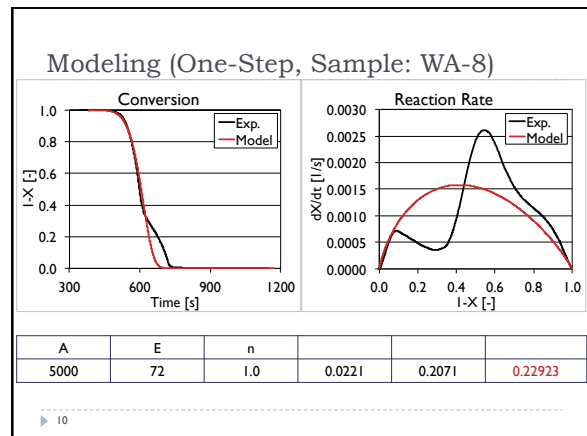
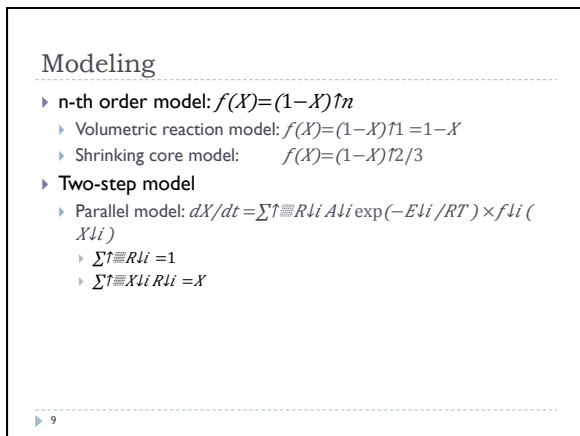
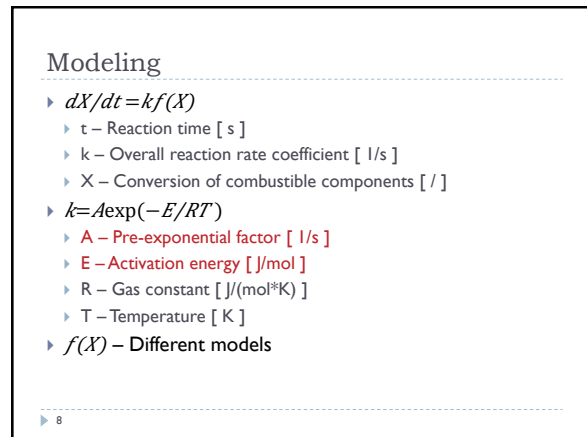
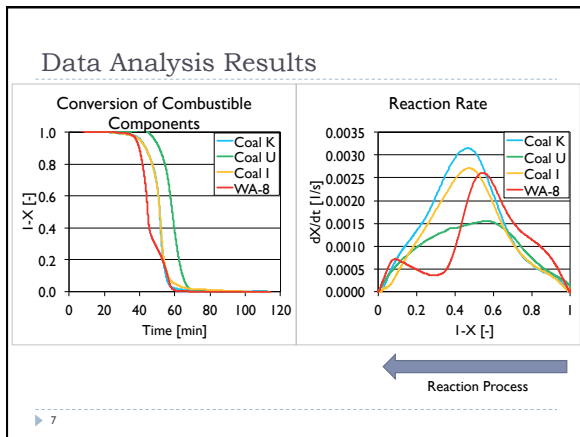
3

Sample Properties

Sample	Coal K	Coal U	Coal I	WA-8	
Composition	Coal	Coal	Bituminous coal	Grinded wood chip	
Mass [mg]	2.00±0.05	5.00±0.05	2.00±0.05	5.00±0.05	
Photo					
Proximate analysis (Dry-based wt%)	Moisture	4.60	0.50	3.3	5.77
	V.M.	44.50	35.03	19.1	80.94
	F.C.	41.00	53.06	72.0	16.85
	Ash	14.50	11.91	8.9	2.21
Ultimate analysis (wt % d.a.f.)	C	65.00	69.8	91.1	48.6
	H	5.47	5.3	4.3	6.8
	N	0.61	1.7	1.9	0.70
	O	14.30	-	2.2	-
S	0.22	0.51	0.5	0.07	

4





Nagoya university
JUACEP

THE FABRICATION OF TISSUE ENGINEERED SMALL BLOOD VESSELS VIA 3D CELL SELF-ASSEMBLY AND ORGANIZATION IN VITRO

DR. FUMIHIITO ARAI¹, DR. TAISUKE MASUDA¹, MITSUHIRU UKIKI¹, ANDREA MANOPPO²

Biorobotics
LAB

¹ Department of Micro-Nano Systems Engineering, Nagoya University, Aichi, Japan
² Department of Biomedical Engineering, University of Michigan College of Engineering, Ann Arbor

INTRODUCTION

- Global severity of cardiovascular diseases**
 - Leading cause of global mortality [WHO reports]
- Gold standard of replacement: By-Pass Surgery**
 - SVG liable to atherosclerosis and neointimal hyperplasia
 - Proper SVG lacking in 30-40% of Patients
 - Donor site morbidity

Images: Nature Outlook: Nature 493, S2-S3

BACKGROUND

- A Brief History in Vascular Replacement Models:**

Artificial material (TERUMO) Polyethylene, ePTFE (For > Φ6 mm)

Polycaprolactone Material
- Biodegradable
- Biocompatible

[S. Serkar et al., Biomaterials, 2006]

Risks

- Clot Formation
- Intimal Thickening
- Poor Cell Interaction

Scaffold and Multi-Layer Cells
For **Tissue-Engineered Small Blood Vessels**

BASIC CONCEPT: VASCULAR TISSUE ENGINEERING

Biodegradable Scaffolds: Nature proteins, Biodegradable polymers, Decellularized vessels, Hybrid scaffolds

Cell Seeding: Autologous cells: Vascular cells, Adult stem cells, Other cell types; Allogenic cells: Vascular cells, Embryonic stem cells, Cord blood cells

Cell Culture & Expansion: Culture chamber, Pump, Media reservoir, Control system, Vessel-reactor

Transplantation: Engineered Vessel

EXPERIMENTAL DESIGN

- Proposal for construction of small blood vessels (<Φ3 mm):**
 - Layer-by-layer Tissue Cell Culturing Technique
 - Construction of a PLCL Scaffold
 - A perfusion system that mechanically tests constructs
 - Three conditions of static, laminar, and pulsatile flow in a perfusion system

- 1) Fibronectin / Gelatin: Layer-by-layer assembly, Single cell, FN-G coated cell
- 2) Cut and Expand PLCL scaffold
- 3) Diced expanded PLCL scaffold
- 4) Seed on expanded PLCL scaffold: FN-G coated cells, Tissue engineered blood vessel
- 5) Open upper JB: Peel PLCL scaffold, Multilayered tissue
- 6) Expanded PLCL scaffold: Vessel capillary
- 7) Diced expanded PLCL scaffold: Biodegradable vessel
- 8) Tissue engineered blood vessel: Multilayered vessel

METHODS: LAYER-BY-LAYER CELLULAR ASSEMBLY

- lbl Technique:**
 - Nano-film coatings of fibronectin and gelatin are deposited onto single cell surfaces of MOVAS 7 cells

(a) Physical stress: Single cell → Losses of cell membrane → Release of cytosol molecules and build-up of cell (dead cell)

(b) Lbl assembly: Single cell → Cell with film → Living cell

Fibronectin: ECM Protein
Gelatin: Gel, Assists Cellular Adhesion

Single cell → FN-G coated cell → Cell accumulation → 1 day → 3D-multilayered tissue (8 Layer)

Y. Yamagishi, et al. 2014

METHODS: DIP-COATING TECHNIQUE

- A dip-coating process used to construct the scaffold
 - PLCL-Chloroform Solution
 - NaCl embedding
 - Automated process using a uniaxial electric stage
 - Salt-leaching to generate porosity

Automated Dip-Coating

7

METHODS: PLCL SCAFFOLD ASSEMBLY

- Expansion
 - PLCL scaffold (PLCL: Poly(L-lactide-co-ε-caprolactone))
- Lamination
 - Multilayered tissue (8 layers)
 - M. Matsusaki et al. Adv. Mater. 2011.
- Assembly
 - Biodegradable bond
 - Residual stress (1 min)
 - Clamp scaffold using jigs

8

METHODS: MICROFLUIDIC PERFUSION CULTURE

9

METHODS: MICROFLUIDIC PERFUSION CULTURE

Blood Vessel Constructs

Layer-by-layer assembly
 ⇒ Multilayer structure (20 layers)
 ⇒ High cell density
 Diameter, Length
 ⇒ 3 mm, 10 mm
 Poly(L-lactide-co-ε-caprolactone):PLCL
 ⇒ 0.8±0.1 MPa, 400±10 μm

Assembled Blood Vessel Constructs

Perfusion Culture system

10

PERFUSION CULTURE CONDITIONS

Signal → Observation

Flow → DIMEM supplement with 1% FBS

Shear stress : 1 Pa (at Maximum volume)

$$\tau = 4\mu Q / \pi r^3$$

[Q : flow volume, r : radius of vessel, μ : coefficient of viscosity 9.6×10⁻⁴ (Pa · s)]

S. Tada, et al., Am. J. Physiol. Heart Circ. Physiol. (2000), (2002).

Flow volume : **165 / 117 ±7 mL/min**
 Pulsatile frequency : **1 Hz**
 Flow pressure : **115 / 90 mmHg**

[sec]

11

EVALUATION

Scaffold ↓ 2 days

Lamination ↓ 2 days

Assembly of Tube ↓ 1 day culture

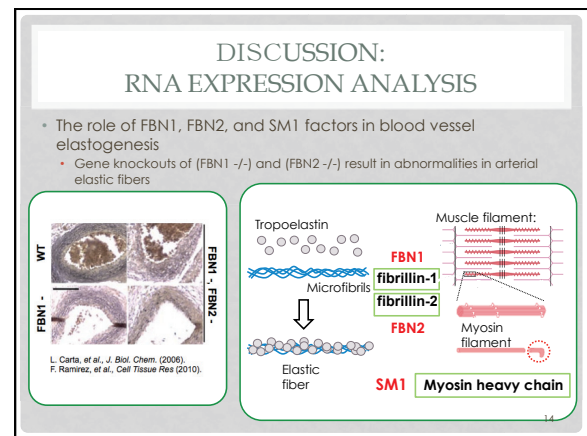
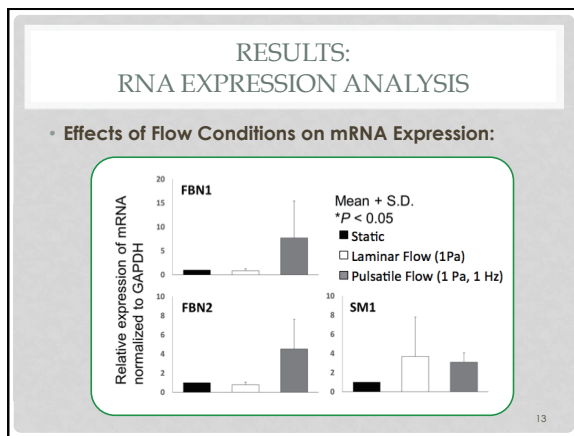
Perfusion Culture ↓ 1 day culture

Evaluations

Mechanical Stress

FBN1 ↑
FBN2 ↑

12



CONCLUSION

- A demonstrated ability to construct a blood vessel construct *in vitro*
 - Method
 - A Multi-Disciplinary Approach
 - LbL Cellular Assembly, PLCL Scaffolding, and Microfluidic Perfusion Culture
 - Results
 - mRNA expression analysis shows cellular response to mechanical stress
 - Material test of scaffold demonstrates accuracy of fabrication
 - Immunohistochemistry shows progress in development of layered conduit
- Future Directions
 - Implantation of constructs in Animal Models

15

THANK YOU!

Arai Laboratories, Nagoya University, Nagoya, Aichi, Japan
Under the supervision of Dr. Fumihito Arai, Dr. Taisuke Masuda,
mentors Ukiki Mitsuhiro and Ayaka Sato

A SPECIAL THANKS TO THE UNIVERSITY OF MICHIGAN INTERNATIONAL
PROGRAM IN ENGINEERING AND NAGOYA UNIVERSITY'S JUACEP STAFF

CONTENT OF PRESENTATION

- Background
 - Global severity of cardiovascular diseases
 - Current standard vascular replacement and a brief history
 - Basic Principles of Tissue Engineering
- Objective
 - Aspects of an effective vessel construct
- Experimentation Methods
 - Cell Culture - LbL Technique
 - PLCL Scaffolding
 - Perfusion System Testing
- Results
 - Tensile Test
 - mRNA expression
 - Immunohistochemistry
- Conclusions
 - Future Directions
- Acknowledgement
- References

17

OBJECTIVES

- Requirements of a good replacement vascular graft or construct
 - Mechanical strength and compliance
 - Non-toxicity, non-immunogenicity, and biocompatibility
 - Availability at a range of diameters
 - Suturability and ease of surgical implantation
 - Non-thrombogenicity and high patency rate
 - Reasonable manufacturing costs
- Potential benefits of tissue engineering
 - Able to fabricate multi-layered structures that are compatible in structure and function to native vessels
 - Composition of multi-layered fibroblasts, SMCs, and endothelial cells from the outer to inner later (among which ECM components should also be incorporated)

18

RESULTS: SCAFFOLD MATERIAL TEST

Test Piece Circumference $L_1 = 2\Delta l + L_0$

$$E = \frac{\sigma}{\epsilon} = \frac{P/A}{\frac{L-L_0}{L_0}} = \frac{P \cdot L_0}{(2\Delta l + L_0) \cdot A}$$

P : Force, t : Thickness, d : Width
 A : Cross-section
 L : Circumference of Scaffold
 L_0 : Jig's circumference
 Δl : Displacement

RESULTS: SCAFFOLD MATERIAL TEST

- n Coatings to PLCL Thickness
 - A positive linear relationship demonstrates the consistency of dip-coating process
 - Controllability of thickness is also demonstration
- Young's Modulus of PLCL Scaffold
 - Able to reproduce the elastic modulus of a native external carotid artery

Conditions	Chloroform : PLCL	95 : 5
	NaCl : PLCL	4 : 6
	Particles diameter of NaCl	53-100 μm
	Number of coating	6
	Pull-up velocity	3.0 mm/s

[A] Scaffold Thickness to Coating Amount
(5 wt % PLCL in Chloroform, NaCl : PLCL = 4 : 6)

[B] Young's Modulus of PLCL Scaffold

RESULTS: IMMUNOHISTOCHEMICAL RESULTS

- Cross-section of nuclear and actin staining (4 days)**
 - High cell density
 - Cell adherence

Blue : Hoechst 33342 Green : Alexa 488 Phalloidin

REFERENCES

- [1] World health organization, global status report on noncommunicable diseases, pp. 28 (2014).
- [2] Chlupáč J., Filová E., Bacáková L. Blood vessel replacement: 50 years of development and tissue engineering paradigms in vascular surgery. *Physiological research*, 58 (2); pp. 119-39 (2009).
- [3] Cleary a., Geiger E., Grady C., Et al. Vascular tissue engineering: the next generation. *Trends in molecular medicine*, 18 (7); pp. 394-404 (2012).
- [4] Peck m., Gebhart D., Dussere N., McCallister T., L'heureux N. The evolution of vascular tissue engineering and current state of the art. *Cells tissues organs*, 195, pp. 144-158 (2012).
- [5] Hasan a., Paul A., Vrana N., Et al. Microfluidic techniques for development of 3D vascularized tissue. *Biomaterials*, 35 (26); pp. 7308-7325 (2014).
- [6] Valentina catto, sylvia faré, giuliano freddi, and maria cristina tanzi, "vascular tissue engineering: recent advances in small diameter blood vessel regeneration," *ISRN vascular medicine*, vol. 2014; article id 923030, 27 pages, 2014.
- [7] Nerem t., Selktar D. Vascular tissue engineering. *Annual review of biomedical engineering*, 3, pp. 225 - 243 (2001).
- [8] Yoshida h., Matsusaki M., Akashi M., Multilayered blood capillary analogs n biodegradable hydrogels for in vitro drug permeability assays. *Advanced functional materials*, 23, pp. 1736 - 1742 (2012).
- [9] Y. Yamagishi, et al., Microfluidic perfusion cultivation system for artery-like tubular tissues with PLCL scaffolds. The 17th international conference on miniaturized systems and chemistry and life science
- [10] Yoshida, M. Matsusaki, Et Al., "Rapid Construction Of Three-dimensional Endothelial Tube Networks By The Cell-accumulation Technique," *Adv Mater*, Vol. 23, Pp. 3506-3510 (2011).

REFERENCES

- [11] R. Ishiwata, U. Yokoyama, M. Matsusaki et al., Three dimensional multilayers of smooth muscle cells as A new experimental model for vascular elastic fiber formation studies, *atherosclerosis*, 233 : 590-600 (2014).
- [12] Fogelgren b., Polgar N., Szauder km., Et al. Cellular fibronectin binds to lysyl oxidase with high affinity and is critical for its proteolytic activation. *J Biol Chem*, 280:24690e7 (2005).
- [13] Y. Yamagishi, et al., Microfluidic perfusion cultivation system for multilayer structured tubular tissues. The 17th international conference on miniaturized systems for chemistry and life sciences, no. 1213 (2013).
- [14] M. Matsusaki, H. Ajiro, T. Kida et al., Layer-by-layer assembly through weak interactions and their biomedical applications, *advanced materials*, 24 (4); pp. 454-474 (2012).
- [15] Nishiguchi a., Yoshida H., Matsusaki M. Et al., Rapid construction of three-dimensional multilayered tissues with endothelial tube networks by the cell accumulation technique. *Advanced materials*, 23 (31); pp. 3506-3510 (2011).
- [16] Yamagishi y., Masuda T., Matsusaki M., Microfluidic perfusion culture system for multilayer artery tissue models. *Biomicrofluidics*, 8, 064113 (2014).
- [17] Wogensell j., Mecham R., Vascular extracellular matrix and arterial mechanics. *Physiological reviews*, 89 (3); pp. 957-989 (2009).
- [18] Aikawa m., Sivam PN, kuro-o M et al., Human smooth muscle myosin heavy chain isoforms as molecular markers for vascular development and atherosclerosis. *Circ res*, 73: 1000e12 (1993).
- [19] Carta l., Wogensell, j., Knutsen R., Et al. Discrete contributions of elastic fiber components to arteriolar development and mechanical compliance. *Arteriosclerosis, thrombosis, and vascular biology*, 29 (12) pp. 2083-2089, (2009).

The 14th JUACEP Workshop

Date: September 2 (wed), 2015

Venue: VBL Hall, Nagoya University

Timetable:

14:35	Opening Address
14:45 - 17:20	Presentations by UCLA students (10 mins. presentation + 4 mins. Q&A each)
17:20 - 17:40	Completion Ceremony
18:00	Farewell Banquet

~Presentation Titles~

1: Douglas Chen

“Direct Production of Highly Pressurized Hydrogen Gas” (p.136)

2: Hongyang Li

“Deep Discharge and Elevated Temperature Performance of Solid-state Thin Film LiCoMnO₄ Batteries” (N/A)

3: Jacob Stremfel

“Fatigue Crack Healing via High-Density Electropulsing” (N/A)

4: Antonio Martinez

“Algorithm for Elevator Travel Distance Detection Using Smartphone” (N/A)

5: Haroula Kyriacou and Lindsey Perry

“Catalytic Cracking of Polyolefins for Fuel Consumption” (p.138)

6: Yifan Jiang

“An Investigation of the Top-Down Approach for Gallium Nitride Nanowires Using Metal Mask and Simple Device Fabrication Using Gallium Nitride Nanowires Grown in HVPE” (p.143)

7: Austin Kuo

“Control for Table Tennis Robot” (p.146)

8: Jimmy Ng

“Electron Field Emission of Graphene” (p.149)

9: Xu Li

“Cell Transportation Based on Vibration-induced Local Flow Control in Open Chip Environment” (p.151)

Direct Production of High-Pressure Hydrogen Gas

Douglas Chen
Thermal Energy Engineering, Nagoya University
Seiichi Deguchi Lab

Outline

- Motivation
- Aluminum
 - Background
 - Experimental Setup
 - Results and Discussion
- Modified TiO₂
 - Background
 - Experimental Setup
 - Results and Discussion
- Conclusion

Motivation

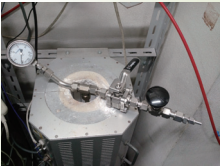
- Sustainable Energy
 - Renewable, environmentally friendly
- Energy Storage
 - Batteries, supercapacitors, pseudocapacitors
 - Hydrogen

Background

- Temperature or solar-driven reactions to produce hydrogen
 - Use ammonia
 - Urea degradation component
- Two methods investigated:
 - Aluminum
 - Platinum-loaded titanium oxide (TiO₂)

Aluminum

- Catalytic conversion of ammonia to hydrogen?
- Experimental Setup:
 - Aluminum powder and aqueous urea solution in steel tube
 - Heat at 200 or 300 °C



Aluminum Results

- Production of pure hydrogen
 - Aluminum reacts with water, not ammonia
- Aluminum is consumed and ammonia (urea) is not
 - Undesirable

Urea Concentration (wt%)	Temp. (°C)	Equilibrium Pressure (MPa)	H ₂ Concentration
40	200	1.5	99.6
40	300	4.0	99.1
0	300	2.5	99.8

Titanium Oxide (TiO₂)

- Catalytic conversion of ammonia to hydrogen, nitrogen

$NH_3 + h^* \rightarrow \cdot NH_2 + H^*$	(1)
$\cdot OH_2 + h^* \rightarrow \cdot OH_2$	(2)
$NH_3 + \cdot OH_2 \rightarrow NH_2 + H_2O$	(3)
$2 \cdot NH_2 \rightarrow N_2H_4$	(4)
$N_2H_4 \rightarrow N_2H_2 + H_2$	(5)
$2N_2H_2 \rightarrow N_2 + N_2H_4$	(6)
$N_2H_2 \rightarrow N_2 + H_2$	(7)

TiO₂ Experimental Setup

- Use glass vessel with two separate sections
- Prepare TiO₂ catalyst by loading with platinum via photodeposition
 - TiO₂ powder with hydrogen hexachloroplatinate (anhydrate) in water/methanol
- Combine catalyst with ammonia solution

TiO₂ Results

- So far unsuccessful
- Sources of error
 - Conditions unmet for catalyst preparation or photocatalytic reaction
 - Age of TiO₂ powder, hexachloroplatinate anhydrate
 - Hexachloroplatinate has absorbed water -> unsure of amount of platinum included in catalyst
 - TiO₂ powder may have changed in chemical composition or structure

TiO₂ Future Plans

- After replicating TiO₂ catalysts:
 - React with urea solution
 - Heat urea solution to decompose
 - Perhaps find one-step process to convert urea to hydrogen

Conclusion

- Two methods of hydrogen production studied
- Aluminum does not behave as catalyst
- TiO₂ catalyst currently problematic
 - Once correctly synthesized, can begin experimenting with urea solutions

Special Thanks

- Professor Deguchi and lab
- JUACEP

Catalytic Cracking of Polyolefins for Fuel Consumption


Haroula Kyriacou and Lindsey Perry
 Department of Materials Science and Engineering, UCLA
 Under the Supervision of Masahiro Hirasawa
 Department of Molecular Design and Engineering, NU

UCLA Engineering
 HENRY SAMUELLI SCHOOL OF
 ENGINEERING AND APPLIED SCIENCE


NAGOYA UNIVERSITY

2 Introduction

- Plastic is a large part of today's society



- Different types of polymers are used for packaging



UCLA Engineering
 HENRY SAMUELLI SCHOOL OF
 ENGINEERING AND APPLIED SCIENCE

NAGOYA UNIVERSITY

3

- Plastic waste requires **recycling**
- It saves **twice** as much energy as burning the same trash!
- In addition, using recycled materials as opposed to raw (new) materials for plastic production saves **two-thirds** of the energy needed for the process!
- Plastic production itself requires a large amount of **oil**—therefore, the creation of fuel oil from waste plastics is a great feedback loop!



UCLA Engineering
 HENRY SAMUELLI SCHOOL OF
 ENGINEERING AND APPLIED SCIENCE

NAGOYA UNIVERSITY

4 Polymer Cracking

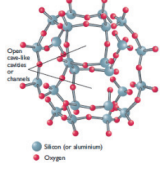
- Recycling waste plastics requires the material to be cracked
- Cracking is the decomposition of heavier hydrocarbons into their small chain petroleum components
- Two Methods:
 - Thermal Cracking
 - Catalytic Cracking
- Each method has different advantages and disadvantages
 - Product quality and type vary
 - Liquid oil for fuel must have a **high octane number**

UCLA Engineering
 HENRY SAMUELLI SCHOOL OF
 ENGINEERING AND APPLIED SCIENCE

NAGOYA UNIVERSITY

5 Catalytic cracking

- Chosen over thermal cracking because of the higher product yield and higher octane number of liquid gasoline at lower T
- We use a solid acid FCC catalyst
 - FCC: Fluid Catalytic Cracking
 - Provided by petrochemical company
- FCC Zeolite Powder
 - Aluminosilicate: $Al_2O_3 \cdot SiO_2$ with various trace elements
 - Porous Honeycomb structure: allows large polymer chains to enter, react and leave as smaller hydrocarbon chains




UCLA Engineering
 HENRY SAMUELLI SCHOOL OF
 ENGINEERING AND APPLIED SCIENCE

NAGOYA UNIVERSITY

6 The Experiment

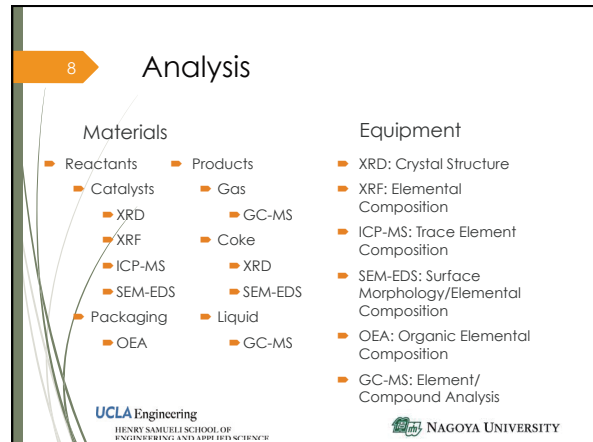
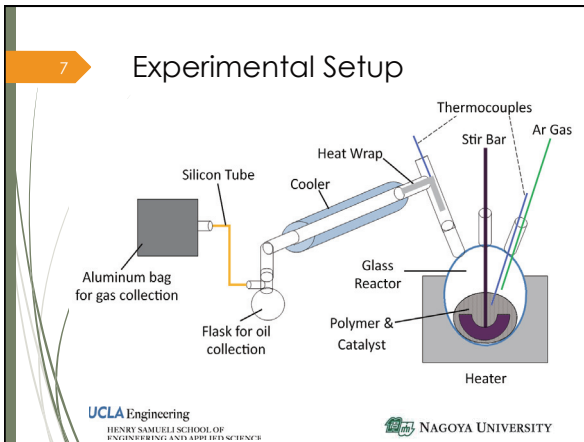
- Five polymer samples:
 - High-Density Polyethylene (HDPE)
 - Low-Density Polyethylene (LDPE)
 - Polypropylene (PP)
 - Polystyrene (PS)
 - Plastic Bottle Label (Packaging)
 - Most likely PE, specifically HDPE
- Two experimental runs per polymer sample
 - One with catalyst and one without catalyst (thermal)
 - HDPE was run with two different catalysts



Plastic Packaging Wrap

UCLA Engineering
 HENRY SAMUELLI SCHOOL OF
 ENGINEERING AND APPLIED SCIENCE

NAGOYA UNIVERSITY



9 Catalyst 1

- XRD: confirmed zeolite aluminosilicate structure.
- Red: EDS, XRF, ICP
- Blue: XRF, ICP
- Green: EDS, ICP
- Orange: EDS

Element	EDS	XRF	ICP
Al	✓	✓	✓
Si	✓	✓	✓
Fe	✓	✓	✓
Ni	✓	✓	✓
Mn	✓	✓	✓
V	✓	✓	✓
La	✓	✓	✓
Ca	✓	✓	✓
Rh	✓	✓	✓
Na	✓		✓
C	✓		✓
N	✓		✓
O	✓		✓

UCLA Engineering
HENRY SAMUELL SCHOOL OF
ENGINEERING AND APPLIED SCIENCE

NAGOYA UNIVERSITY

10 Catalyst 2

- XRD: confirmed zeolite structure, substituted Ti (for Al) in silicate
- Red: EDS, XRF, ICP
- Blue: XRF, ICP
- Green: EDS, ICP
- Orange: EDS
- Purple: XRF

Element	EDS	XRF	ICP
Al	✓	✓	✓
Si	✓	✓	✓
Ti		✓	✓
Mn		✓	✓
Fe		✓	✓
Rh		✓	✓
Ca	✓		✓
C	✓		✓
O	✓		✓
Pd		✓	

UCLA Engineering
HENRY SAMUELL SCHOOL OF
ENGINEERING AND APPLIED SCIENCE

NAGOYA UNIVERSITY

11 Packaging

- Organic Elemental Analysis (OEA)

Sample	H (%)	C (%)	N (%)
HDPE	14.38	84.96	0.27
LDPE	14.43	85.54	0.22
PP	14.44	85.27	0.24
PS	8.08	92.04	0.2
Packaging	13.99	83.51	0.23

UCLA Engineering
HENRY SAMUELL SCHOOL OF
ENGINEERING AND APPLIED SCIENCE

NAGOYA UNIVERSITY

12 Coke

- Remaining catalyst is transformed into a solid residue called coke
 - Analysis performed on coke from packaging run
- XRD
 - Quartz (SiO₂)
 - Calcium
 - Magnesioferrite
- EDS (performed 5 times)
 - In 5 runs: Al, Si, O
 - In 4 runs: C, Ti
 - In 3 runs: Ca
 - In 1 run: Cl, V, Mn, Fe, Ni, Cu, Zn, La

UCLA Engineering
HENRY SAMUELL SCHOOL OF
ENGINEERING AND APPLIED SCIENCE

NAGOYA UNIVERSITY

13 Gas & Liquid Products

- GC-MS identified both structure type and carbon number of products

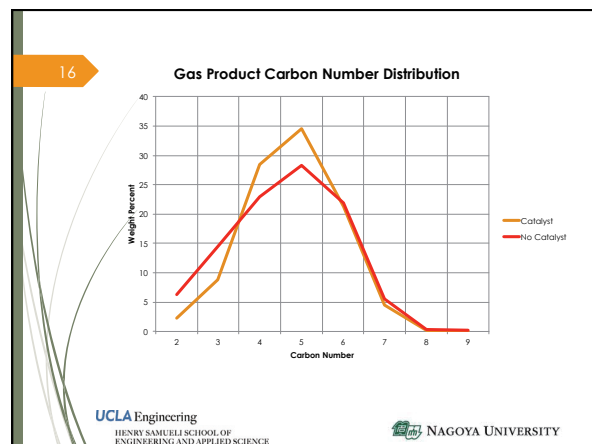
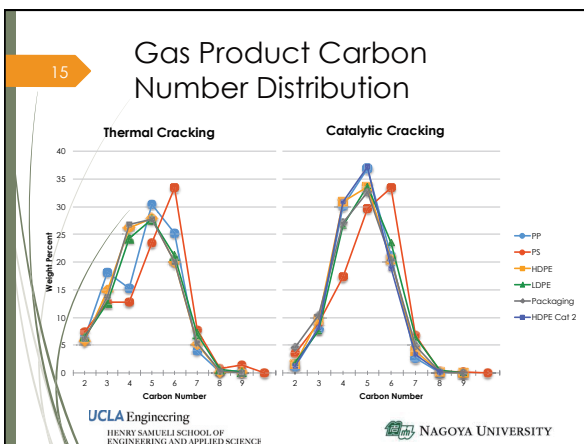
Hydrocarbon Terms	Definition
Bond Type	<ul style="list-style-type: none"> Paraffin: all single bonds Olefin: one ore more multiple bond Diene: two double bonds
Structure Geometry	<ul style="list-style-type: none"> n: straight chain Iso: branched chain

UCLA Engineering HENRY SAMUELLI SCHOOL OF ENGINEERING AND APPLIED SCIENCE NAGOYA UNIVERSITY

14 Gas Products

Product	Catalytic	Thermal
n-paraffin	13.3	21.0
iso-paraffin	20.9	10.6
n-olefin	29.4	36.7
iso-olefin	35.8	30.9
aromatics	0.6	0.8
other	0.02	0.06

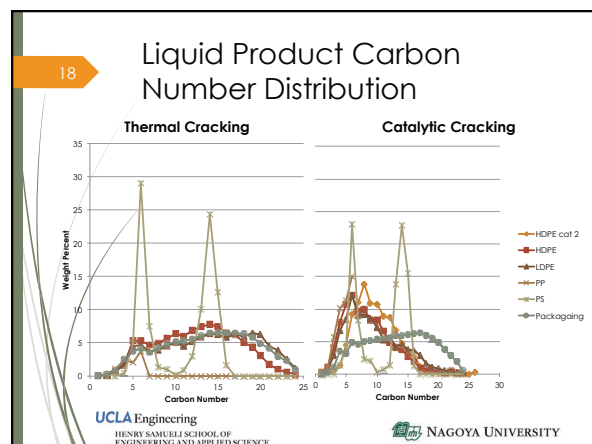
UCLA Engineering HENRY SAMUELLI SCHOOL OF ENGINEERING AND APPLIED SCIENCE NAGOYA UNIVERSITY

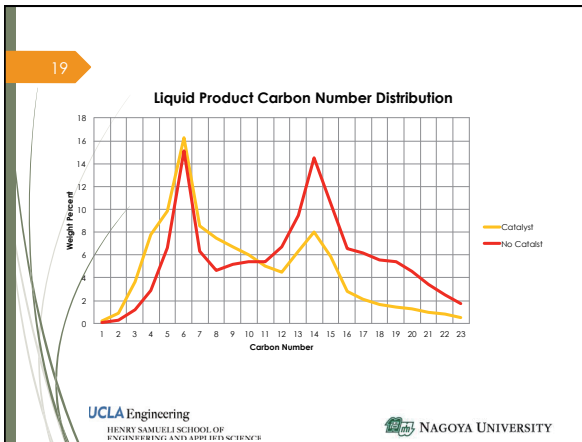


17 Liquid Products

Product	Catalytic	Thermal
n-paraffin		3.1
iso-paraffin	8.2	6.7
n-olefin	13.5	8.4
iso-olefin	33.5	22.4
aromatic	20.8	0.4
other	20.7	53.3

UCLA Engineering HENRY SAMUELLI SCHOOL OF ENGINEERING AND APPLIED SCIENCE NAGOYA UNIVERSITY





20

Conclusions

- Catalytic vs. Thermal
 - Produced compounds of lower carbon chains, increased branching and aromatics
 - Cracking occurred at lower temperatures, therefore requiring less energy
- Waste Packaging vs. Polyolefin Samples
 - Analyses confirm similar to HDPE
 - Products mirror that of PE samples
- Polystyrene is the best candidate for plastic packaging due to its high yield of aromatics

UCLA Engineering
HENRY SAMUELL SCHOOL OF
ENGINEERING AND APPLIED SCIENCE

NAGOYA UNIVERSITY

21

Scooter Fuel

- Approx. one liter of oil produced
- Distilled to 500 mL of usable fuel
- Tested in a motorized scooter

UCLA Engineering
HENRY SAMUELL SCHOOL OF
ENGINEERING AND APPLIED SCIENCE

NAGOYA UNIVERSITY

22

Scooter

- After siphoning out the remaining gas...

UCLA Engineering
HENRY SAMUELL SCHOOL OF
ENGINEERING AND APPLIED SCIENCE

NAGOYA UNIVERSITY

23

Adding the Fuel

UCLA Engineering
HENRY SAMUELL SCHOOL OF
ENGINEERING AND APPLIED SCIENCE

NAGOYA UNIVERSITY

24

And...

UCLA Engineering
HENRY SAMUELL SCHOOL OF
ENGINEERING AND APPLIED SCIENCE

NAGOYA UNIVERSITY

25 Success!



UCLA Engineering
HENRY SAMUELI SCHOOL OF
ENGINEERING AND APPLIED SCIENCE

NAGOYA UNIVERSITY

26 Future work

- Analysis
 - NMR: packaging element composition
 - TGA: coke composition
 - Chlorine: packaging component
- Liquid Oil Product
 - Test for fuel power and efficiency in the scooter
 - Obtain octane number rating
- Experiment
 - Increase trial number of polymer type
 - Multiple use of catalyst to observe activity

UCLA Engineering
HENRY SAMUELI SCHOOL OF
ENGINEERING AND APPLIED SCIENCE

NAGOYA UNIVERSITY


27 Acknowledgements

- The Hirasawa Lab
 - Prof. Masahiro Hirasawa
 - Prof. Haruki Tani
 - Takashi Shirao
 - Shiori Saino
 - & the rest of our labmates!
- JUACEP & JASSO
 - Chiharu Yada
 - Tomoko Kato

UCLA Engineering
HENRY SAMUELI SCHOOL OF
ENGINEERING AND APPLIED SCIENCE

NAGOYA UNIVERSITY

28 Thank You & ありがとう
Questions?



UCLA Engineering
HENRY SAMUELI SCHOOL OF
ENGINEERING AND APPLIED SCIENCE

NAGOYA UNIVERSITY

An Investigation of the Top-down Approach for Gallium Nitride Nanowires Using Metal Mask and Simple Device Fabrication Using Gallium Nitride Nanowires Grown in HVPE

Jiang, Yifan
University of California, Los Angeles

1

GaN nanowire is a promising competitor for applications in different fields

2

Outline

- Different approaches for GaN nanowires: the explanation of methods for bottom-up approach and top-down approach
- Experiment results
 1. Top-down approach:
 - metal islands
 - nanowires by etching
 2. Bottom-up approach:
 - long nanowires grown in HVPE
 - simple single nanowire device

3

There are two approaches for GaN nanowire growth or generation

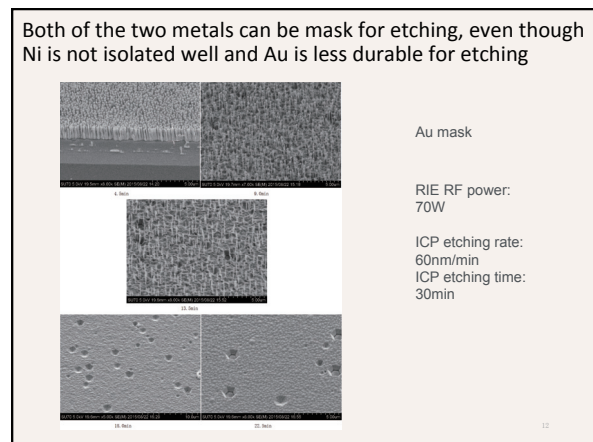
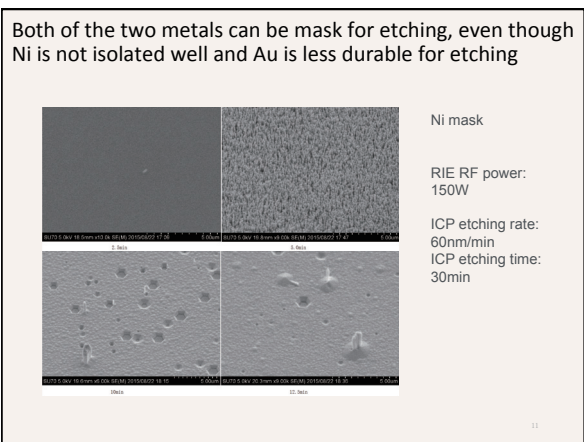
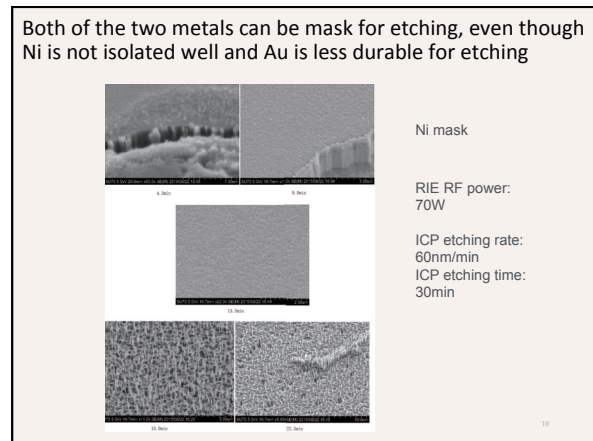
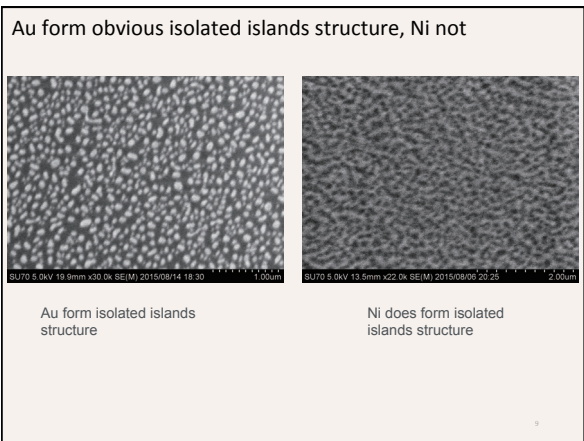
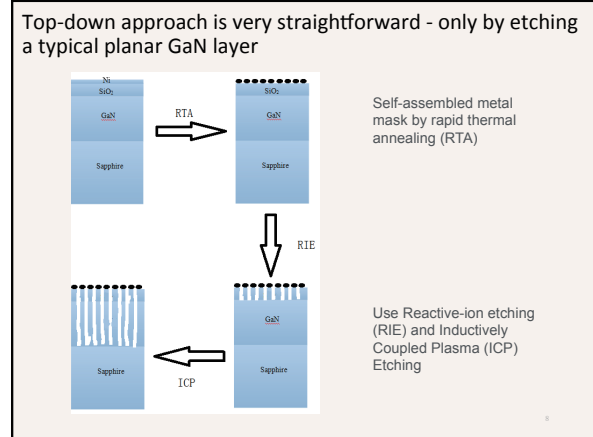
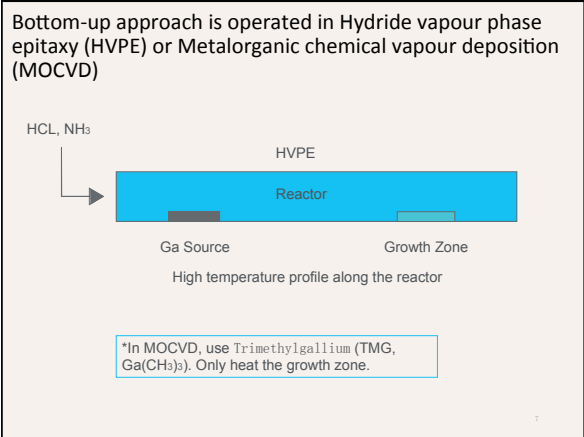
4

Bottom-up approach is operated in Hydride vapour phase epitaxy (HVPE) or Metalorganic chemical vapour deposition (MOCVD)

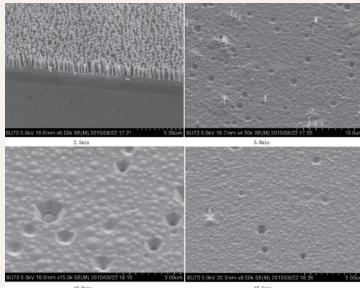
5

Bottom-up approach is operated in Hydride vapour phase epitaxy (HVPE) or Metalorganic chemical vapour deposition (MOCVD)

6



Both of the two metals can be mask for etching, even though Ni is not isolated well and Au is less durable for etching



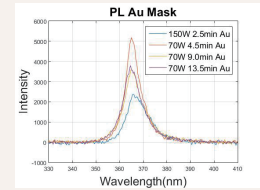
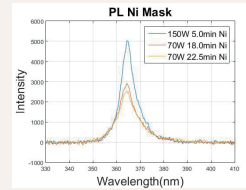
Au mask

RIE RF power: 150W

ICP etching rate: 60nm/min
ICP etching time: 30min

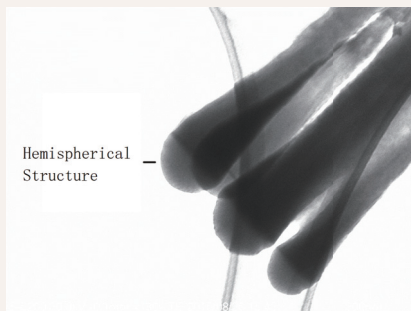
13

Photoluminescence (PL), Transmission electron microscopy (TEM) and Energy-dispersive X-ray spectroscopy (EDX) shows that the nanowires are GaN



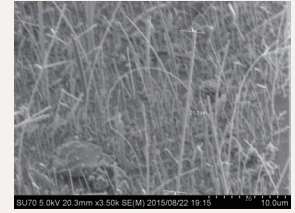
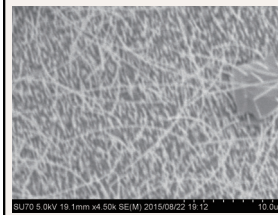
14

Photoluminescence (PL), Transmission electron microscopy (TEM) and Energy-dispersive X-ray spectroscopy (EDX) shows that the nanowires are GaN

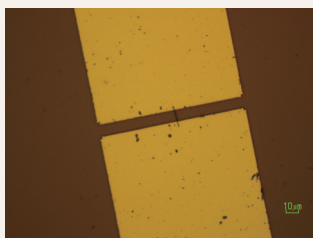


15

The GaN nanowires grown in HVPE is very long



The length is decent for single-nanowire device fabrication



17

Questions?

18

1

Control of Table Tennis Robot

Austin Kuo, UC Los Angeles
 Prof. Yoshikazu Hayakawa, Nagoya University

2

Introduction

Advanced robots operate:

- In a dynamic, unstructured environment
- Autonomously
- Quickly, smoothly, with sophisticated motion

3

Notation

Racket Var.		Ball Var.	
$V \in RT3$	Racket velocity	$p_i(t) \in RT3$	position
α	Yaw	$v_i(t) \in RT3$	Trans. velocity
β	Pitch	$w_i(t) \in RT3$	Ang. velocity
		t_i	time
		m, r, I	Mass, Radius, MOI

PA-10 Robotic Manipulator

- Four points of interest: $i=0,1,2,3$
- $-,+$ subscripts denote just before and after

4

Physical Modeling

Three Models:

- Aerodynamic Model (ADM)
- Table Rebound Model (TRM)
- Racket Rebound Model (RRM)

PA-10 Robotic Manipulator

5

Physical Modeling

Three Models:

- Aerodynamic Model (ADM)
- Table Rebound Model (TRM)
- Racket Rebound Model (RRM)

PA-10 Robotic Manipulator

6

Aerodynamic Model

- Consider Drag and Magnus Terms
- $g := [0 \ 0 \ g]^T$

$$\dot{p}(t) = -g - 1/2 C_{LD}(t) \rho / m S_{1b} \|p(t)\| p(t) + C_{LM}(t) \rho / m V_{1b} (\omega \times p(t))$$

Physical Modeling

Three Models:

- Aerodynamic Model (ADM)
- Table Rebound Model (TRM)
- Racket Rebound Model (RRM)

PA-10 Robotic Manipulator

Table Rebound Model

Assumptions:

- Ball makes point contact with table
- Impulse Momentum Theorem:

$$m\mathbf{v}^+ - m\mathbf{v}^- = \mathbf{P}$$

$$I\boldsymbol{\omega}^+ - I\boldsymbol{\omega}^- = \mathbf{r} \times \mathbf{P}$$
- $v_z^+ = -e v_z^-$
- $v^+ T = \gamma v^- T$ $\gamma > 0$ or $\gamma = 0$
- $\mathbf{P} \perp \mathbf{x}y = -\lambda (v^- T - \|v^- T\|) : 0 < \lambda < \mu \|P\| z^-$

Result:

$$[\mathbf{v}^+ - \mathbf{v}^-] = [\mathbf{A}t \ \mathbf{B}t \ \mathbf{C}t \ \mathbf{D}t] [\mathbf{v}^- \ \boldsymbol{\omega}^-]$$

Physical Modeling

Three Models:

- Aerodynamic Model (ADM)
- Table Rebound Model (TRM)
- Racket Rebound Model (RRM)

PA-10 Robotic Manipulator

Racket Rebound Model

Assumptions:

- Ball makes point contact with racket
- Impulse Momentum Theorem:

$$m\mathbf{v}^+ - m\mathbf{v}^- = \mathbf{P}$$

$$I\boldsymbol{\omega}^+ - I\boldsymbol{\omega}^- = \mathbf{r} \times \mathbf{P}$$
- $v_z^+ = -e v_z^-$
- $1/2 m \|\mathbf{v}^+ T - \mathbf{v}^- T\|^2 = \int_0^t \mathbf{x} \cdot \mathbf{f} \, dt$
- $\mathbf{P} \perp \mathbf{x}y = \int_0^t \mathbf{T} \boldsymbol{\omega} - k \mathbf{s} \mathbf{x}(t) \, dt$

Result:

$$[\mathbf{v}^+ - \mathbf{v}^-] = [\mathbf{R}1r \ \mathbf{R}2r \ \mathbf{R}3r] [\mathbf{v}^- \ \boldsymbol{\omega}^-]$$

Forward Calculation

Given: $\{p10, v, \alpha, \beta\}$

Find: $\{p13, v13, w13\}$

$p10 \rightarrow v1-, w1-, p11 : \text{ADM}$
 $v1-, w1- \rightarrow v1+, w1+ : \text{RRM}$
 $v1+, w1+ \rightarrow v2-, w2- : \text{TRM}$
 $v2-, w2- \rightarrow v2+, w2+ : \text{TRM}$
 $v2+, w2+ \rightarrow v3-, w3- : \text{ADM}$
 $v3-, w3- \rightarrow v3+, w3+ : \text{TRM}$

PA-10 Robotic Manipulator

Inverse Calculation

Given: $\{p13, v13, w13\}$

Find: $\{V, \alpha, \beta\}$

$v13+, w13+ \rightarrow v13-, w13- : \text{TRM}$
 $v13-, w13- \rightarrow v12+, w12+ : \text{ADM}$
 $v12+, w12+ \rightarrow v12-, w12- : \text{TRM}$
 $v12-, w12- \rightarrow v11+, w11+ : \text{ADM}$
 $v11+, w11+ \rightarrow V, \alpha, \beta : \text{RRM}$

PA-10 Robotic Manipulator

Inverse Relations

- $TRM^{-1} : [v_x, v_y, v_z]^T = [A]^{-1} [v_{x1}, v_{y1}, v_{z1}]^T + [B] [v_{x2}, v_{y2}, v_{z2}]^T$
- ADM (w/o drag, Magnus, $\dot{p}_3(t) = -\dot{p}_1 - 1/2 \dot{p}_2$
- $p_{12} = p_{11} + p_{21} + p_{11} - 1/2 p_{12} + p_{12} = p_{11} - 1/2 p_{12}$
- $p_{13} = p_{11} + p_{21} + p_{11} - 1/2 p_{12} + p_{12} = p_{11} - 1/2 p_{12}$
- $v_{12} = v_{11} + v_{21} - g T^2 / 2$ $v_{13} = v_{11} + v_{21} + v_{12} - 1/2 g T^2$
- $w_{12} = w_{11} + w_{21}$ $w_{13} = w_{11} + w_{21} + w_{12}$ $T^2 = t_{13} - t_{12}$
- $RRM^{-1} :$
- $V = RJR(1 - A)r^{-1} [RJR^T(v) - \dot{r}(v)] = B\dot{y}$
- $RJR^T(v) = \dot{r}(v)$
- $\sin(\alpha) = -b \pm \sqrt{b^2 - 4ac} / 2a$ $a = \xi_1 y^2 + \xi_2 x^2 + \xi_3 z^2$
- $\eta_1 y / \cos(\alpha) = -\xi_1 x \cos(\beta) + \xi_2 z \sin(\beta)$ $b = 2(\eta_1 z \xi_1 x - \eta_2 x \xi_2 z)$
- $c = \eta_1 z^2 + \eta_2 x^2 - \xi_1 y^2$

Numerical Simulation

1. Assign output variables $\{p_{13x}, p_{13y}, v_{13x}, v_{13y}, v_{13z}\}$
2. Perform inverse calculation to find $\{V, \alpha, \beta\}$ as well as T_{11}, T_{12}

Ass.	p_{13x}, p_{13y}	$v_{13x}, v_{13y}, v_{13z}$	$\omega_{13x}, \omega_{13y}, \omega_{13z}$
Ass.	0.342, 0.381	-4, -0.5, 2.15	***, ***, ***

V	α [deg]	β [deg]	T_{11}	T_{12}
-3.48, -1.25, 1.59	5.3	120.0		
With	0.195	0.433		
W/O	0.199	0.471		

With	p_{13x}, p_{13y}	$v_{13x}, v_{13y}, v_{13z}$	$\omega_{13x}, \omega_{13y}, \omega_{13z}$
With	2.209, 0.627	0.24, -0.04	0.00, 0.00
W/O	2.195, 0.622	0.18, -0.03	0.00, 0.00

With	p_{13x}, p_{13y}	$v_{13x}, v_{13y}, v_{13z}$	$\omega_{13x}, \omega_{13y}, \omega_{13z}$
With	0.624, 0.449	-3.69, -0.38, 2.08	19.1, -184.7, -72.4
W/O	0.343, 0.381	-4.00, -0.50, 2.15	25.0, -200.0, -72.4

Physical Experiment

1. Assign output variables $\{p_{13x}, p_{13y}, v_{13x}, v_{13y}, v_{13z}\}$
2. Inv Calculations performed in C++
3. Robot executes command

Conclusion

- ADM, TRM, RRM define physical model
- Forward calculations find final ball state given racket state and initial ball state
- Inverse calculations find racket state given final and initial ball state
- Numerical and Physical experiments confirm model

Thanks to:

- Professor Yoshikazu Hayakawa
- Mizuki Owada
- Yuki Isomura
- JUACEP Office

Electron Field Emission of Graphene

Jimmy Ng
Prof. Yahachi Saito
Dept of Quantum Engineering, Nagoya University
JUACEP 2015

Introduction

WELCOME TO THE GRAPHENE AGE

A CLOSER LOOK AT GRAPHENE

Introduction cont.

- ▶ Goal: Obtain a graphene-based electron emitter with a stable emission pattern activated by a low threshold voltage
- ▶ Zr deposition on graphene:
 - Zr has a lower work function
 - Zr has a tendency to adsorb molecules to the surface

Quantum Tunneling

classical physics: climbing the hill

quantum physics: "tunnelling"

Schrodinger Equation:

$$-\frac{\hbar^2}{2m} \frac{d^2\Psi}{dx^2} + V(x)\Psi = E\Psi$$

$\Psi = Ae^{-\alpha x}$ where $\alpha = \sqrt{\frac{2m^*(U_0 - E)}{\hbar^2}}$

Reduced probability, but ~~not~~ reduced energy!

Electron Field Emission (Fowler-Nordheim)

$$D(E_x, F) = \exp\left\{-\frac{8\pi(2m)^{\frac{1}{2}}}{3\hbar e F} (E_0 - E_x)^{\frac{3}{2}}\right\}$$

$$n(E_x)dE_x = \frac{4\pi m k T}{h^3} \ln\left[1 + \exp\left\{-\frac{E_x - E_f}{k T}\right\}\right] dE_x$$

$$J = \frac{4\pi e m k T^3}{h^3} \int_0^\infty \ln\left[1 + \exp\left\{-\frac{E_x - E_f}{k T}\right\}\right] \times \exp\left\{-\frac{8\pi(2m)^{\frac{1}{2}}}{3\hbar e F} (E_0 - E_x)^{\frac{3}{2}}\right\} dE_x$$

$$V(F, x) = E_0 - \frac{e^2}{4x} - eFx$$

$$J = 1.54 \times \frac{10^{-6} A(\beta V)^2}{\phi} \exp\left[-\frac{6.83 \times 10^7 \phi^{\frac{3}{2}}}{\beta V}\right]$$

Graphene's Characteristic FEM

Dragonfly like pattern predicted by Zibing Li and Ningsheng Xu from the State Key Laboratory of Optoelectronic Materials and Technologies at Sun Yat-Sen University in China

Experimental Procedures

Making W needles

1. 試料ホルダにグラフェンエミッタを装着する (Load the graphene emitter into the sample holder).
2. 金線ファイヤフィラメントを準備する (Prepare the tungsten filament).
3. 球状になった金線 (Spherical tungsten filament).

Zirconium deposition onto emitter

Obtaining graphene by scraping carbon surface inside SEM

7

Field Emission Microscope (FEM)

8

Results: Current vs Time

Current vs Time of Bare Graphene

Current (A) vs Time (seconds)

Bare graphene
20 min
V=440V

SEM of bare graphene emitter

Current vs Time of Graphene with 19A Zr

Current (A) vs Time (seconds)

Graphene with 19A Zr deposited
20 min
V=550V

- ▶ Causes of current decay: change in emitter's surface morphology over time
- ▶ Causes of current fluctuations: frequent absorption and desorption of surface molecules

9

Results: I-V curves

I-V curves for Bare Graphene, Graphene with 4A Zr, and Graphene with 19A Zr

Current (A) vs Voltage (V)

- Bare Graphene
- Graphene with 4A Zr
- Graphene with 19A Zr

More Zr deposition leads to better fit to Fowler–Nordheim equation

Zr deposition decreases the threshold voltage. Threshold voltages are:

- Bare: 0.5467 kV
- 4A Zr: 0.4781 kV
- 19A Zr: 0.4853 kV

10

Results: FEM Images

Bare graphene

Graphene with 19A Zr


- ▶ Bare graphene has dragonfly-like FEM pattern but its unstable
- ▶ Deposition of Zr alters FEM pattern

11

Conclusion

- ▶ Goal: Obtain a graphene-based emitter with a stable characteristic FEM pattern activated by a low threshold voltage
- ▶ Current fluctuations in bare graphene
- ▶ Current decay in emitters
- ▶ Deposition of Zr lowers threshold voltage, but also alters FEM pattern




12


Japan-US Advanced Collaborative Education Program
 Gain Engineering Research Experience in Nagoya and USA

Cell Transportation Based on Vibration-Induced Local Flow Control in Open Chip Environment

Xu Li, Takeshi Hayakawa
Advisor: Fumihito Arai

Department of Micro-Nano Systems Engineering, Nagoya University

Page 1 Nagoya University, Biorobotics LAB

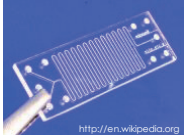
Outline

- Background
- Theoretical Analysis on Vibration-induced Flow
- Fabrication Process and Experimental Setup
- Experimental Results
- Summary

Page 2 Nagoya University, Biorobotics LAB

On-Chip Cell Manipulation

Microfluidic Chip



http://en.wikipedia.org

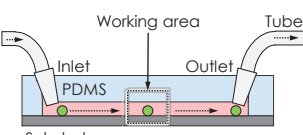
- ✓ Low initial cost
- ✓ Disposable

- ✓ Operator skill independent
- ✓ High throughput

Page 3 Nagoya University, Biorobotics LAB

Cell Manipulation on Opened & Closed Chip

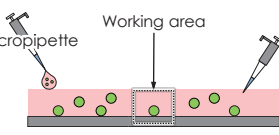
Closed Chip



- ✓ High-speed flow control
- ✓ Environmental control
- ✓ Difficult to access
- ✓ Complex experimental setup

Application ➤ Huge number of cells
➤ One-time process

Opened Chip



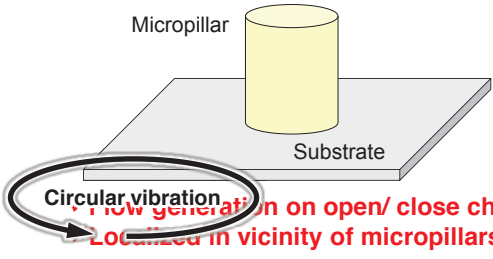
- ✓ Easy to access
- ✓ Easy to setup
- ✓ Difficult to control the flow
- ✓ Difficult to control the environment

Application ➤ Rare cell handling
➤ Time-lapse observation

Purpose Flow control on **open chip** for cell manipulation

Page 4 Nagoya University, Biorobotics LAB

Vibration-Induced Flow



Flow generation on open/ close chip
Localized in vicinity of micropillars

Page 5 Nagoya University, Biorobotics LAB

Theoretical Analysis

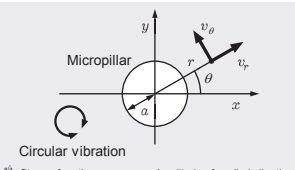
1st Order Stream Function: $\psi^{(1)}$

$$\psi^{(1)} = \pm \left[\frac{1}{48} \int_a^r \frac{1}{x} \rho(x) dx + c_1 \right] + r^2 \left(-\frac{1}{16} \int_a^r x \rho(x) dx + c_2 \right) + \left(\frac{1}{16} \int_a^r x^3 \rho(x) dx + c_3 \right) + \frac{1}{r^2} \left(-\frac{1}{48} \int_a^r x^3 \rho(x) dx + c_4 \right)$$

$$\rho(r) = \frac{f^2 A^2}{32\pi^3 \eta^2} \left[2X + 2X^* - 2\frac{\alpha^2}{r^2} CZ^* - 2\frac{\alpha^2}{r^2} C^* Z - 4XX^* + 4ZZ^* \right]$$

Flow Velocity: v_r, v_θ

$$v_r = -\frac{1}{r} \frac{\partial \psi}{\partial \theta}, \quad v_\theta = \frac{\partial \psi}{\partial r}$$

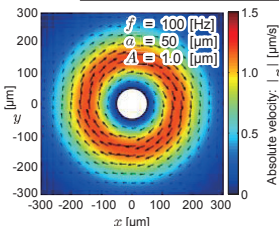


Circular vibration

ψ : Stream function
 η : Kinematic viscosity
 ω : Frequency of applied vibration
 α : Phase difference of x and y

Control Parameter

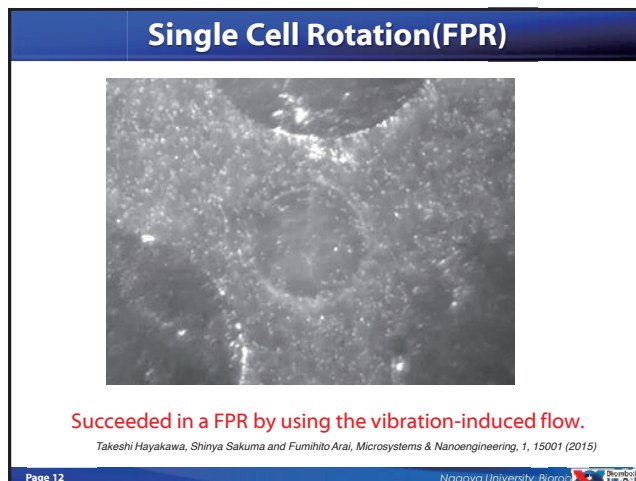
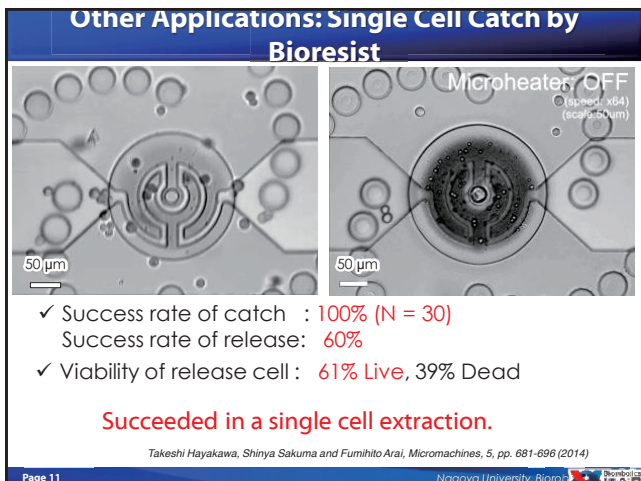
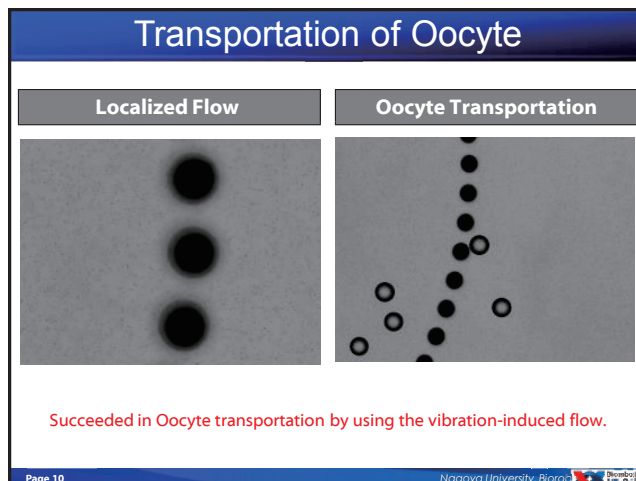
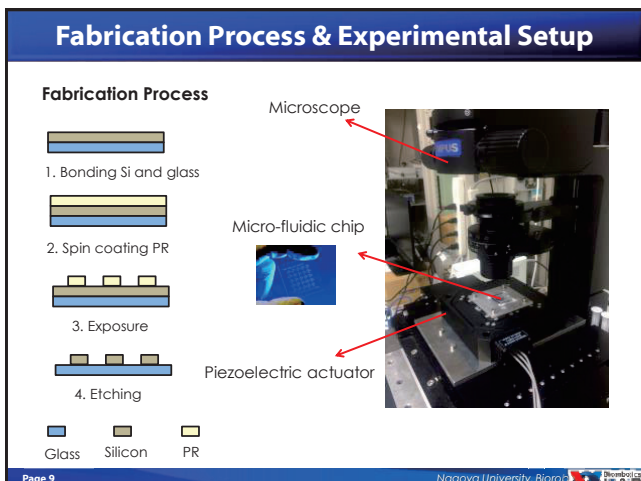
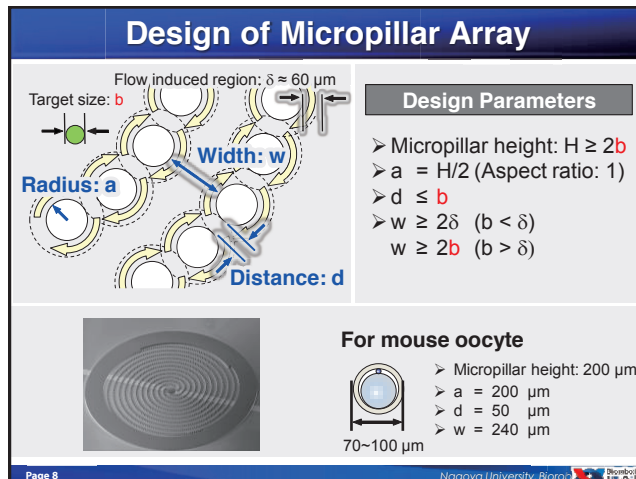
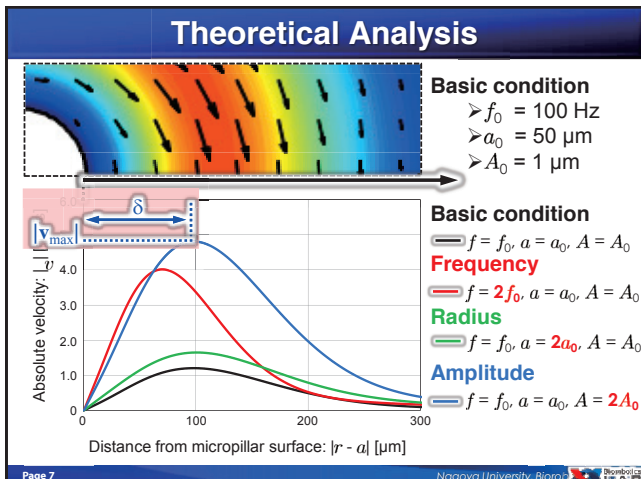
- > Frequency: f
- > Amplitude: A
- > Micropillar radius: a



Absolute velocity: v [$\mu\text{m/s}$]

$f = 100$ [Hz]
 $a = 50$ [μm]
 $A = 1.0$ [μm]

Page 6 Nagoya University, Biorobotics LAB



Acknowledgement

Thank you for your kind attention.



References

1. Takeshi Hayakawa, Shinya Sakuma and Fumihito Arai, *Micromachines*, 5, pp. 681-696 (2014).
2. Takeshi Hayakawa, Shinya Sakuma and Fumihito Arai, *Microsystems & Nanoengineering*, 1, 15001 (2015)

Special Thanks To ...



<3>

Reports & Questionnaires
on JUACEP Program

3-a. Reports

Findings through JUACEP

Name: Emanuel Antony Chirayath

Affiliation: Department of Aerospace Engineering,
University of Michigan, Ann Arbor.

Participated program: Summer 2015

Research theme: Rotating Detonation Gas-Turbine Engine

Advisor at Nagoya University: Prof. Jiro Kasahara

Affiliation: Aerospace Engineering



The JUACEP program has been a very valuable opportunity for me to pursue research in Aerospace Engineering. I have been able to collaborate with my colleague from University of Michigan, on a joint project to design, develop and test a Rotating Detonation Gas-Turbine Engine. My experience in Kasahara Lab has been very excellent. Prof. Kasahara and Prof. Matsuoka have been diligently guiding us from the very beginning of the project. My Teaching Assistant Mr. Ishihara has been very helpful at every step of the process. Besides them, all other members in the Kasahara Lab have been very welcoming and helpful in dealing with life in a different place. The staff at the JUACEP office, especially Ms. Yada and Ms. Kato, have been very helpful at all times.

Life in Nagoya has been quite busy. I found the International Residence to be a very excellent and well-kept place. It allowed me to relax after coming back from a busy day at the lab. The excursion to the Toyota Motors plant at Motomachi was an eye opening opportunity for me to see an advanced Japanese industrial plant. The Japanese pottery class and the chance to make our own pottery was a unique experience in my life.

I was able to visit places like Kyoto, Osaka, Tokyo, Mount Fuji and Kamikochi. Every place had its own charm and story to tell. Kyoto exuded old heritage and culture, while Osaka was a picture of modernity. Tokyo was the busy, bustling city that I had expected it to be. The trip to the Japanese Alps in Kamikochi was very relaxing and refreshing. Watching the sunrise at Mount Fuji was something I would describe as a once-in-a-lifetime opportunity. The whole experience of climbing and staying on the mountain is something I would cherish forever.

The most important aspects of Japanese culture that I personally recognized were the punctuality, hospitality and politeness of its people. I realized how discipline could lead a nation to greatness. The Japanese way of life also enlightened me to a sustainable use of the limited resources available to humankind. I felt that everything in Japan tried to blend with the environment.

I hope these experiences will have a positive influence in my life. The research experience I have gathered in the Kasahara Lab would be very valuable for my career in Aerospace Engineering. I hope to continue pursuing research with similar themes in the future as well.

Findings through JUACEP

Name: Fang Dai

Affiliation (Dept & Univ): Mechanical Engineering. University of Michigan

Participated program: Summer 2015



Research theme: IMPLEMENTATION AND PARAMETERS IDENTIFICATION OF WIEDEMANN VEHICLE FOLLOWING MODEL

Advisor at Nagoya Univ: Prof. Tatsuya Suzuki

Affiliation (Dept.): Mechanical Engineering

My research topic in Nagoya University is 'Implementation and Parameters Identification of Wiedemann Vehicle Following Model for Fuel Consumption'. My supervisor is Prof. Tatsuya Suzuki and I gain much more than I expected both in academic and non-academic. For research itself, I enhanced the skills of programming in Matlab and got access to an amazing software, Carmaker, which is an advanced vehicle simulation tool.

The life in lab is casual and people here are very kind and easy-going. They organized the welcome party for me and after that we went to play bowling together. Beside the research experience in the lab, I like the culture here. We travelled to many cities in Japan like Kyoto, Osaka and Tokyo. We experienced the firework festival here with the traditional yukata and tried a lot of traditional and delicious food like Takoyaki, Sashimi and Ramen, which I would never forget.

JUACEP program was very kind and considerate to organized many meaningful activities for us. The handcraft exercise was one of these and it offered us a good chance to well apply the theory into real-life. The pottery training was also very interesting and we were absorbed in making our own work. I believe all things I learned and all experiences I gained in Japan must have positive impact on my future career.



Findings through JUACEP Experience 2015

Name: Ulka Dandekar

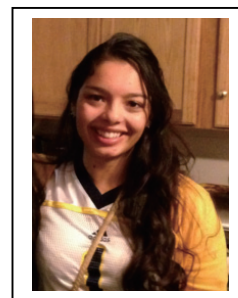
Affiliation (Dept & Univ): Pharmaceutical Engineering, University of Michigan

Participated program: Summer 2015

Research theme: siRNA as gene silencing system for therapeutic use

Advisor at Nagoya Univ: Prof. Hiroyuki Asanuma

Affiliation (Dept.): Molecular Design & Engineering



Firstly, I would like to thank Kato-san and Yada-san, as they both worked hard to make our experience as pleasant as possible, and always did so with a smile. Also, thank you to the coordinators of JUACEP and the UMich IPE Office, for making this opportunity possible. JUACEP is my first study-abroad experience, and I was more apprehensive than excited at the prospect of spending 3 months in Japan. However, this program has been a wonderful experience and I would be happy to return if ever given such a chance.

Working in Asanuma Sensei's lab, I learned several new methods and analytical techniques including RNA synthesis and purification, gel electrophoresis, and mass-spectrometry. Learning such academic concepts was difficult, but even using things like MS Office and other computer software was challenging because it was all in Japanese. I found it interesting that most of the students in lab are undergraduate and master's students, with only one PhD student, yet they worked long hours coming in around 9:30 am and staying until 9 pm. My lab mates always made efforts to include me in social activities, despite the language barrier - they invited me to play softball, eat lunch with them, and recommended fun places for me to visit in Nagoya and other cities. Asanuma-sensei was even kind enough to take me and a few others to watch the Grand Sumo tournament!

JUACEP activities outside of research such as the field trip and Japanese class were a great opportunity to take a break from lab and also interact with the other students. Even though I am hardly well-versed in Japanese, I highly recommend taking the Japanese class because by studying the language we inherently learned about the cultural norms. I thoroughly enjoyed the field trip because before coming to Japan, I interned at Toyota in Ann Arbor, MI for eight months and at the field trip to Toyota City we were able to witness examples of the Toyota Production System in practice. Also, that day the UM students were able to socialize with JUACEP staff and UCLA students at dinner and karaoke.

Since the first day I arrived, I kept learning new things about Japan - both small and big details. For example, Japan truly is the "the land of the rising sun" as the sun came up every day before 5 AM. Additionally, punctuality is followed here quite closely, not just by people but by the trains and subways, too. Before my arrival, I was initially very nervous about eating in Japan, because I am vegetarian. At times I missed food from home and it was difficult to find food without meat or fish, but never impossible. Unfortunately, I could not eat much authentic Japanese cuisine, but I was still able to eat new fruits like yellow kiwi and yellow grapefruit, and enjoy Japanese culture in other forms.

The program allowed for free time, giving the opportunity to visit Kyoto, Osaka, Tokyo, and more. A few of my favorites include seeing temples and downtown Kyoto, Ise Jingu shrine, the beach at Toba, Osu Kannon shopping in Nagoya, and learning to make sushi in Tokyo.

As a final note, my sincerest thank you to Asanuma Lab, especially Kamimoto-san, as well as JASSO, UM-IPE, and JUACEP for an unforgettable summer of new and exciting opportunities. ありがとうございます!!

Findings through JUACEP

Name: Yuting Gao

Affiliation (Dept & Univ): Chemical Engineering, UM

Participated program: Summer 2015

Research theme: Analytical Study on Combustion Kinetics of Various Solid Fuels / Waste Products

Advisor at Nagoya Univ: Prof. Ichiro Naruse

Affiliation (Dept.): Mechanical Engineering



On May 13th 2015, I arrived at Nagoya, and started the 3-month program. As a Chinese, I am always interested in our neighbor country, Japan. I have been here once about ten years ago. However, I believe that if you want to experience a different culture, the best way is to live there rather than just travel there. Thanks to JUACEP for providing me a great opportunity to experience authentic Japanese culture.

Japan is a country that is totally different from America. People here are really care about others. When I first arrived at my room, I found that everything was well prepared, including beddings, internet cable, cloth hangers, and even a lamp. As long as you had your personal belongs, you could settle down within one hour. Maybe in America we can have more freedom to prepare our own living supplies, but when I saw a well-prepared room, I could feel that they really cared about our residents and was truly grateful for that.

Daily life in Nagoya was just going to lab and work with lab students. Japanese students were relative shy compared to American people. Maybe because of language problem, they seldom came to talk with me, but if I had some problems and ask them what to do, they were all willing to help me. Getting along with them made me believe that all the engineers around the world are funny people. When they introduced a new student to me, I was told that his English was very good and his Chinese was also very good.

Besides experiments, lab students also invited me to the softball game and lab trip. They played softball very well and I only knew a little about that, but they taught me and practice with me with great patience and enthusiasm. During the lab trip, the two professors helped me a lot. They explain the similarity and difference between Chinese and Japanese cultures, and interpreted for me when I bought souvenirs. They lived with students in the same Japanese style room and even play mahjong and games together. They were not like professors, but just close friends with everyone, making me feel like the lab was like a family.

On weekends, I hung around with other JUACEP students. We bought yukata and went to the firework festival, traveled to Kyoto, enjoyed the hot spring in Inuyama, and etc. Before JUACEP, I did not know anyone of them, but now we are really close friends. It is always hard to live alone in an unfamiliar city thousands of miles away from hometown, especially when you hardly speak their native language. Thanks to these friends, life in Japan was never hard but enjoyable, although language was still the biggest problem.

I really like this JUACEP program. The simplest words express the truest feelings. The lab experience impresses me greatly. If there is a chance, I will consider to apply for a PHD program in Nagoya University and even work in Japan for some years in the future.

Findings through JUACEP

Name: Xudong Hao

Affiliation (Dept & Univ): Department of Mechanical Engineering,
University of Michigan

Participated program: Summer 2015

Research theme: Evaluation of Contact States Using A Wound Testing System
with Slip and Force Sensors for Estimating Skin Scratch Risks

Advisor at Nagoya Univ: Prof. Yoji Yamada

Affiliation (Dept.): Mechanical Science and Engineering, Nagoya University



It is my first time visiting Japan. The three-month experience makes me love the life here. I had a lot of fun with friends from University of Michigan and students of Nagoya University.

The first thing we learnt in Japan is the one-month Japanese class. It is not that long but very helpful. We learned a lot daily words and conversation sentences with a kind professor. The limited Japanese we had learnt helped us a lot during our later travel in Japan. We could tell which were the shops, what was the sushi we wanted to eat and ask some basic questions in Japanese.

Furthermore, I also like the research experience at Professor Yamada' lab. People here work very hard, which inspires me to do my research diligently. Professor Yamada and post-doctor Akiyama warmly answered my questions and pointed out the problems of my work. My lab mates are from different countries, such as Japan, China, Germany and Ecuador. We had wonderful parties and helped each other with the researches.

Also, JUACEP office held a lot of interesting activities to enrich our life in Japan. We had a field trip to Toyota Motor Company assembly work and Toyota Museum. We were shocked by the automation of robots and achievements they had made. In the afternoon of that day, we made potteries of different shapes. I made my first heart-shape pottery with pink color. That day ended with a BBQ feast. It was one of the most wonderful days in Japan. The handcraft exercise later made me understand the basic structures of a gasoline internal combustion engine by disassembling and assembling it.

What's more, I also travelled in Nagoya, Kyoto and Tokyo with friends from University of Michigan. We tried different kinds of Japanese food and visited many places of interest, like shrines and skyscrapers.

All in all, it is an amazing experience in Japan that I will never forget. After this program, I am much interested in working and living in Japan or working for a Japanese company in Japan or in US.

Findings through JUACEP

Name: Chadwick Harvey

Affiliation (Dept & Univ): Aerospace Engineering, University of Michigan

Participated program: Summer 2015

Research theme: Rotating Detonation Gas-Turbine Engine

Advisor at Nagoya Univ: Prof. Jiro Kasahara

Affiliation (Dept.): Aerospace Engineering, Nagoya University



My experience in Japan through the JUACEP program is certainly something that I will never forget. After arriving, I was presented with cutting-edge research in aerospace propulsion that will have a profound effect on my life. Every person that I've interacted with in my lab has been extremely welcoming and always willing to help. My TA has gone above what was required of him to help integrate me with the lab, and I feel that after only three months we are all working as a team.

This program has not only exposed me to life at a new university, but to an entirely new country and culture. Through the program I've been able to explore many cities in Japan including Tokyo, Osaka, and Kyoto, as well as to participate in adventures such as hiking through Kamikochi in the Japanese Alps and climbing Mt. Fuji to watch the sunrise. Having lived in a completely foreign culture for three months has exposed me to a great deal of understanding that I previously did not have. I feel more connected to the rest of the world and certainly more well rounded as an individual. I'm also great with chopsticks now!

I strongly believe that both my research here as well as my cultural experiences will have a significant contribution to my future, and for that I am forever grateful. In Michigan, my focus has been entirely on the class aspect of learning. Here at Nagoya University in Kasahara-sensei's laboratory, I have been able to thrive in a completely new aspect of learning in the research and laboratory setting. Even though it was only for three months, my experiences here will apply significantly to my future careers as a strong asset. My experience will make me more marketable when looking for a job, as well as more versatile when I have found it.

Findings through JUACEP



Name: Jiahong Ju

Affiliation (Dept & Univ): EECS University of Michigan

Participated program: Short (Summer) 2015

Research theme: Investigation of Performance of the Modified MCCB with A New-Developed Fault Current Limiter in Low Voltage DC Distribution System

Advisor at Nagoya University: Prof. Matsumura and Associate Prof. Yokomizu

Affiliation (Dept.): Electrical Engineering

I feel so lucky to have the chance to attend the last year of the JUACEP program. Before attending the JUACEP program, many imaginations are in my mind about Japan. Just like other people around me, I knew and started to contact with and be interested in Japan from the Japanese animations during my childhood, especially from the Japanese movies when I grow up. Most of all, the power system protection is always my favorite topics in electrical engineering. Unfortunately, there is no such minor field in University of Michigan, so it is definitely a great gift for me to be here, in Prof. Matsumura' lab, in Nagoya University and in Japan.

The management of JUACEP is really a good combination of research and pleasure. In the first several weeks, I take the Japanese class with all the students from Michigan, it is helpful to have an overview about the Japanese language and Japanese culture. During the weekdays, I stay in my lab to read papers and conduct experiments. All the lab mates are really hardworking. Sometimes we talked about the topics in our major field and it is found that all the things in electricity has some things in common around the world but also with minor differences, which actually reflects the difference behind each culture. We also discussed about the difference culture between Japan, America and China and there are always some interesting stories to share with each other. People in my lab are also very friendly to help me both in research and the life in Japan. They taught me how to configure each equipment when I have difficulty in reading about the Japanese instruction manual. As all the experiments in my lab are about large current and power system protection, so they instructed me how to conduct the experiments safely. Sometimes when I want to travel to some neighborhood cities around Nagoya for sightseeing, they helped me make the travel plan and recommended me interesting places and good restaurants, which made my travel experience incredibly amazing.

For my favorite aspect about Japan is definitely the Japanese food. Not to mention all the good restaurants outsidess the campus, the food in the Dining hall in campus is much better than that in America, what's more? They are much cheaper. Normally I will go to the cafeteria for lunch and dinner with my lab mates together. What surprised me most is the small portion of the Japanese dishes and also the small stomach size of Japanese people. I might eat almost twice portion of the food as my lab mates ate and they were also surprised to my good appetite.

Besides the food, I also want to behave like Japanese people. I wear Yukata to attend the Nagoya University festival and the firework festival in Nagoya harbor. When I choose the hotels during traveling, I preferred to choose to stay in Tatami and Capsule hotels. All these experiences enrich my life in Japan and makes me understand Japanese culture better.

The only concern for me is that English is not so popular in Japan. Although people cannot speak too much English, they are still willing to talk with you and help you, which always gives me a good impression of Japanese people.

In a word, I never imagine I could have the opportunity to be in Japan like this. I really want to thank JUACP and all the officers, TAs and professors working in JUACEP. Thanks to their kind help and good management of this program, I have this wonderful experience in Japan. For me, three month program goes so fast and I am still not ready to leave here, but I am sure that I will have more opportunities to come back to meet all you people in the future. I will miss all of you.

Life and Research in Japan with JUACEP

Name: Andrea Manoppo

Affiliation: Biomedical Engineering, University of Michigan

Participated program: Summer 2015

Research theme: Fabrication of Tissue-Engineered Small Blood Vessels via 3-Dimensional Cell Self-Assembly and Organization In Vitro

Advisor at Nagoya University: Professor Fumihito Arai

Affiliation: Nagoya University, Micro-Nano Systems Engineering



I am very happy to have had the opportunity to participate in the JUACEP research program. I am grateful to the Arai Lab for hosting me and grateful to both the JUACEP and IPE program staff for their support. The research project that I worked with alongside my mentor was highly innovative. It was fascinating to learn novel approaches to tissue engineering. I have a fondness for cellular and tissue research, microfluidics, and micro-mechanics – so needless to say, that was a great learning process for me. The Arai lab seems to be famous on Nagoya University campus for their incredibly rigorous approach to research and for their accomplishments in bio-robotics and micro-nano systems. It's unfortunate that I am not fluent in the Japanese language (and even less so in a scientific setting). In that sense, the most difficult challenge was the language barrier. Laboratory protocols are also written in Kanji, so I felt like I required a lot of assistance. However, challenges were overcome with the enthusiasm of my fellow lab mates at Arai Laboratories. I always felt welcome here; both their intellect and their helpfulness always impress me.

While the project at Arai Laboratories expanded my knowledge in a biomedical topic that I am passionate about, the JUACEP events allowed me to see aspects of engineering outside my concentration that I wouldn't have seen otherwise. For example, I learned about car manufacturing techniques during the Toyota Factory tour, learned to assemble internal combustion engines by hand, and attended production-engineering seminars. From there, it's easy to see why everyday technological convenience and environmental conservation is so exceptional in Japan.



Regarding culture differences, actually I felt like I fit in right away. The change in diet was no problem for me; I tried every type of sushi, okonomiyaki, yakitori, udon, ramen, or takoyaki imaginable. I made many Japanese friends who pushed me to try new things. One of my favorite moments was when friends taught me how to play card games (such as daifugo) on the train to visit Osaka. I participated in traditional tea ceremony at Nagoya castle, took classes in traditional fan dance, spotted geisha in Kyoto, fed deer in Nara, bought antiques in Takayama city, saw temples in Ise and huge fireworks festivals in Gifu. I stayed in Tokyo and even climbed to the top of Mount Fuji. All this activity combined with research was quite exhausting – but the good kind of exhaustion. I made efforts to talk to all kinds of Japanese people and make use of the Japanese language that I learned. I discussed philosophy with locals to get a sense of new attitudes and approaches to life.

In the end, it is not just the opportunity to contribute to a cutting-edge biomedical research project that is so valuable, but the global aspect as well. It was an impactful experience in terms of learning to communicate and work toward common goals with others in a new environment. I learned a lot with JUACEP and I hope to visit all in Japan someday in the future!



Findings through JUACEP

Name: Haodong Shen

Affiliation (Dept & Univ): Electrical Engineering and computer science

Participated program: Summer 2015



Research theme: All-polarization-maintaining Er-doped ultra-short pulse fiber laser using carbon nanotube saturable absorber

Advisor at Nagoya Univ: Prof. Nishizawa

Affiliation (Dept.): Electrical Engineering

Firstly, I want to express the appreciations for the JUACP programs. It is really a good experience. I'm impressed by the kindness of Japan.

My professor is a hard-working and talented professor who is the pioneer of his area. He taught me by himself and I learned a lot from him. In the past 70 days, I learned many practical skills in the laboratory which I believe will help me in the future career. I was warmly welcomed by the lab mates. They helped me to solve the problem in research and life. Also, I went out and drank with them. Thus, I knew how was Japanese. They are very shy outside and very nice in their deep heart.

The lectures and the excursion organized by JUACEP are fantastic. I learned a lot of knowledge about the manufacture. And I was shocked by the steam-line of the Toyota. In the BBQ, It was very delicious Japanese style BBQ. Also, I felt the "craziness" of Japanese. They

This program did a good preparation for my future career. Moreover, it teaches me how to live. I traveled many places in Japan, Kyoto, Gifu, Mt.Fuji and Sapporo. It's different from China and USA. It is just like the Japanese animation. I will come to Japan next time in a different season. I could imagine what is the altitudes of Japanese towards life: they just do things extremely good and enjoy the nature.

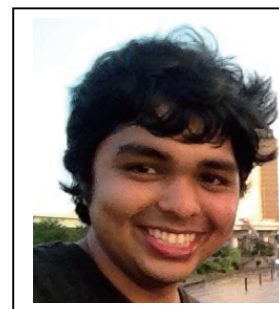
The culture in Japan is very interesting. In the Nagoya University, it has Meidai Festival. In different places, they have their own festivals. I remember that we wore Japanese traditional suit Yukata to join the atsutajingu festival. There were lots of people joining different kind of activities and also many small stores to sell interesting items.

It is very worthy to be here.



Findings through JUACEP

Name: Goutham Thangaraj
Affiliation (Dept & Univ): AOSS, UM
Participated program: Summer 2015



Research theme: Solar Neutron Data Assimilation and Analysis obtained through SciCRT

Advisors at Nagoya Univ: Prof. Itow, Prof. Matsubara and Prof. Shiokawa
Affiliation (Dept.): Solar Terrestrial Environment Lab

The JUACEP program was the perfect blend of education and fun. It challenged me in many ways and helped my growth both professionally and personally. In the program, I was able to perform research in my chosen field with my peers. They were not only very intelligent but also witty and very welcoming. The professors were very kind and helpful and were always willing to help me through my troubles. I learned a lot during my stay here and the research project provided me with valuable experience that has strengthened my knowledge in the field of Space Science.

Attending the Japanese Language Course was very helpful and it made conversation and travelling the country much easier. By learning simple phrases and keywords, I was able to connect with my lab mates and not be totally lost during any conversation.

The excursion was simply amazing. The tour of the Toyota factory and the museum were very informational and the watching a robot play the violin was truly marvelous and a testament to the hard work and compassion that the Japanese people have for progress. The Seto Pottery Museum was also interesting and making a pot for the first time was exciting and surprisingly fun! The two and a half hour all-you-can eat restaurant was the truly one of the best places I have been to, the different kinds of food and drink along with the live performance all added to the great ambience of the place. This was all topped off with a trip to the Karaoke where we all sang our hearts out and had a great time!

Life in Nagoya is very vibrant with plenty of places to visit such as the Nagoya Castle, the Aquarium, Science Museum (one of my favourite places in the city), Osu Kanon, Nagoya Station and many more. It will be a long time before anyone can cover the whole city but I tried my best to cover as much as I could during my stay here. I also visited Kyoto, a city that maintains the country's cultural heritage to this day. I visited a lot of shrines such as Fushimi-Inari, Heian-Jingu, Yoshida as well as temples such as Kinkakujin (Golden Temple), Ginkakujin (Silver Temple) and Kiyomizu Dera. Japan is a lovely country to stay in as the people are very polite and patient. Even if you do not speak a word of Japanese they will try to help you out in any way they can.

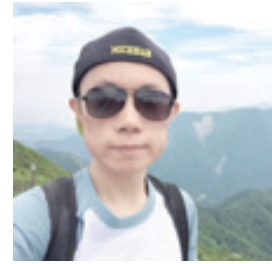
JUACEP provided me with the opportunity to work in Space Science field thereby strengthening my knowledge and providing me with the technical background to further establish myself in the sector. It also helped improve my communication and analytical skills as language was often a barrier and other forms of communication such as non-verbal language needed to be adopted. It provided me with a chance to experience a different culture thereby helping me understand the intricacies of the difference in personality between people from varying backgrounds.

Research and Fun

Name: Chen Wang

Affiliation (Dept & Univ): Department of Mechanical Engineering, UM

Participated program: Summer 2015



Research theme: A Study on Topology Optimization with FEM Based on Iterative Mesh Division

Advisor at Nagoya Univ: Prof. Toshiro Matsumoto

Affiliation (Dept.): Department of Mechanical Science and Engineering

This is my second time to Japan. So everything here is not totally new to me. I can even speak some simple Japanese. But this time I have experienced more compared to last time thanks to JUACEP.

First of all, let me talk about the lab life and research. I join Matsumoto Lab in the Department of Mechanical Science and Engineering here, of which lab members are really nice and helpful. They've organized a welcome party for me and really helped me a lot about both my daily and academic life. As to the research, Prof. Matsumoto is always happy to answer any question I raised. I have learnt a new programming language Fortran and used it to use a practical problem in finite element analysis. With this experience, in the future, I think it may help me to start my job as an FEA engineer.

Secondly, I really love the introductory courses given by experts from different automobile related companies like TOYOTA and DENSO. Although the lectures are not deep into specific techniques themselves, they show me a general pic of the current situation and development of Japanese vehicle industry. Moreover, as my major and concentration is automobile technology, this is the first opportunity that I can start to get to know the big car corporations. I hope, in the near future, I can obtain a job in such kind of companies in Michigan.

Furthermore, I have improved my Japanese proficiency during this stay in NU. Although I didn't take the language classes provided by JUACEP, I found many chances to communicate with natives like lab members and local people through daily life. I think it is the best to come to Japan if you want to learn its language!

Last but not the least, I really enjoy the trips this time. Since this is not my first time to Japan, some big cities or hot tourists spots are so appealing to me. And thus I tried to find some beautiful places that Japanese natives would like to go. I went to 湘南 and 伊豆 areas to see sceneries of sea and Mt. Fuji. And I also went camping in national park of Mie prefecture and watched the fireworks in Nagoya. It is really good memory for me to keep all the time.



Life Experience in Japan

Name: Hanyi Xie

Affiliation: Mechanical Engineering, College of Engineering;
Engineering Sustainable Systems, School of Natural Resources & Environment;
University of Michigan

Participated program: Short (summer) 2015

Research theme: Annealing effect on Hardness of DLC Coating

Advisor at Nagoya University: Prof. Noritsugu Umehara

Affiliation (Dept.): Mechanical Science Engineering



Photo I. With my TA: Eitaro Nakatani



Photo II. Umehara Lab

It's the second time I came to Umehara Lab in Nagoya University. Compared to previous experience, I achieved more than I expected not only because I learned advanced technology in tribology area, but all lab members treated me as if I have never left here before.

After last year's JUACEP program, I started to learn Japanese since I returned to Umich until now. I did not think about coming again until I got the offer from School of Natural Resources & Environment for pursuing my second Master's degree. During the time I was thinking about how I would spend this summer, I received encouraging email from both Chiharu and Prof. Umehara saying I was permitted to take one more time part in the JUACEP. I was moved a lot. And even now, it sounds like a dream for me and I feel thankful for being able to get involved in this wonderful program again.

Due to the achievements of my Japanese learning, it was possible for me to communicate much better and more deeply with people in our lab. I witnessed how hard M2 students were doing the job hunting and how much effort B4 students paid on preparing the entrance exam. I stayed up whole night with my TA working on our research. I was also shared the success and happiness when M2 students got good news from companies. Even though I spend most of time together with lab members and even have not been to Tokyo, I feel satisfied so much. For me, accompanying with my friends in this lab is much more significantly meaningful than travelling to places of interests by myself. Three months is too short. But it was good enough to give me a start to learn the surface of tribology, to get to know Japanese culture, to develop friendship and to build an unforgettable memory here.

Again, thanks to JUACEP for giving me such a chance to enrich my life experience, meeting trustful friends. If my Japanese is getting good enough, I would also be glad to have job hunting in Japan since I really like the culture and people here. I believe it would make me live a great life in Japan as well.

Findings through JUACEP

Name: Yalim Yıldırım

Affiliation (Dept & Univ): Mechanical Engineering, Michigan

Participated program: Summer 2015

Research theme: Human Running Assist Exoskeleton

Advisor at Nagoya Univ: Prof. Yasuhisa Hasegawa

Affiliation (Dept.): Micro-Nano Systems Engineering



When I received the email about the JUACEP program in Winter semester, it seemed like it was just what I needed. I had just recently been admitted to the one-year Master's program at Michigan, and I had been looking for summer opportunities where I would gain some experiences that would help me with my work next year. JUACEP seemed to be the perfect opportunity because it allowed me to travel in Japan, work with world-class faculty on one of dozens of research opportunities, and transfer research credits to my Master's. And over two months into the program, I can say that it was a once in a lifetime opportunity and am glad to have done it.

At Nagoya I joined Prof. Yasuhisa Hasegawa's lab to work on a Human Running Assist Exoskeleton. It was already a relatively mature project that had started about 4 years ago, and it is currently given to one of the experienced graduate students in the lab. So working with him on the project taught me a lot about how to navigate through a research project and helped me gain skills not only like engineering design and data collection and analysis, but also more academic skills like article and presentation writing and communication.

Apart from my time at the lab, I also had the chance to take Japanese classes, go on field trips to exciting places like a Toyota plant, and attend seminars by faculty from Nagoya, Michigan and UCLA. The Japanese classes, although having only lasted 5 weeks, covered most of the basic conversation skills. I cannot say I retained most of the material we learned during class, but it was still a good opportunity to become acquainted with the language, read the Japanese alphabets, and learn how to say the basic daily-life phrases. The field trips were well organized and were a great opportunity to get to know other students from Michigan and UCLA. Although the seminars were often about fields unrelated to each student's interests, they were still a good opportunity to become acquainted with research going on in various fields and universities.

Aside from the activities organized by JUACEP, I also joined the Judo Club. Looking for an exciting way to stay in shape, I searched for clubs at the university and emailed their president before coming to Nagoya. He returned my emails very quickly, helped me arrange my first training, and introduced me to the members in my first week here. During my first training I found out that they practiced a special kind of Judo called Kosen that was only done in the 7 former imperial universities, and that they are very competitive. I was surprised about how welcoming they were to a foreigner with minimal martial arts training. I went to practice every week during the program and made great friends, including a Danish visiting medical student, a Brazilian law PhD student, and a Japanese senior who is going to study in Michigan next year. So it was a great opportunity to not only stay in shape, but also to learn a true Japanese martial art and make a lot of friends.



The biggest difficulty that I can mention about coming to Japan for a research program is the language barrier. Because Japan is an island country with dominant popular and academic cultures, most students are not good at English. It still is a very safe and organized country and the people are very welcoming and helpful, which makes daily life a lot easier. But as research is based mostly on exchange of information, the language barrier can become frustrating and limiting. That is why I believe that this program was as much about experiencing a laboratory and work environment in Japan as about doing actual research, if not more so.

Findings through JUACEP, Summer 2015

Name: Douglas Chen

Affiliation (Dept & Univ): Materials Science and Engineering, UCLA

Participated program: Summer 2015

Research theme: Hydrogen Production

Advisor at Nagoya Univ: Prof. Seiichi Deguchi

Affiliation (Dept.): Thermal Engineering



I have thoroughly enjoyed the time spent living in Japan and working at Nagoya University and am grateful to have had the opportunity to do so. During my time here, I explored much of Nagoya and Japan, including Kyoto and Tokyo. Being able to experience Japanese culture firsthand has been an eye-opening adventure, and I have learned much both academically and personally. The chance to learn Japanese both via classes as well as through communication and reading in society has been great, and I look forward to learning more upon my return to the United States. The necessity to learn some Japanese in order to navigate and communicate with people has also been a catalyst to make me learn Japanese, a goal that I have been attempting for many years. I have also been grateful for the chance to experience the vast amount of media and anime in Japan: I have enjoyed the music, animation, manga, and videogames available here which I would find back home. Having the chance to explore Kyoto and Tokyo gave me glimpses of a variety of subcultures and building architectures present throughout Japan. Japanese culture as a whole proves to be very different compared to the United States, but it is a culture that I quickly and easily adapted to as a quiet, introspective, and respectful person. The summer weather proved to be difficult, but I managed to withstand the heat and humidity even while continuing to wear long pants. It has shown me that I can live in environments that I previously felt I would not be able to live in for long periods of time. I also extremely enjoyed the food in Japan, whether it was ramen, onigiri, pork katsu – just about anything I ate was delicious.

Academically, the research I have been working on has been fulfilling. Being able to physically work in order to attempt hydrogen production has been satisfying, and trying to find an environmentally friendly method to produce and store energy coincides with my desires and life goals. The experiments run so far have proven to be unsuccessful, but even the process of determining and assembling experimental setups and analyzing why experiments did not work are good mental exercises for scientific purposes. My lab mates have proven to be good friends, and have introduced me to much of Japanese culture and humor. I enjoyed spending time within both within and outside of the lab, bonding with them while learning each other's' languages.

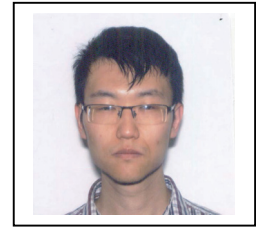
Overall, the time I have spent in Japan thanks to JUACEP has thoroughly introduced me to many aspects of Japanese culture and has greatly assisted in making me learn the Japanese language. It has shown me that I would be more than willing to live in Japan if given the chance and financial ability to do so.

Findings through JUACEP

Name: Jiang, Yifan

Affiliation (Dept & Univ): Department of Electrical Engineering, UCLA

Participated program: Summer 2015



Research theme: Characterization of the Properties of GaN Nanowires and Their Devices

Advisor at Nagoya Univ: Prof. Amano, Hiroshi

Affiliation (Dept.): Electrical Engineering and Computer Science

It is amazing for me to see that there are so many people in Prof. Amano's group. The group is large and many research topics are covered. I am very exciting to get involved in the study of GaN nanowires and related devices. It is the first time for me to do experiments in this field. I appreciate that many group members are willing to help. I learned the operation of many devices and learned many knowledge and skills about this area. The more important thing is that I see a relatively large picture of the development of GaN nanowires and nanowire-based devices after this experience.

I want to pursue a PhD and get involved in a research institute in the future. Of course, the best is to find a faculty position in a university. For my career goal, the research internship provides me opportunities. I hope that I can take advantage of what I learned in Nagoya University for my career goal. It is really a valuable experience in my life.

Besides the research internship, there are many interesting activities in this program. I love the experience to assemble a motor and the experience to create a mug. Furthermore, the field trip to the factory provides me the opportunity to learn about how a vehicle is produced. It is always exciting to see big machines and large scale production. Prof. Amano's lab also had a trip. I went with other group members in the lab. It is interesting to see and live in a Japanese style hotel and took part in a Japanese style party. Japanese food is good.

The Japanese language course is also very useful. As a relatively widely used language (for me, it is), Japanese is very useful. I have wanted to learn Japanese for many years. There are so many conditions in which I really want to know Japanese. The course is short and only elementary; however, I still learned the basics of Japanese. It is a good start for me. Moreover, now it is more possible for me to learn Japanese by myself.

I appreciate Prof. Amano to provides me with this good opportunity. I also appreciate those group members who help me with my research. Overall, It is a nice experience.

My Experience in Japan

Name: Austin Kuo

Affiliation (Dept & Univ): HSSEAS, UC Los Angeles

Participated program: Summer 2015

Research theme: Autonomous and Dynamic Robotics

Advisor at Nagoya Univ: Prof. Hayakawa

Affiliation (Dept.): Mechatronics Laboratory



JUACEP has provided a unique opportunity for American students to immerse themselves in Japanese culture with special regard to academia and graduate life in Japan. I am very thankful to have such an opportunity to learn more about my field of study and develop a professional and social network of contacts.

My work at Professor Hayakawa's lab was an excellent primer into the burgeoning field of applied robotics. I was amazed at how intellectually-graspable kinematic equations can translate into highly sophisticated motion by a robot. The design process was, to me, a mysterious 'black box' that magically turned theory into application. But by meticulously poring over the 5+ years of work put into the robot, as well as conducting some experiments with the robot, the box's opacity was rendered null, and the design process was elucidated. I can now appreciate the competency and interdisciplinary knowledge that is required in the undertaking of such a project. The project demands fluency in mathematics, programming, and engineering concepts as well as the ability to integrate those topics into a coherent system.

During my time here, I was able to visit several places that were eminently reachable by bus or train: Nagano, Ise, Tokyo, Kyoto, Lake Suwa, Mt Fuji, and more. I tried many foods: ramen, sushi, sashimi, yakitori, katsu, and a plethora of regional specialties (usually sweets). They were both delicious and cheap when compared to food of similar quality in the states. With the JUACEP program, I visited Toyota's automotive manufacturing plant, and got to experience karaoke, izakaya (Japanese gastronomic bar), onsen (bath house), and shrines. There was never a shortage of things to do in Japan.

I am most grateful for the opportunity to learn Japanese language and culture, and interact with Japanese people. I have come to greatly admire the collective propriety of effusive cordiality and obsequious humility that is a trademark of Japanese culture. I learned a great deal about subtlety, an art perfected by the Japanese, and was astounded by how everything from syntax to gesticulations could impart a colloquial vibe or formal atmosphere and everything in between. While some may regard the observance of such customs as tedious or even trivial (my own immoderacy tolerated because I was a foreigner/guest), I believe many cultures can study Japanese culture and adopt some of their values to great effect. I hope that my presence here was also beneficial for my Japanese counterparts who may have learned a little about how to interact with Americans or other Westerners.

I would like to thank JUACEP, Professor Hayakawa, the members of the mechatronics laboratory, and the many people I met on this trip for an unforgettable time and a learning experience in the laboratory and well beyond. Thank You.

Findings through JUACEP

Name: Haroula Kyriacou

Affiliation (Dept & Univ): Materials Engineering, UCLA

Participated program: Summer 2015

Research theme: Polyolefin Catalytic Cracking for Fuel Consumption

Advisor at Nagoya Univ: Professor Hirasawa

Affiliation (Dept.): Molecular Design and Engineering



To say I was a bit skeptical about traveling across the Pacific is a bit of an understatement. As a proud Southern Californian Greek Princess, traveling to a country and continent unfamiliar to me seemed like the end of the world. Luckily, the world kept spinning. Though I would say I enjoy traveling, until this summer, I don't think I was able to classify myself as an expert traveler. However, after managing the Tokyo subways like a boss and planning extensive weekends trips around Japan, goal reached: I am on my way to becoming a world traveler! More than that, I have learned so much about myself, in both the academic and social worlds.

At UCLA, I purposely avoided laboratory settings as much as possible. The constant attention to detail as well as monotonous work seemed like something I could not possibly accomplish. However, through JUACEP, I was able to spend the summer mastering a laboratory with my best friend by my side. Though the language barrier was immense, the Hirasawa lab members did their best to welcome fellow Bruin MSE Lindsey and I to Nagoya and aid us in our research. It has been amazing to not only experience hands-on research but to also perform it in a country whose approaches and standards are different than our own. As Structural Master's students with a concentration in Characterization, the opportunity to use such a wide variety of analysis was a great help for our future careers. From SEM-EDX, to XRF, XRD, ICP-MS, OEA, NMR and GC-MS, it is incredible to say that I now have experience with all of these machines. As the avid student I am, I especially enjoyed the Japanese language course offered through JUACEP and loved our adorable Sue Sensei-I only wish it was longer, or even better, brought to the States to allow us to prepare before our arrival!

Lastly, to talk about the amazing experiences that Japan has offered me. From exploring all the wonderful parts of Nagoya- Kanayama, Osukannon, Sakae, Fushimi, Higashiyama, Motoyama, Yagoto- to weekend adventures throughout Japan- Osaka, Nara, Kyoto, Gifu, Gujo, Tokyo, Chiba, Mt Fuji, Seki- this trip has been nothing short of non-stop fun (and sweating, atsuide). My favorite events have been all the wonderful summer festivals found throughout the country. From the Hanabi Festival in Gifu to the Fukagawa Festival in Tokyo, I find the Japanese cultural fascinating. As a lifelong Greek folk dancer and instructor, you can imagine my favorite would be an Odori Festival and the small town of Gujo made the event something magical. The live music and hundreds of yukata-clad locals adorning the streets took my breath away. The love and respect felt for their culture was felt in every word sung and step taken.

Thank you JUACEP for a wonderful summer, filled with laughter, friendships, accomplishments and self-realizations. Though I never imagined myself a lover of laboratory research or matcha (the holy green grail of Japan), I can now proudly say I am both! ありがとうございます & じゃあまた!

Findings through JUACEP

Name: Hongyang Li

Affiliation: Department of Materials Science and Engineering

Participated program: Summer 2015

Research theme: Deep Discharge and Elevated Temperature Performance of Solid-state Thin Film LiCoMnO₄ Batteries

Advisor at Nagoya Univ: Prof. Yasutoshi Iriyama

Affiliation: Department of Materials, Physics, and Energy Engineering



As a student majoring in materials science and engineering, I know it very well that Japan has accomplished a lot in the field of material research, and the commercialization of lithium ion batteries is one of the shining achievements of Japan. That is also my motivation for coming to Nagoya University through the JUACEP program.

The first thing that impressed me is the orientation for us. It was the first time to meet a Noble Prize winner. I cannot express how excited we were when we met Prof. Amano, such an approachable and humble man who has achieved a lot and changed the world to some extent. And of course I shared the photo I took with Prof. Amano with all my friends in America and China.

My research life here started with a talk with my two advisors, Prof. Iriyama and Prof. West. Before coming here, I was a little bit worried whether I could truly get involved in the research here as an exchange student who will only stay here for less than three months. However, this talk made me believe that I could have a satisfying summer here and I feel pretty lucky that I could work under the guidance of two experts in my research area. Not only does the advanced and creative research perspectives inspire me, the rigorous research spirit in my lab offers me a lot as well. From working with my advisors and the experienced students in my lab, I learned a lot about lithium ion battery research and I do consider it useful for my following study and career.

The field trip to Toyota impressed me a lot as well. I have never thought about how a car is made and was astonished when went to Toyota factory. The highly automatic assembly line and the complex but efficient system running the whole factory are what I really appreciate. As a highly developed industrial country, Japan has a lot of things that are worth learning. The advanced technology, the in-depth of fundamental research and attention to details make Toyota a great company, and also make Japan an admirable country in the world.

Life in Nagoya is enjoyable and I really appreciate this opportunity to have a nice summer here.



Findings through JUACEP

Name: Xu Li

Affiliation (Dept & Univ): Mechanical and Aerospace Engineering

Participated program: Summer 2015



Research theme: Design of magnetically driven microfluidic chip

Advisor at Nagoya Univ: Prof. Fumihito Arai

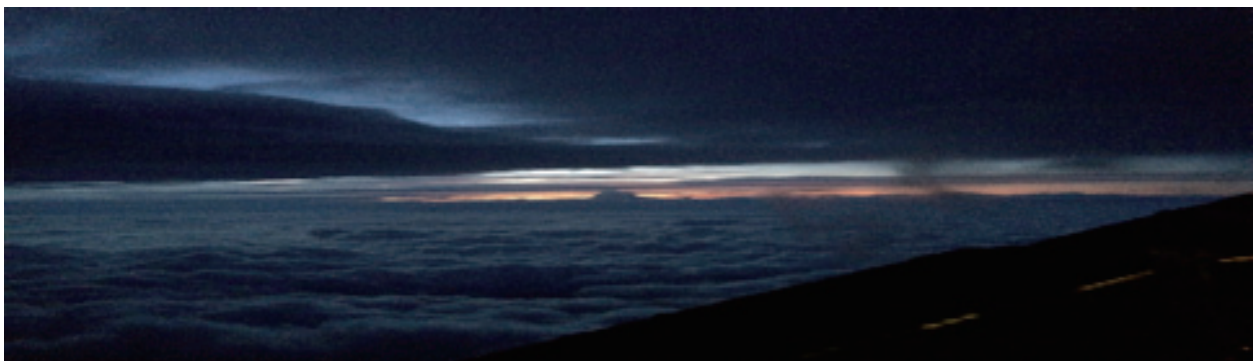
Affiliation (Dept.): Micro-nano systems engineering

At this moment I'm typing, there is only one week left before the end of the program. I have to say, this is the most amazing summer I ever had, which is definitely a valuable memory in my life. I have always been seeking for a chance to come to Japan. Not only because I'm a big fan of manga, sushi and kendo, I also would like to live in Japan for a period of time so that I could truly enjoy the culture of this country. The first impression I had on Japan is that people here are so friendly. When I got off the plane and had to manage to go to Nagoya University by myself, I was actually a little worried for being lost, since I don't speak Japanese and not all Japanese people speak English. But still what surprised me is that when I asked a lady for help, though she may not fully understand what I was saying. But when she figured out my destination, she guided me in person to the subway station and also led me inside to the right platform. Later on I found she is not the only one for being so kind. All the Japanese people are very friendly and willing to help others, which made my life in Japan much easier.

During this period I visited some famous places, such as Osaka, Kyoto and Nara. I love the architecture in Kyoto, which remained the old fashion of Japanese style. I fed the deer in Nara and visited toodai-ji. I like Osaka most, because takoyaki and okonomiyaki in Dōtonbori are so delicious, the best in the world. I also went to Tokyo and Hakone. But I think the most unforgettable trip is to Mt.Fuji. Hiking is my favorite sport, so one of the main purposes of coming to Japan is to see the sunrise on the top of Mt.Fuji. It took me about 4.5 hours from Mt.Fuji 5th station to the top. Unfortunately it was very cloudy that day. We couldn't see the sunrise. But still it was such a great view when you were overlooking from the peak point.

I also enjoyed life in the lab very much. Our lab is like a big family with almost 30 members. When I first joined the lab, they threw a welcome party for me. Before the party we spent the whole afternoon to prepare the 手巻き寿司, sashimi and soba ourselves. It was really fun and I finally found out why my seaweed was too sticky to the rise to be cut perfectly when I made 巻き寿司 in Los Angeles. I have to COOL THE RICE DOWN first. We are going to have a lab tour to 高取山ふれあい公園 the day after tomorrow. I'm so looking forward to it.

I'm glad I joined JUACEP program. I will never forget this wonderful summer.



Findings through JUACEP

Name: Antonio Martinez

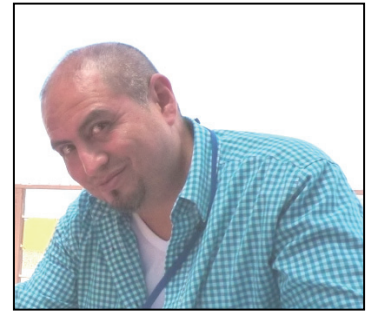
Affiliation (Dept & Univ): Electrical Engineering, UCLA

Participated program: Summer 2015

Research theme: Algorithm For Estimation Of Elevator Travel Distance Using Smartphone

Advisor at Nagoya Univ: Prof. Nobuo Kawaguchi

Affiliation (Dept.): Department of Computational Science and Engineering



As my second time participating in JUACEP, I have again most enjoyed from this program the research lectures. Researchers from well-known companies and institutions come to the Nagoya University campus to offer a research lecture about the work they are currently engaged on. For instance, I enjoyed the research lecture of Professor Akihiro Iiyama, from Yamanashi University, who talked about technological innovations in fuel-cell for future automobiles. Another part of the program that I appreciated was the engine assembly/disassembly. This hands-on activity was not only fun, but also very interesting as we were able to closely learn the basic engineering principles seen on an engine.

I found my lab a bit crowded this second time. It has about fifteen members and two professors. Most of my lab mates are master students, but there are also undergrad and PhD students. The lab has a good feeling of camaraderie, which is one of the aspects I like the most because this has a positive effect on teamwork, especially in a research setting like this.

I am glad that Nagoya University has a beautiful and large campus, the Higashiyama campus that is, where the graduate school of engineering is located at. There are many facilities to serve the students, like cafeterias, convenience stores, coffee shops, etc. Also, there is a gym, which I've been using regularly. In general, the campus area is in a nice and quiet location of Nagoya.

Life in Nagoya has been enjoyable in many aspects, with the exception of the summer weather. It was a bit hotter and humid than last year, but the good thing was that there was always air conditioning on most places, including my lab, and my room. Nagoya is centrally located in Japan. That made it easy to travel not far distances to visit interesting places like Kyoto, Osaka, Tokyo, among others. Even within Nagoya there are many places to visit, like the Nagoya castle, several temples, and even the Nagoya zoo.

I believe having participated in the JUACEP program twice will not only have an impact on my future career as a researcher, but also, on my life. I have been able to observe the differences and similarities on how a research lab functions here in Japan compared to a lab back home in the US. This has definitely improved my own research practices and it will keep doing it in the future too. Similarly, the cultural differences I have experienced in Japan enriches the way I see life and will keep helping me appreciate contributions of other cultures to my own.

Findings through JUACEP

Name: Jimmy Ng

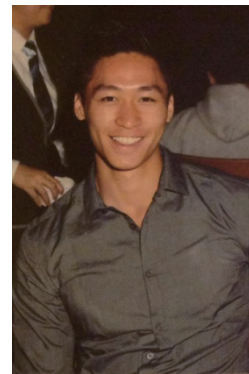
Affiliation (Dept & Univ): Materials Science and Engineering

Participated program: Summer 2015

Research theme: Electron field emission of graphene

Advisor at Nagoya Univ: Prof. Yahachi Saito

Affiliation (Dept.): Quantum Engineering



Being in Japan through the JUACEP program has been a truly amazing experience. When I first arrived in Japan, I had no idea what to expect. I couldn't speak the language at all, nor was I familiar with its culture and customs. My anxiousness was soon put to rest when I met my advisor, Yahachi Saito. A very intelligent and wise man with a friendly happy-go-lucky attitude, I could tell he really cared about his students. I was no exception and he made a huge effort to make me feel welcome.

Professor Saito also assigned me a project that was interesting and challenging but doable in the 10 weeks I was in Japan. Working on my research project, I was able to learn new material and become familiar with equipment that I did not have an opportunity to learn while I was at UCLA. Furthermore, doing research here challenged me to work and communicate with people in an unfamiliar setting. In the process, my interpersonal skills with people of different cultures grew. In the globalized world that we live in today, these soft skills are invaluable and I cannot thank the JUACEP program enough for allowing me the opportunity to cultivate them.

Luckily, Nagoya University had many extracurricular activity clubs. To de-stress from a busy day in the lab, I joined the campus' boxing club and participated in their practices. Having some kickboxing background, I had no problems keeping up with the practices despite there being a communication barrier at times. Doing boxing, I was able to meet many cool people outside my major and keep healthy during my stay at Nagoya University! I would recommend everyone participating in this program to seek out a club that sparks their interest and put themselves out there to meet people.

During the weekdays, I stayed around the university focusing on my research efforts and going out nearby some nights. But on the weekends, I got the chance to explore the city of Nagoya and also venture off to other cities in Japan. Being one of Japan's major cities, Nagoya has many tourist attractions to visit as well as a lively nightlife. Weekend excursions to farther cities were also planned with other JUACEP students. I partied in Osaka, learned about traditional Japanese culture in Nara and Kyoto, went to a summer fireworks festival in Gifu, visited Japan's most sacred shrine in Ise, had many adventures in Tokyo, and climbed to the summit of Mt Fuji!

However, the most memorable part of my time in Japan were the people that I met in my lab. All of the lab mates from the Saito lab were very friendly and made a genuine effort to make me feel welcome. When we were not working and studying hard inside the lab, we were outside the lab having fun. I will never forget the times we went out eating out, drinking, partying, watching movies, playing sports, karaoke-ing, and even to a music festival in Tokyo together! And when we were stressed out or when we had issues in our lives, we supported each other. Through them, I not only learned about Japanese people, life, and culture, I got to experience it. I consider this the most important experience I gained during my stay in Japan. I feel truly blessed that I was able to make such good friends during my short stay and am eternally grateful!

The JUACEP program not only had an impact on my future career as a scientist, but also on my life. Living and working in Japan made me greatly appreciate Japanese people and culture. Because of this experience, I am no longer hesitant to apply to jobs that involve travel to Japan, or even engineering companies in Japan. I am very glad I got the opportunity to come to Japan and would recommend this to anyone who wants to gain useful skills while delving into a new country and culture.

Findings through JUACEP

Name: Lindsey Perry

Affiliation (Dept & Univ): Materials Engineering, UCLA

Participated program: Summer 2015

Research theme: Polyolefin Catalytic Cracking for Fuel Consumption

Advisor at Nagoya Univ: Prof. Hirasawa

Affiliation (Dept.): Molecular Design and Engineering



Even though I was excited to apply for JUACEP, I was still nervous to actually travel to Japan. I had never been outside of North America or away from home for longer than a week - 3 months in Asia sounded crazy in comparison! I am so glad I did not let that stop me from coming because this was a once in a lifetime experience. I traveled around a new country, learned a new language, ate new foods, and experienced a completely new culture! In addition, I gained research experience and now feel much more confident in a lab setting.

To start with the reason we were all here: research. With one of my friends and labmates from UCLA, Haroula Kyriacou, we accomplished more than I could have imagined in 3 short months. We researched polymer recycling in Professor Hirasawa's lab, going into lab almost daily, performing experiments and doing several forms of analysis, including GC, SEM, XRD, XRF, and ICP-MS. We were also taken to a nearby university to perform NMR analysis on some samples. Overall, we gained valuable experience and were able to put into action the skills we had learned in our classes at UCLA. I feel much more confident in my ability to run my own experiments and perform independent research.

While I will always appreciate the experience I gained as an engineer through JUACEP, I think what I will remember most from this trip is exploring Japan. We visited many of the sites in our own city of Nagoya, such as the Higashiyama Zoo, Nagoya Castle, Atsuta shrine, and Nagoya Aquarium, among others. We also went exploring in the downtown area of Sakae and had a lot of fun with the night life! With JUACEP we went to Seto and made some traditional Setomono, or pottery – you can see my beautiful cat in the picture above. On our own we visited several other cities and places, including Osaka, Nara, Kyoto, Gifu, Gujo, Tokyo, Chiba, Seki, and Mt. Fuji! In Chiba we went to the huge music festival Summer Sonic and rocked out to some of our favorite American bands, like Imagine Dragons! Even though we were in lab during the week, 3 months has been plenty of time to venture out of the University. My personal favorite place was Gujo, where we went white water rafting, ate delicious chanko nabe, danced the night away at an Odori festival, and jumped into their famously clean river off a 30 foot bridge! That trip was completely due to the kindness of new Japanese friends, for which I am eternally grateful. I have made so many friends in Japan, all of whom I hope to stay in touch with and see again!

I can't believe my time in Japan has come to an end! I will always remember this trip and the experiences I have had (and the pounds of matcha I consumed). I am so grateful to JUACEP for this opportunity. I learned so much, not only in lab, but about an entire culture. Not to mention my skills with hashi (chopsticks) are going to be the envy of all of my friends back in the U.S. the next time we get sushi!

Findings through JUACEP

Name: Jake Stremfel

Affiliation: Materials Science & Engineering / University of California, Los Angeles

Participated Program: Summer 2015

Research Theme: Fatigue Crack Healing via High-Density Electropulsing

Advisor at Nagoya: Prof. Yang Ju

Affiliation: Mechanical Engineering



My time in Nagoya, and Japan in general, has been one of my most rewarding experiences. When I first arrived in Japan, I thought that ten weeks was a rather long time and enough time to fully experience Japan and its culture. However, having now almost finished the program, I wish I had more time. There is so much to experience in Japan, and I feel that I have just scratched the surface.

My research under Prof. Yang Ju at Nagoya was the study of fatigue crack healing via the application of high-density electropulsing. Being able to conduct research outside of my own area of research at UCLA was extremely useful. Due to the limited amount of time in Japan, my research was somewhat restricted but still fruitful. My time in lab was sometimes slow due to the inability to read/operate some of the pieces of equipment, but all of my labmates were extremely patient and helpful with anything I needed.

Outside of my time spent on campus, I did quite a bit of traveling. Besides traveling in and around Nagoya, I spent two weekends in Kyoto, almost a full week in Tokyo, and a harrowing two nights in Fuji. On both of my round trips to Kyoto I took the Shinkansen. The Shinkansen trains were very impressive and just taking them was an experience in itself. However, after two round-trip tickets, I quickly knew I would have to find an alternative way to travel as a one-way ticket was about 50 USD.

The most memorable and intense experience of my trip is by far Mt. Fuji. Climbing Mt. Fuji tested me both physically and mentally. There was nothing inherently difficult about the terrain of the mountain that made it difficult to hike, but the altitude, temperature, wind, and sheer distance made the climb relentless. I reached the summit about 15 minutes before the sunrise which unfortunately was largely masked by clouds, but it was beautiful nonetheless. Once I experienced the sunrise, I quickly made my way into one of the buildings and passed out on a bench along with other weary climbers before I faced the arduous journey back down the mountain.

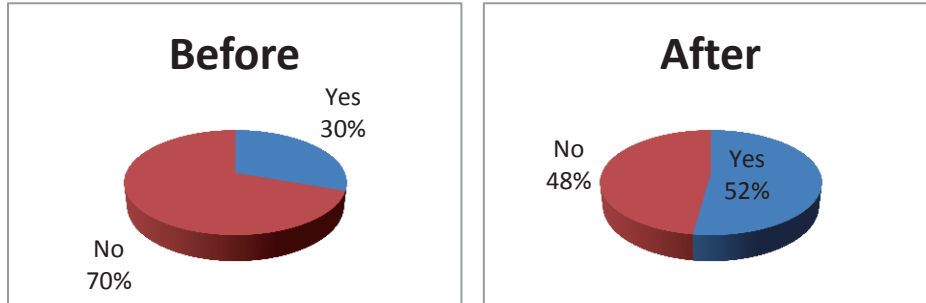
I wish I could write at more length about all my experiences in Japan, but doing so would require significantly more than one page. While I do miss home back in Los Angeles, I am quite sad to leave Japan and all the new friends that I have made. I honestly hope that I will some day return to Japan so that I can explore more of the country and get to know more of the culture and people.



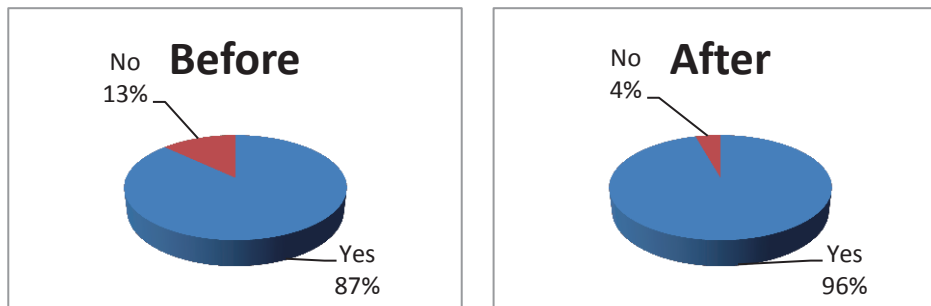
3-b. Questionnaires

**For Q1-4, we asked the same questions BEFORE and AFTER the program.*

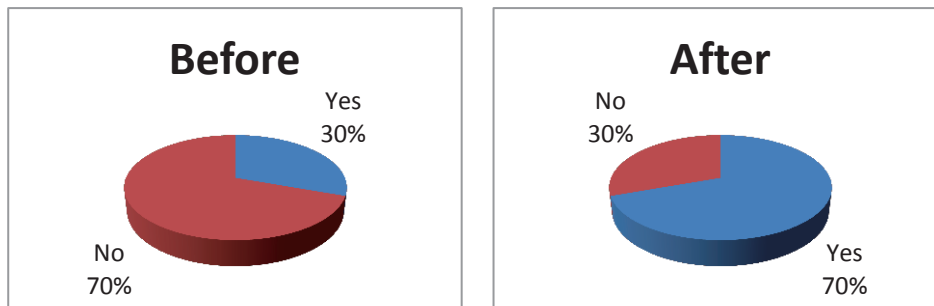
Q1: Are you interested in studying at a Japanese University for PhD?



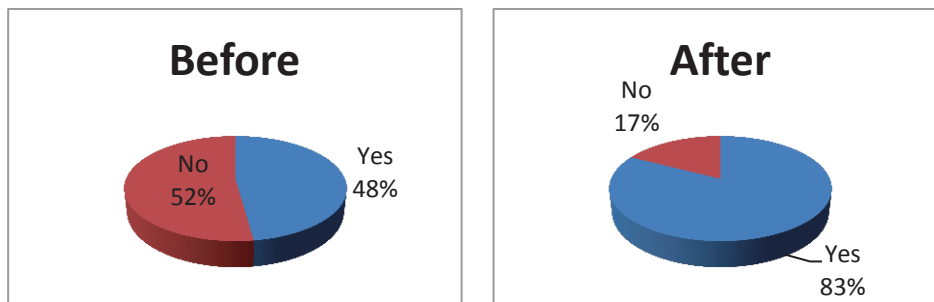
Q2: Are you interested in working at a Japanese company in USA?



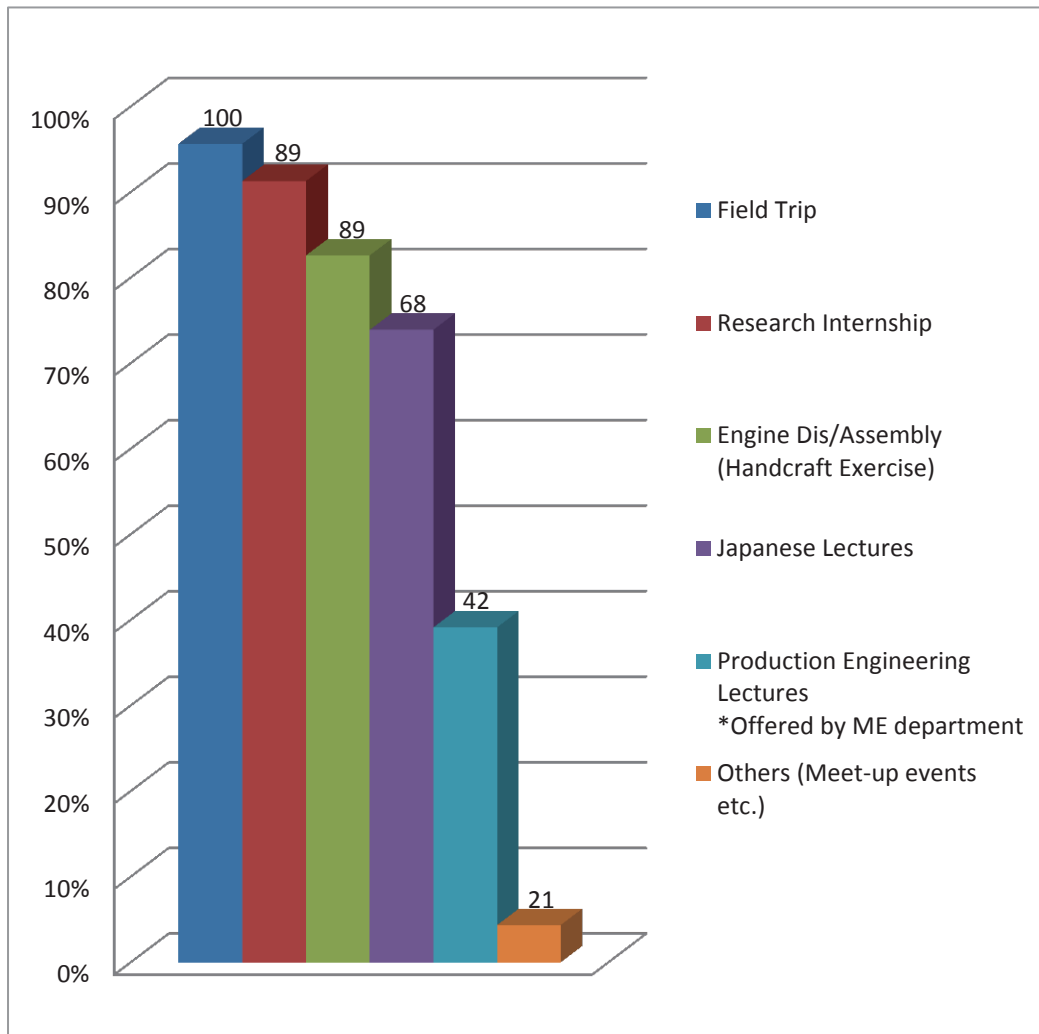
Q3: Are you interested in Working at a Japanese company in Japan?



Q4: Are you interested in working at a non-Japanese company in Japan?



Q5: Which programs of the JUACEP did you like?



Q6: In what did you find difficulty? What could be improved?

Time limitation (10 weeks) of research internship

- I hope we could have the option to extend the length of it to finish an on-going work.
- The time restriction to conduct a good research project. In the laboratory, there were many days where I was waiting for things to be prepared or certain choices to be made. I think it was because the people in my laboratory are incredible busy, but I was often worried about what I was supposed to be doing. I wish I had more time to connect with my professor.

Time limitation (10 lectures) of Japanese lectures

- The language course could extend over the entire program instead of only five weeks.
- The Japanese language class could have been longer.
- If JUACEP could have also provided higher-level Japanese language courses, it would be better.

Production engineering lectures

- *The production engineering lectures were soft-spoken and hard to hear and understand.*
- *Although the lectures were in English, you could not understand the lecturer and the presentations were poorly executed.*

Language barrier

- *There was a large language barrier that was difficult to surmount, and in my case, a translator was required. It's not necessarily a problem, as long as the program is focused on the cultural aspect of the exchange rather than the academic aspect.*
- *Unfortunately, not many people spoke English in our laboratory and those who did, they had difficulty explaining scientific matters to us.*
- *I believe I found the most difficulty is the language barrier in the lab setting. It was difficult to try and convey challenging concepts and ask questions without knowing how to express myself in Japanese (the opposite was true as well in English).*

Opportunity for more social settings

- *I wish there were more opportunities to meet and spend time with the other international students. There was one day-long trip that involved us traveling to the Toyota production plant and an all-you-can-eat dinner, and it really helped me get to know everyone in my program as well as other international students outside my program.*

Q7. Write comments freely.

Everything in Japan in this program has been a very positive experience for me. I worked very well with all the students in my laboratory and other graduate students at Nagoya University. I think we all really connected well so I'm very happy about my experiences here.

I obtained a lot through this program and thought it was thoroughly fruitful coming here. I am definitely giving thought to learning the language and coming here again, either for a PhD or to work.

I had a really good time this summer exploring Japan.

I felt that the opportunity to pursue cutting edge research through the JUACEP program was the most valuable part of it. Thanks.

Very well organized program due to good professors and organizers.

I hope this program could be held every year.

Overall, the JUACEP program is a very excellent program. It not only enables us to get much research experience, but also lets us enjoy a different culture in Japan. The dorm was very nice and clean with modern facilities and amenities. It would be nice if the policies were a little more lax, like allowing guests into the suites.

Really appreciate this opportunity to study and have a nice summer here.

Overall, JUACEP is a wonderful program and is an amazing opportunity for American students. I only wish that the language barriers were less but that may be our own faults.

The JUACEP booklet was helpful in the beginning since it contained a lot of information (in English!).

The program is really good and mature for holding so many years. I will always remember the days here. Thanks.

For me, three month program goes so fast and I am still not ready to leave here, but I am sure that I will have more opportunities to come back to meet all you people in the future. I will miss all of you.

<4>

Appendix

4-a. Pictures

-Orientation-



-Welcome Luncheon-



-Japanese Language Class-



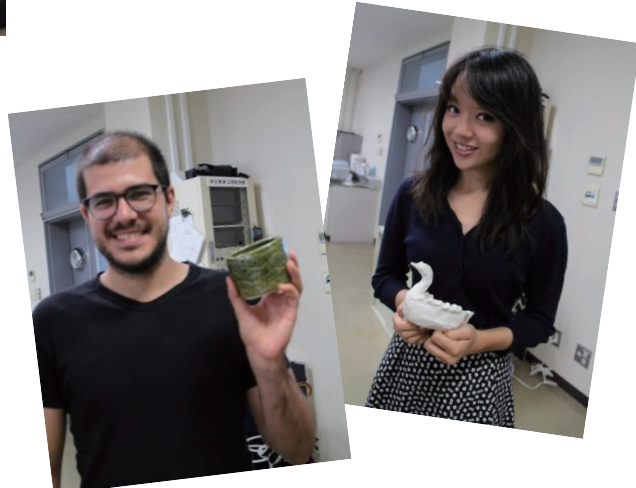
-Field Trip-



Toyota Motomachi Plant



Seto Pottery Museum



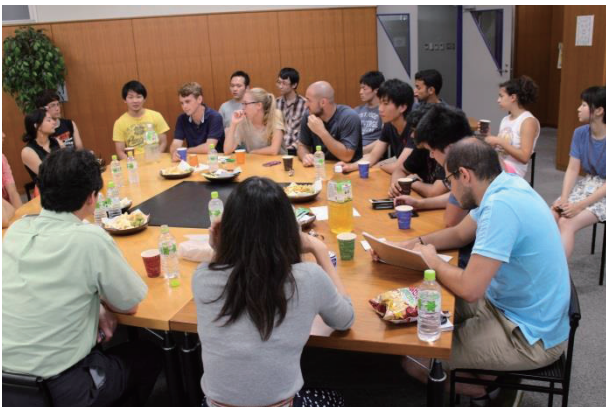
BBQ in Sakae



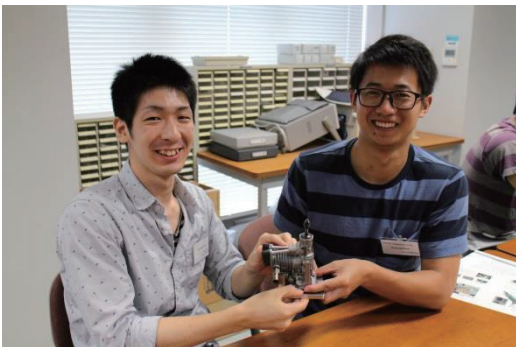
-Round-table Discussion with Prof. Yang-



-Meet-up event with NU students-



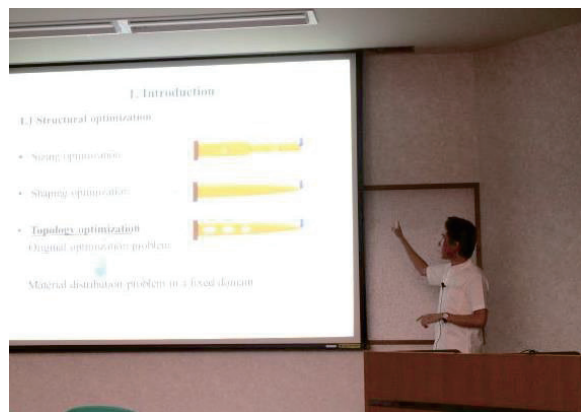
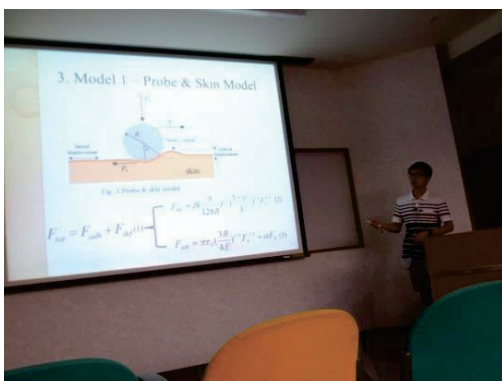
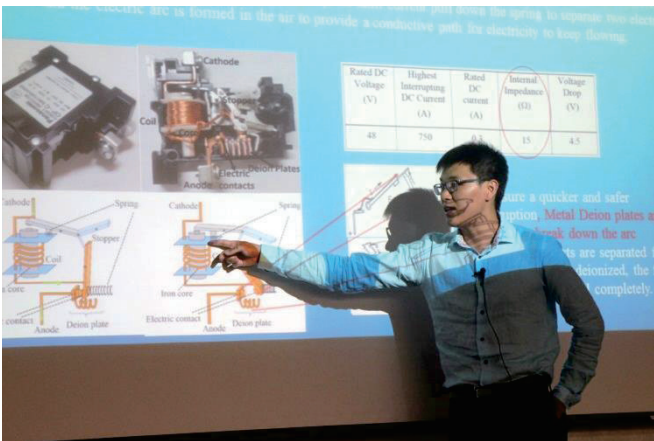
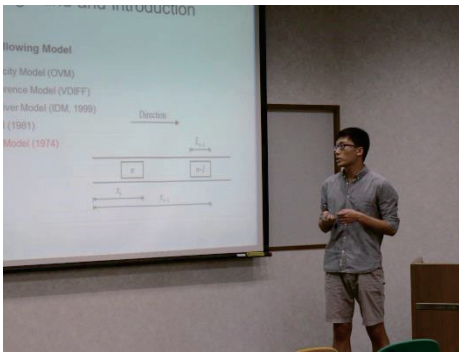
-Handcraft Exercise-

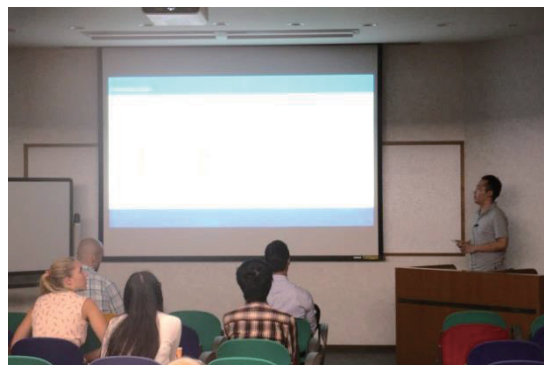
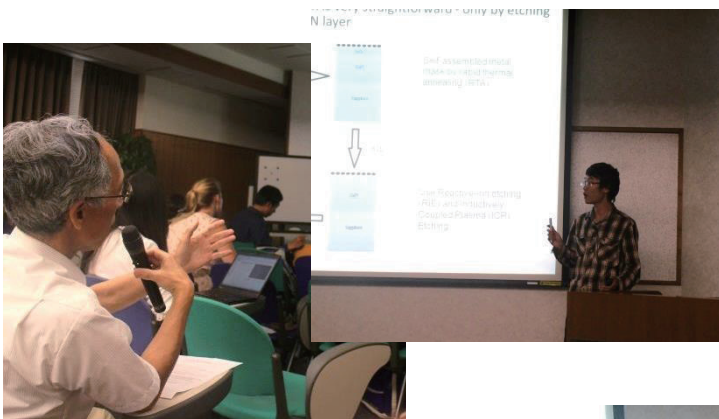
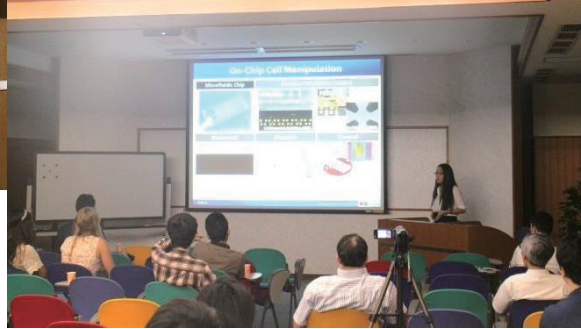


-@ Lab.-



-Workshop-





-Awarding Ceremony-



-Farewell Party-



JUACEP Summer Program 2015

Thursday, May 14, 2015 for UM students

10:00 Reception at VBL Hall: payment of admission fee, student health insurance

10:30 **Orientation** --VBL Hall

Welcome address from JUACEP Leader

Introduction of faculty, staff and participating students

Academic Information

- A) Schedule
- B) Japanese Language Class
- C) JUACEP Seminars
- D) Introduction to Production Engineering
- E) Handcraft Exercise
- F) Field Trip
- G) 3 Reports (Research report, Scholarship report, Finding through JUACEP)
- H) Evaluation

Life Information

- A) Housing
- B) Use of PC on Campus -- set up with TA
- C) Student ID Card
- D) Medical and Health Care
 - Medical Services
 - Health Precautions
- E) Student Life
 - Refuse Disposal at Nagoya University
 - Public Transportation in Nagoya City
 - If involved in a Traffic Accident
 - Compliance with Japanese Law
 - Safety Guide
 - Culture Shock
 - Differences in Academic Culture
 - Cope with Stress
 - Harassment

11:30 **Introduction of the lab mentors and TAs**

12:00 **Welcome lunch** --VBL Hall

13:30 Japanese Language Class --Room 441, Engg. Bldg.3

Friday, May 15, 2015

13:30 Receiving stipend and tuition fee payment --ES031, 3F, ES Bldg

*stipend: 80,000 yen

*tuition: 44,400 yen for research internship (3 credits)

14,800 yen for Japanese class (1 credit) + 3,780 yen for text

JUACEP Summer Program 2015

For UCLA students

Wednesday June 17, 2015

10:00 Reception at VBL Hall: payment of admission fee, student health insurance

10:30 **Orientation** --VBL Hall

Welcome address from JUACEP Leader

Introduction of faculty, staff and participating students

Academic Information

- A) Schedule
- B) Japanese Language Class
- C) JUACEP Seminars
- D) Introduction to Production Engineering
- E) Handcraft Exercise
- F) Field Trip
- G) 3 Reports (Research report, Scholarship report, Finding through JUACEP)
- H) Evaluation

Life Information

- A) Housing
- B) Use of PC on Campus --set up with TA
- C) Student ID Card
- D) Medical and Health Care
 - Medical Services
 - Health Precautions
- E) Student Life
 - Refuse Disposal at Nagoya University
 - Public Transportation in Nagoya City
 - If involved in a Traffic Accident
 - Compliance with Japanese Law
 - Safety Guide
 - Culture Shock
 - Differences in Academic Culture
 - Cope with Stress
 - Harassment

11:30 **Introduction of the lab mentors and TAs** --ES Meeting Room

12:00 **Welcome lunch** --Chez Jiroud

Welcome address from Prof. Niimi, Dean of Grad School of Engineering

13:30 Receiving stipend and tuition fee payment --ES031, 3F, ES Bldg

*stipend: 80,000 yen

*tuition: 29,600 yen for research internship (2 credits)

14,800 yen for Japanese class (1 credit) + 3,780 yen for textbook

Campus Life Information

Housing

International Residence Yamate

(10 minutes' walk from Higashiyama Campus)

Address: 165 Takamine-cho, Showa-ku, Nagoya 466-0811, Japan

Phone: 052-835-5575 (office)

Facilities: This is a three-story building with 106 single rooms (approximately 15m²).

It houses a lounge, a recyclable trash area, two laundry rooms, mail boxes, and an administrative office.

Each room is furnished with a bed with bedding(*), desk, chair, desk lamp, open closet, storage shelf, air conditioner, Internet connection, TV connection, wastepaper bin, sink, induction heating (IH) cooker (1), microwave oven, refrigerator-freezer, ventilation fan, unit bathroom/ toilet and curtains (2 sets), etc.

(*):Bedding: Set for each room comprises quilt (1), blanket (1), bedpad (1), pillow (1), quilt cover (2), bedsheet (2), pillow slip (2).

Three Japanese graduate students live on each floor in International Residence Yamate as tutors.

PC & ID

Use of PCs on Campus

Wireless internet connection is available on campus including the Satellite PC Lab in the main library, and other areas on campus. If you want to connect our lap top PC to Nagoya University Wireless Network (NUWNET), please go to 'ECIS computer web page' (<http://eee.ecis.nagoya-u.ac.jp/computer/instr.html>) After receiving your ID and password, you must take the online Information Security Training and pass the test within a week. To pass the test, you must score at least 80% and retake the test until your score 80% or above.

Student ID Card

A student ID card has many functions. It will let you into the university libraries, and with the card you may borrow books from the library. The card lets you get student discounts at museums, theatres and so on.

Medical and Health Care

1. Medical Services

If you suffer from continuous headaches, a loss of appetite, or you cannot sleep well, etc., you should seek the advice of a doctor before the condition gets worse. These symptoms may be a sign of fatigue or exhaustion. They may also be psychological or psychosomatic symptoms, which are treatable by specialist

doctors. In addition to taking care of your own health, please pay attention to your friends' health and encourage them to see a doctor, if they are feeling unwell.

(1) The Health Administration Office

Students can undergo physical examinations, receive health advice, first-aid and arrange psychiatric counseling at this facility. There is no charge for using any of these services.

Tel: 052-789-3970

[Office Hours for Health Services]

Treatment	Time	Mon	Tue	Wed	Thu	Fri
Physical Examinations & First-Aid	10:00 – 11:30	○	○	○	○	○
	13:30 – 16:30	○	○	○	○	○
Psychiatric Counseling	10:00 – 12:00	○	○	○	○	○
	13:30 – 16:30	○	○	-	○	○

*Note: Appointments are necessary for psychiatric counseling services. Please call the office 052-788-6276 for appointments.

The Health Administrative Office is open between 9:00 - 12:00, 13:00 - 17:00 for first aid.

Map: http://en.nagoya-u.ac.jp/map/higashiyama/research_center_of_health_physical_fitness_sports.html

(2) Calling an Ambulance

Telephone 119 or press the RED button on a public phone for connection, free of charge. Although it is possible to speak English, it would probably be helpful for you to say the following: **Kyukyusha** (ambulance) **o onegai shimasu. Basho wa** (your location) **desu.** (I am calling for an ambulance. I am at...location.) This number is also used for requesting fire engines (**shobosha**). In Japan, ambulances are available 24 hours a day, free of charge.

2. Health Precautions

(1) Food Poisoning

Great care should be taken with regard to eating habits during the extreme summer weather in Japan. To avoid food spoilage, check the expiration date before buying food, apply heat to raw foods and be careful not to keep food in the refrigerator for an excessive amount of time. To guard against food poisoning, always wash culinary items with hot water. In the past, there was a frightening outbreak of O-157, a bacterial food poisoning disease. There was also an incident where students enrolled at Nagoya University were poisoned by eating wild mushrooms.

(2) Necessary measures to prevent the spread of infectious diseases

If you are traveling from Japan to another country, please seek travel advice regularly until the time of departure. Please follow the basic rules of hygiene to avoid being infected.

The Ministry of Foreign Affairs of Japan: <http://www.anzen.mofa.go.jp/>

Student Life

1. Refuse Disposal at Nagoya University

A sorting system for refuse disposal is used at Nagoya University. There are trash cans for “combustible refuse”, “incombustible refuse”, and recycle bins for “empty bottles”, “empty cans”, and “PET bottles” all over campus. In addition, there are boxes and a reverse vending machine near the Co-op. The sorted refuse will be recycled. Newspapers or magazines are collected by recycle companies. Used paper products such as used copy paper are collected and recycled. Students are kindly requested to be mindful when they throw away their rubbish and to use the correct bins to help waste reduction and the reuse of recyclable materials.

2. Public Transportation

1. Subway and City Bus Tickets:

- ① Manaca: Manaca is a pre-paid pass that can be used for both subway trains and buses operated by Nagoya City. Various types of Manaca can be purchased. It can be used for Meitetsu buses and trains, Aonami lines, Yutorito lines and Toyohashi railroad. It is a rechargeable card.
- ② One-day ticket: One-day tickets allow for unlimited rides for one day. One-day tickets for all bus, subway, and bus & subway routes are available. Ticket, Donichi-Eco-Kippu, that can be used on Saturdays, Sundays, holidays and the 8th of every month can be also purchased.

These tickets include a discounted admission fee for some tourist facilities in Nagoya city such as Nagoya Castle or the Tokugawa Museum.

They can be purchased at any subway station. For further information, refer to the following website:

<http://www.kotsu.city.nagoya.jp/> (Japanese)

2. Useful Links:

The following websites provide information on available transport services, time-tables, etc..

HYPERDIA: <http://www.hyperdia.com/en/>

3. If involved in a traffic accident.

If you are involved in a traffic accident, remain calm and do the following:

1. If anyone is injured, dial 119 for an ambulance.
2. Move any dangerous including vehicles, off the road to prevent other accidents.
3. Report the accident immediately, even if it is small, to a nearby police station and obtain a report of the accident.

4. Write down the license plate number of the car concerned as well as the name, address and age of the driver, after requesting to see his/her driver's license.
5. If there are witnesses, write down their names, addresses and telephone numbers.
6. Make detailed notes of the accident and take photographs, if possible.
7. See a doctor, even if you think that you are all right, because sometimes symptoms can take time to occur.
8. Consult your insurance company as soon as possible.

4. Compliance with Japanese Law

During their stay in Japan, any student who commits a crime, misdemeanor or any other illegal act, will be subject to legal procedures according to Japanese Law. Nagoya University also takes strict disciplinary measures against students who commit crimes or misdemeanors, and may expels them from university.

(1) Prohibition of Narcotics

In Japan, the possession and sale, for personal use or otherwise, of all narcotics and any illegal substances are strictly prohibited. If offered, refuse them. If leaving Japan temporarily, never agree to look after a stranger's luggage at the airport.

(2) Drinking and Smoking Restrictions

In Japan, people aged under 20 are not allowed to drink or smoke. Smoking is not allowed in many places, including stations, public facilities and within the campus. Nagoya city has special zones where smoking on the street is banned. If found smoking there, you will be fined.

Driving a car, riding a motorcycle or bicycle after drinking any amount of alcohol is a serious offence in Japan, and can also cause accidents. Never drive after drinking. Those who accept a ride in a car that is driven by a drunk driver or those who offer alcohol to a driver are all subject to punishment under Japanese law.

(3) Others

Whilst inside a shop, removing product wrappers, price tags or putting products into pockets or bags before actually paying for them may be treated as an attempt to shoplift in Japan. Talking loudly on your mobile phone or chatting with friends in public places, such as on a train, can cause disturbance in Japan.

5. Safety Guide

Japan is not as safe as most people think. There is the risk of crime anywhere in the world, including Japan. This is what you can do avoid problems.

- ◆ Avoid going out alone at night and keep away from deserted places.
- ◆ Many bag-snatchings occur in Nagoya. Keep your handbag close when walking on the street.
- ◆ Do not answer phone calls from unknown numbers. Do not open the door to strangers, even if they claim that they are representing certain companies. Lock and chain the door of your apartment when you are at home.

- ◆ There are deserted or dark places on campus which you should avoid. There is the risk of theft inside and outside of buildings. Please always protect your property.

6. Culture shock

Although “culture shock” is generally understood as a temporary shock felt when confronted by different cultural customs, ways of thinking and behavior patterns, it actually refers to a psychological state of depression caused by a succession of failure experiences in unfamiliar social situations. Culture shock is temporary and everybody goes through it to some extent in the process of cultural adaptation. General symptoms of culture shock include negative feelings such as: losing self-confidence, feeling depressed, attributing all failure to yourself, feeling that nobody understands you, feeling inadequate, etc. Accordingly, you may lose all motivation to talk with Japanese people or to attend classes. Most of these psychological reactions are, again, very natural in the process of cultural adaptation. Please take time to cope with each single event in your life, and you will be able to overcome these emotions sooner or later.

7. Differences in “academic culture”

It is widely accepted that different values, behavioral and communication patterns exist from culture to culture. However, we often fail to realize that there are also differences in “academic culture”, such as expected roles of academic advisers and students, classroom communication, evaluation criteria, etc. Such differences can also be a major cause of your stress. For example, the relationship between academic adviser and advisee is considered particularly important at the graduate level education in Japan. Some knowledge of the Japanese academic culture will help you achieve your goal more smoothly.

8. Cope with Stress

If you feel pressured by stress or lose confidence in your ability to study, you should think about releasing yourself from these negative emotions. Achieving good results in your studies may take a certain amount of time, and ought to be viewed as an accumulative process. Sometimes, you will need to take a break. If you feel tired, do not push yourself too hard and try to enjoy some of your favorite foods, recreation, and physical exercise. It is also recommended that you talk with your friends, academic adviser, or international students advisors/counselors. Moreover, please do not consider the process of cultural adaptation solely as a cause of stress; you can learn tremendously about various cultures, including your own, from this process.

< Visit the office of ECIS Advising & Counseling Services >

If you feel that you cannot deal with stress or feel a sense of isolation or frustration, do not hesitate to ask for help from international counselors at the ECIS Advising & Counseling Services. There is an international student counselor who will support your personal and psychological concerns. A discussion with an international student counselor can help achieve a useful perspective on culture shock and insights into Japanese culture.

ECIS Advising & Counseling Services (7th floor, West Wing of IB Bldg.)

<http://www.isa.provost.nagoya-u.ac.jp/en/>

9. Harassment

Nagoya University has set up a Harassment Consultation Center to prevent and eliminate the occurrence of any kinds of harassment, such as sexual harassment and academic harassment. Professional counselors deal with inquiries with utmost respect for their clients' feelings and wishes. Where the necessity arises, claims will be referred to the Committee for the Prevention of Harassment for investigation and arbitration. The Harassment Consultation Center works on issues of any degree of gravity. If you observe someone suffering from any kind of harassment, you may also come and report the case. In addition to the Harassment Consultation Center, each School at Nagoya University has appointed a faculty member as contact person (cf. see below). For English language consultation, you may visit the representative at the Education Center for International Students (ECIS). All consultation will be kept strictly confidential.

Nagoya University Harassment Consultation Center (Appointments by fax or E-mail)

Tel: 052-789-5806 (9:30-16:00)

Fax: 052-789-5968

E-mail: sh-help@post.jimu.nagoya-u.ac.jp

URL: <http://www.sh-help.provost.nagoya-u.ac.jp/>Contact persons at each School (including ECIS)

URL: <http://www.sh-help.provost.nagoya-u.ac.jp/pdf/madoguchi.pdf>>

Campus Map

Higashiyama Campus



Main Buildings

- 1 Administration Bureau Buildings
- 2 Toyoda Auditorium / Symposion
- 3 Nagoya University Museum
- 4 University Library (Central Library)
- 5 Noyori Conference Hall
- 6 Noyori Materials Science Laboratory
- 7 Akasaki Institute

Graduate School / School Buildings

- 8 Graduate School / School of Engineering Buildings
- 9 Engineering and Science Building (Central Building of Graduate School of Engineering / Particle and Astrophysical Science Building)
- 10 Graduate School / School of Science Buildings
- 11 Graduate School of Mathematics Building
- 12 Science and Agricultural Building
- 13 Graduate School of Bioagricultural Sciences / School of Agricultural Sciences Building
- 14 Environmental Studies Hall
-Graduate School of Environmental Studies
- 15 Graduate School / School of Economics Building
- 16 Graduate School / School of Law Building
- 17 Graduate School of International Development Building
- 18 Graduate School of Education and Human Development / School of Education Building
- 19 Integrated Research Building (Arts and Social Sciences)
- 20 Graduate School / School of Letters Building
- 21 Central Building for Liberal Arts and Sciences
-School of Informatics and Sciences Building
-Institute of Liberal Arts & Sciences
- 22 Building A for Liberal Arts and Sciences
- 23 Graduate School of Languages and Cultures Building
- 24 Graduate School of information Science Building

Centers / Institute Buildings

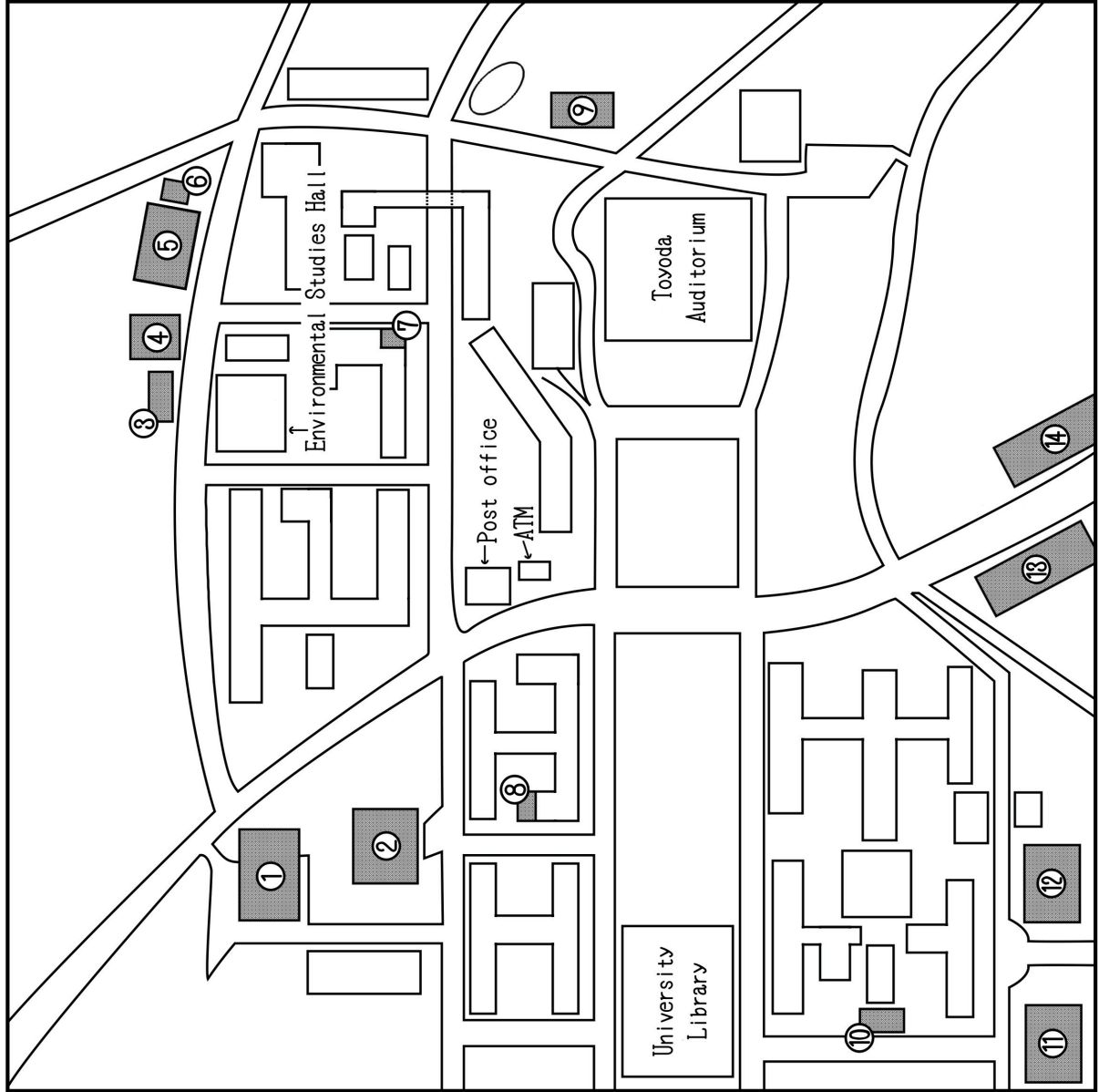
- 25 Center for Developmental Clinical Psychology and Psychiatry
- 26 Center for the Studies of Higher Education
- 27 Education Center for International Students
- 27₂ Advising & Counseling Services, ECIS
- 28 Center for Asian Legal Exchange
- 29 Information Technology Center
- 30 Kobayashi-Maskawa Institute for the Origin of Particles and the Universe (KMI)
- 31 Research Center for Materials Science
- 32 Bioscience and Biotechnology Center
- 33 Radioisotope Research Center
- 34 Research Institute of Environmental Medicine
- 35 Hydrospheric Atmospheric Research Center
- 36 Institute for Advanced Research Hall
- 37 Solar-Terrestrial Environment Laboratory
- 38 Eco Topia Science Institute
- 39 International Cooperation Center for Agricultural Education
- 40 Research Laboratory Building
- 41 Research Center of Health, Physical Fitness and Sports

Conference Halls & Galleries

- 42 Noyori Conference Hall
- 43 Noyori Materials Science Laboratory, Lecture Hall
- 44 Engineering and Science Building, ES Auditorium
- 45 Science South Building, Sakata & Hirata Hall
- 46 Environmental Studies Hall, Lecture Hall
- 47 Integrated Building (IB), Lecture Room
- 48 Graduate School / School of Economics, Conference Hall
- 49 Graduate School of International Development, Auditorium
- 50 Integrated Research Building (Arts and Social Sciences), Conference Room

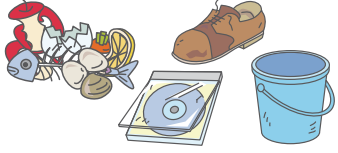















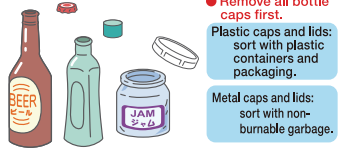

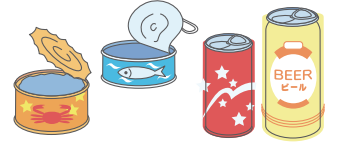


DINING MAP

- ① Hokubu Shokudo / Cafeteria
- ② Shichimittei / Cafeteria
- ③ Cafe Fronte / Coffee Shop
- ④ Dining Forest / Cafeteria
- ⑤ Restaurant Haranoki
- ⑥ Rikei Shop / Convenience Store
- ⑦ Craig's Cafe / Coffee Shop
- ⑧ IB Cafe / Coffee Shop
- ⑨ Shokuin Shokudo / Cafeteria
- ⑩ Family Mart / Convenience Store
- ⑪ Friendly Nanbu / Cafeteria
- ⑫ Nanbu Shokudo / Cafeteria
- ⑬ Hello Kid / Hamburger Steak Restaurant
- LAWSON / Convenience Store
- Bento Man / Lunchbox Shop
- Botantei / Chinese Restaurant
- ⑭ Cafe Terrace Cremes / Coffee Shop
- Tsubovakitei / Grilled-meat (yakimiku) Restaurant
- Kourantei
- GRAN PIATTO / Italian Restaurant



Sorting of Domestic Recyclable an Non-recyclable Refuse

Collection days are determined by neighborhood. Use this chart by circling the collection day in your area.

Collection	Sorting Category	Main Items (Examples)	Frequency	Collection Days <small>(収集日を丸で囲ってお使いください)</small>	Designated Bag
Usually Collected House-to-House	Burnable Garbage		Twice a Week	Mon. & Thu. (月・木) Tue. & Fri. (火・金)	
	Hazardous Flammable Items	 <p>● Remove all lids.</p> <p>Use up all the contents first. Punch holes in spray cans.</p>		Mon. & Thu. (月・木) Tue. & Fri. (火・金)	
	Non-Burnable Garbage		Once a Month	First (第1) Mon. (月) Second (第2) Tue. (火) Third (第3) Wed. (水) Fourth (第4) Thu. (木) Fri. (金)	
	Large-Sized Garbage By Prior Request Fee required	 <p>● Large items exceeding 30 cm diagonally</p> <p>Call the Large Waste Service Center at least one week in advance of the collection day to request collection.</p>	Once a Month	First (第1) Wed. (水) Second (第2) Thu. (木) Third (第3) Fri. (金) Fourth (第4)	Large Waste Service Center 0120-758-530 When calling by cell phone or from outside Aichi 052-950-2581 9 a.m. – 5 p.m. (excluding Sat./Sun./New Year's) *Service only available in Japanese.
	Plastic Containers and Packaging 		Once a Week	Mon. (月) Tue. (火) Wed. (水) Thu. (木) Fri. (金)	
Collected at Collection Station	Paper Containers and Packaging 		Once a Week	Mon. (月) Tue. (火) Wed. (水) Thu. (木) Fri. (金)	
	Recyclable Plastic Bottles 	 <p>● Remove all bottle caps first.</p> <p>Bottle caps: sort with plastic containers and packaging.</p> <p>Be sure to crush plastic bottles first.</p> <p>Plastic bottles can also be recycled at convenience stores.</p>		Confirm the day of the week on which collection occurs.	
	Empty Glass Jars and Bottles Beverage Bottles Food Jars Makeup Vials	 <p>● Remove all bottle caps first.</p> <p>Plastic caps and lids: sort with plastic containers and packaging.</p> <p>Metal caps and lids: sort with non-burnable garbage.</p>		Sort by category before placing out for collection	Remove bottles from plastic bags. Place them directly in the blue bin.  Place bottles on sides when placing in the bin.
	Empty Cans Beverage Bottles Food Jars			Chikusa, Higashi, Kita, Nishi, Nakamura, Naka, Showa, Mizuho, Atsuta, Minami, Moriyama, Midori, Meito, and Tempaku Wards  Nakagawa and Minato Wards Place in the yellow bin. 	

名古屋市

*For the time being, any see-through transparent or semi-transparent bag may be used in place of designated recyclable garbage bags.

< Chinese version >
< Hangul version >

http://www.city.nagoya.jp/zh/cmsfiles/contents/000022/22540/guide_ch.pdf
http://www.city.nagoya.jp/ko/cmsfiles/contents/000022/22541/guide_ha.pdf

Hospitals around Nagoya University (※English OK)

Nagoya Daini Red Cross Hospital

Address: 2-9 Myoken-cho, Showa-ku, Nagoya

Tel: (052) 832-1121

Mon-Fri: 8:00-11:00

Closed on Sat, Sun, holidays

Watanabe Clinic

Address: 1F Nikkou Yamate-dori Building, 3 -9-1 Yamate-dori, Showa-ku, Nagoya

Tel: (052)861-3450

Mon-Sat: 9:00-11:30

Mon, Wed-Fri: 16:00-17:30

Closed on Sun, holidays

Kai Clinic

Address: 32-2 Myoken-cho, Showa-ku, Nagoya

Tel: (052)836-9136

Mon-Sat: 9:00-12:00

Mon-Wed, Fri: 18:00-20:30

Closed on Sun, holidays

Yamate Dermatologist

Address: 2-9-1 Yamate-dori, Showa-ku, Nagoya

Tel: (052)836-4115

Mon, Tue, Thu-Sat: 9:30-12:30

Mon, Tue, Thu, Fri: 16:30-19:30

Sat: 14:30-17:30

Closed on Wed, Sun, holidays

Fujimi Dentist

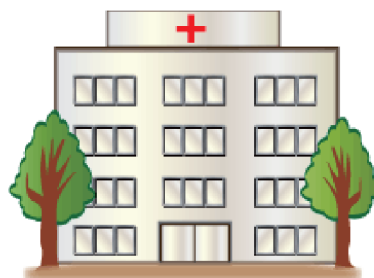
Address: 139 Yagotohujimi, Showa-ku, Nagoya

Tel: (052)835-3200

Mon-Wed, Fri, Sat: 9:30-12:30

Mon-Wed, Fri, Sat: 14:00-19:00

Closed on Thu, Sun, holidays



Copyright © JUACEP 2015 All Rights Reserved.

Published in November, 2015

Leaders of JUACEP

Professor Noritsugu Umehara

Professor Yang Ju

Japan-US Advanced Collaborative Education Program (JUACEP)

Graduate School of Engineering

Nagoya University  NAGOYA UNIVERSITY

Furo-cho, Chikusa-ku, Nagoya, 464-8603, JAPAN

JUACEP@engg.nagoya-u.ac.jp

<http://www.juacep.engg.nagoya-u.ac.jp>

